EFFECTS OF ADHESIVE Z-CONNECTIONS ON THE PROPERTIES OF A MODEL WOOD COMPOSITE

by

Wenchang He

B.Sc. Beijing Forestry University, 2011

A THESIS SUBMITTED IN PARTIAL FULFILLMENT OF

THE REQUIREMENTS FOR THE DEGREE OF

DOCTOR OF PHILOSOPHY

in

The Faculty of Graduate and Postdoctoral Studies

(Forestry)

THE UNIVERSITY OF BRITISH COLUMBIA

(Vancouver)

April 2017

Abstract

Adhesive is a costly and critical component of wood composites. The relationship between adhesive distribution and properties of wood composites has been explored, but few studies have attempted to alter the distribution of adhesive in wood composites as a way of improving their properties. In this thesis, I hypothesize that creating a 3-dimensionally inter-connected adhesive network by introducing adhesive Z-connections will improve two key properties of wood composites (thickness swelling and fracture toughness). Both experiments and computer simulation (finite element analysis) were carried out to test this hypothesis. I developed a methodology to precisely perforate veneer to facilitate the creation of adhesive Z-connections when the composite was pressed. Adhesive Z-connections are defined as the cured adhesive distributed in the Z- (thickness) direction (in addition to the X-Y directions) of the laminated wood composite due to the perforation in veneer. I examined factors affecting the ability of Z-connections to improve dimensional stability and fracture toughness of a model wood composite. I visualized the adhesive distribution in the composite in 2D and 3D using macro-photography, X-ray micro-computed tomography and scanning electron microscopy. Significant improvements in dimensional stability and fracture toughness of some of the composites were observed. Key parameters affecting the ability of adhesive Z-connections to reduce thickness swelling were diameter and spatial arrangement of Z-connections, adhesive level and wood species used to make the composite. Key parameters affecting the ability of adhesive to increase the fracture toughness of a model wood composite were area-density of Z-connections and reinforcement of the adhesive in the composite. I conclude that introducing adhesive Z-connections can reduce thickness swelling and enhance fracture toughness of wood composites, but the effectiveness of such an approach is affected by wood species, area-density and spatial arrangement of the Z-connections. I discuss the implications of my findings for the development of wood composites with enhanced dimensional stability and fracture

toughness and further research needed to capitalize on the concept of creating an inter-connected 3D adhesive network in wood composites by introducing adhesive Z-connections.

Preface

Portions of Chapter 4 were presented at the International Panel Products Symposium held in the UK and published in the conference proceedings (He and Evans 2015). The conference paper was subsequently reviewed and published in a special issue of the International Wood Products Journal:

He, W. and Evans, P.D. 2016. Reducing the thickness swelling of a model wood composite by creating a three-dimensional adhesive network. International Wood Products Journal, 7(4): 202-207.

Portions of Chapter 7 have been published in the open access journal: Advances in Materials Science and Engineering:

He, W. and Evans, P.D. 2017. Adhesive through-reinforcement improves the fracture toughness of a laminated birch wood composite. Advances in Materials Science and Engineering, published online: https://doi.org/10.1155/2017/5637248.

I conducted all the experimental research described and discussed in this thesis and I wrote the thesis. I received assistance from my supervisor with experimental design, statistical analysis and preparation of the final thesis. My committee members, Dr Chunping Dai and Dr Thomas Tannert commented and gave me feedback on parts of the thesis.

Table of Contents

List of Tables

List of Figures

Acknowledgements

I would like to express my sincere thanks to Professor Philip D. Evans for his professional supervision and valuable assistance during my Ph.D program. His mentoring has inspired me to be a better scientist and a better person in general. His deep knowledge and wide-ranging experience have greatly contributed to the quality of the research in this thesis. His forward thinking has encouraged me to be more innovative and interested in science. His method of organizing his group where everyone works together as a team has benefited every aspect of my life. I am very grateful for the opportunities Professor Evans has given me and also the funding he provided, which was essential for the completion of this research.

I thank my supervisory committee members Dr Thomas Tannert and Dr Chunping Dai for their support and help throughout my doctoral research. I thank all of the people at The Australian National University (ANU) who helped me with FEA, SEM and X-ray micro-CT: Dr Shankar Kalyanasundaram, Dr Mohammad Saadatfar (Department of Applied Mathematics); Ajay Limaye (Visualization Lab, ANU Supercomputing Facility); Dr Hua Chen and Dr Frank Brink (ANU's Centre for Advanced Microscopy). I thank Professor Dorin Ruse (Department of Biomaterials at UBC) for generous access to his Instron tensile testing equipment; Professor Markus Haapasalo (Department of Oral Biological & Medical Sciences at UBC) for letting me use his precision dental drilling equipment.

I would also like to thank China Scholarship Council for a scholarship which enabled me to come to Canada for my Ph.D, and supported me for the first four years of my Ph.D. I thank Tolko Industries for in-kind support, and Kevin Blau and Dan Price of Tolko for valuable feed-back and advice.

I’m greatly indebted to my many friends at UBC, especially those in my research group: Siti Hazneza, Kenny Cheng, George Chan, Barend Lötter, Vinicius Lube and Yuner Zhu. Thanks for all your valuable help and your friendship.

I also thank the Biocomposites Centre at Bangor University (Wales) for the honour of being the first recipient of the Harry Earl Memorial Scholarship which enabled me to travel to the UK in 2015 to present my work at the International Panel Products Symposium. My thanks also go to the Faculty of Graduate and Postdoctoral Studies and the Faculty of Forestry at UBC, for providing me with travel grant. I also thank Cindy Prescott, Gayle Kosh and Dan Naidu from the Graduate Office in Forestry for their help with my study and life at UBC.

My sincere gratitude to the donors of the Mary and David Macaree Fellowship in Forestry for their financial support, and all of the people in Forestry at UBC (too numerous to mention) who helped me throughout my time at UBC. Thank you all very much.

My warmest thanks go to my mother and father, whose unconditional love and unselfish support have encouraged me to pursue my career far from home. I will always be in debt to you.

Dedication

To science and all seeking mind.

1 General Introduction

1.1 Introduction

Wood composites are manufactured by hot pressing veneer, strands, particles or fibres of wood together with a thermo-setting adhesive. Adhesive bonding influences most of the properties of wood composites (Collett 1972; Frihart and Hunt 2010). For example, poor adhesive bonding is often associated with delamination at wood-adhesive interfaces and strength losses of wood composites (Bucur 2011). The levels of adhesive added to wood composites are far lower than the matrix materials used for composites such as glass or carbon fibre reinforced composites. Therefore, the adhesive in wood composites has to be 'efficient' at bonding wood elements together.

The term 'efficiency of adhesive bonding' in wood composites was first coined by Burrows (1961) who defined it as the state 'giving the best bonding characteristics with the minimal consumption of adhesive'. A variety of approaches have been used to increase the efficiency of adhesive bonding of wood composites, for example, chemical or physical modification of the surface of woody elements to enhance wood-adhesive interactions (DeVallance et al. 2007; He et al. 2007; Dai et al. 2011). Alternatively, modification to the chemical or physical properties of the adhesive used in wood composites can improve efficiency of adhesive bonding (Stephens and Kutscha 1987; Ellis and Steiner 1991). However, it is important to minimize the cost of such modified adhesives because adhesives are a costly component of wood composites. For example, the structural wood composite oriented strand board (OSB) contains only 2% to 4% by weight of adhesive. Nevertheless, adhesive represents up to 25% of the raw material cost of OSB (Spelter et al. 2006).

An alternative approach to increasing the efficiency of adhesive bonding in wood composites is to optimize the distribution of adhesive in the composites. The distribution of adhesive in veneer-based wood composites, such as plywood, laminated veneer lumber (LVL)

and glue laminated timber (glulam), is obviously only oriented in the X-Y plane (Fig. 1.1) due to the nature of the layered structure of these composites. Adhesive in these composites needs to wet and spread across adherend surfaces and then interact with the surface to create strong bonds. The surface area of woody elements in particulate composites is higher than that of veneer-based composites, and complete coverage of surfaces by adhesive is not achieved. However, early research by Lehmann (1970) demonstrated that more even distribution of adhesive in particleboard and improved mechanical properties of the composite were obtained when adhesive was applied to wood particles as a fine rather than a coarse mist. Recently, Evans et al. (2010, 2015) probed the 3D distribution of adhesive in particleboard and oriented strand board using X-ray micro-computed tomography. Their results suggested that the adhesive network in these wood composites is mainly oriented in the X-Y plane, and there are relatively few cross-links in the Z- (thickness) direction of the board (Fig. 1.2). Hence, the distribution of adhesive in particulate wood composites forms layers in 2D rather forming a 3D inter-connected network structure. Their studies also indicate that adhesive layers are interrupted by voids particularly in the core of the composites.

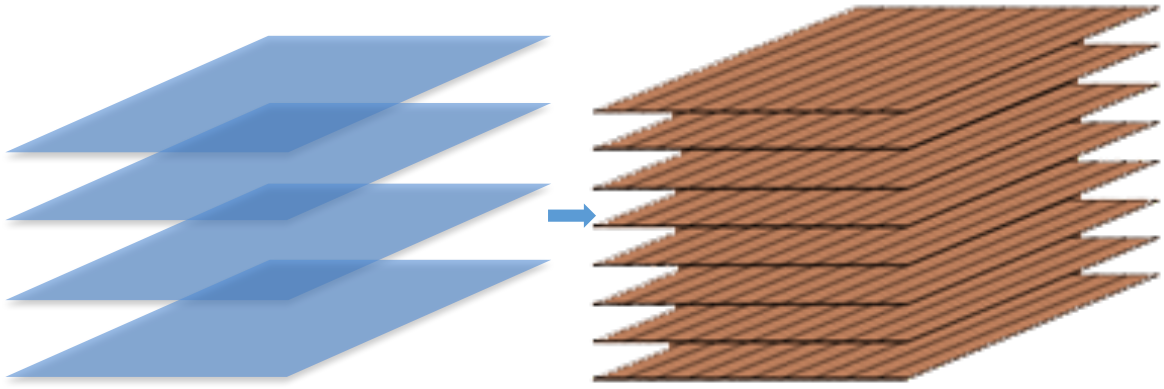

Figure 1.1 Schematic illustration of the separated adhesive distribution (blue) in the X-Y plane and veneer (brown) in veneer-based wood composites such as plywood and laminated veneer lumber (LVL)

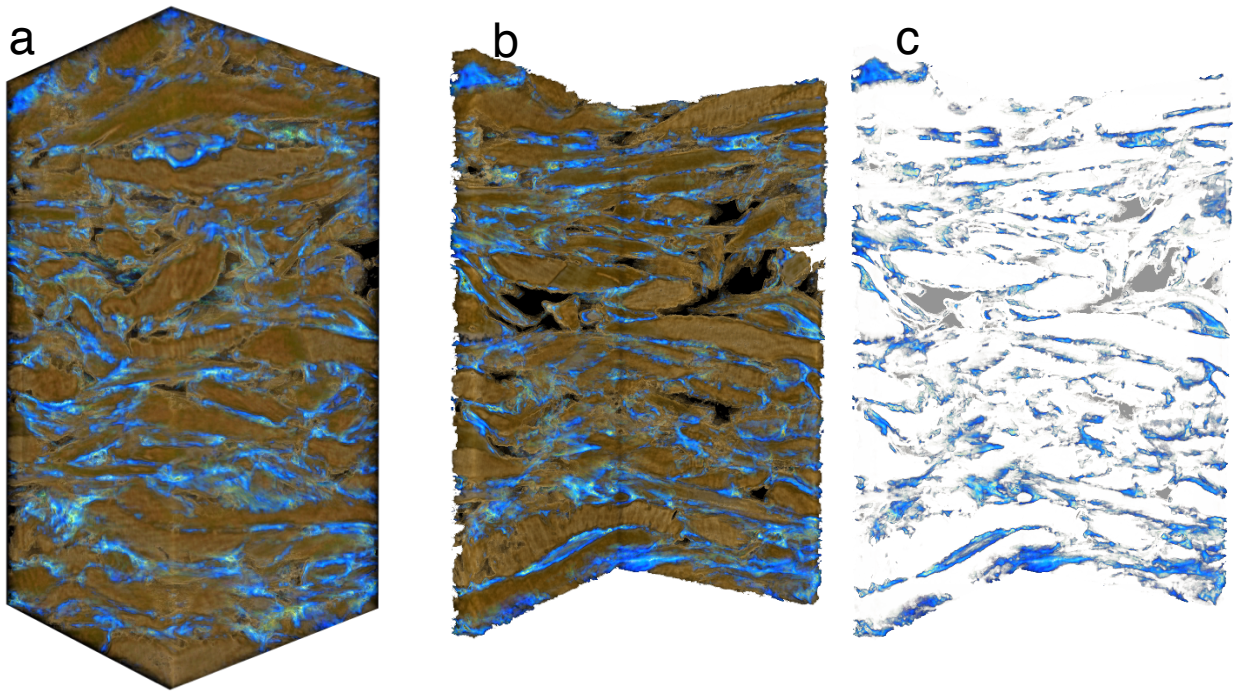

Figure 1.2 X-ray micro-computed tomography images of particleboard showing the distribution of the adhesive (blue) in the matrix of wood particles (brown): (a) Rendered image showing the 3D spatial distribution of adhesive in particleboard; (b) Cross-section of a 3D rendered model showing that adhesive is mainly oriented in the X-Y plane with relatively few connections in the Z-direction; (c) Adhesive in the composite (Evans et al. 2010)

3D inter-connected network structures are the preferred architecture of many natural biological materials, including bone, nacre and wood (Fig. 1.3a~c) (Thompson 1917; Weiner and Wagner 1998; Jeronimidis 2000; Wegst et al. 2014). For example, wood employs a sophisticated multiscale 3D architecture which is responsible for its superior strength to weight properties (Mattheck and Kubler 1997; Fratzl and Weinkamer 2007). Lessons learnt from natural composites' structures were first adapted for structural optimization of man-made composites by Thompson (1917). They were further explored by Jeronimidis (2000) who stated that 'microstructure of nature's biological materials should provide inspiration and stimulation for new material concepts, efficient design strategies and structural optimization'. Studies by Vincent and Mann (2002) also point out the benefit of technology transfer from biology to engineering (biomimetics). The concept of creating 3D inter-connected networks to improve the properties of materials and structures is clearly apparent in modern reinforced concrete, which

uses a network of steel or fibre-plastic reinforcing bars that are tied together with wire to create a 3D inter-connected network structure (Fig. 1.3d). Such an inter-connected network improves the tensile and flexural strength of the reinforced concrete (Yeih et al. 1997; Saleem et al. 2013).

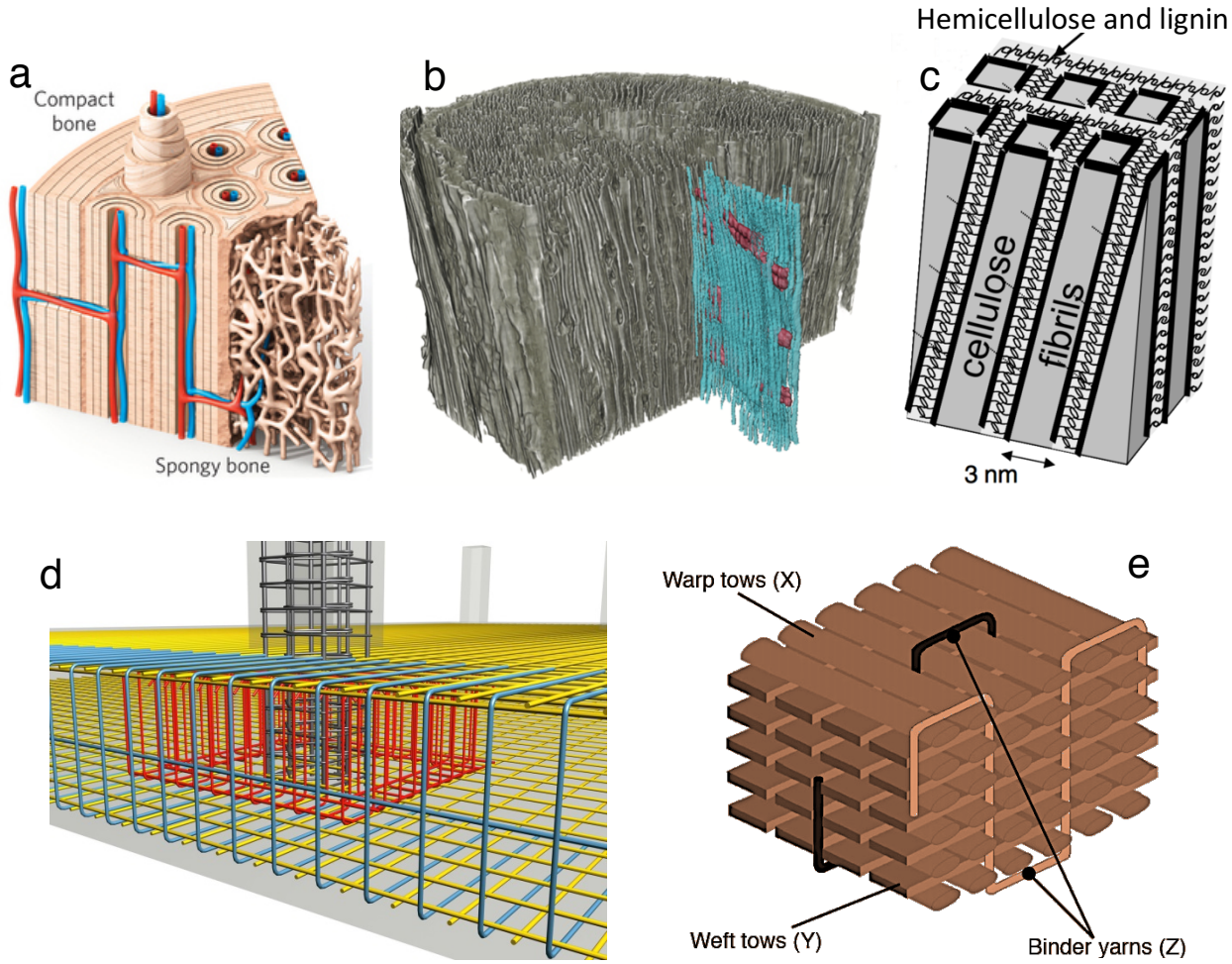

Figure 1.3 Illustration of 3D structures in natural biological materials and man-made structural composites: (a) Hierarchical structure of bone showing the sophisticated 3D network of bone tissues (modified from a figure in Wegst et al. 2015); (b) 3D X-ray µCT reconstruction of wood showing the interpenetrating networks of rays and tracheids (in two different colours) (modified from a figure in Brodersen 2013); (c) Schematic illustration of the structure of the cell-wall of softwood tracheids showing the nanoscale 3D structure created by cellulose, hemicellulose and lignin (modified from a figure in Fratzl and Weinkamer 2007); (d) Schematic illustration of the 3D inter-connected structure of rebars used in reinforced concrete; (e) Schematic illustration of a 3D woven polymer composite showing the binder yarns bonding the tows in the Z-direction (modified from a figure in Mouritz et al. 1999)

Similarly, polymer composites with 3D fibre architectures are stronger than traditional 2D layered polymer laminates (Fig. 1.3e) (Mouritz et al. 1999). For example, 3D woven composites

have better impact damage resistance, higher in-plane tensile modulus and improved inter-laminar fracture toughness compared to 2D laminates (Farley et al. 1992; Ding et al. 1995; Mouritz et al. 1999). In addition to 3D weaving, there are a series of approaches used to provide 3D architecture in advanced composites, for example stitching, braiding, embroidery, tufting and z-anchoring (Mouritz 2007). The concept of 3D structural optimization has not been fully explored in wood composites, whose adhesive is mainly oriented in the X-Y plane, as described above. However, based on the architecture of natural materials and advanced composites, the creation of a 3D inter-connected adhesive network in wood composites should improve a range of properties. Therefore, in this thesis I explore a novel way of modifying adhesive distribution to improve the efficiency of adhesive bonding and properties of a model wood composite. My concept involves altering the geometry of the adhesive distribution to form a 3D inter-connected adhesive network in a model wood composite with potential relevance to composites made from veneer or flakes.

1.2 General hypothesis

There is some evidence, mainly in the field of interpenetrating polymer networks or IPNs (Sperling 1981), that increasing 3D cross-links between two polymer networks in a composite can influence the swelling property of the IPN composite. For example, Jakes et al. (2015) suggested that an IPN formed between phenol-formaldehyde resin and the wood cell wall may help decrease moisture sorption by mechanically restraining the swelling of wood polymers during moisture adsorption. There is also ample evidence in the literature, mainly from studies of the through-thickness reinforcement (Z-connections) of advanced polymer composites, that a 3D inter-connected network structure provides superior material properties such as impact tolerance and fracture toughness (Mouritz et al. 1999; Mouritz 2007), etc. compared to a 2D layered structure. Introducing Z-connections, as a way of structural optimization, is an efficient way of improving properties of advanced polymer composites (Lander 2008). Wood composites

are a sub-set of polymer composites and some of them lack adhesive connections in the Z-direction or when they are present they are sporadic and poorly formed (Evans et al. 2010, 2015). Therefore, it is plausible that introducing a designed array of adhesive Z-connections will improve some properties of wood composites.

In this thesis, I hypothesize that altering the distribution of adhesive in wood composites to create adhesive Z-connections, thus forming a 3D inter-connected adhesive network will significantly improve properties of wood composites.

The properties examined in this thesis include those in which wood composites are deficient, for example, dimensional stability and fracture toughness (see below). My aim is to alter the adhesive distribution in a model composite and obtain property improvements. Throughout my experimental work, composites with an inter-connected (3D) adhesive network contain the same level of adhesive as controls. At the outset of my work I had to develop a practical and efficient way of altering the adhesive distribution and introducing the adhesive Z-connections in wood composites. The approach I adopted involved drilling holes in woody elements used for wood composites and allowing the adhesive in the composite to form adhesive Z-connections linked to adhesive bond lines in the X-Y plane. Thus an inter-connected adhesive network was created in the composite. To my knowledge this is a novel approach although related to ones used in advanced composite materials.

1.3 Outline of study

My thesis consists of eight chapters. Following this introductory chapter, Chapter 2 reviews the literature on the structural architecture of wood composites and some other composites. Relevant literature on wood-adhesive interactions, and previous research on improving efficiency of adhesive bonding in wood composites is reviewed, as well as methods used to improve dimensional stability and mechanical properties of wood composites. Chapter 3 describes the preliminary research mentioned above that developed methodology to create a

3D inter-connected adhesive network in a model wood composite. Chapter 4 sought to test the concept that the introduction of adhesive Z-connections would reduce the water-induced thickness swelling of a model wood composite. Chapter 5 further examined the effect of adhesive Z-connections on the thickness swelling of the model wood composite, looking specifically at whether property improvements were influenced by wood species, and orientation of wood veneer (radial vs. tangential). Chapter 6 used finite element analysis (FEA) as a tool to model the effectiveness of adhesive Z-connections at reducing thickness swelling of the model wood composite. This chapter modelled the effects of different combinations of diameter, area-density and spatial distribution of the Z-connections on the thickness swelling of the model composite. The aim of the modelling was to find an optimal solution to minimize the surface heterogeneity of composites containing adhesive Z-connections after they had been exposed to water. Chapter 7 examined whether the adhesive Z-connections can improve the fracture toughness of a laminated wood composite. This chapter also compared the ability of glass-fibre reinforcement of adhesive bond lines to improve fracture toughness with that of adhesive Z-reinforcement. Finally, Chapter 8 discusses the findings of all experimental chapters, and I also suggest further research needed to more fully explore the concept of Z-direction reinforcement as a way of improving the properties of wood composites, and also whether it can be extended to composites that resemble those in commercial production.

2 Literature Review

2.1 Introduction

Wood composites have numerous end-uses because they are inexpensive, have many excellent properties and are mainly derived from a renewable material. However, they also have a number of disadvantages (Humphrey 1982). For example, the dimensional instability (especially in the thickness direction) of particleboard and oriented strand board (OSB) in response to moisture absorption, and the susceptibility of plywood to cracking and delamination places restrictions on their end-uses (Suchsland 1959; Kelly 1977; Walker 1993). Thickness swelling of OSB is the combination of two components: reversible thickness swelling due to natural hygroscopic swelling of wood, and irreversible thickness swelling mainly due to the release of compression strains applied to form mats during hot-pressing (Neusser et al. 1965; Halligan 1970; Kelly 1977; Wu and Suchsland 1996, 1997). Garay et al. (2009) reported 19% thickness swelling of OSB after it was exposed at 40°C and 95% relative humidity for 800 hours. The comparable figure for plywood was 9%. Such thickness swelling can cause high internal stresses in OSB (Constant et al. 2003) and affect its strength in service (Wu and Suchsland 1996). Thickness swelling may also cause uneven OSB sub-floors, which can be expensive and time-consuming to fix (Evans et al. 2013). On the other hand, cracks and delamination of adhesive bond lines commonly occur in laminated composites such as plywood when they are exposed to water (Huang 2011). According to Bucur (2011), delamination of laminated composites is ‘de-bonding of two adjoining wood layers resulting from imperfect bonding or excessive structural loading during service’. To reduce the incidence of such defects, it is important to have a good understanding of the interaction of wood and adhesive in wood composites, and in particular the distribution of adhesive between and within woody elements.

There has been a large amount of research on the distribution of adhesive in some wood composites (Burrows 1961; Quirk 1968; Côté and Vasishth 1970; Hare and Kutscha 1974;

Murmanis et al. 1983; Johnson and Kamke 1992; Kamke 2004; Xing et al. 2004, 2005; Cyr et al. 2008; Pakdel et al. 2008; Walther and Thoemen 2009; Evans et al. 2010). Adhesive distribution affects both the dimensional stability and some mechanical properties of wood composites even though it only makes up 2~14% by weight of the composites (Spelter et al. 2006; Irle and Barbu 2010). This chapter reviews the literature on structural architecture of wood composites, particularly the distribution of adhesive in wood composites and its effect on a variety of properties. There has been relatively little research on 3D distribution of adhesive in wood composites. Therefore, this chapter also reviews 3D structure of some advanced polymeric composites including the effect of introducing Z-direction (through-thickness) reinforcement on some mechanical properties of carbon fibre composites.

2.2 Structural architecture of wood composites

There are four major types of wood composites based on the form size and distribution of their constituent elements (Table 2.1). The main focus of this thesis is on creating an inter-connected adhesive network in a layered 'model' wood composite with relevance to composites made from veneer and larger flakes, particularly plywood, laminated veneer lumber (LVL) and oriented strand board (OSB). Plywood is manufactured by gluing thin sheets of wood veneer together with liquid resin or resin films and pressing the veneer together at elevated temperatures with the grain of adjacent veneer perpendicular to each other (Perry 1948; Kollmann et al. 1975; Baldwin 1981; Walker 1993). Laminated veneer lumber (LVL) is also made from wood veneer, but the grain of adjacent veneer is parallel to each other (Koch 1967; Schaffer et al. 1972; Walker 1993). These veneer-based wood composites have a layered laminate structure. In such composites, as stated by Voronko et al. (2014), the adhesive is distributed as layers in 2D planes. OSB is also a multi-layered panel manufactured by laying down a resinated mat of thin rectangular strands and then pressing the mat at high pressure and temperatures (Irle and Barbu 2010; Stark et al. 2010). The strands in the mat are arranged

into three primary layers with varying grain orientation: the strands in the two outer layers are aligned parallel to the long edges of the mat (board), whereas the strands in the core layer are often aligned at right angles to the strands of the face layers (Irle and Barbu 2010).

Table 2.1 Major categories of wood composites

Wood constituent	Constituent element	Composite product	Adhesive used	Product end-use
Sawn wood laminae		Glulam, Cross-laminated timber	PF, RF, pMDI	Structural headers, beams, girders, columns, and trusses, walls
Thin veneer (rotary peeled or sliced)		Plywood, LVL	UF, PF, pMDI	Subfloors, roof and wall sheathing, furniture frames, shipping containers, aircraft, boats
Long strands		Parallam	PF	Structural I-joists, beams
Flakes		OSB, OSL	UF, PF, pMDI	Subfloors, roof and wall sheathing, packaging, I-beams
Particles/sawdust		Particleboard	UF, MF, MUF	Furniture, subfloors, kitchen cabinets
Fibre		MDF, Masonite (hardboard)	UF, MF, MUF, PF	Furniture, kitchen cabinets, wall sheathing

Source: Irle and Barbu (2010). Wood-based panel technology. In: (Thoemen, Irle and Sernek ed.) Wood-Based Panels - An Introduction for Specialists; Kollmann et al. (1975). Principles of Wood Science and Technology II Wood Based Materials. Note UF = urea formaldehyde, MF = melamine formaldehyde, PF = phenol formaldehyde, RF = resorcinol formaldehyde, MUF = melamine urea formaldehyde, pMDI = polymeric methylene diphenyl isocyanate.

2.2.1 Wood species

Wood species used for plywood manufacturing in North America mainly include Douglas fir (*Pseudotsuga menziesii*), southern pine (*Pinus spp.*), western hemlock (*Tsuga heterophylla*), etc. for softwood plywood; and yellow birch (*Betula alleghaniensis*), yellow poplar (*Liriodendron tulipifera*), red oak (*Quercus rubra*), etc. for hardwood plywood (Kollmann et al. 1975; Walker 1993; Shmulsky and Jones 2011b). According to Shmulsky and Jones (2011b), wood species that have been used to manufacture structural plywood in North America can be categorized by stiffness and strength properties into four groups as listed in Table 2.2. The plywood is graded and classified for strength purposes as Group 1, Group 2, etc.

Laminated veneer lumber (LVL) has historically been manufactured from softwood species such as Douglas fir and lodgepole pine (*Pinus contorta*) (Hesterman and Gorman 1992; Vlosky et al. 1994). Hardwood species, such as aspen (*Populus tremuloides* Michx.), beech (*Fagus sylvatica*), poplar and eucalypts (*Eucalyptus obliqua*) have been also used in North America, Europe and Australia (Hoover et al. 1987a, 1987b; Hsu 1988; Ozarska 1999).

Wood species commonly used to manufacture oriented strand board (OSB) include aspen, southern pine, paper birch (*Betula papyrifera*), red maple (*Acer rubrum*), sweetgum (*Liquidambar styraciflua*), and yellow poplar (Stark et al. 2010).

Table 2.2 Grouping of wood species used for the manufacture of commercial structural plywood in North America into stiffness and strength categories (1 = highest, 4 = lowest)

Group 1	Group 2	Group 3	Group 4
Birch, sweet/yellow	Fir, pacific silver/white	Cedar, Alaska	Aspen
Douglas fir	Hemlock, western	Fir, subalpine	Cottonwood, eastern/black
Larch, western	Pine, red/Virginia	Hemlock, eastern	Cedar, western red
Maple, sugar	Spruce, black/red/Sitka	Pine, lodgepole/ponderosa	
Pine, southern	Sweetgum Poplar, yellow	Spruce, Engelmann/white	

Source: Shmulsky and Jones (2011b). Forest Products and Wood Science: An Introduction (sixth edition)

'Wood species' significantly influences properties of laminated wood composites (Walker 1993) as well as particle/strand-based wood composites (Kelly 1977). The influence of 'wood species' on properties of wood composites is primarily related to wood density and its interaction with various processing parameters (Dai et al. 2007a). Wood density is negatively correlated with compression ratio of composite panels during hot-pressing. A higher compression ratio generally yields stronger wood-adhesive bonding because of increased contact area between woody elements in both particleboard and OSB (Kelly 1977; Humphrey 1982; Dai and Steiner 1993; Drolet and Dai 2010) and LVL (Ozarska 1999). For example, one of the reasons that aspen and poplar are suitable for the manufacture of LVL is due to their relatively low density (ranging from 390 to 500 kg/m^3), which is similar to that of many North American softwoods (O'Halloran 1995). There has been some research on the effects of wood species on mechanical properties of structural LVL. For example, Durand-Raute Industries Ltd. (1988) reported that LVL made from aspen tended to have higher bending strength but lower stiffness than LVL made from southern yellow pine. Hsu (1988) carried out ASTM D 143-83 testing and demonstrated that aspen LVL had bending properties comparable to softwood LVL. Hesterman and Gorman (1992) compared some key mechanical properties of LVL made from Douglas fir and lodgepole pine and reported a 15% difference in bending and compressive strength between Douglas fir LVL and lodgepole pine LVL.

2.2.2 Adhesive in wood composites

Adhesive is the single most expensive raw material other than wood used in the manufacture of wood composites, as mentioned above. Adhesive typically represents up to 25% of total manufacturing costs even though it only accounts for 2~14% of total mass of wood composites (Dunky 2002; Spelter et al. 2006; Irle and Barbu 2010). For example, the cost of adhesive represents 18% and 8%, respectively, of total manufacturing costs of OSB and plywood, according to Spelter et al. (2006) (Fig. 2.1).

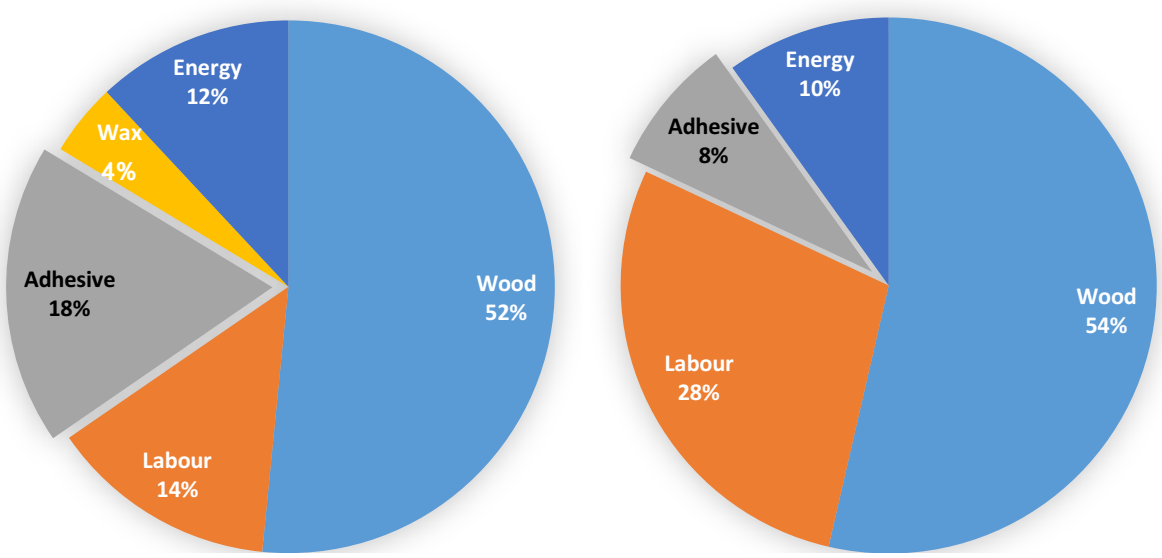

Figure 2.1 Manufacturing costs for benchmark northcentral United States OSB plants (left) and southern United States plywood plants (right) in 2006 (figures based on data from Spelter et al. (2006))

2.2.2.1 Adhesive bonding mechanisms

An understanding of adhesive bonding mechanisms in wood and wood composites should emphasize the unique properties of wood at different spatial scales: macroscopic, microscopic, and molecular levels, according to Frihart (2006).

At the macroscopic scale, wetting of wood surfaces upon contact with adhesive is one of the essential steps involved in adhesive bond formation (Comyn 2006). Bartell and Osterhof (1927) developed a method based on Thomas Young's equation (1805) for determining wettability of a solid surface by a liquid. Their 'method is based upon the measurement of the pressure with which one liquid will displace another from a powdered material which has been compressed within a cylinder'. 'By measuring the displacement pressure it is possible to determine the adhesion tension between a solid and a liquid phase'. Their method was used to examine the wettability of silica surfaces by water and some organic liquids. The wettability of a wide range of materials, such as metal, glass and polymers has been extensively studied since then (Zackay et al. 1953; Zisman 1963; Petri et al. 2002; Hedberg et al. 2014; Wallinder and Herting 2016). Wettability of wood surfaces has been studied by various research groups, for

example, Chen and Wangaard (1968), Collett (1972); Young (1976), Gardner et al. (1991), Podgorski et al. (2000), Frihart (2006). The most common method used to measure the wettability of wood surfaces is sessile drop method (Gray 1962; Zisman 1963; Collett 1972; Jordan and Wellons 1977; Gardner et al. 1991). This method uses a goniometer consisting of a liquid dispenser (syringe), a height-adjustable stage for wood samples and a digital camera for real-time observation of contact angle between a droplet of a liquid and the wood surface (Fig. 2.2). Contact angle refers to the equilibrium of a drop of a liquid inserted by resting on a plane solid surface under the action of three surface tensions: (1) at the interface of the liquid phase and vapor phase, γ_{LV}; (2) at the interface of the solid phase and the liquid phase, γ_{SL}; and (3) at the interface of the solid phase and vapor phase, γ_{SV} (Fig. 2.2). The angle θ between γ_{LV} and γ_{SL} is defined as the contact angle of the liquid (Zisman 1963, Collett 1972).

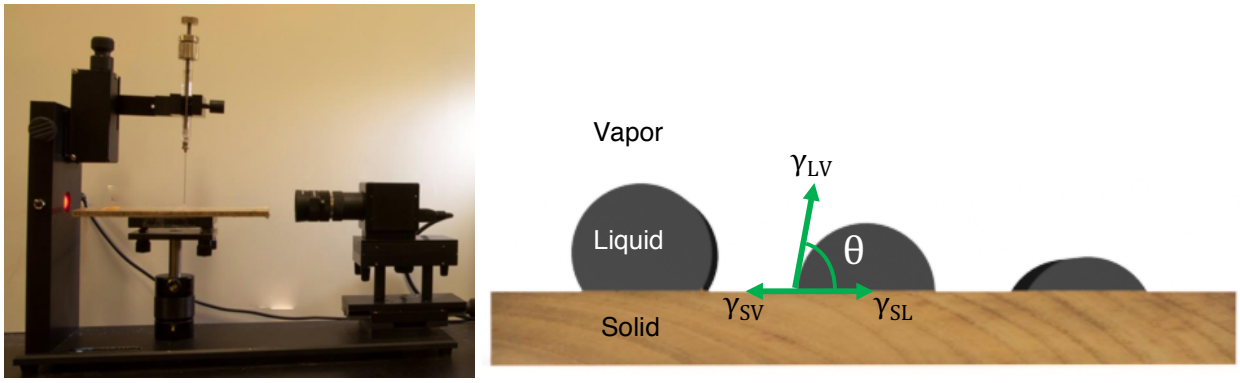

Figure 2.2 Photo of the sessile drop method equipment (left) and schematic illustration of contact angle measurement (right)

Wetting is followed by flow of the adhesive on the wood surface (Fig. 2.3). Flow of adhesive is desirable because the adhesive will cover a greater surface area allowing a more uniform distribution of adhesive at bonding interfaces (Collett 1972; Frihart 2006). Flow of adhesive on wood strands is increased during hot-pressing (Dai et al. 2011) and influenced by some other parameters (Dai et al. 2007a, 2007b). The wetting and flow of adhesive on wood surfaces can be enhanced by chemically modifying wood surfaces (Chow 1975; Gardner and Elder 1988; Kurt et al. 2008) or mechanically roughening surfaces to increase contact area

between adhesive and wood (Belfas et al. 1993; Aydin 2004). Plasma treatment can chemically and mechanically modify wood surfaces to increase wettability and, in some cases, improve adhesion (Rehn et al. 2003; Scholz et al. 2010; Avramidis et al. 2011; Jamali and Evans 2011; Acda et al. 2012).

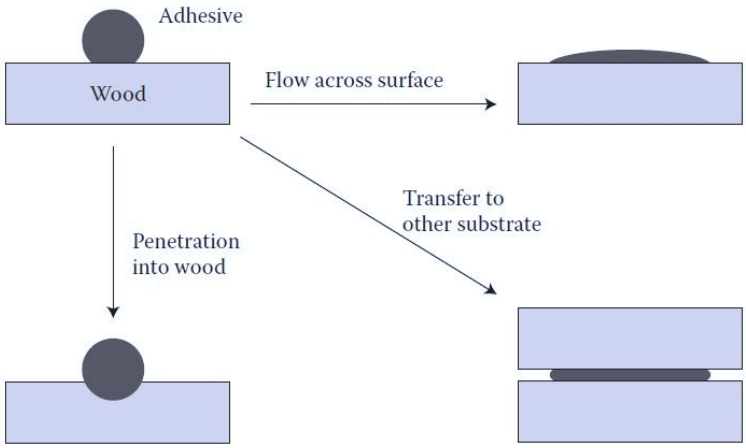

Figure 2.3 Schematic illustration of adhesive wetting, flow and penetration on substrate surfaces (modified from a figure in Frihart 2006)

At the microscopic scale, penetration of adhesive from glue-lines into wood can occur. Therefore, the mechanical interlocking theory of adhesion is relevant to adhesive bonding of wood (McBain and Hopkins 1926; Browne and Brouse 1929; Comyn 2006; Gardner 2006). Porosity and irregular surface characteristics of wood facilitate adhesive penetration into wood cells, and the resulting mechanical interlocking of wood and adhesive (Pizzi 1994; Gardner 2006). Pocius (2012) suggested that porous and rough bonding surfaces create detour cracking paths for adhesive. These detour paths cause plastic deformation during adhesive debonding which dissipates significantly more energy compared to adhesive debonding at a smooth surface (Pocius 2012). Irregular and rough surfaces also have substantially greater contact area than a smooth surface, which increases total energy of surface interaction and bond strengths (Pocius 2012). In support of this suggestion, Belfas et al. (1993) found that coarse abrasive sanding (80 grit) of wood surfaces was significantly better than smooth sanding at improving the shear strength of karri (*Eucalyptus diversicolour*) and jarrah (*E. marginata*) lap-shear specimens

bonded with resorcinol formaldehyde adhesive. Cool and Hernández (2011) compared bonding performance and adhesive penetration at wood surfaces subjected to different machining processes (Fig. 2.4 a & b). They found that poly vinyl acetate adhesive penetrated deeper into the sub-surface of black spruce (*Picea mariana* [Mill.] B.S.P.) when it was applied to a rougher surface containing more deformed and crushed cell walls (Fig. 2.4d) compared to a smoother surface that was relatively damage-free (Fig. 2.4c). However, a weak boundary layer caused by mechanical damage to wood surfaces during machining and surface aging can weaken adhesive bond lines (Bikerman 1961; Stehr 1999; Frihart 2006; Gardner 2006; Frihart and Hunt 2010; Pocius 2012).

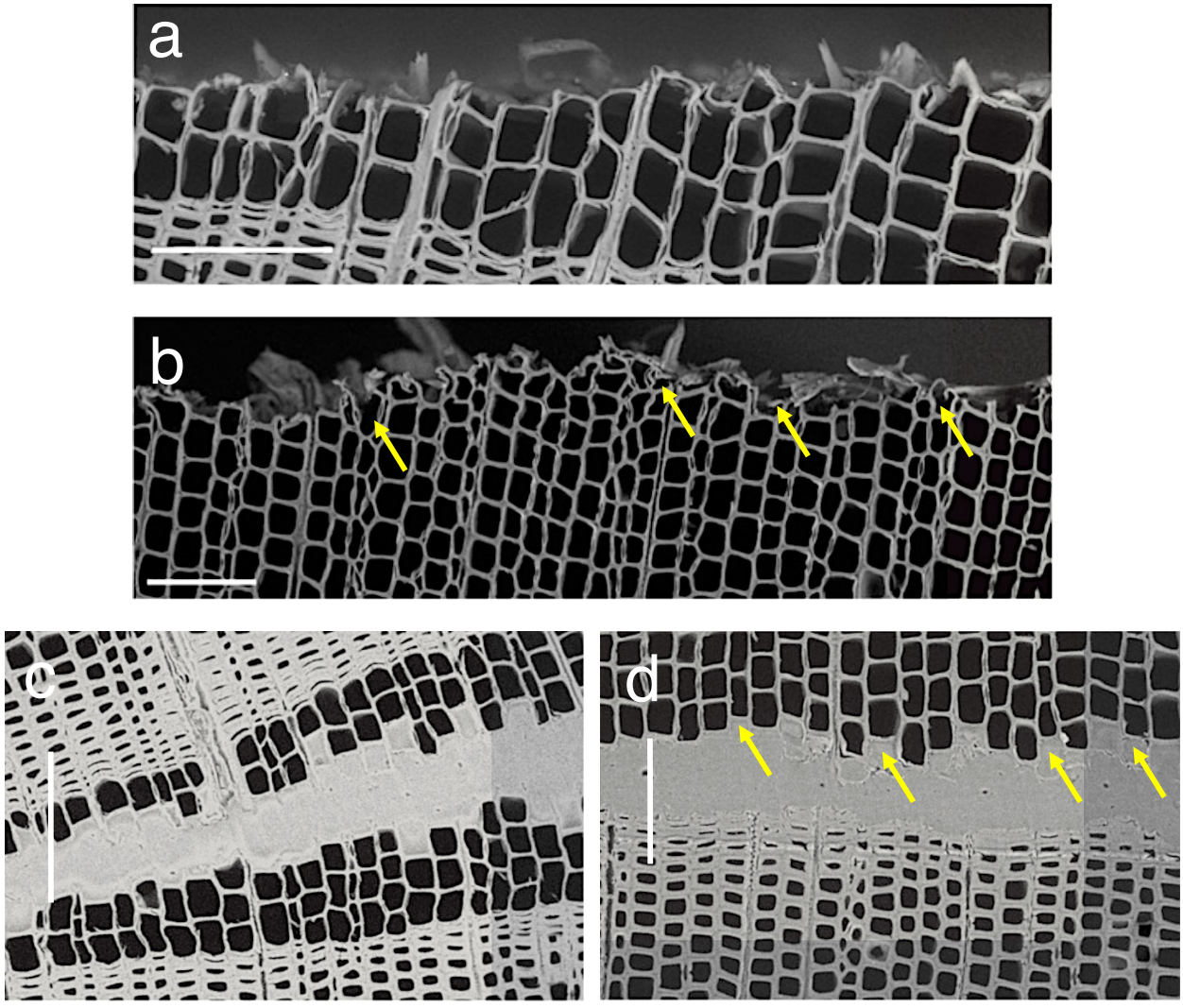

Figure 2.4 Environmental scanning electron photomicrographs of black spruce wood surfaces that were (a) oblique-cut, (b) conventional-planed, (c) oblique-cut and then glued, and (d) conventional-planed and then glued. Note that deformed and crushed cell walls are more common at a surface that was conventionally panned (arrowed in (b)), which facilitated adhesive penetration (arrowed in (d)). Scale bars = 100 μm. (modified from figures in Cool and Hernández 2011)

At the molecular scale, interaction between wood's molecules and adhesive's molecules may occur resulting in bond formation. Such molecular adhesion is thought to be universal for all types of materials, and therefore it has been thoroughly studied (Schultz and Nardin 2003; Comyn 2006; Pocius 2012). Texts on adhesion state that there are four adhesive bonding mechanisms that operate at the molecular scale: (1) electronic or electrostatic; (2) adsorption (thermodynamic); (3) diffusion; (4) chemical (covalent) bonding. All these theories can be used to explain wood bonding, according to Pizzi (1994); but the extent to which they are relevant to specific situations depends on the adhesive as well as the wood involved in bonding (Pizzi 1994). The electronic or electrostatic theory of adhesives is not relevant to conventional adhesive bonding of wood or wood composites, as there is unlikely to be electron transfer between the adhesive and wood surfaces, according to Pizzi (1994). However, electronic theory is relevant to wood finishing and coating operations (Gardner 2006). The adsorption theory, on the other hand, is the most widely accepted and applicable theory of adhesion for wood bonding (Pizzi 1994) and has been studied for over 50 years, according to Shi and Gardner (2001). The adsorption theory states that adhesion occurs because of intermolecular and interatomic forces between atoms and molecules of adjacent adherends (Schultz and Nardin 2003). In the case of wood adhesion, three main types of secondary forces, namely van der Waals forces, hydrogen and covalent bonds appear to play a role (Shi and Gardner 2001). For example, wood's molecular components contain numerous hydroxyl groups (-OH) which can form secondary forces with methylol groups, methylene groups and isocyanate groups which are found in major wood adhesives (Pizzi 1994). One of the most debated aspects of wood adhesion is the existence of covalent (chemical) bonds between wood and adhesives (Pizzi 1994). There is evidence in the literature that covalent bonds exist and can contribute to bond strength of

certain adhesives with wood (Troughton 1967; Rowell and Ellis 1981; Pizzi 1994). For example, Rowell and Ellis (1981) suggested that the isocyanate group in pMDI adhesive can form chemical bond with hydroxyl groups in lignin of wood. However, there is evidence to the contrary (Johns 1989; Gardner 2006). Diffusion theory is unlikely to be applicable to regular thermosetting adhesive bonding with wood, according to Pizzi (1994). However, diffusion theory may be relevant to the thermal softening of lignin in wood subjected to hot-pressing and the intermixing of lignin with thermosetting adhesives such as phenolic resin (Pizzi 1994; Sarkar and Adhikari 2000). Most recently, the theory of interpenetrating polymer networks (IPN) has been applied to wood-adhesive interaction at the molecular-scale. Such an IPN is created when lower molecular weight components of adhesives penetrate amorphous layers of wood cell walls. An IPN may mechanically stiffen the cell walls (Marcinko et al. 1998, 2001; Gardner 2006). For example, Marcinko et al. (1998, 2001) concluded that pMDI and southern pine wood interacted with each other at the molecular level to create an IPN that stiffened wood cell wall elements. Gardner (2006) also suggested that both PF and pMDI adhesives formed IPNs in wood.

2.2.2.2 Major adhesive types used in wood composites

In general, thermosetting synthetic adhesives are used for the manufacture of wood composites. The most commonly used thermosetting adhesives include urea formaldehyde (UF), melamine formaldehyde (MF), phenol formaldehyde (PF), resorcinol formaldehyde (RF) and isocyanate-based adhesives (such as diphenylmenthane-4,4'-diisocyanate (MDI)). These adhesives are commonly used to bond wood composites depending on the type of composite and its end-use (Table 2.1). For example, RF, PF and MF are commonly used for glue laminated timber (glulam). PF is the main adhesive used to manufacture structural plywood and laminated veneer lumber (LVL). Both phenolic and isocyanate-based adhesives are used for oriented strand board (OSB), oriented strand lumber (OSL) and other structural engineered

wood composites. The most commonly used adhesive for the manufacture of medium density fibreboard (MDF) and particleboard is UF (Koch et al. 1987; Grunwald 2002a; Irle and Barbu 2010).

2.2.2.3 Basic properties and water resistance of major wood adhesives

Urea formaldehyde (UF) adhesive is primarily found in wood composites used indoors. UF is hydrophilic due to the presence of free methylol groups, which can interact with the hydroxyl group in water (Delmonte 1947). Cured UF resins can be hydrolysed under moist conditions especially at elevated temperatures due to weak bonding between the nitrogen of the urea and the carbon of the methylene bridge (Dunky 2002). However, the moisture resistance of UF can be improved by fortifying it with melamine to form a MUF resin (Pizzi 1994; Irle and Barbu 2010), because MF is resistant to hydrolysis unlike UF (Dunky 2002). The advantages of UF are that it is relatively cheap, cures to a clear or white glue-line, and provides good dry strength.

Phenol formaldehyde (PF) adhesive is much more moisture and weather resistant than UF (Dunky 2002; Irle and Barbu 2010), because of the stability of the C-C bond between the aromatic nucleus and the methylol group or methylene bridge (Dunky 2002). The main drawbacks of PF are its dark red colour when cured and its high cost (twice that of UF) (Irle and Barbu 2010). PF also requires higher temperatures and longer press times to cure compared to UF. Therefore, the cost of using PF to manufacture wood composites is higher than that of UF (Dunky 2002).

Isocyanate-based adhesives provide excellent bond strength, although they are more expensive than formaldehyde-based adhesives (Irle and Barbu 2010). For example, pMDI is commonly used as an adhesive when high tensile strength, toughness and heat resistance are required, according to Lay and Cranley (1994). pMDI is also less susceptible to water degradation and hydrolysis than formaldehyde-based adhesives. Hence, pMDI is extensively

used in applications that require a hydrolytically stable bond for moisture resistant properties with high durability, according to Grunwald (2002b). Composites bonded with pMDI do not emit formaldehyde, unlike UF, PF and MF adhesives, which is an advantage in countries where legislation places limits on the emission of formaldehyde from wood composites (Dunky et al. 2002). The main disadvantages of pMDI are its tendency to stick to metals, for example hot press platens and its toxicity (Dollhausen 1983; Grunwald 2002b).

2.2.2.4 Bond strengths of major wood adhesives

Bond strengths of adhesives are associated with their mechanical performance and durability, which influence their end-uses. This is particularly important for adhesives used in wood composites because their end-uses can vary significantly (Table 2.1). There are two main ways to assess bond strengths of adhesives used in wood composites. One way is to evaluate strength of cured glue-lines in composites. There are various standard testing methods used in different countries to evaluate the strength of glue-lines. The choice of strength properties to be tested is governed by the test method, according to Gustafsson (2002). A typical testing method examines the stress-deformation relationship of bond lines in either shear or tension. Such tests are described in various national standards, for example, American Society for Testing and Materials (ASTM) D905-08, German Institute for Standardization (Deutsches Institut für Normung, DIN) EN 205: 2016-12, and British Standard (BS) 1204 (Gustafsson 2002). Wernersson (1990) used the DIN test method to examine the shear stress-strain relationship and fracture energy of different adhesives, PF and polyurethane, at two different glue-line thicknesses (Table 2.3). Another study by Wilson (1980) compared bond strengths of pMDI and PF in Douglas fir particleboard. He found that internal bond (IB) strength of the particleboard bonded with pMDI and PF were 1.52 MPa and 0.91 MPa, respectively, when the resin content was 6%. Modulus of rupture (MOR) of the particleboard bonded with pMDI and PF were 15.4 MPa and 13.1 MPa, respectively, when the resin content was 6%. This indicates that pMDI is

stronger than PF in bonding particleboard. One of the reasons pMDI is stronger than PF is because pMDI resin and wood's molecular components can mix together forming an 'anchored' interphase (Marcinko et al. 1998).

Table 2.3 Shear strength and fracture energy of polyurethane and PF glue-lines at two different thicknesses

Adhesive	**Glue-line thickness (mm)**	**Shear strength (MPa)**	**Fracture energy (kNm/m^2)**
Polyurethane	0.1	2.15	0.6
	0.25	0.45	0.18
PF	0.1	10.9	0.85
	0.25	10	0.79

Source: Wernersson (1990). Wood adhesive bonds - fracture softening properties in shear and in tension. Report TVSM-3012, Division of Structural Mechanics, Lund University, Sweden.

There are a variety of factors during the manufacturing of wood composites that influence adhesive bond strength (Kollmann et al. 1975). Kim and Humphrey (2001) examined the effects of different hot-pressing temperatures on bond strength of pre-catalyzed and filled resol-type PF adhesive on maple (*Acer spp.*) wood. Their results, which were obtained using an automated bond evaluation system, showed that bond strength decreased from 0.8 MPa to 0.2 MPa when hot-pressing temperature increased from 50°C to 65°C. River (1984) examined the effects of exposure to heat and moisture on shear strength of wood bonded with a polyurethane adhesive. His data clearly shows that shear strength was impaired by both elevated wood moisture content and temperature (Fig. 2.5).

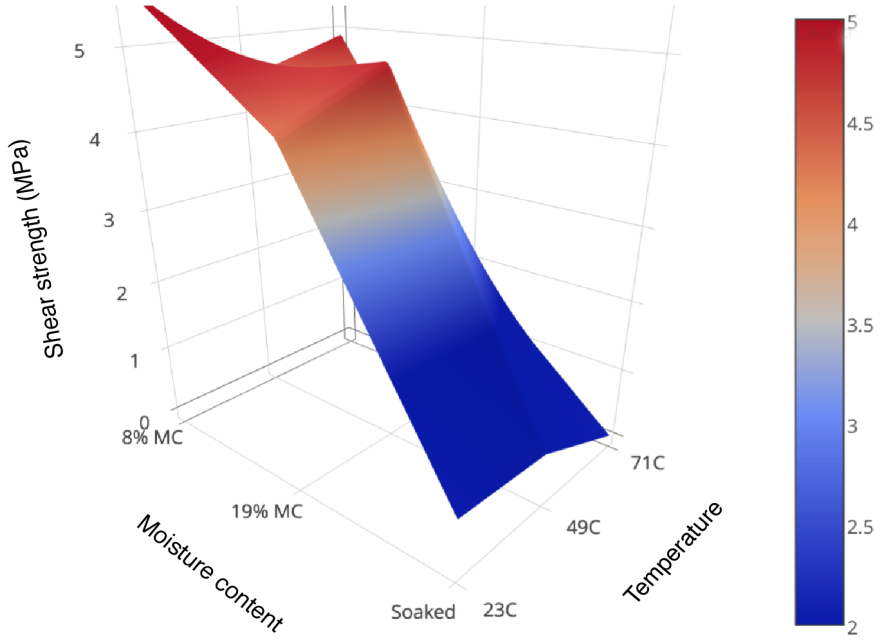

Figure 2.5 Average shear strength of polyurethane adhesive using ASTM D3983 testing method (figure based on data from River (1984))

An alternative method of assessing bond strengths of adhesives is to test physical properties of samples of the adhesive (Gustafsson 2002). For example, a test method used to create samples of pure adhesive was initiated by Page of Ciba-Geigy (Duxford) Ltd., improved by Beele (1983), and further developed by Irle and Bolton (1987, 1988, 1991). They described a method of producing thin dumb-bell shaped samples of pure UF resin. These samples were then used to examine the strength characteristics of the resin (Bolton and Irle 1987). They found a good (R^2 = 0.83) negative correlation between modulus of elasticity (MOE) of the UF resin and moisture content (Bolton and Irle 1987). They also noted that cured UF polymers were far more rigid than PF's (Bolton and Irle 1988).

2.2.3 Visualization of adhesive distribution in veneer-based wood composites

Quirk (1968), and Côté and Vasishth (1970) used light and fluorescence microscopy to examine the structure of phenol formaldehyde (PF) glue-lines in Douglas fir plywood. They found gross penetration of PF into wood cell walls, especially the cell walls immediately adjacent to the bonding interface (Fig. 2.6). Koran and Vasishth (1972) used scanning electron

microscopy to examine the shear-fracture surfaces of Douglas fir plywood bonded with PF adhesive. They found accumulation of glue in lathe checks at the veneer surfaces, suggesting that the PF adhesive penetrated into the checks. Their SEM images also suggested that the PF adhesive penetrated into rays.

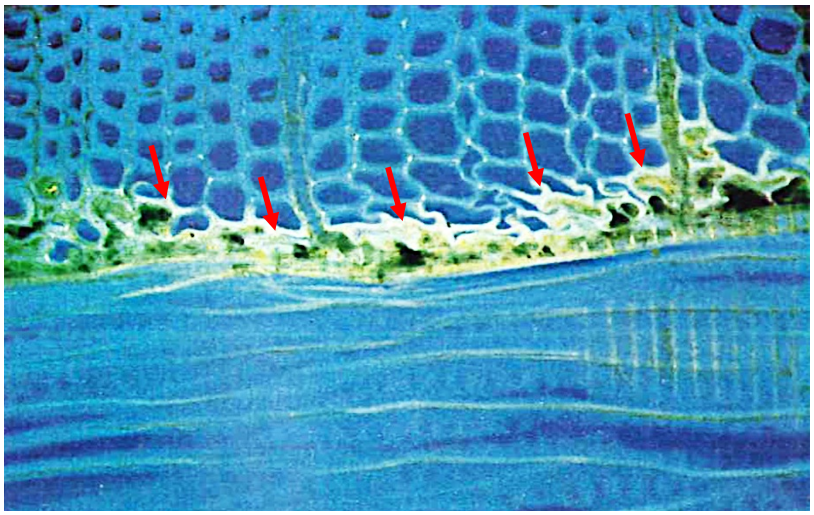

Figure 2.6 Fluorescence photomicrograph (150 x) of phenol-formaldehyde (PF) resin in Douglas fir plywood. Note the penetration of PF glue-line into adjacent wood cell walls evidenced by the fact that middle lamella region (arrowed) fluoresces like the PF resin at the interface, but with less intensity (modified from a figure in Côté and Vasishth 1970)

Hare and Kutscha (1974) examined the structure of PF glue-lines in eastern spruce plywood using both light microscopy and scanning electron microscopy. Light microscopy showed that wood cells that ruptured during the peeling of veneer were filled with PF adhesive (Fig. 2.7a). Their SEM images showed deep penetration of PF adhesive into lathe checks (Fig. 2.7b), resin canals (Fig. 2.7c) as well as rays (Fig. 2.7c). They suggested that even penetration of adhesive into wood at the adhesive interface (Fig. 2.7d) and good contact of adhesive with the cell lumen inner walls (Fig. 2.7c) contributed to good bond strength. However, undesirable voids were observed in glue-lines (Fig. 2.7e), which may be caused by steam pockets that formed within plywood as it was hot-pressed.

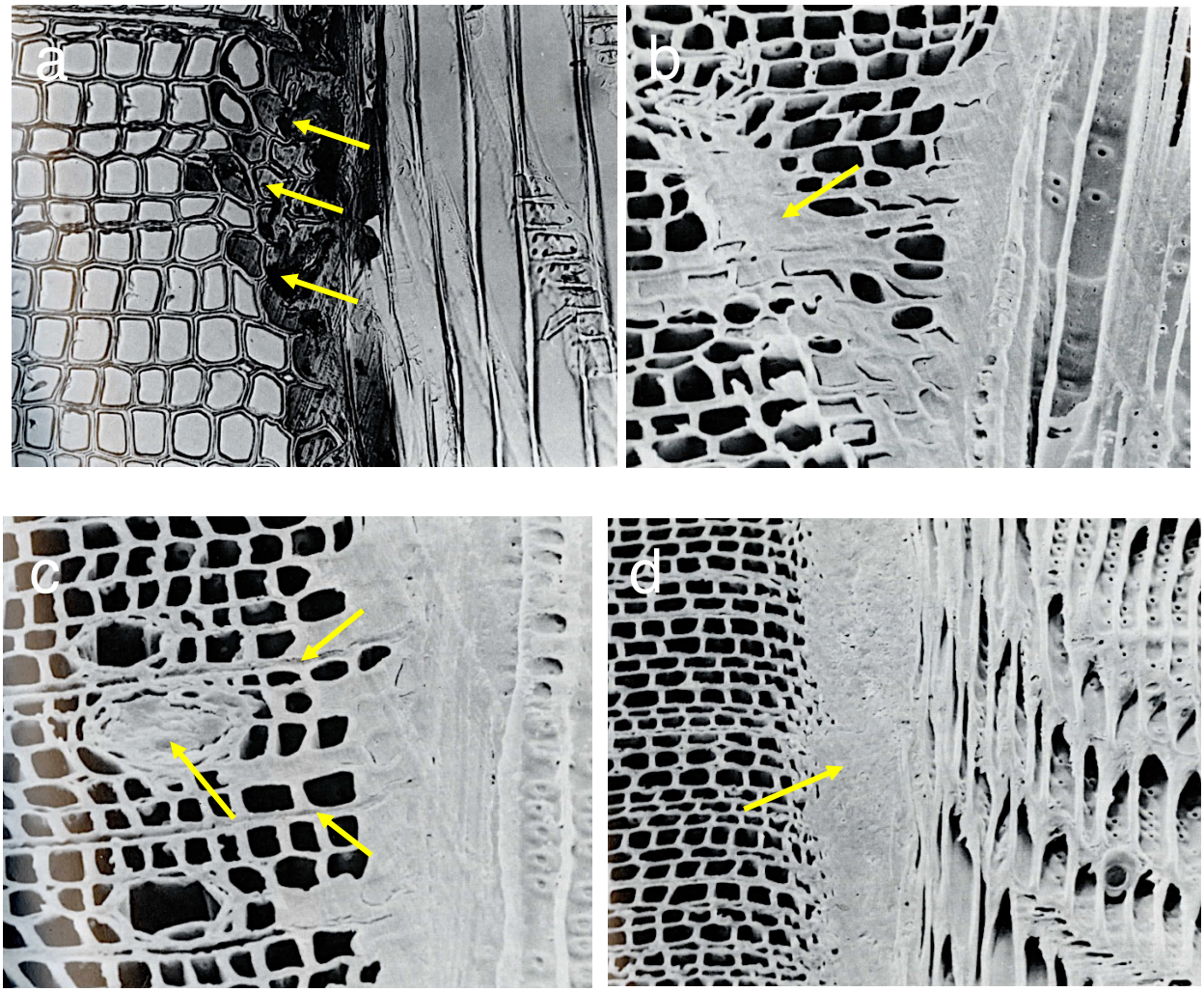
a
b
c
d

Figure 2.7 (a) Light microscopy; and (b ~ e) Scanning electron microscopy images of PF glue-lines in eastern spruce plywood: (a) Penetration of PF (dark areas) into ruptured cells; (b) Penetration of PF into a lathe check and close contact between adhesive and cell lumens; (c) Adhesive in resin canals and rays; (d) A uniformly thick glue-line; and (e) Voids in the glue-line (modified from figures in Hare and Kutscha 1974)

Murmanis et al. (1983) used fluorescence microscopy to visualize wood-adhesive bond lines. Their images showed penetration of PF adhesive into adjoining Douglas fir tracheids, but there was little penetration of adhesive into rays. Johnson and Kamke (1992) also used fluorescence microscopy and an image analysis system to examine the distribution of urea formaldehyde (UF) and phenol formaldehyde (PF) adhesives in yellow poplar veneer. They found that penetration of PF in poplar occurred mainly via vessel elements, as arrowed in Fig. 2.8a. Kamke (2004) visualized the distribution of pMDI (Fig. 2.8b), epoxy (Fig. 2.8c), and polyvinyl acetate (Fig. 2.8d) adhesive bond lines in southern pine and southern red oak, respectively, using epi-fluorescence. He demonstrated that fluorescence microscopy could distinguish between the various adhesives, as mentioned above, when the wood was stained with 0.5% safranin O. He observed that both epoxy and polyvinyl acetate adhesives penetrated into vessels adjacent to glue-lines in southern red oak (Kamke 2004).

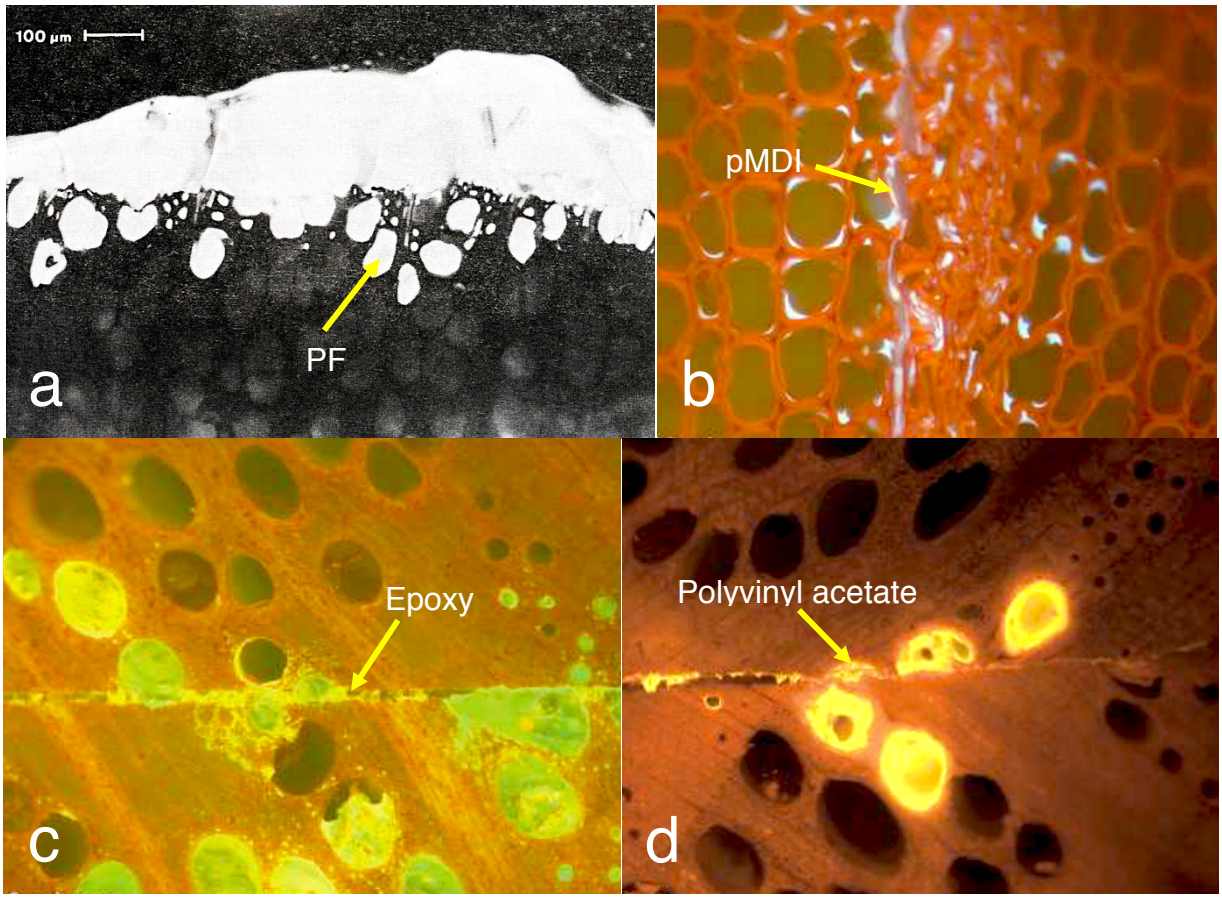

Figure 2.8 Fluorescence microscopic photomicrographs of (a) Penetration of PF adhesive (arrowed) in yellow poplar veneer via vessels adjacent to the glue-line (modified from a figure in Johnson and Kamke 1992); (b) Distribution of MDI bond line (arrowed) in southern pine veneer (modified from a figure in Kamke 2004); (c) Distribution of epoxy bond line (arrowed) in southern red oak (modified from a figure in Kamke 2004); and (d) Distribution of polyvinyl acetate bond line in southern red oak (modified from a figure in Kamke 2004)

There have been a few recent attempts to visualize adhesive distribution in plywood and also LVL. For example, Šrajer et al. (2013) used image analysis of light microscopy images to examine macroscopic and microscopic structure of glue-lines in spruce and beech plywood. They observed that adhesive penetrated into different wood cells including vessels, tracheids and parenchyma. Adhesive also penetrated into a crack oriented in the thickness direction of veneer (arrowed in Fig. 2.9).

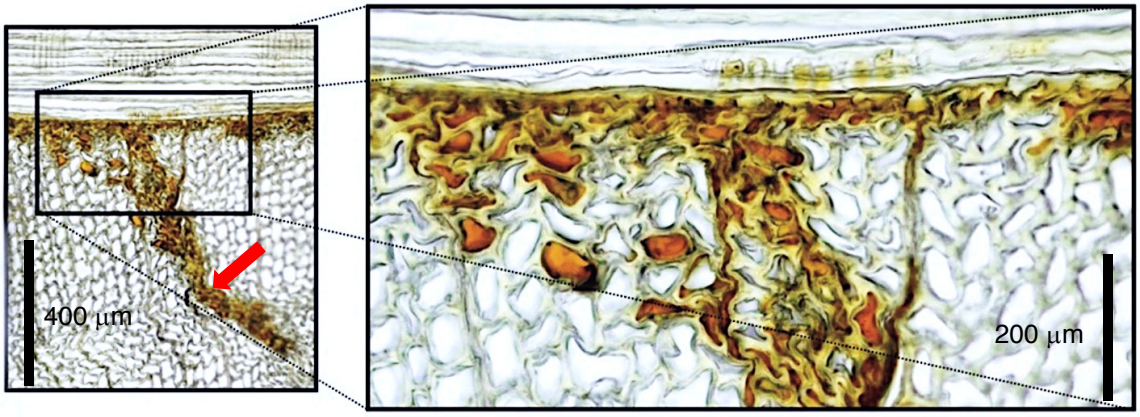

Figure 2.9 Microscopic images of urea formaldehyde adhesive (dyed with red coloured filler) between two spruce wood veneers. Note penetration of adhesive via a crack in the thickness (Z) direction of veneer (modified from a figure in Šrajer et al. 2013)

Another recent study by Li et al. (2014) used X-ray micro-computed tomography (X-ray μCT) developed in Ghent University (Vlassenbroeck et al. 2007; Dierick et al. 2014) to examine internal micro-structure of PF bonded okoumé (*Aucoumea klaineana* Pierre) and poplar (*Populus* spp.) plywood exposed to water. Their X-ray μCT images (Fig. 2.10) clearly showed that adhesive is distributed in 2D planes between wood veneer and there are no adhesive cross-links in the thickness (Z) direction of the plywood. They also used X-ray μCT to study moisture ingress and distribution in plywood.

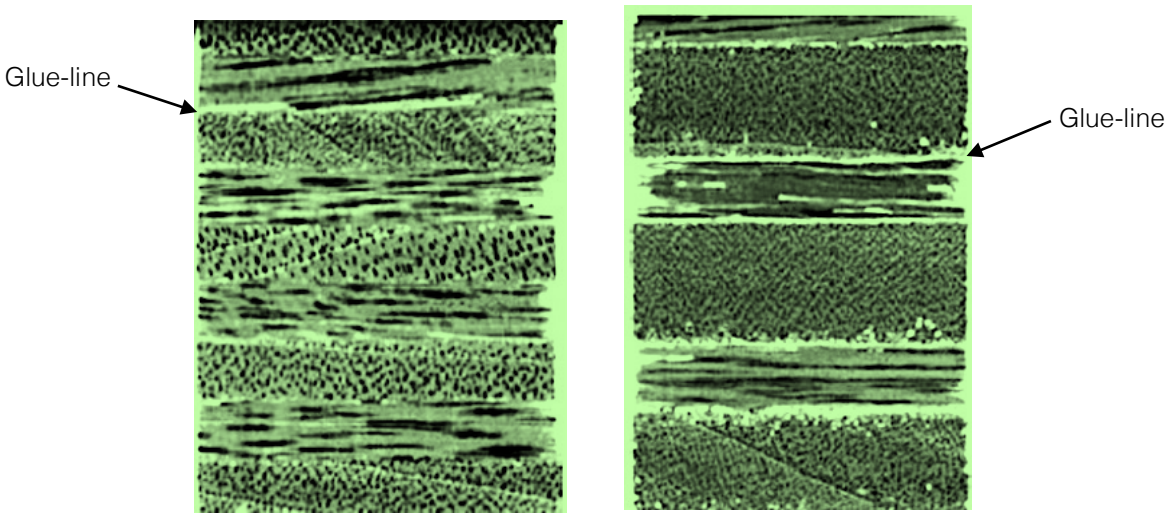

Figure 2.10 X-ray μCT images of adhesive distribution in PF-bonded okoumé (left) and poplar (right) plywood. Note that adhesive is distributed in 2D planes with no cross-links in the thickness (Z) direction of the plywood (modified from a figure in Li et al. 2014)

2.2.4 Visualization of adhesive distribution in strand and fibre-based wood composites

Early work on adhesive distribution in strand-based wood composites used light microscopy and spectroscopy to examine adhesive distribution on wood flakes before pressing (Burrows 1961). Burrows (1961) observed that some phenol formaldehyde (PF) adhesive droplets were deeply embedded in surface cracks and fissures in the flakes (Fig. 2.11), and he concluded that these adhesive droplets did not contribute to adhesive bonding.

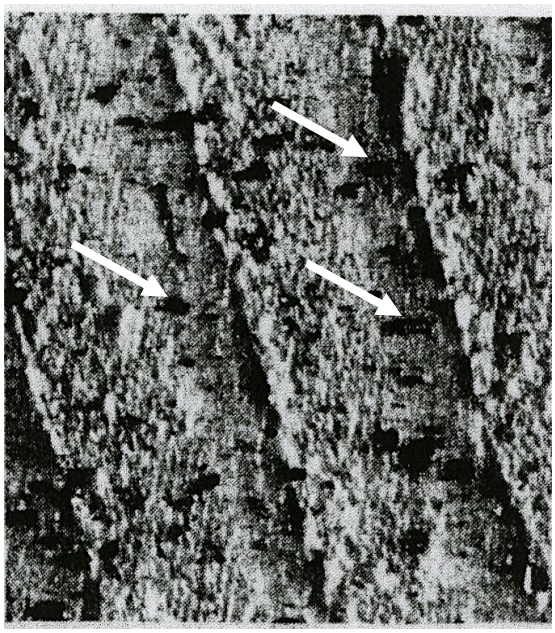

Figure 2.11 Light microscopic image of phenol formaldehyde resin droplets (arrowed) embedded in cracks and fissures at a flake surface (modified from a figure in Burrows 1961)

Lehmann (1965) conducted research during the 1960s and 1970s on adhesive distribution and efficiency in particleboard. He examined the effects of different types of adhesives, i.e. urea formaldehyde (UF) and phenol formaldehyde (PF) adhesives, percentage of solids in adhesives, atomization characteristics of adhesives, and some other variables on adhesive efficiency. He used various techniques, including ultraviolet light photography (1968) and photoelectric reflection microscopy (1970), to visualize the distribution of adhesives on wood flakes. He concluded that optimal adhesive efficiency was obtained with adhesives that had a high solids content. He was the first to show the presence of both continuous (Fig. 2.12a)

and discontinuous (Fig. 2.12b) glue-lines within particleboard. His findings suggested a strong relationship between droplet size during adhesive atomization and adhesive distribution in wood composites.

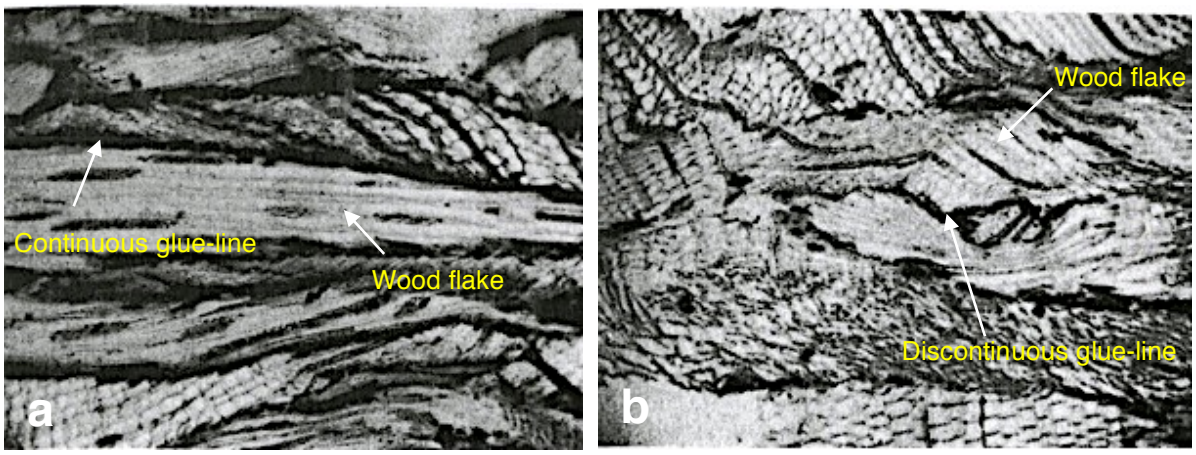

Figure 2.12 Cross-sections of particleboard bonded with phenol formaldehyde resin: (a) Black glue-lines between flakes sprayed with a fine mist of adhesive are almost continuous; (b) Glue-lines between flakes sprayed with a coarse mist of adhesive are discontinuous (modified from figures in Lehmann 1970)

Kasper and Chow (1980) examined PF adhesive distribution in flakeboard using X-ray imaging. Their study was one of the first to relate adhesive distribution in flakeboard to mechanical properties of the composite. They found that as adhesive droplet size became normally distributed, internal bond strength of the flakeboard was improved.

Early work on visualizing adhesive distribution by light microscopy mainly focussed on PF adhesive because its dark colour contrasted well with lighter coloured woody elements in the composite (Kamke et al. 1996). Visualizing UF adhesive is more challenging because it is colourless. However, UF adhesive is the primary adhesive used to manufacture particleboard and MDF especially in Europe (Lukkaroinen and Dunky 2005; Riegler et al. 2012). Hence, a number of techniques have been used in combination with microscopy to visualize colourless UF adhesive in wood composites, including use of stains, dyes and chemical labeling (Pakdel et al. 2008). Stains and dyes used to distinguish UF from wood particles under visible light include the dye Patent Blue V (Otterstätter 1995), copper sulphate in combination with rubeanic acid

(Johansson 1988), and a 'stain system' that has higher affinity to UF than to wood particles (Ginzel and Stegmann 1970). A fluorescent dye, Rhodamine B, in combination with fluorescence microscopy was also used by Murmanis and Youngquist to visualize PF adhesive in fibreboards (Murmanis et al. 1986a & 1986b; Youngquist et al. 1987). Their results suggested that fibreboard samples with more uniformly deposited resin had higher internal bond strength. Riegler et al. (2012) used a fluorescent dye, Brilliant Sulphaflavine (BSF), in combination with fluorescence microscopy to visualize UF adhesive at wood particle surfaces in particleboard. They successfully identified resin distributed between two particles (Fig. 2.13a) as well as agglomerated resin spots (Fig. 2.13b).

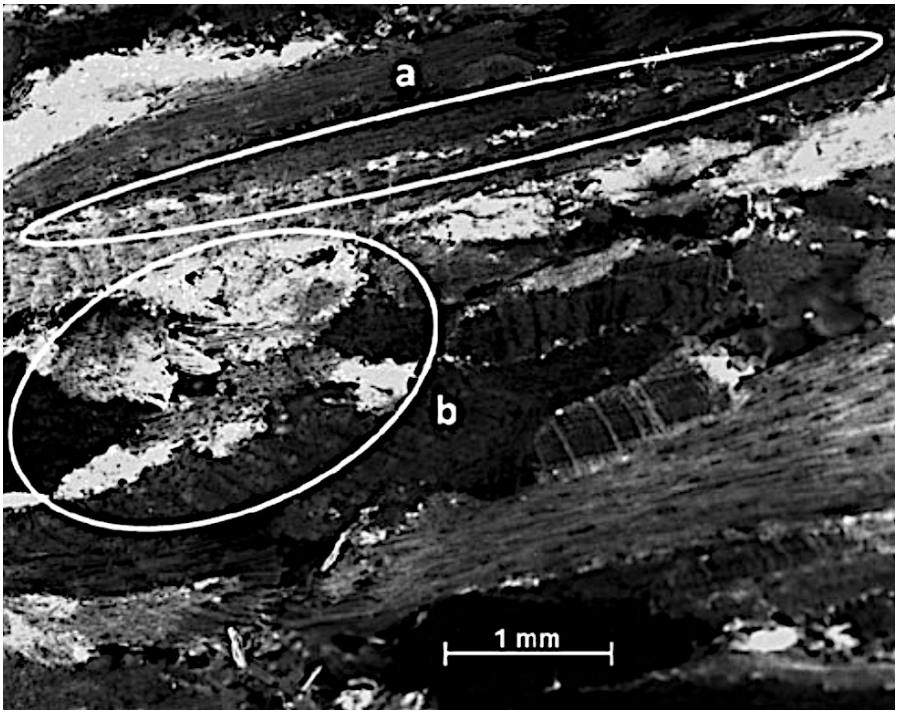

Figure 2.13 Cross-section of particleboard stained with Brilliant Sulphaflavine showing (a) a glue-line between two particles, and (b) agglomerations of resin at one spot (modified from a figure in Riegler et al. 2012)

Apart from fluorescence microscopy, confocal laser scanning microscopy (CLSM) has also been used to visualize adhesive distribution in wood composites (Xing et al. 2004; Cyr et al. 2008). For example, Cyr et al. (2008) used CLSM and a fluorescent dye to investigate the distribution and penetration of urea-melamine-formaldehyde (UMF) resin in medium density

fibreboard (MDF). They observed deep penetration of UMF resin into wood cells while the fibre surface was still well covered with resin (Fig. 2.14a). Wood fibre surfaces were irregular, but large areas were still covered with resin (Fig. 2.14b). Another important finding was that UMF resin penetrated through pores from cell surfaces to cell lumens (Cyr et al. 2008). This finding suggested that pits were a penetration pathway for the UMF adhesive through wood cell walls.

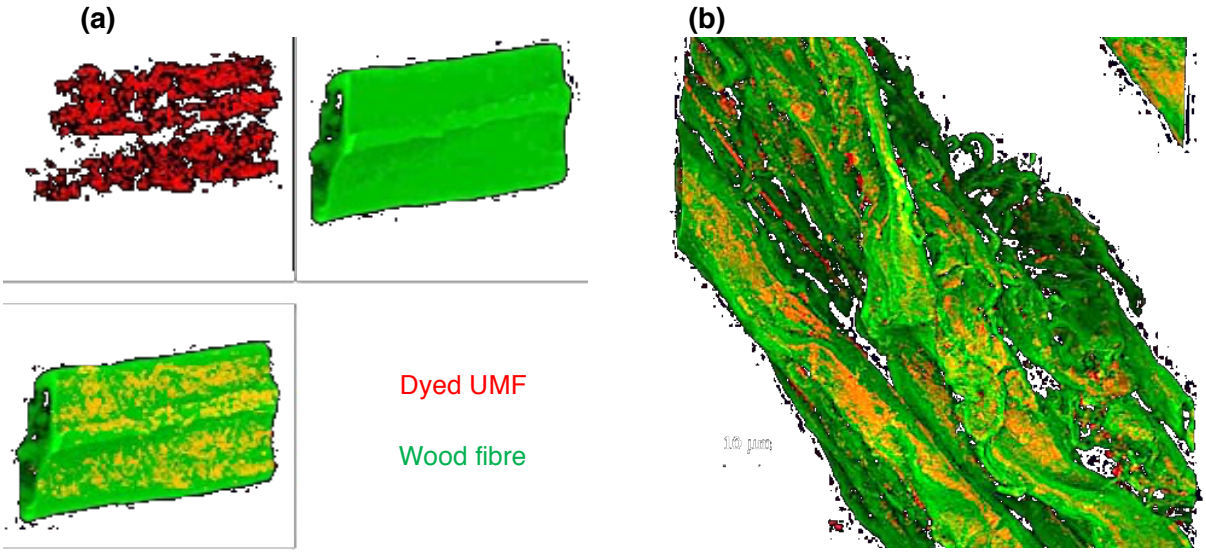

Figure 2.14 Urea-melamine-formaldehyde resin in medium density fibreboard obtained using confocal laser scanning microscopy: (a) Resin (red) covers a single spruce fibre (green) surface as well as penetrating into cells; (b) Magnified view of resin penetration across irregular fibre surfaces (modified from a figure in Cyr et al. 2008)

Grigsby and Thumm (2002, 2012) also used CLSM to visualize UF resin in MDF. They showed that the UF resin was mainly distributed parallel to the radiata pine (*Pinus radiata*) fibres in the composite. There were few adhesive connections between different layers of UF resin in the Z-direction (Fig. 2.15).

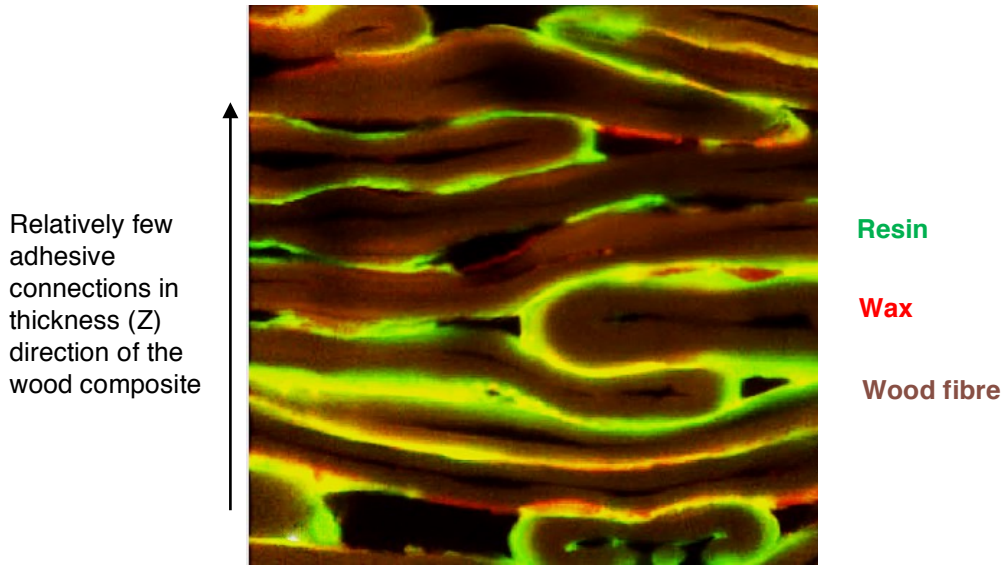

Figure 2.15 Confocal laser scanning microscope image showing urea formaldehyde resin (green) and wax (red) between radiata pine wood fibres (brown) in medium density fibreboard (modified from a figure in Grigsby and Thumm 2012)

In addition to microscopy, a range of other techniques have been used to examine adhesive distribution in wood composites. For example, X-ray photoelectron spectroscopy (XPS) was used to quantify UF resin content at wood fibre surfaces (Grigsby et al. 2004; Pakdel et al. 2008). Pakdel et al. (2008) examined the influence of some manufacturing parameters on resin coverage of fibre during MDF production. One interesting finding was loss of approximately 1.17% of resin during blowline blending of resin and fibre. Pakdel et al. (2008) attributed this loss of resin to the penetration of resin into surface pores or fibre defects during MDF refining, or alternatively to evaporation of the resin during drying.

More recently, X-ray micro-computed tomography (μCT) has been used to visualize the microstructure of wood composites (Shaler 1998; Wang and Shaler 1998; Groom et al. 1999; Sugimori and Lam 1999; Lux et al. 2006). Walther and Thoemen (2009) used synchrotron X-ray μCT to visualize labelled UF adhesive in MDF. UF was labelled with barium sulfate to increase its density and enable it to be distinguished from wood (Fig. 2.16). Walther and Thoemen (2009) concluded that adhesive distribution could be visualized using X-ray μCT, however, the

resolution of the system they used was not high enough to clearly separate the labelled adhesive from wood.

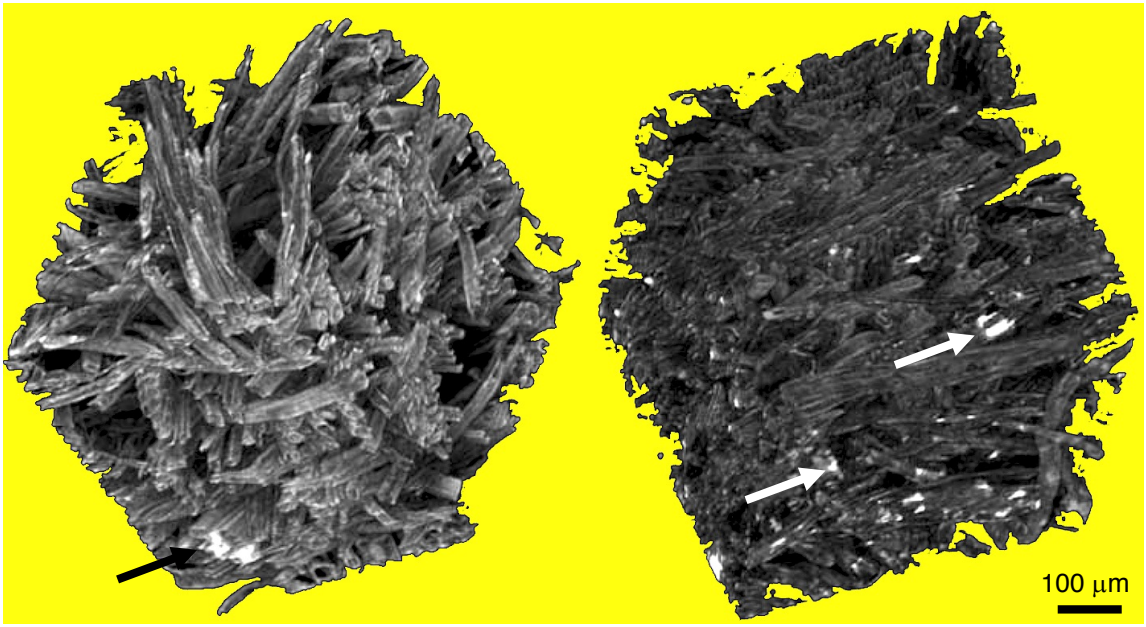

Figure 2.16 X-ray micro-CT image of iodine (left) and barium sulfate (right) labelled UF adhesive (bright white areas, arrowed in picture) in medium density fibreboard. Note the sparse distribution of UF in the fibre matrix (modified from a figure in Walther and Thoemen 2009)

Evans et al. (2010) used X-ray µCT to visualize the distribution of a UMF adhesive in particleboard. They found that the adhesive was mainly distributed in the X-Y plane with relatively few connections in the Z-direction (Fig. 2.17a). This lack of Z-connections can be more clearly seen when the adhesive network was segmented (Fig. 2.17b). Evans et al. (2010) confirmed previous findings that adhesive tended to penetrate cracks or splits in flakes. They also observed that the continuity of glue-lines in particleboard appeared to depend on the degree of contact between flakes. The glue-lines were longer and more continuous in areas where there was better inter-particle contact.

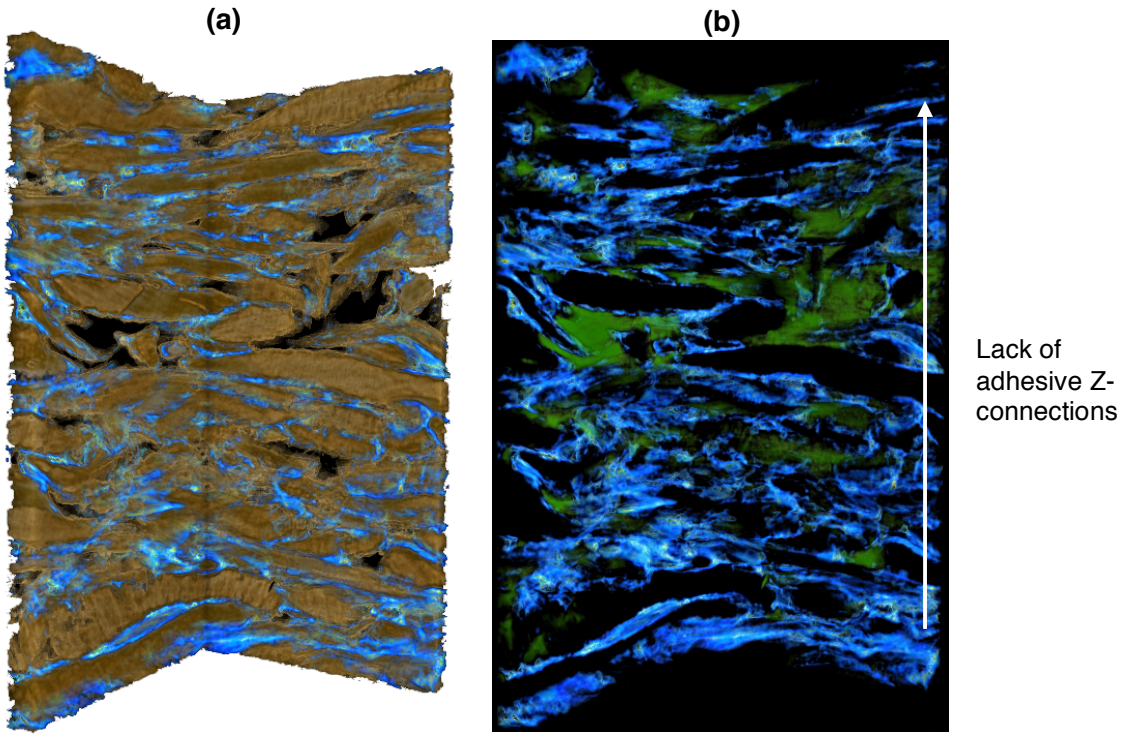

Figure 2.17 Rendered X-ray micro-CT images of distribution of resin (blue), voids (black) and wood flakes (brown) in particleboard: (a) Wood flakes present; (b) Wood flakes excluded (Evans et al. 2010)

2.2.5 Adhesive penetration into wood substrates

Studies by Rice (1965) and Smith (1971) on adhesive bonding in plywood showed that UF and PF penetrated wood veneer. White et al. (1977) developed a method for quantifying adhesive penetration into southern pine wood. Their results showed that adhesive penetration into earlywood was greater than that of latewood. They also found that adhesive penetration was inversely related to adhesive viscosity.

Several studies have examined factors that can influence adhesive penetration into wood veneer. For example, Brady and Kamke (1988) examined the effects of hot-pressing parameters on penetration of a PF into sliced aspen and Douglas fir wood veneers. They found that higher veneer moisture contents were correlated with increased adhesive penetration because the adhesive's viscosity increased more slowly during pressing. The effect of hot platen pressure on adhesive penetration was not consistent as it interacted with different moisture content levels. Pressing time and temperature also affected adhesive penetration

because they influenced adhesive curing rate and viscosity. They also found that adhesive penetration varied with wood species. Johnson and Kamke (1992) developed a quantitative method of examining UF and PF adhesive penetration into yellow poplar, and they then examined the effects of various parameters on adhesive penetration. They found that adhesive penetration into wood was inversely correlated with the molecular weight of the PF. Sernek et al. (1999) examined the effects of moisture content and growth ring orientation on penetration of a liquid UF adhesive into beech wood. They found that the application of mechanical pressure to the bond line greatly increased penetration. Maximum penetration of UF adhesive during hot pressing occurred at 9% moisture content. Penetration in the tangential direction was greater than that in the radial direction after hot-pressing. The authors attributed such directional difference in penetration to: (1) the presence of thin latewood bands with fewer and smaller vessels in the radial direction; (2) greater numbers of pits on the radial surfaces of vessels than on tangential surfaces; (3) greater permeability (90 x) of beech in the tangential direction than in the radial direction.

Stamm (1964) and Sellers (1994) suggested that polymers with a molecular weight of 1000 or less have the ability to effectively diffuse into wood cell walls. In accord with these suggestions, Nearn (1974) detected the presence of PF adhesive in wood cell walls using scanning electron microscopy. Marcinko et al. (1998, 2001) used solid-state nuclear magnetic resonance spectroscopy (NMR) to show that pMDI resin and wood's molecular components mixed together forming an 'anchored' interphase. Xing et al. (2005) used confocal laser scanning microscopy (CLSM) and a Toluidine Blue O staining to investigate the relationship between viscosity of UF resin and its penetration depth in MDF fibres. They found that resins with viscosities ranging from 80 mPa·s to 250 mPa·s exhibited similar penetration depths after the resins were in contact with fibre for 30 minutes at room temperature.

Penetration of adhesive into the porous microstructure of wood has a strong influence on adhesive bond strength in wood composites, according to Collett (1972), Jakal (1984), Kedziersk (1986), and Brady and Kamke (1988). Hare and Kutscha (1974) suggested that deep and even penetration of adhesive into wood is associated with higher glue-line shear strengths. However, the depth of penetration had a limit beyond which shear strength decreased (Hare and Kutscha 1974). White et al. (1977) suggested that deeper penetration of adhesive in earlywood compared to latewood accounted for the stronger bond that developed between earlywood and the adhesive. Subsequent research (Kamke and Lee 2007) also suggested that a moderate degree of adhesive penetration is desirable. However, excessive penetration may lead to 'starved' bond lines with insufficient adhesive remaining at the interface to effectively bond the two adherend surfaces (Marra 1992; Sernek et al. 1999; Xing et al. 2005). However, it is not known how much adhesive bond strength is derived from true interface contact and how much is derived from penetration of adhesive into wood cell walls, according to Frihart (2006).

2.3 Effects of adhesive on thickness swelling of wood composites

Plywood and OSB are the most widely-used load-bearing wood composite panels in North America. They are often used for wall sheathing, roof decking or as a sub-floor for various flooring materials in residential and commercial construction (Shmulsky and Jones 2011b). In these applications, wood composites are sometimes unavoidably exposed to water. Water absorption causes moisture-induced dimensional changes, particularly thickness swelling (Lawniczak and Nowak 1962; Johnson 1964; Wu et al. 2002). Moisture-induced thickness swelling of wood composites is mainly the sum of two components - swelling of the wood itself and release of compression strains imparted during hot pressing (Halligan 1970). The latter is not recovered even when the wood composites return to their original moisture content and, hence, wood composites undergo irreversible thickness swelling. Irreversible thickness swelling is a costly problem in some end-uses of wood composites, as mentioned above (p. 8).

Therefore, reducing thickness swelling of wood composites has always been a priority for those interested in improving the properties of wood composites. Previous research on this subject has focused on the effects of density distribution on the thickness swelling of wood composites and also on treatments that can reduce swelling. These studies are briefly reviewed below (Section 2.3.2). Additional information can be found in publications by Suchsland (1962), Wang and Winistorfer (2000), and Tackie et al. (2008). The following section gives greater emphasis to the effects of adhesive in wood composites on thickness swelling.

2.3.1 Adhesive level, type and distribution on thickness swelling of wood composites

Adhesive plays an important role in controlling dimensional stability of wood composites because it can mechanically interlock wood elements and create bonds of sufficient magnitude to resist delamination when the composites are exposed to water. Adhesive can block penetration of water into plywood and increase the dimensional stability of wood by bulking cell walls (Stamm and Baechler 1960; Rowell and Banks 1985; Kajita and Imamura 1991; Li et al. 2014).

Previous studies have found that the dimensional stability of wood composites is greatly influenced by the level, type and distribution of adhesive. Linville and Wolcott (2001) found that the dimensional stability of OSB was positively correlated with the level of pMDI adhesive in panels. They suggested that 'a pMDI resin level of approximately 12.5% should minimize the non-recoverable swelling component in OSB'. Generalla et al. (1989) as well as Avramidis and Smith (1989) observed positive correlations between adhesive level and dimensional stability of OSB bonded with PF resin. Abdalla and Sekino (2004) found that increased PF resin application rates between strands improved the dimensional stability of a composite flange composed of Japanese red pine (*Pinus densiflora* Seib. et. Zucc). However, there is an optimal level of adhesive, above which additional adhesive no longer reduces thickness swelling (Kelly 1977; Suchsland and Xu 1991). The optimal adhesive level for OSB has been reported to be between

6 ~ 12 %, depending on adhesive type (Kelly 1977; Generalla et al. 1989; Biblis 1990). The positive correlation between dimensional stability of wood composites and resin level has been attributed to bulking of wood cell walls (Kajita and Imamura 1991) and intra-cell bonding (Krzysik and Young 1986). Cell wall bulking is favoured when wood is impregnated with a water-soluble resin that penetrates into the wood cell walls and forms insoluble polymers, which will not leach from wood (Stamm and Baechler 1960; Rowell and Banks 1985; Kajita and Imamura 1991).

Adhesive type also has a significant influence on the thickness swelling of wood composites. For example, several studies have shown that OSB and particleboard bonded with iscocyanate resin (pMDI) show reduced thickness swelling compared to those bonded with PF resin (Deppe 1977; Wilson 1980; Galbraith 1986; Abdalla and Sekino 2004; Taylor et al. 2008). For example, Wilson (1980) reported that thickness swelling of particleboard bonded with 5% pMDI or PF were 5% and 15% after a 24-hour water soaking test, respectively. Brochmann et al. (2004) suggested that using PF as a surface resin and pMDI as a core resin was an effective combination for reducing the thickness swelling of OSB. However, the higher cost of pMDI limits the percentage that can be used in wood composites, according to Koch et al. (1987) and Chapman (2006). Some North American companies manufacture OSB with enhanced moisture resistance and dimensional stability by either using higher loadings of PF resin and wax or replacing some of the PF resin with pMDI resin. These ‘enhanced’ OSB products are used as sub-floors (Taylor et al. 2008). These products are up to three times more expensive than commodity grade OSB (Fig. 2.18).

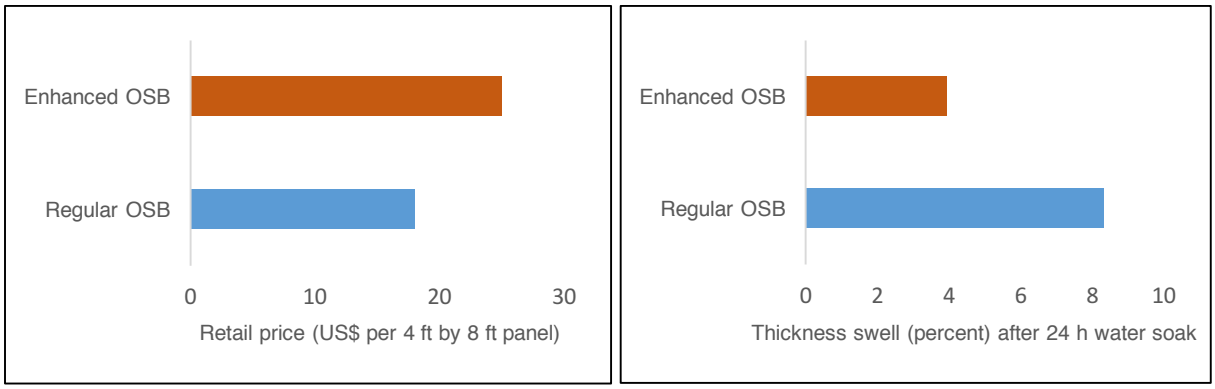

Figure 2.18 Comparison of retail price (US$) and thickness swell (percent) of regular commodity grade OSB and an 'enhanced' OSB (figure based on data from Taylor et al. 2008)

Adhesive distribution can also significantly influence the thickness swelling of wood composites. For example, Ellis (1993) reported that thickness swelling of a waferboard was lowest when the particle size of a powdered PF resin was < 45 μm. In contrast, thickness swelling was highest when the particle size of the powdered PF resin was 150 ~ 212 μm.

2.3.2 Alternative approaches to reduce thickness swelling of wood composites

Some alternative approaches, other than increasing adhesive level, have been used to reduce the thickness swelling of OSB. For example, pre-treatments that chemically or mechanically modify wood particles and strands, before adhesive application, can be employed to improve dimensional stability of OSB. These pre-treatments include acetylation (Rowell et al. 1986a, 1986b, 1990) and steam treatment (Hsu et al. 1988) of wood strands. Alternatively, post-treatment of panels, such as heat treatment, can improve their dimensional stability (Shen 1974, Hsu et al. 1989, Suchsland and Xu 1991).

The dimensional stability of wood composites can also be improved by using surface coatings (Williams et al. 2005). Coatings and water repellents create a physical barrier at wood surfaces and impede water absorption (William et al. 2005). Evans and Cullis (2008) assessed the effects of applying UV-cured finishes on the dimensional stability of OSB. The UV-cured finishes were able to reduce the thickness swelling of coated OSB by 65% compared to the

uncoated controls. Water repellents, including wax and oil emulsions, have also been used to dimensionally stabilize OSB (Baileys et al. 2003; Mantanis and Papadopoulos 2010). Coatings applied to the edges of OSB, commonly referred to as edge seals (Fig. 2.19), are widely used to prevent moisture ingress into the edges of particleboard and OSB (Johnson 1984; Winterowd et al. 2003). Edge tapers (Fig. 2.19) and drainage channels (Fig. 2.20) are used commercially to reduce the differential thickness swelling of OSB (Evans et al. 2013)

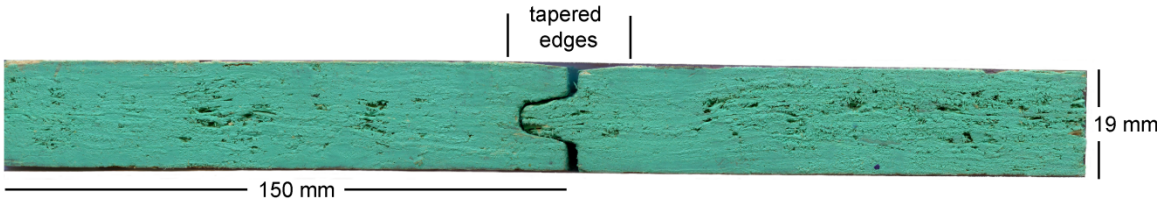

Figure 2.19 OSB samples containing a 0.6 mm deep and 10 mm wide edge taper. The samples are coated on their edges with a green coloured edge seal (Evans et al. 2013 & 2015)

Figure 2.20 Commercial OSB panels containing water drainage channels: Louisiana-Pacific's TopNotch® 350 enhanced OSB sub-floor panel with drainage notch in the tongue of the panel (left, http://www.lpcorp.com); Weyerhaeuser's Edge Gold® OSB sub-floor panel with 'Down Pore' hole (right, http://www.woodbywy.com)

No previous research has modified adhesive distribution in wood composites in three dimensions as a way of restraining thickness swelling. But related approaches have been tested in other fields.

2.4 Effects of inter-connected 3D structure on some properties of advanced composite materials

There has been use of metal nails and screws to bond wood composites. For example, Keating from Australia's Commonwealth Scientific and Industrial Research Organization (CSIRO) mentioned the use of 'nail laminating' to prevent spreading of structural timber laminations (Keating 1973). Screws have also been used to connect glulam with cross laminated timber (CLT) components, according to Jacquier and Girhammar (2014). These fixings provide additional reinforcement in the through-thickness (Z) direction of structural wood composites. This type of reinforcement has been more widely used in some advanced composite materials and structures. I review these uses of through-thickness reinforcement in the following sections.

2.4.1 3D rebar structure in concrete

Reinforced concrete is a good example of a composite with an inter-connected 3D structure. It was invented by Joseph Monier in 1849 and patented in 1867 in Paris, France (Hassoun and Al-Manaseer 2012). Reinforcing steel bars (also known as rebars) are aligned in the X, Y and Z directions forming an inter-connected 3D network (Park and Gamble 1980). Rebars increase tensile strength (Cosenza et al. 1997; Yeih et al. 1997; Anwar Hossain 2008) and flexural strength (Hassoun and Al-Manaseer 2012; Saleem et al. 2013) of concrete.

There have been numerous studies on optimization of rebars to improve the performance of concrete. For example, Harajli et al. (2002) examined the bond strength of plain and steel-fibre reinforced concrete embedded with steel rebars of varying diameters. Their results indicated that maximum load at bond failure increased with increasing rebar size. Rebars with a diameter of 16 mm withstood a maximum slipping load of 36 kN, whereas rebars with a diameter of 32 mm withstood a maximum slipping load of 68 kN. More recently, fibre-reinforced polymer (FRP) rebars have been used in concrete to overcome the corrosion problem that

occurs when steel rebars are used in concrete (Nanni and Dolan 1993; Burgoyne 2001; Benmokrane et al. 2002; Sayed Ahmad et al. 2011). Several studies examined the bond strength (rod pull-out resistance) of FRP rebars with concrete. For example, Nanni et al. (1995) suggested that the shape and form of rebars (such as circular vs. polygonal cross-sections; straight, twisted vs. braided forms) significantly affected the bond strength of FRP rebars with concrete. Physical properties (Young's modulus and Poisson's ratio) of FRP rebars also influence the bond strength between the FRP rebars and concrete (Nanni et al. 1995). Nanni et al. (1995) also mentioned that the differential thermal expansion coefficients of FRP rebars and concrete may cause considerable stress in the concrete adjacent to the rebars. Cosenza et al. (1997) examined bond-slip curves of different FRP rebar designs and came to the conclusion that smooth rebars were less effective at reinforcing concrete than sanded and twisted rebars because there was less friction between the smooth rebars and the surrounding concrete matrix than the sanded and twisted rebars. Cosenza et al. (1997) also suggested that the bond strength between the FRP rebars and concrete is largely dependent on polymer properties rather than concrete strength. Tighiouart et al. (1998) investigated bond strength of FRP rebars with concrete using a pull-out test. They examined the effects of rebar diameter (12.7 mm, 15.9 mm, 19.1 mm and 25.4 mm) on bond strength. Their results indicated that average maximum bond strength decreased when the diameter of rebars increased. They attributed this inverse correlation to the bleeding of water that had been trapped beneath bigger rebars, creating voids and reducing contact between the rebars and surrounding concrete. Their work indicated that rebar design parameters significantly influence the bond strength of FRP rebars with concrete. On a related issue, Burgoyne (2001) suggested that the spatial layout of FRP rebars in the concrete matrix can also affect bond strength of rebars to concrete.

2.4.2 Advanced textile composites with 3D architecture

Advanced polymer composites have been extensively used for aircraft structures (Archer et al. 2010). Originally, such composites were mainly 2D laminates, but to overcome delamination problems with these composites, research was performed to develop more 'advanced' reinforced polymer composites with 3D fibre architectures (Farley and Dickinson 1992). Mouritz et al. (1999) published an extensive review on advanced fibre textile composites with 3D architectures created by 3D weaving, braiding, stitching and knitting. These advanced composites have superior properties compared to traditional laminates. For example, 3D woven composites have higher ballistic damage resistance, higher tensile strain values and less delamination than traditional 2D laminates (Fig. 2.21) (Ding et al. 1995; Mouritz et al. 1999).

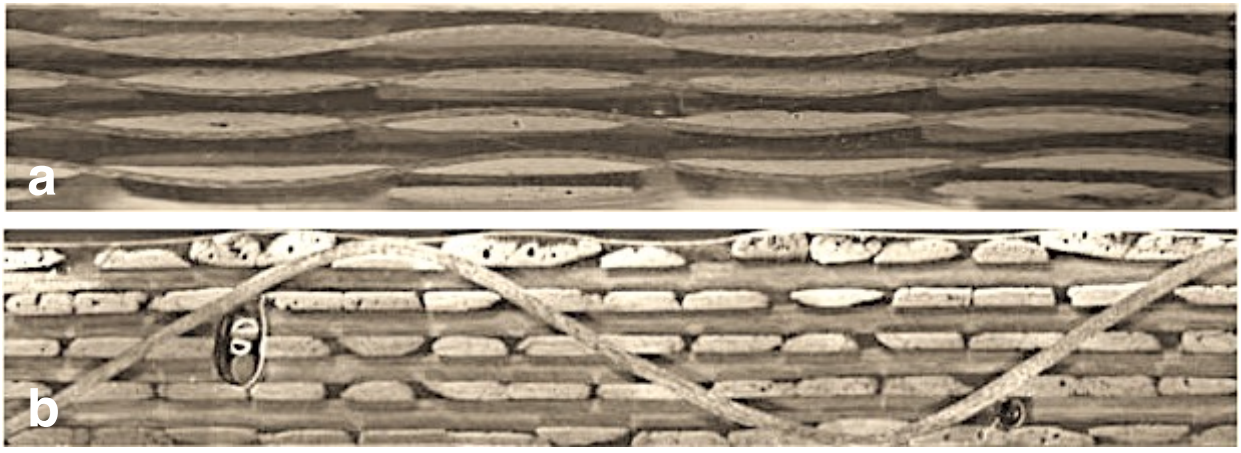

Figure 2.21 Longitudinal micrographs of (a) 2-D laminate, and (b) 3-D interlocking carbon fibre composites (modified from figures in Mouritz et al. 1999)

One of the most common weaving architectures has an orthogonal structure (Fig. 2.22). The proportion of Z-direction reinforcement (binder yarn) is usually less than 5% (Mouritz et al. 1999). However, the Z-direction binder yarn significantly improves impact resistance. For example, Chou et al. (1992) reported that the impact energy required to initiate damage in 3D woven composites was up to 60% higher than that of 2D laminates.

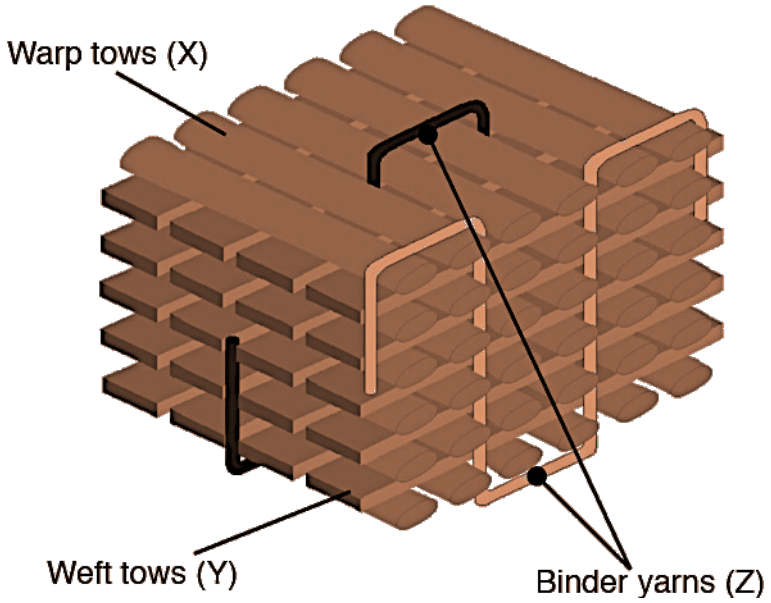

Figure 2.22 Orthogonal woven fibre architecture commonly used in 3-D woven composites (modified from a figure in Mouritz et al. 1999)

2.4.3 Z-fibre (through-thickness) reinforcement in advanced polymer composites

The process of inserting small, solid and cylindrical composite rods through polymer laminates (also known as Z-fiber™) was originally developed by the U.S. military tech company Foster-Miller Inc., and further developed by Aztex Inc. Z-rods are inserted through polymer laminates using an ultrasonic procedure (Freitas et al. 1994, 1996). Freitas et al. (1996) claimed that 'Z-fibers can be a cost-efficient way to increase out-of-plane strength, damage resistance, and through thickness thermal conductivity of polymer laminates that are used for modern aircraft structures'. They also reported that Z-fibres significantly increased fracture toughness of polymer laminates, because 'as a crack propagates the number of reinforcing fiber rows which are activated increases resulting in increased fracture toughness'. They also examined the mechanical properties that were compromised by using the Z-fibre technology. They stated that 'for Z-fiber areal densities less than 1.5 percent, a negligible reduction in tension (2~9%) and compression (1%) strength of the composite was seen'. However, in another study, Steeves and Fleck (2006) found that Z-pins decreased the tensile strength of the composite by 27%, and the compressive strength by at least 30% even though the Z-pins reduced the composite's

susceptibility to delamination. Their results also indicated that the distribution pattern of the Z-pins influenced the compressive strength of the composites.

There are a variety of other factors, apart from distribution pattern, that have important effects on the ability of Z-fibres to improve mechanical properties of polymer composites. Rugg et al. (1998) reported a near doubling of the delamination resistance of carbon-epoxy polymer lap shear specimens when they were reinforced with 1.7 mm diameter Z-fibres inserted at an angle of 45° to the delamination plane. They also found that the deformation and damage of the rods and surrounding laminates were very different for rods of different orientations. In a subsequent study, Rugg et al. (2002) examined the mechanisms of bridging and crack propagation in Z-fibre reinforced composites. They stated that 'Z-fibres can bridge cracks thus reducing the driving force for crack growth', and 'in some cases, the presence of Z-fibers resulted in a change in the failure mechanism from delamination to microbuckling of the laminate'. The effect of Z-fibre pinning on Mode I fracture toughness (using double cantilever beam test) of a polymer laminate with different areal densities of Z-fibres was examined by Partridge and Cartié (2005). They found that 2% area-density produced a load carrying capability and Mode I fracture toughness that was at least two times higher than that of a composite with 0.5% area-density of Z-pinning. The effects of Z-pin area-density as well as the diameter of the pins on the compressive strength of textile laminates was examined by Huang and Waas (2009). They concluded that higher area-density and smaller diameter Z-pins reduced the compressive strength of laminates. They attributed these negative correlations to unintended fibre waviness resulting from the insertion of the Z-pins into the laminates.

Finite element analysis (FEA) has been used to model the effects of Z-fibres on some mechanical properties of polymer composites. For example, Grassi et al. (2002) used finite element analysis to model the mechanical behaviour of z-pinned laminates. Their simulation showed that by adding 2% volume percentage of Z-fibres, the through-thickness Young's

modulus of laminates was increased by 22~35%, while undesirable reductions in in-plane moduli were limited to 7~10%. Bianchi et al. (2012) also used finite element analysis to model structural deformation, strength properties and delamination fracture behaviour of composite T-joints reinforced with Z-pins. Their FE model indicated that 'Z-pinned joint does not fail catastrophically at the initial load drop point (unlike the unpinned controls) due to bridging traction loads generated by the pins along the delamination crack'.

The insertion of Z-fibres in polymer laminates, however, has been associated with thermal stress mismatch in the composite due to differential thermal conductivity between the Z-fibres and the polymer. Such thermal stresses can occur because advanced polymer laminates are generally cured at temperatures between 120°C and 180°C (Sweeting and Thomson 2004). Sweeting and Thomson (2004) used FE modelling to calculate thermal residual stresses for laminates with Z-pins. Their model indicated that the stress levels in resin pockets around the Z-pins could be greater than the failure stress of the epoxy resin, suggesting that cracks may develop around the Z-pins. Byrd and Birman (2006) examined the effect of temperature on Z-pinned joints and confirmed the cracking of the composite around the Z-pins at elevated temperatures.

The effects of Z-fibre reinforcement on properties of laminates that are peripheral to this thesis are reviewed by Mouritz (2007).

2.5 Finite element analysis (FEA) of hygroscopic swelling of wood composites and some advanced composite materials

2.5.1 Finite element analysis of hygro-mechanical deformation of solid wood and MDF

Finite element analysis (FEA) has been used to simulate hygro-mechanical deformation of solid wood (Ormarsson et al. 1998, 1999), glue-laminated timber products (Deteix et al. 2008; Ormarsson and Dahlblom 2013), and fibre-based wood composites (Suchsland and McNatt 1986; Tong and Suchsland 1993; Cloutier et al. 2001; Ganev et al. 2005). However, the majority

of the studies have modelled a system composed of a single material. For example, the FEA model developed by Ormarsson et al. (1999) simulated dimensional change of a solid wooden board during drying. They used the commercial FEA program ABAQUS® to model the deformation of a solid wood panel during drying. Models for simulating the hygroscopic warping and cupping of medium density fibreboard (MDF) mainly treated the MDF as a 'homogeneous' material, with the exception of variation in density in the vertical direction (Cloutier et al. 2001; Ganev et al. 2005). These models form the basis for modelling complex systems composed of two different materials such as wood and adhesive Z-pins.

On the other hand, the model developed by Deteix et al. (2008) to predict cupping of laminates incorporated an adhesive layer in the laminate. Their work showed the importance of the adhesive layer in the FEM simulation of hygroscopic cupping. The model was able to simulate the cupping provided that the mesh was sufficiently dense in the adhesive layer. FEA models can graphically show changes in geometry and form of composites resulting from hygroscopic swelling and shrinkage. However, it is still challenging to model the hygroscopic deformation of wood composite systems that contain more than one material. Therefore, it is informative to review relevant literature that has modelled other composites for example silicon laminates used by the semi-conductor industry.

2.5.2 Finite element analysis of hygroscopic swelling of silicon laminates in integrated-circuit packages

FEA has been extensively used to model hygroscopic swelling of silicon wafers because their failure sometimes arises due to moisture-induced deformation during their manufacture or storage (Shirangi and Michel 2010). Specifically, differential hygroscopic swelling within such wafers creates a stress mis-match which reduces interfacial adhesion and leads to delamination (Hsu and Hsu 2009). The residual moisture also induces elevated vapor pressure at higher temperatures, which results in 'popping crack failure' (Hsu et al. 2008). Hsu et al. (2008) used

the FEA software ANSYS® to predict the hygroscopic swelling and residual stress distributions in a multi-material integrated-circuit consisting of epoxy molding compound, die attach, substrate, solder mask and acrylic adhesive. They used the similarity between thermal diffusion and moisture diffusion within the thermal module of ANSYS® to solve moisture diffusion problems. The approach that Hsu et al. (2008) used to model moisture diffusion was first developed by Lam (2000). He introduced the term 'wetness' to overcome the difficulty of solving differential equations with discontinuous moisture concentration at multi-material interfaces (Lam 2000). Such an approach can be adapted to model the hygroscopic swelling of laminated wood composites containing adhesive Z-insertions.

2.6 Overview

It is clear from this review of literature that adhesive plays an important role in dimensional stability (thickness swelling) and mechanical properties of wood composites. One focus of the literature is the relationship between adhesive characteristics, content and distribution in wood composites and their properties. However, the effects of spatial distribution of adhesive on key properties remain largely unexplored.

Clearly, veneer-based (such as plywood and LVL) and, less obviously, strand-based composites (such as OSB) have layered structures in which woody elements and adhesive are distributed in two dimensions with few connections in the Z-direction. On the other hand, it has been shown that some adhesives have the ability to penetrate into checks, cracks, voids, cell lumens and even cell walls at the adhesive interface. Mechanical interlocking at sites of glue penetration explains in part the bonding between adhesive and wood (Pizzi 1994; Gardner 2006). Therefore, it is possible that this kind of bonding could be spatially engineered by altering the penetrating pathways of adhesive in wood composites.

Structural modification of matrix and reinforcing materials has been employed to create inter-connected 3D networks in concrete, textile laminates and advanced polymer composites in

order to improve selected properties. Relevant approaches include Z-pin insertions which provide through-the-thickness reinforcement in advanced polymer composites. Many properties including fracture toughness have been enhanced by such Z-reinforcement.

This thesis explores whether it is possible to improve dimensional stability and fracture toughness of some wood composites by altering adhesive distribution, hence forming inter-connected 3D adhesive networks in wood composites. This review provides evidence that adhesive can wet, flow and penetrate into the wood matrix. Therefore, it should be possible to create adhesive Z-connections by manipulating and modifying adhesive distribution pathways.

3 Development of Methodology to Create Adhesive Z-connections in Wood Composites

3.1 Introduction

The general hypothesis of this thesis, as stated in Chapter 1, is that altering adhesive distribution in wood composites to introduce adhesive Z-connections and hence create a 3-dimensionally (3D) inter-connected adhesive network will significantly improve some key properties of wood composites. One of the most important properties of wood composites is their dimensional stability, particularly against hygroscopic thickness swelling (see Chapter 2). Therefore, large parts of this thesis are devoted to testing the hygroscopic thickness swelling of wood composites with adhesive Z-connections. To my knowledge, this approach is novel and has not been used before. Hence, to be able to test my hypothesis, the first preliminary step in my research was to develop the methodology to create a 3D inter-connected adhesive network in wood composites and to test whether such an approach influenced the hygroscopic thickness swelling of the composites.

Hygroscopic thickness swelling of wood composites is mainly the sum of two components - swelling of the wood itself and release of compression strains from hot pressing, as mentioned above (Halligan 1970). The latter is not recovered even when wood composites return to their original moisture content. Therefore, it is called irreversible thickness swelling. It is possible that adding 'restraining' reinforcement in the thickness direction could impede the release of such compression strains. There are some studies suggesting that adding Z-direction reinforcement can restrain thermal expansion of some advanced composite materials, although no previous studies have examined the restraining effect of adding Z-direction (through-thickness) reinforcement on reducing hygroscopic swelling of any composite materials. For example, 3D stitching introduces polymeric materials in the Z-direction between 2D laminates to form an inter-connected 3D structure (Tong et al. 2002). A 3D stitched carbon fibre reinforced

silicon carbide polymer composite had up to three times less through-thickness thermal expansion than that of a 2D laminate (Kumar et al. 2009). Therefore, it is plausible that Z-direction (through-thickness) reinforcement might restrain hygroscopic swelling of wood composites. To introduce this kind of restraining reinforcement in wood composites, the Z-direction reinforcement should have superior water resistance and hygroscopic dimensional stability compared to wood. Interestingly, one of the two major components of wood composites, the adhesive, is already a good candidate because it has such properties. For example, adhesive impedes the penetration of water into plywood (Li et al. 2014), and some adhesive mechanically interlocks wood cells and restrains swelling (Jake et al. 2015). Thus, it is possible that mechanical interlocking of adhesive in the thickness (Z-) direction, albeit at a larger scale in wood composites, might restrain moisture ingress and thickness swelling. One possible way to create such interlocking is to drill holes in woody elements, such as veneers, flakes and strands. The adhesives may then be able to flow and penetrate into the holes upon pressing, and form adhesive Z-connections after the adhesive has cured.

In this chapter, I describe the preliminary research that was carried out to explore such an approach. Wood veneers containing both perforated and unperforated (control) sections were used to manufacture a model wood composite (laminate). The veneers were bonded together using a polyurethane adhesive after preliminary research showed that this adhesive was better able to form adhesive Z-connections than epoxy or PVA adhesive. The model wood composites were then submerged in water and their thickness swelling was measured to examine differential thickness swelling between the sections with holes and the sections without holes on the same composite. Key parameters for the ‘hole drilling’ procedure were defined at the end of this research.

3.2 Materials and methods

3.2.1 Experimental design

A two-factor split-plot randomized block design was used to examine the effects of nine (3 x 3) treatments (Table 3.1) on the thickness swelling of a model wood composite. The factors examined were size of the holes drilled into veneer, and amount of glue applied to each veneer. These two factors were selected because of their possible influence on the formation of adhesive Z-connections in the composites, as related to study by Tighiouart et al. (1998) (Chapter 2). Veneer cut from six different veneer sheets provided replication at the higher level (six blocks). The two factors had different levels as shown in Fig. 3.1. A model wood composite was designed to eliminate variations in wood properties that could affect thickness swelling. The model composite consisted of three different sections (Fig. 3.2) enabling measurement of differential thickness swelling between marked sections with holes and the sections with no holes (Fig. 3.2).

Table 3.1 Two factors examined and their different treatment levels

Hole size (diameter, mm)	Glue amount per hole (μL)
1 (small)	5
2 (medium)	10
3 (large)	20

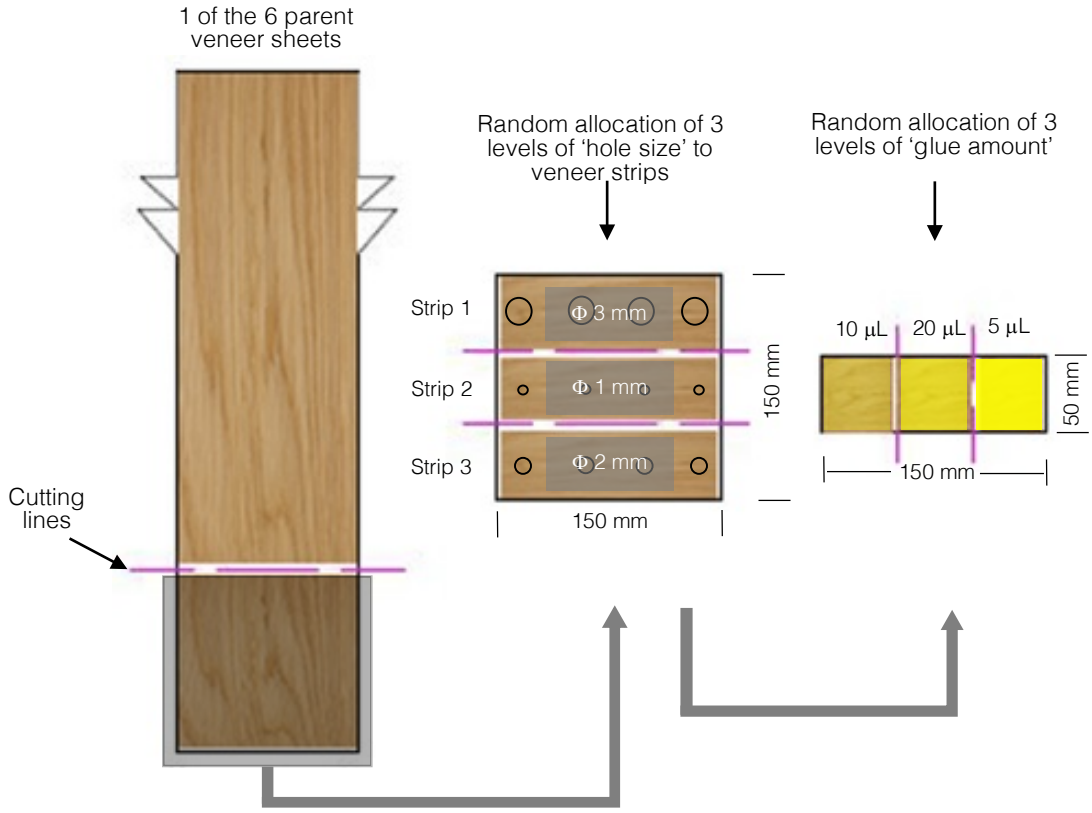

Figure 3.1 Schematic diagram of the split-plot experimental design used to examine the effects of two factors on the performance of adhesive Z-connections in a model wood composite

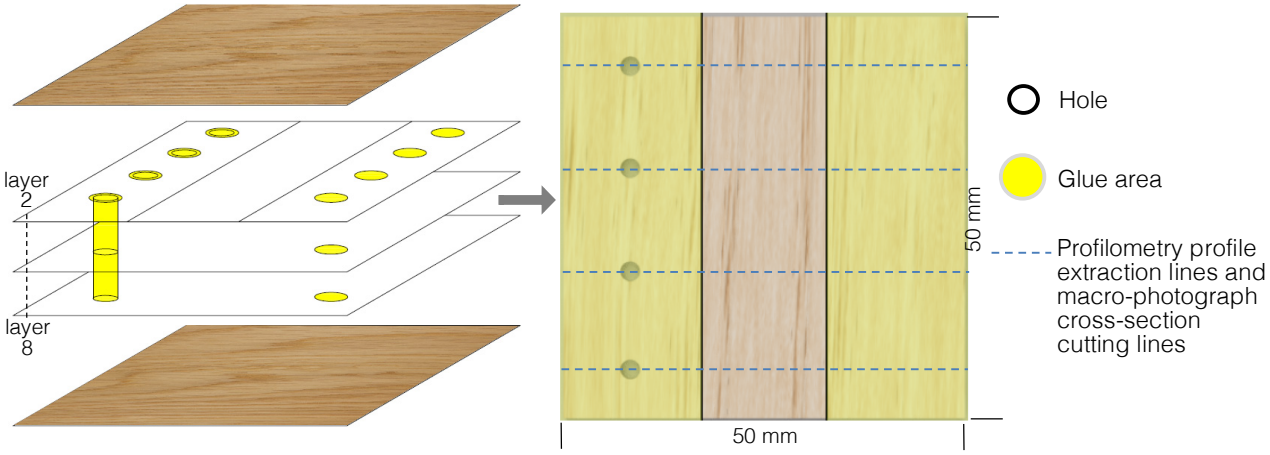

Figure 3.2 Schematic illustration of the structure of the model wood composite consisting of 7 core perforated veneers and two intact surface veneers. Each of the 7 perforated veneers had 3 sections: from left to right: holes & glue; no holes & no glue; no holes & only glue

3.2.2 Preparation of wood veneer and veneer perforation

Six birch (*Betula alleghaniensis*) veneer sheets (representing six blocks) measuring 15 cm (width) x 200 cm (length) with a thickness of 1 mm were purchased from ENE Wood Product (Surrey, BC, Canada) and stored in a conditioned environment (20 ± 1ºC temperature and 65 ±

5% relative humidity) for one month to ensure they reached equilibrium moisture content and stable dimensions before experimentation. The first veneer sheet (block #1) was then cut into nine pieces (each model composite specimen consisted of nine veneer laminae) measuring 150 mm x 150 mm using a desk-top band saw (Ryobi® B5902). Each of the nine pieces was then cut into three veneer strips measuring 50 mm x 150 mm using a paper cutter (Boston™ 2658) as shown in Fig. 3.1. Each of the three veneer strips was further cut into three veneer squares measuring 50 mm x 50 mm using the paper cutter (Fig. 3.1). Finally, a total of 9 x 9 = 81 veneer squares were prepared. They were all stored in the same conditioned environment, as above, for seven days.

All the veneer squares from block #1 were then perforated as shown in Fig. 3.2, with the exception of the top and the bottom veneers of each composite, which were not perforated (Fig. 3.2). Wood veneers were perforated with holes of different sizes. Small holes (1 mm in diameter) were drilled using a micro-hand drill (Fig. 3.3). Medium (2 mm in diameter) and large (3 mm in diameter) holes were created using a corded electric drill (Fig. 3.3). A method was developed to ensure that the seven core veneers were accurately aligned in the Z-direction and fixed while holes were drilled (Fig. 3.3). This method ensured that holes were perfectly aligned in the Z-direction, as desired (Fig. 3.2).

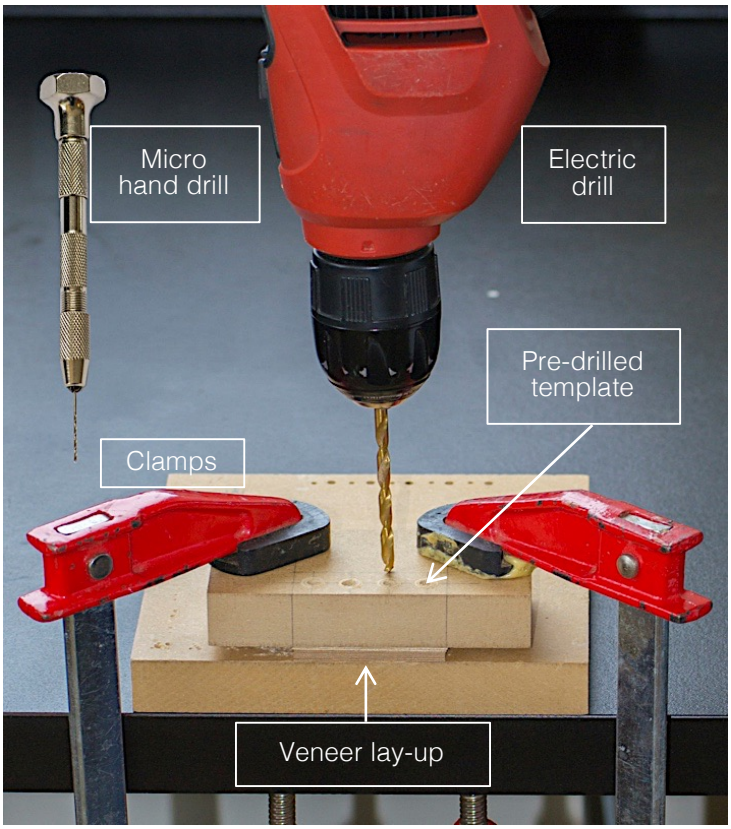

Figure 3.3 Drilling procedure to create Z-direction holes in veneers using either a micro hand drill (for small (1 mm diameter) holes) or an electric drill (for medium (2 mm) and large (3 mm) holes). Pre-drilled MDF templates with different hole diameters were used on top of the veneers to ensure accurate alignment of holes in the Z-direction

3.2.3 Adhesive application and preparation of model wood composites

Perforated veneer squares were stored in the conditioned environment described above for two weeks. Adhesive was applied to veneers and the assembly of veneers was pressed. A polyurethane adhesive (5, 10, or 20 µL), Gorilla® glue (The Gorilla Glue Company, Cincinnati, Ohio, USA), was applied onto each veneer using a syringe (BD® 1 mL syringe) (Fig. 3.4). The adhesive resin droplet was applied using the syringe onto the 'glue & holes' section. The same amount of adhesive was applied onto the 'glue & no holes' section. The glue was then spread evenly and quickly across each section using a glass coverslip (Matsunami®). This procedure ensured that the same amount of adhesive was applied to each of the matching sections on the same veneer square. Gorilla glue was chosen because it cured in the presence of moisture at

room temperature and flowed to form adhesive Z-connections, as mentioned above. Hence, there was no need to add catalyst or to use elevated temperatures to cure the glue. Furthermore, polyurethane adhesives are being increasingly used to manufacture wood composites (Dunky 2002). Technical information on the adhesive is listed in Tables 3.2 & 3.3.

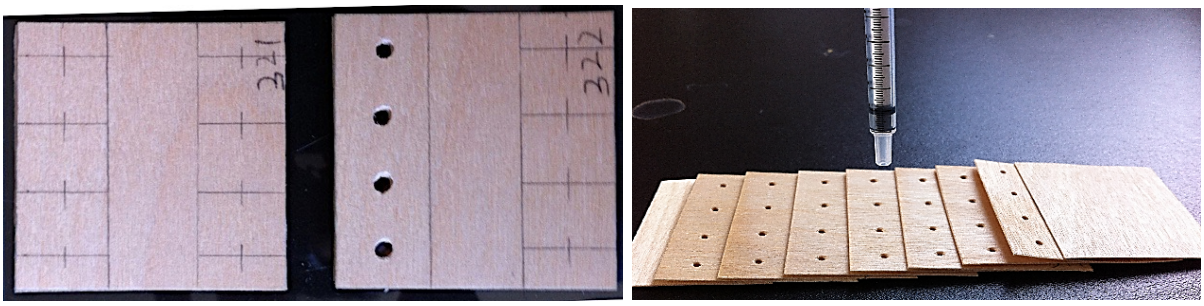

Figure 3.4 Adhesive application on veneer squares using a 1 mL syringe to control the adhesive application rate. There were two types of veneers for each model composite: 2 unperforated surface veneers and 7 core veneers containing perforations

Table 3.2 Chemical composition of the polyurethane adhesive (Gorilla® glue)

Composition	Product CAS number	Percentage (w/w)
Polyisocyanate Prepolymer based on MDI	(CAS No) 67815-87-6	40~70
Polymeric Diphenylmethane Diisocyanate (pMDI)	(CAS No) 9016-87-9	10~30
4,4'-Methylenediphenyl diisocyanate	(CAS No) 101-68-8	10~30
Diphenylmethane Diisocyanate (MDI) Mixed Isomers	(CAS No) 26447-40-5	1~5
Additive	(CAS No) Trade Secret	0.1~1

Source: Gorilla Glue NA GHS SDS (http://www.gorillatough.com/sds)

Table 3.3 Basic physical and chemical properties of the polyurethane adhesive (Gorilla® glue)

Physical and chemical properties	State/Value
Physical state	Liquid
Boiling point	208°C
Flash point	> 93°C
Vapor pressure	<0.0001 mm Hg at 25°C
Density	1.138 g/cm^3 at 20°C

Source: Gorilla Glue NA GHS SDS (http://www.gorillatough.com/sds)

After adhesive application, all the nine veneer squares were laid up with their grain direction parallel to each other to make one laminated wood composite. Each composite was placed in a small laboratory press (Carver® hydraulic press 3912, Fig. 3.5) and pressed one at a time at room temperature at a pressure of 15.7 MPa for 8 minutes. The resulting composites were then stored in a conditioned environment at 20 ± 1ºC and 65 ± 5% r.h. for three days.

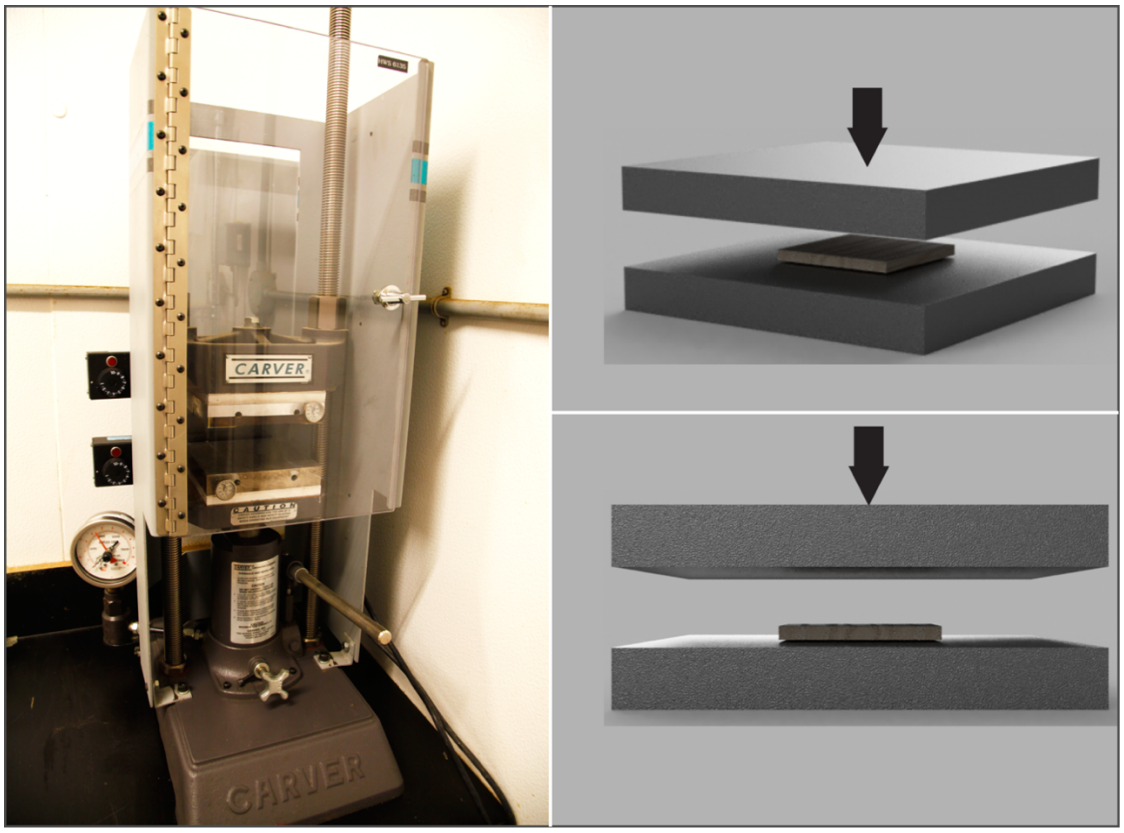

Figure 3.5 A photograph of the small hydraulic press (left) used to press wood composites, and schematic illustration (right) of the two press platens (plates) with a composite specimen in between

3.2.4 Water soaking, re-conditioning and measurement of differential thickness swelling using confocal profilometry

Replicate composite specimens made from the first veneer sheet were submerged in water to a depth of 2 cm. Rubber bands were used to keep specimens submerged for 24 h in a tank measuring 150 cm x 80 cm x 60 cm as recommended in ASTM standard D7519 (Fig. 3.6).

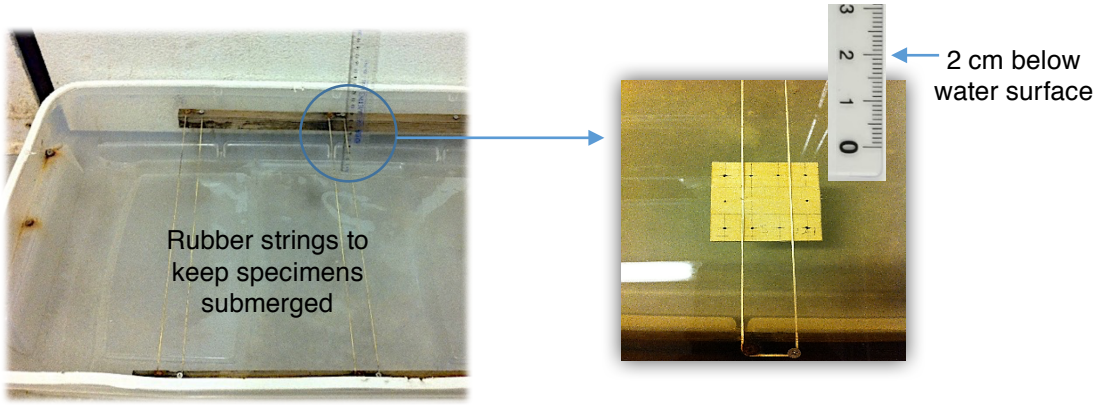

Figure 3.6 Water immersion of the composite specimens. Note the use of rubber bands to keep specimens submerged in water to a depth of 2 cm

Composite specimens were removed from the water tank after 24 h and then re-conditioned for two weeks. Surface topography of the re-conditioned specimens was then measured using confocal profilometry (AltiSurf® 500, Altimet, France). Confocal profilometry operates as follows: Light passes through a lens with chromatic aberration and is split into different components with different wavelengths (Fig. 3.7). Light with a certain wavelength (μm) is focused on a point at the surface of the material and reflected back (Browne et al. 1992). A detection device transforms the reflected light signal into an electrical signal that is then recorded by a computer. The central wavelength of this monochromatic light corresponds to the exact height of the measured point (see http://nanovea.com/chromatic-confocal). By electromechanically regulating the object's surface in the x and y directions, the 3D topography of the scanned surface can be reconstructed with a resolution of 2 nm in the Z (height) direction of the probe (Altimet 2007). Confocal profilometry was used to generate topography maps of the surface of composite specimens after water immersion and re-conditioning. The maps were used to visualize thickness differences across each composite specimen.

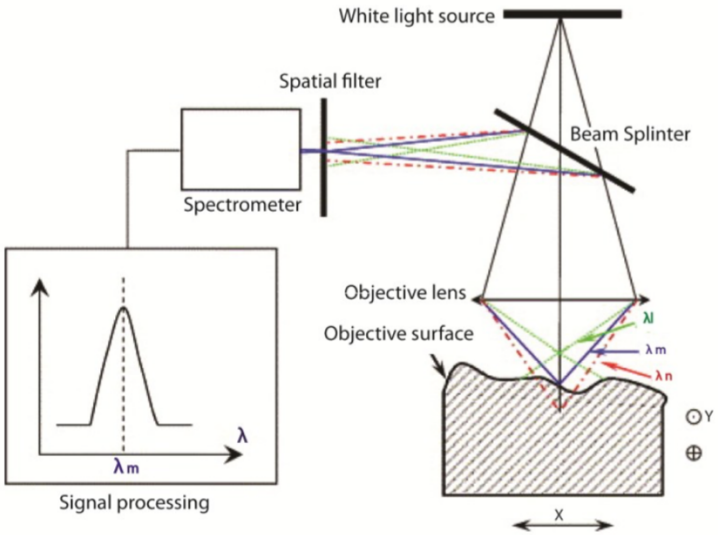

Figure 3.7 Principles of confocal profilometry (Altimet: http://www.altimet.fr/?page_id=1591&lang=en)

Line profiles were extracted from the surface topography maps using image analysis software, AltiMap® 6.2 (Altimet, France). Four line profiles per specimen were extracted (Fig. 3.2) and used to quantify differential thickness swelling (DTS) of the specimens. Differential thickness swelling is defined as the swelling difference between the glued sections with and without holes on a same specimen (Fig. 3.2 & 3.8). This measure of differential thickness swelling indicated whether the adhesive Z-connections restricted thickness swelling of the model composite. Greater differential thickness swelling values indicate that adhesive Z-connections were better at restraining thickness swelling.

The aforementioned procedures were repeated on composites made from the 2nd parent veneer sheet and so on until differential thickness swelling measurement were made on composites made from all six parent veneer sheets.

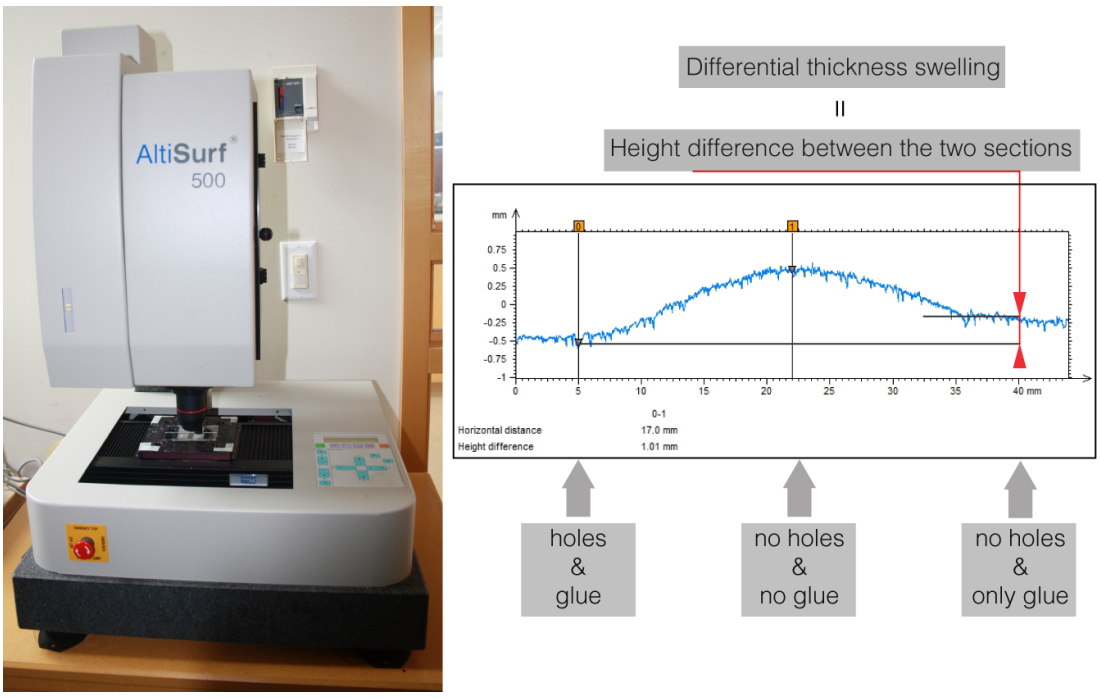

Figure 3.8 Confocal profilometer (left) used to measure the surface topography of composites after water immersion and re-conditioning, and the method of calculating differential thickness swelling (right)

3.2.5 Visualization of the adhesive Z-connections in the model wood composites using macro-photography

Model composites (laminates) were cut using a desk-top band saw along a line that was very close to a profilometry profile scan (Fig. 3.2). Then the cross-sections were carefully sliced using a hand-held, single-edged, razor blade while being viewed under a stereo-microscope until the adhesive Z-columns were completely exposed. Then a digital single lens reflex (DSLR) camera (Canon® EOS 5D Mark II) equipped with a macro lens (Canon® Macro Photo MP-E 65 mm lens) and mounted on a Polaroid® MP4 Land Camera Stage was used to photograph cut surfaces. Four halogen lights (150 Watt each, Sylvania®) were mounted around the stage to illuminate the cross-sections. The camera used an aperture setting of F/8, optical zoom-in 5 x, and ISO 100. Tethering capture used Cannon® EOS Utility software on a laptop computer, which enabled remote camera control for maximum macro-photograph quality. All the macro-photographs were saved as RAW files and processed using Adobe® Photoshop® Raw processor and then saved as TIFF files.

3.2.6 Statistical analysis

Analysis of variance (ANOVA) was used to examine the fixed effects of three levels of hole size and three levels of glue amount and random effects on the differential thickness swelling of the model wood composites. Statistical computation used Genstat® (Release 17.1). Mean values are plotted on graphs and error bars representing least significant difference (LSD) are included on graphs to assess whether difference between individual means are statistically significant ($p < 0.05$).

3.3 Results

3.3.1 Effects of the adhesive Z-connections on restraining thickness swelling of model wood composites

Surface topography maps show that the section of the composites with adhesive Z-connections swelled less compared to the section with no Z-connections after 24 h water immersion and re-conditioning (Fig. 3.9).

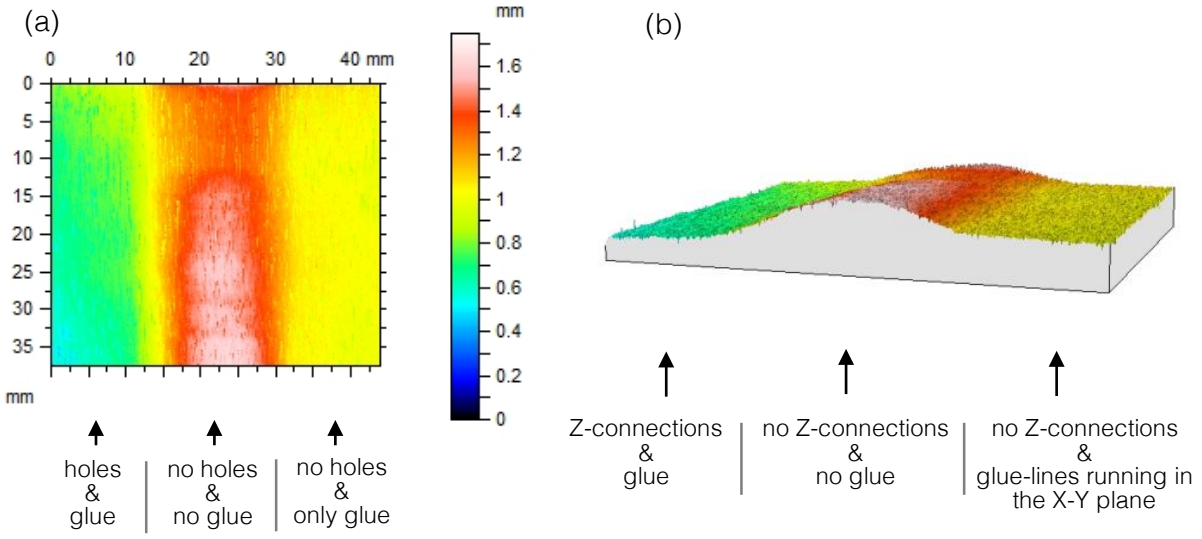

Figure 3.9 Colour-coded profilometry height maps of a composite specimen after 24 h water immersion and re-conditioning: (a) 2D view of the top of the composite; (b) 3D view showing the height difference between the different sections on the same composite specimen

3.3.2 Effects of different hole sizes and quantity of glue on differential thickness swelling

The effects of all of the nine treatments (hole size x glue amount) on differential thickness swelling of the model wood composites are summarized in Fig. 3.10. Differential thickness swelling is defined as the swelling difference between the glued sections with and without holes on a same specimen. In other words, a larger differential thickness swelling indicates that the adhesive Z-connections were more effective at restraining thickness swelling. This figure also shows the variation within each treatment. Composites with smaller holes (1 mm diameter) showed relatively small variation in the thickness swelling across the three

different levels of glue amount. In contrast, composites with the largest holes (3 mm diameter) showed relatively large variation. The 10 µL glue level in combination with 1 mm (small) hole size generally had the lowest variation indicating a consistent effect of this treatment.

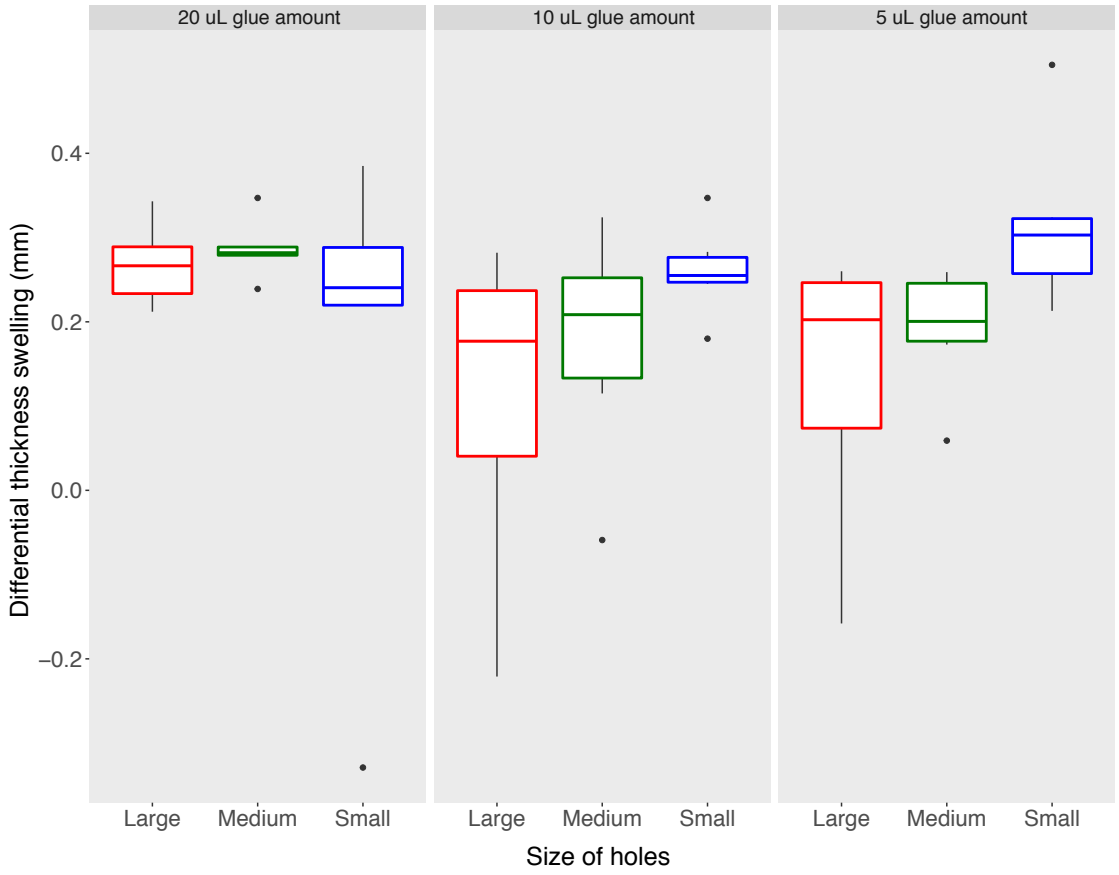

Figure 3.10 Differential thickness swelling (DTS) of model wood composites after 24 h water immersion and re-conditioning. Note the variation within each treatment. Diameter of holes were 3 mm (large), 2 mm (medium), or 1 mm (small)

There was a significant ($p = 0.02$) effect of level of glue (20, 10 or 5 µL) on the differential thickness swelling of the model wood composites. The effect of diameter of the Z-connections approached statistical significance ($p = 0.06$). However, there was no significant ($p = 0.2$) interaction of glue level and diameter of Z-connections on swelling. Therefore, the effect of each of the factors on thickness swelling is examined separately (Figs. 3.11 & 3.12). The highest level of glue (20 µL/hole) produced the largest differential thickness swelling, which was significantly greater than that of composites containing 10 µL of glue per hole (Fig. 3.11).

Composites with the narrowest Z-connections (Φ1 mm hole size) had the greatest differential thickness swelling of 0.28 mm compared to composites with wider Z-connections (Φ2 mm hole size = 0.22 mm and Φ3 mm hole size = 0.17 mm) (Fig. 3.12).

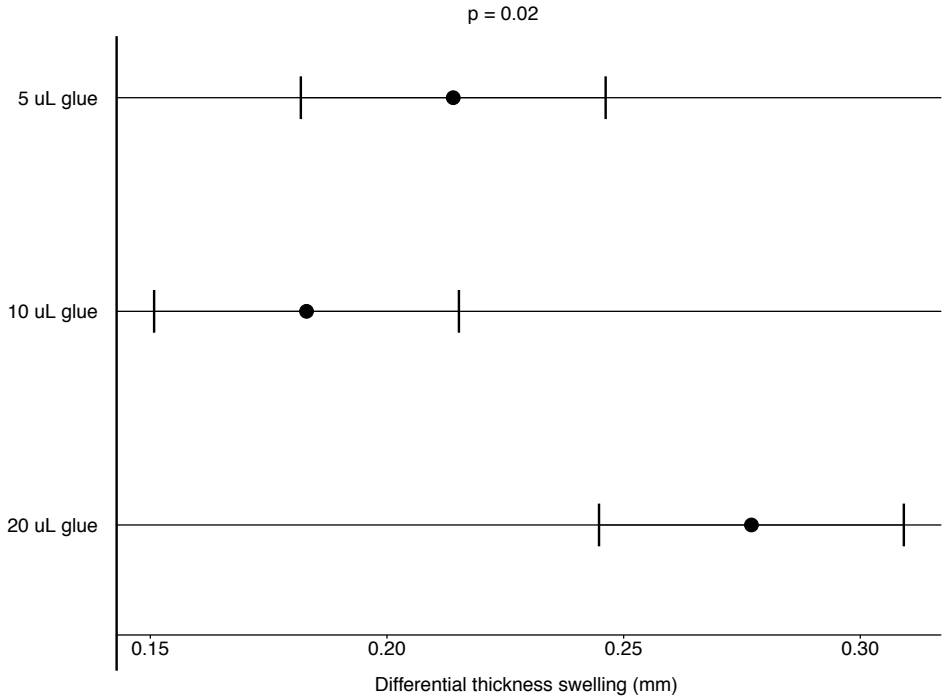

Figure 3.11 The effects of different levels of glue on differential thickness swelling of the model wood composites. Error bars represent ± standard error of difference which can be used to assess whether differences between means are statistically significant ($p < 0.05$)

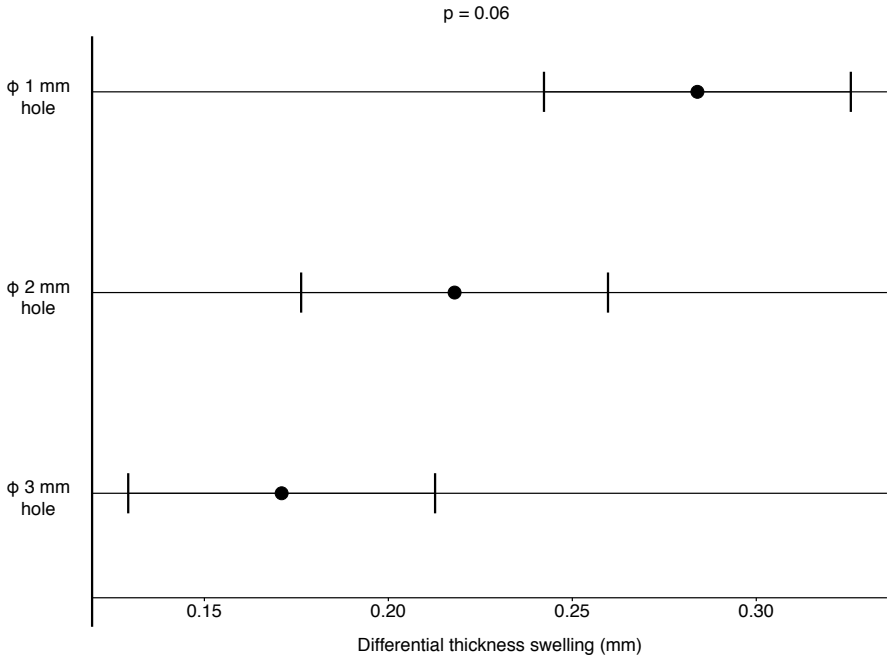

Figure 3.12 The effects of the different diameters of Z-connections on differential thickness swelling of the model wood composites. Error bars represent ± standard error of difference

3.3.3 Macro-photographs of the adhesive Z-connections in the model wood composites

Macro-photographs of the cross-sections of the model wood composites clearly showed the presence of the adhesive Z-connections in the perforated section (Figs. 3.13 & 3.14). The 1 mm diameter Z-column is completely filled with cured adhesive and voids are rarely present (Fig. 3.13). In contrast, voids are more common in the 3 mm diameter adhesive Z-connection (Fig 3.14).

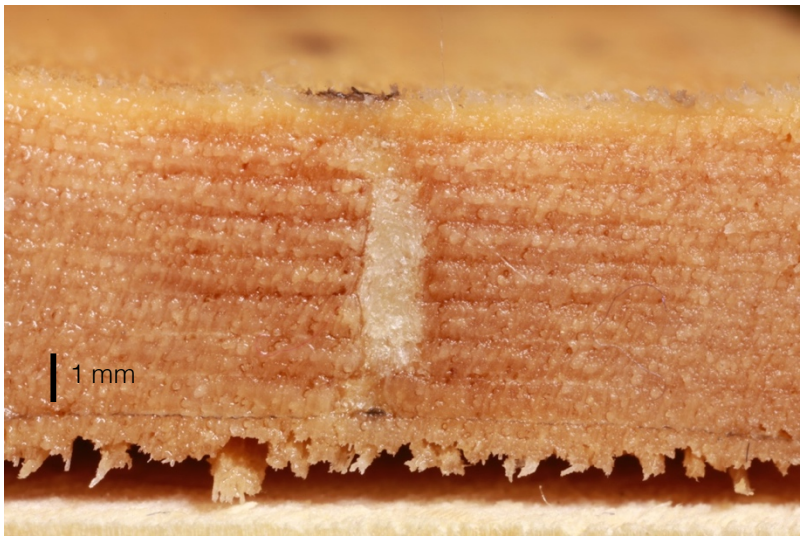

Figure 3.13 Macro-photograph of a cross-section of a perforated section of a model wood composite containing a 1 mm diameter adhesive Z-connection. Note that voids are absent from the Z-connection

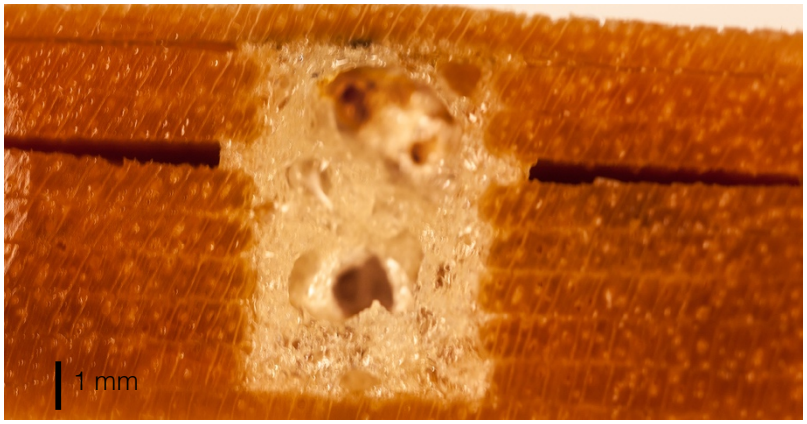

Figure 3.14 Macro-photograph of a cross-section of a perforated section of a model wood composite containing a 3 mm diameter adhesive Z-connection. Note the 3 mm diameter hole is not completely filled with adhesive and voids are present in the adhesive Z-connection

3.4 Discussion

This chapter describes the preliminary research that developed the methodology that is refined in subsequent chapters. Macro-photographs clearly showed the presence of adhesive Z-connections in holes that were aligned in the Z-direction of the composite. This observation supports the approach of drilling holes in wood veneers to facilitate the creation of adhesive Z-connections. The Z-connections appeared to restrain the thickness swelling of the wood

composite, but the effectiveness of the Z-connections varied depending upon the amount of adhesive used to create the Z-connections. The diameter of the holes used to create Z-connections was inversely correlated with restraint of swelling, but ANOVA indicated that the effect of hole size on differential thickness swelling was not statistically significant ($p = 0.06$). Nevertheless, these findings are important because one of the goals of this preliminary research was to hone in on design parameters (hole size & glue amount) for Z-connections that can restrain thickness swelling. Results suggested that the Φ1 mm hole size rather than larger holes favoured the creation of adhesive Z-connections that were effective at restraining thickness swelling (Fig. 3.11). The greater effectiveness of smaller diameter holes at restraining swelling may be related to the ability of the adhesive to completely fill the Z-columns without leaving voids in the columns. Therefore, continuity of the adhesive in the Z-columns appears to favour their ability to restrain thickness swelling. Therefore, 1 mm diameter holes were used for subsequent experimentation. Another issue favouring 1 mm diameter holes is that their use minimizes the impact of removing wood on the structural integrity of the composites. The combination of Φ1 mm hole size and 10 µL of glue amount per hole worked well at restraining swelling. Furthermore, I observed that when higher levels of glue (20 µL/hole) were used, the glue flowed out of the holes. There was no significant difference in the differential thickness swelling of composites containing 5 or 10 µL of glue per hole (Fig. 3.11). However, there was less variability in the differential thickness swelling of composites with small holes and 10 µL of glue per hole compared to those with 5 µL of glue per small hole (Fig. 3.10). Hence, I selected 10 µL of glue per hole (an application rate of 0.05 µL/mm^2 (4 x 10 µL/800 mm^2)) for subsequent experimentation.

Clearly, drilling holes in wood veneers encouraged the creation of adhesive Z-connections in glued wood composites. However, holes drilled using both the micro-hand drill and also the electric drill had rough edges, and it was difficult to produce holes that were all the

same diameter and precisely aligned in the Z-direction. Therefore, I explored other methods of perforating veneers. After several trials, I selected high-speed dental drilling as a preferred method of drilling holes in arrays of veneer. Dental drilling employed a precision drill (W&H® Trend WD-56) with a Φ1 mm drill bit (Dentsply® TN) connected to a control motor (Dentsply® DTC). This drill operated at 6000 rpm rotary speed and 100 g/cm of torque and was able to accurately drill holes with a consistent diameter of 1 mm. This system produced accurately-sized, smooth, cylindrical 1 mm diameter holes in wood veneers. Thus, this micro-hole drilling procedure was adopted for all subsequent experimentation.

Results in this chapter also demonstrated that confocal profilometry was able to accurately measure small differences in thickness swelling of the wood composites with Z-connections and also the controls. Confocal profilometry also produced colour-coded surface height maps of the wood composites which made it possible to visualize surface topography of the composites. Macro-photography was also useful for visualizing the adhesive Z-columns in the wood composites. However, scanning electron microscopy and X-ray micro-computed tomography might provide more detailed information on the morphology of the Z-columns and the 3D inter-connected adhesive network.

3.5 Conclusions

In the Introduction, I suggested that drilling holes in wood veneers would encourage the formation of adhesive Z-connections when an assembly of perforated and resinated veneers were pressed together. My results support the feasibility of this approach and have successfully established some key design parameters that facilitate the creation of adhesive Z-connections in a model wood composite. In summary, these key design parameters are:

(1) High-speed precision drilling is needed to accurately and consistently produce smooth-walled, cylindrical holes in assemblies of wood veneers;

(2) A suitable diameter of holes for adhesive Z-connections to be able to restrain thickness swelling of the model wood composite was 1 mm;

(3) The preferred adhesive application rate for the adhesive to penetrate the Z-columns created by drilling was 0.05 μL/mm^2 (10 μL/hole) at each veneer surface;

The procedures developed in this Chapter were adapted and refined in subsequent experimentation described in Chapters 4, 5, 6 and 7.

4 Effects of Adhesive Z-connections on the Thickness Swelling of a Model Wood Composite Made from Commercial Wood Veneers

4.1 Introduction

My thesis is that the dimensional stability and fracture toughness of wood composites can be enhanced by altering the geometry of the adhesive network in the composites so they are better able to resist the strains that develop when the composites are exposed to water or subjected to mechanical testing.

In this chapter, I refine the methodology developed in Chapter 3 to test the specific hypothesis that the creation of Z-direction adhesive connections will restrain the moisture-induced thickness swelling of a model wood composite.

4.2 Materials and methods

4.2.1 Veneer preparation and perforation

Twenty rotary-cut (tangential) white spruce (*Picea glauca* (Moench) Voss), yellow birch (*Betula alleghaniensis* Britton) veneer sheets and a similar number of sliced (radial) yellow cedar (*Cupressus nootkatensis* D. Don) sheets, measuring 15 cm (width) x 225 cm (length) were purchased from a local retailer of commercial veneer (ENE Wood Products, Surrey, BC, Canada). The thickness of the white spruce, yellow birch and yellow cedar veneer were 0.87 mm, 0.65 mm and 1.09 mm, respectively. Six sheets were selected for each species and stored in a conditioned environment (20 ± 1ºC temperature and 65 ± 5% relative humidity) for one month. Samples measuring 25 mm x 25 mm square were cut from each of the six conditioned sheets using a paper cutter (as described in Chapter 3). A veneer species was selected at random and fourteen veneer squares were selected at random from the first veneer sheet and allocated to two different types of model composites, each consisting of seven veneer squares: (1) Composite composed of perforated veneer squares; (2) Composite composed of unperforated veneer squares (control). Veneer squares were perforated with a hand-held high-

speed dental drill (W&H® Trend WD-56) with a 1 mm diameter drill bit (Dentsply® TN burr) operating at 6000 rpm with 100 g/cm of torque (Fig. 4.1).

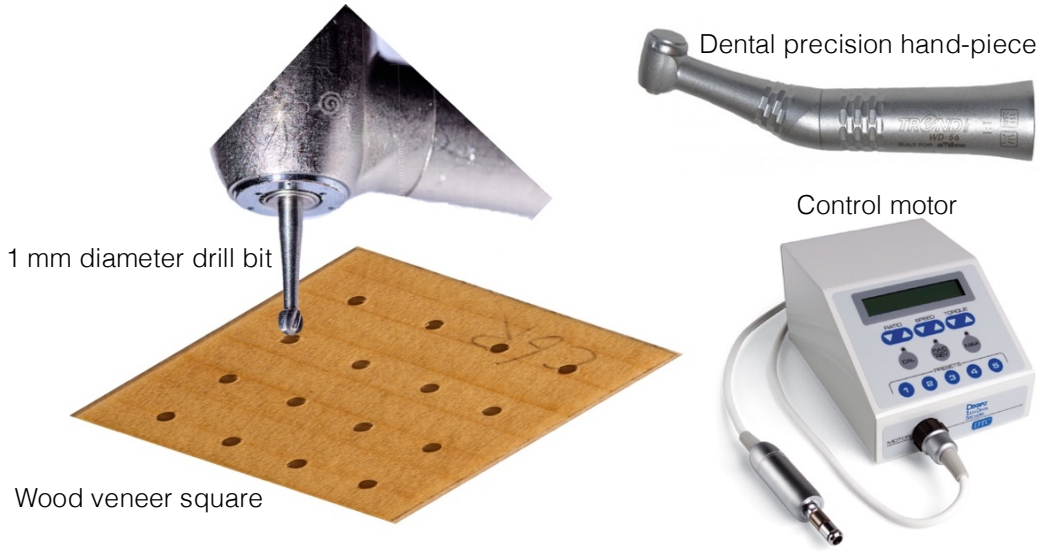

Figure 4.1 Micro-hole drilling of wood veneer used a high-speed precision dental drill to produce smooth holes in wood veneers with accurate and consistent diameter

The drill produced accurately sized, smooth, cylindrical, 1 mm diameter holes in the veneer. Seven veneer squares were placed in a customised mould to align them vertically and all seven were perforated together in the mould (Fig. 4.2a). The spacing between holes was 5.5 mm (Fig. 4.2b). All the perforated and unperforated veneer squares were stored in a conditioned environment (as above) for seven days.

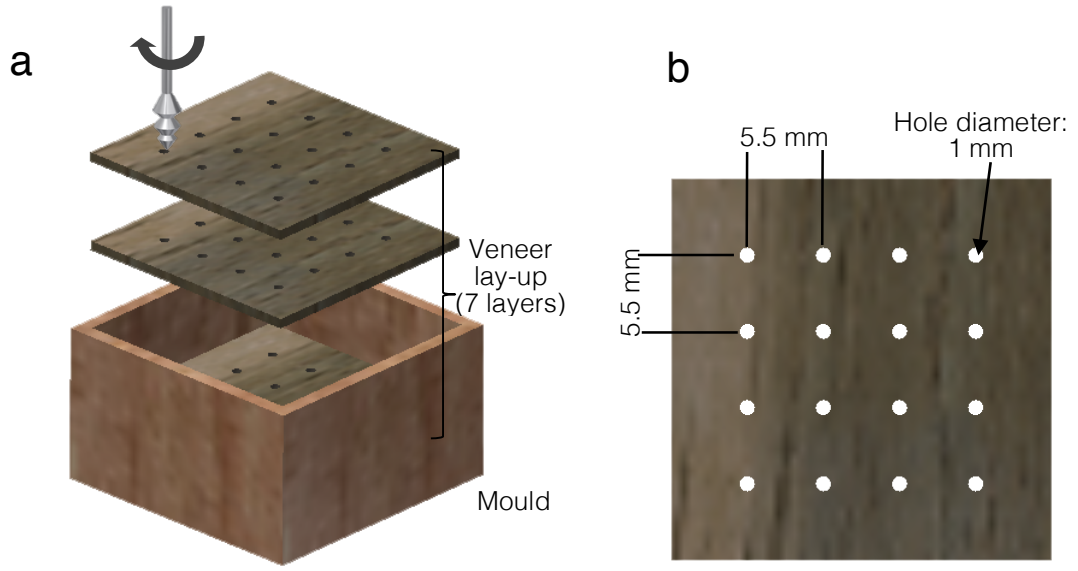

Figure 4.2 Schematic illustration of (a) veneer lay-up in the mould during drilling, and (b) hole size and pattern in each veneer square

4.2.2 Adhesive application and pressing of composites (laminates)

Two matching groups of perforated or unperforated veneer squares cut from the same parent veneer sheet were selected, and 0.044 g ± 0.0005 g (40 µL) of a polyurethane adhesive (Gorilla glue®) was applied to each veneer using a syringe and evenly spread across each veneer square surface using a glass coverslip (as described in Chapter 3). The same amount of adhesive was applied to perforated and unperforated veneers. Veneers were laid up with their grain direction parallel to each other to make model composites containing either perforated or unperforated veneer squares. Composites were placed in a small laboratory press and pressed at room temperature at 13.8 MPa for eight minutes, as described in Chapter 3. The resulting composite specimens were conditioned at 20 ± 1ºC and 65 ± 5% r.h. for three days and the thickness of each specimen was measured in 12 places using a digital calliper. The average thickness of composites (with and without adhesive Z-connections) made from the three species is summarized in Table 4.1.

Table 4.1 Thickness of pressed composites made from the three different wood species

Species	Thickness of pressed composites (mm)						
	Block 1	Block 2	Block 3	Block 4	Block 5	Block 6	**Average**
White spruce	4.12	4.46	4.39	4.27	4.34	4.29	**4.31**
Yellow cedar	5.99	6.17	5.82	5.96	5.94	5.98	**5.98**
Yellow birch	4.00	3.99	3.91	4.06	3.99	3.87	**3.97**

4.2.3 Measurement of absolute thickness swelling and differential thickness swelling

Composite specimens from the first veneer sheet for each species were submerged in water to a depth of 1 cm for 24 h in a tank measuring 15 cm x 8 cm x 6 cm. Afterwards they were reconditioned for three days and their thicknesses were re-measured, as above. The percentage increase in thickness of the conditioned composite specimens (mm) was calculated. The changes in surface topography of the conditioned specimens after immersion in water and drying was measured using confocal profilometry, as described in Chapter 3. The model composites (perforated and unperforated control) for each species and veneer sheet were placed together on the stage of a confocal profilometer and the heights of the entire surface of each specimen were measured with a 3 mm probe at a scanning speed of 6 mm/s. The spacing between measurement points was 10 µm x 10 µm (x and y-directions) and the accuracy of measurements in the Z-direction was 0.00033 µm, according to the manufacturer of the profilometer. Following these area scans, separate line scans along the four rows of holes in x and y directions in each specimen were also carried out using the same instrument parameters used for the area scans (Fig. 4.3). Height information from all the scans was imported into image analysis software (AltiMap® Premium v. 6.2.) in a PC. This software was used to obtain topographical information on the model wood composites including the difference in swelling of the wood and Z-connections (adhesive plugs), and also to produce colour-coded height maps of

the surface of the composites. Once all measurements were completed on composites produced from the first veneer sheet for each species, the process was repeated for composites produced from sheet #2 and so on until measurements of irreversible thickness swelling on composites from all 6 sheets per species were completed.

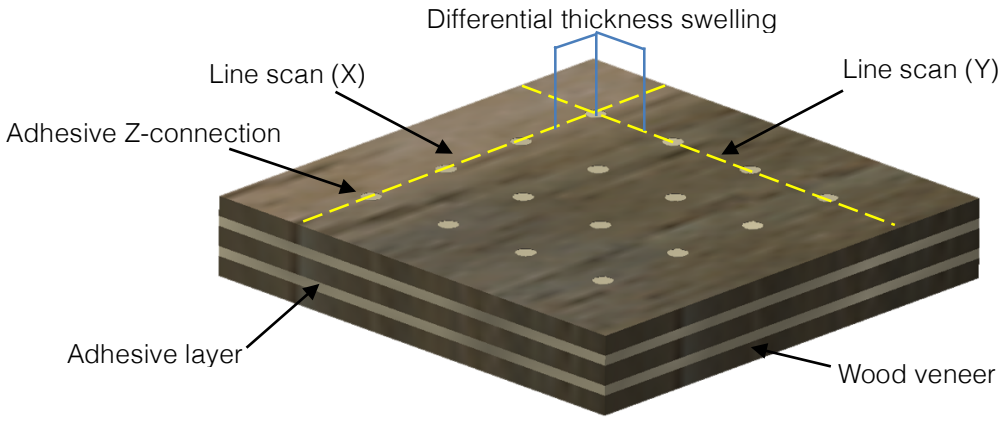

Figure 4.3 Schematic view of part of a perforated model composite showing wood veneers, adhesive layers and Z-connections as well as profilometry profile line scans

4.2.4 Scanning electron microscopy, X-ray micro-computed tomography and macro-photography of the adhesive network in the model wood composite

A separate set of composites (one perforated and one unperforated for each species) were prepared as above except the polyurethane adhesive contained 2% w/w of a fine copper-zinc alloy powder (Metal Effects® Deep Gold). Composites were soaked in water and reconditioned as above. A small specimen measuring 10 x 6.5 mm was sawn from the centre of each composite specimen using a small desk-top band saw (Ryobi® B5902). The specimens were clamped one at a time in a small vice and cut with a hand-held, single-edged, razor blade while being viewed under a stereo-microscope. Specimens were stored over silica gel for two days, trimmed to a final size of 8.5 (length) x 5 (height) mm and mounted on aluminium stubs using doubled-sided adhesive tabs (Electron Microscopy Sciences). Specimens were coated with a thin layer of gold and viewed using Hitachi 4300 Se/N or Zeiss UltraPlus analytical field emission scanning electron microscopes using an accelerating voltage of 15 kV, and working distances of 13.3 to 14.3 mm. The contrast between adhesive and wood was greatest when

images were formed from back-scattered electrons and therefore, we employed a back-scattered electron detector in addition to a secondary electron detector to image samples. Selected back-scattered and secondary electron images of the cross-sections of the composite specimens were saved as TIFF files.

X-ray micro-computed tomography (X-ray μCT) was used to probe the internal structure of a pair of model spruce wood composites. X-ray μCT can produce virtual cross-sectional images - tomograms - of the inner structure of materials, based on transmission measurements of penetrating X-ray ionizing radiation (Davis and Wells 1992; Freyburger et al. 2009). Each white spruce specimen (perforated vs. the control) was divided in two, and one half of each type was probed together using X-ray μCT. Micro-CT was performed in the Department of Applied Mathematics at The Australian National University. The X-ray μCT device consisted of an X-ray source (X-Tek RTF-UF225), rotation stage (Newport RV120PP), and a flat-panel X-ray detector (PerkinElmer XRD 1621 xN) with 2048 x 2048 pixel array mounted on a parallel rail (Sakellariou et al. 2004). Spruce composite specimens were placed together on the rotation stage, located 95 mm from the X-ray source, and probed with a polychromatic X-ray beam (Bremsstrahlung radiation) that was generated by a focused electron beam (60 kV, beam current of 140 μA). A charge coupled device (CCD) camera recorded the X-ray transmission radiograph (projection data) while the stage was rotated 360 degrees over a period of 20 hours. Projection data were processed with a Feldkamp-Davis-Kress (FDK) reconstruction algorithm to generate a tomogram (Feldkamp et al. 1984). The quality of the tomogram was optimized using a range of measures to overcome the limitations imposed by using a polychromatic X-ray cone beam (Feldkamp et al. 1984). The tomogram had sufficient quality to segment the wood and adhesive phases. Volume rendering of tomographic data was used to visualize the internal structure of the composites in three dimensions. Volume rendering used the software Drishti, which is an open source volume exploration and rendering tool for visualizing tomographic data

(http://sf.anu.edu.au/Vizlab/drishti) (version 2.0) (Limaye 2017). Thresholding of the density-related intensity histograms allowed separation of higher density adhesive (1.138 g/cm^3) from lower density wood (0.45 g/cm^3) and voids within composite specimens.

Composite specimens soaked in water and re-dried were also cross-cut to expose the Z-direction adhesive connections. The cross-sections were photographed using a single lens reflex camera with a macro lens, as described in Chapter 3.

4.2.5 Statistical analysis

The experiment was a randomized block design with six blocks (veneer sheets) and two fixed factors (sample type and wood species). Analysis of variance (ANOVA) was used to examine the effects of these fixed factors (and random effects) on the following parameters: (1) Percentage thickness swelling of composites (from calliper measurements); (2) Differential thickness swelling of composites from profilometry data. Statistical computation was carried out using GenStat® (17th edition). Significant results are presented in graphs that include error bars to estimate whether differences between means are statistically significant at the 5% level.

4.3 Results

4.3.1 Effects of adhesive Z-connections on reducing thickness swelling of the model wood composite

The Z-connections restricted thickness swelling of the yellow cedar and white spruce composites (Fig. 4.4). However, the effect of Z-connections on restraining thickness swelling of yellow birch composites was not significant ($p > 0.05$). The difference in thickness swelling of yellow cedar and white spruce was highly significant ($p < 0.001$), and there was also a significant ($p < 0.001$) interaction of Z-connections and species on thickness swelling because the Z-connections were ineffective at restraining thickness swelling of the yellow birch specimens (Fig. 4.4).

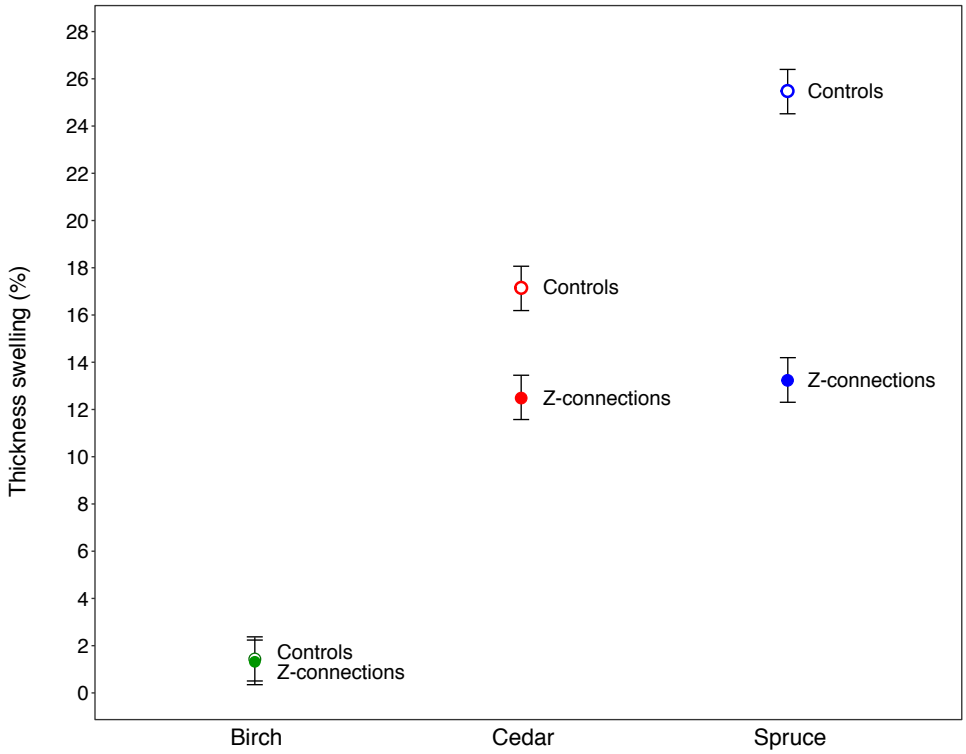

Figure 4.4 Thickness swelling of yellow birch, yellow cedar and white spruce specimens after immersion in water for 24h and re-drying. Note the difference in swelling of the specimens with Z-connections (filled symbols) compared to the controls (open symbols)

The restraining effects of the Z-connections on swelling was not uniform across the surface of the specimens as can be seen in Fig. 4.5. This figure shows confocal profilometry images of the surfaces of specimens after immersion in water and re-drying. The surfaces of the specimens containing Z-connections are not flat, and depressions (dimples) can be seen around individual Z-connections, indicating local restriction of thickness swelling. The dimples around the Z-connections are deeper and wider in white spruce than in yellow cedar, and much less noticeable in yellow birch (Fig. 4.5). Figure 4.5 also shows that the Z-connections restricted swelling along the grain (X-direction) to a greater extent than across the grain (Y-direction) especially in spruce. This effect was confirmed by the analysis of variance of differences in thickness swelling of specimens in the X and Y directions, which showed a highly significant ($p < 0.001$) interaction of Z-connections and wood species (yellow birch, yellow cedar and white spruce) on differential thickness swelling (Fig. 4.6).

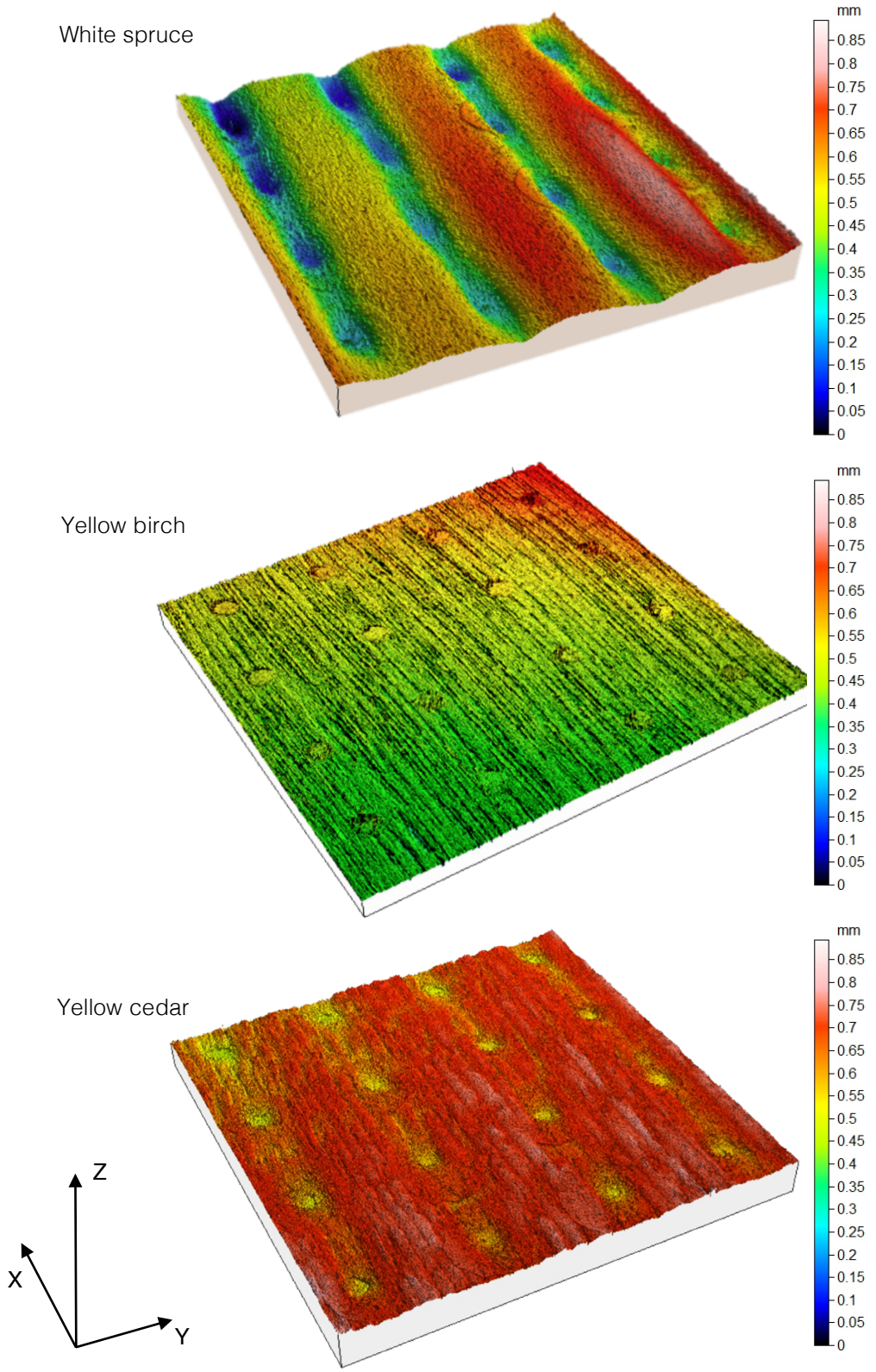

Figure 4. 5 Confocal profilometry scans of the surface of white spruce, yellow birch and yellow cedar specimens after immersion in water and re-drying. Note localised restraint of swelling around Z-connections

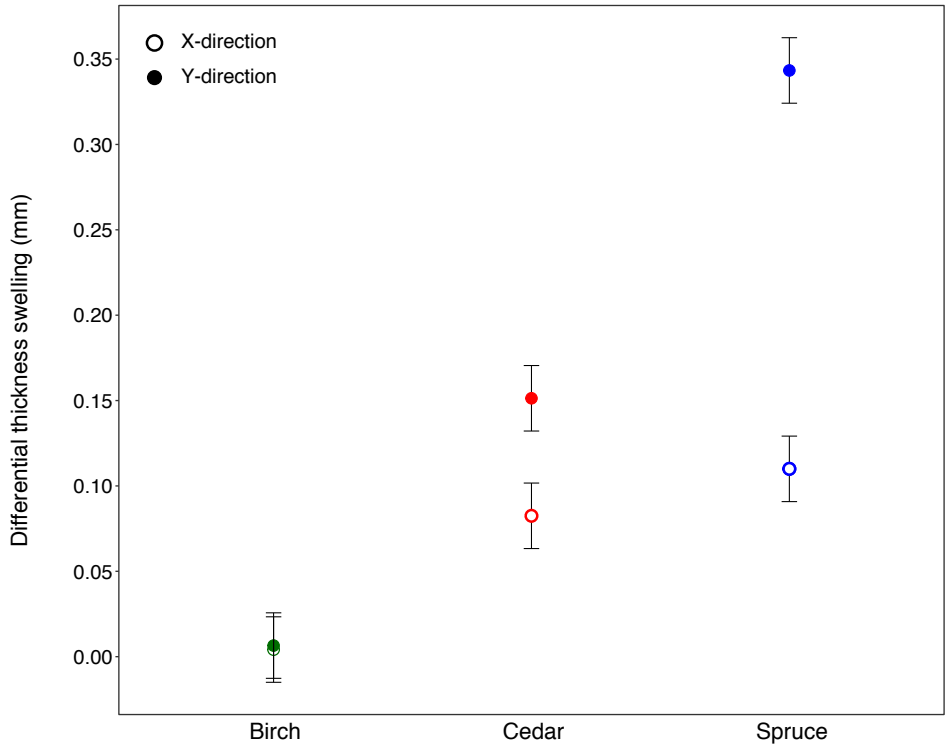

Figure 4.6 Difference in swelling of adhesive Z-connections and the adjacent wood along the grain (x-direction) vs. across the grain (y-direction)

4.3.2 Visualization of 2D and 3D adhesive distribution in the model wood composite

4.3.2.1 Macro-photography

Confocal profilometry revealed noticeable differences in swelling of the surface of the Z-connections (adhesive plugs) and adjacent wood in white spruce and yellow cedar. The difference was much less pronounced in yellow birch. The differential swelling of white spruce and yellow cedar specimens can be clearly seen in macro-photography images (Figs. 4.7a & b). These images also show that that there was delamination of individual veneers in the specimens (arrowed in Fig. 4.7). Such delamination was more pronounced in yellow cedar than in white spruce, which possibly accounts for the reduced effectiveness of the Z-connections at reducing thickness swelling of yellow cedar compared to spruce. Fig 4.7b shows that the adhesive Z-connections in yellow birch were not completely filled. There were considerably more voids present (arrowed in Fig. 4.7) in the adhesive Z-connections in yellow birch compared to white spruce and yellow cedar.

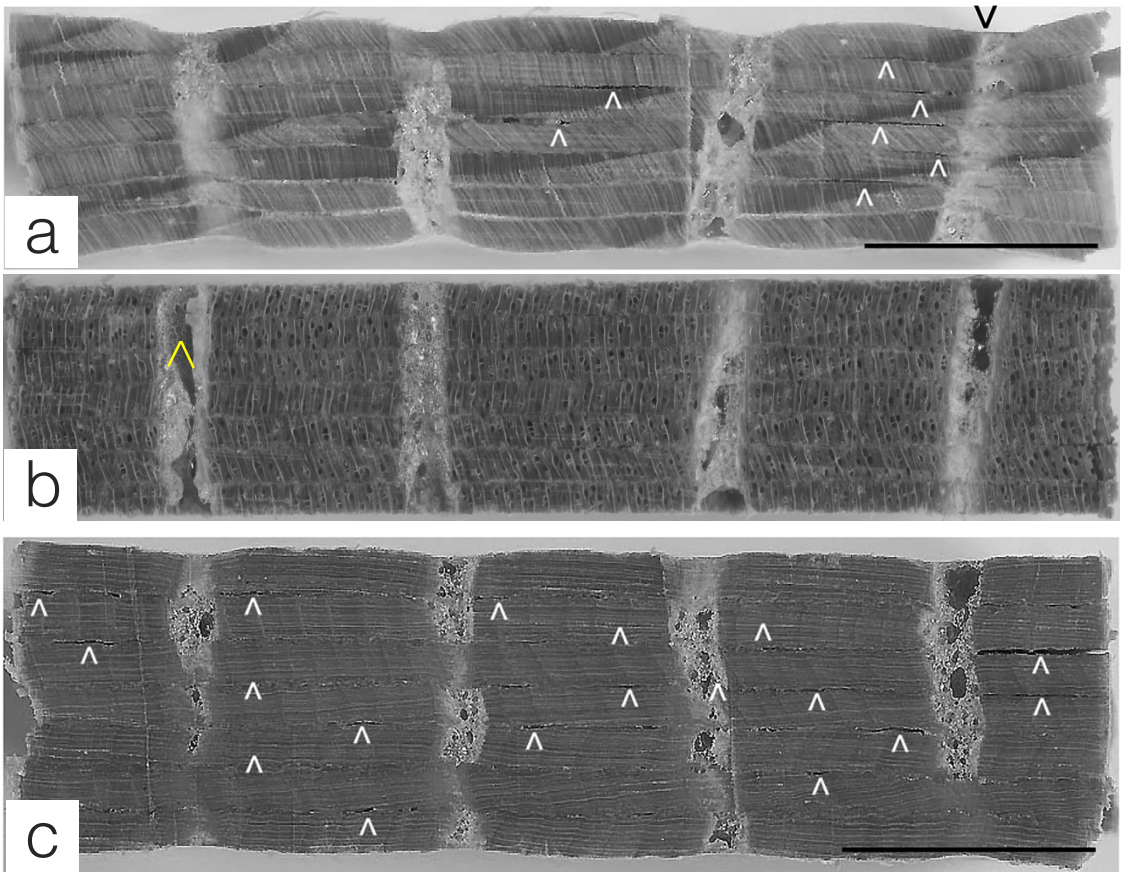

Figure 4.7 Macro-photography images of cross-sections of (a) white spruce, (b) yellow birch, and (c) yellow cedar specimens containing Z-connections after immersion in water and re-drying. White arrows indicate delamination of glue-lines, black arrows indicate lower restraint of swelling of latewood, and yellow arrow indicates voids in adhesive Z-connections. Scale bars = 5.5 mm.

4.3.2.2 SEM

Scanning electron microscope (SEM) images of adhesive Z-connections and horizontal glue-lines in yellow cedar and white spruce specimens are shown in Figure 4.8. This figure shows that the Z-connections in both the yellow cedar and white spruce specimens (Fig. 4.8a, c) restrained the swelling of the wood adjacent to the Z-direction adhesive connection. However, the Z-connections did not restrain the swelling of yellow birch specimens (Fig. 4.8e). The horizontal glue-lines that bond individual veneers together are clearly visible and remain connected to the adhesive Z-connection in a white spruce specimen (Fig. 4.8c). Furthermore, there is less delamination of glue-lines in white spruce than in yellow cedar and yellow birch (Fig. 4.8a~f). Whereas, delamination is more common in a yellow birch specimen (Fig. 4.8e~f),

which may be, in part, due to penetration of adhesive into vessel elements adjacent to the horizontal glue-lines at the bonding interface in birch composites (Fig. 4.8f). Figure 4.8 confirms what is readily apparent in Figs. 4.4 and 4.6 that the Z-direction adhesive connections were less effective at restraining swelling of yellow cedar than white spruce specimens. Figure 4.8c shows that such restraint in white spruce was associated with deformation of low density earlywood that is adjacent to the Z-direction adhesive connection. There is some deformation of earlywood immediately adjacent to the Z-direction adhesive connection in the yellow cedar specimen (Fig. 4.8a), but it is far less pronounced than that in the white spruce specimen.

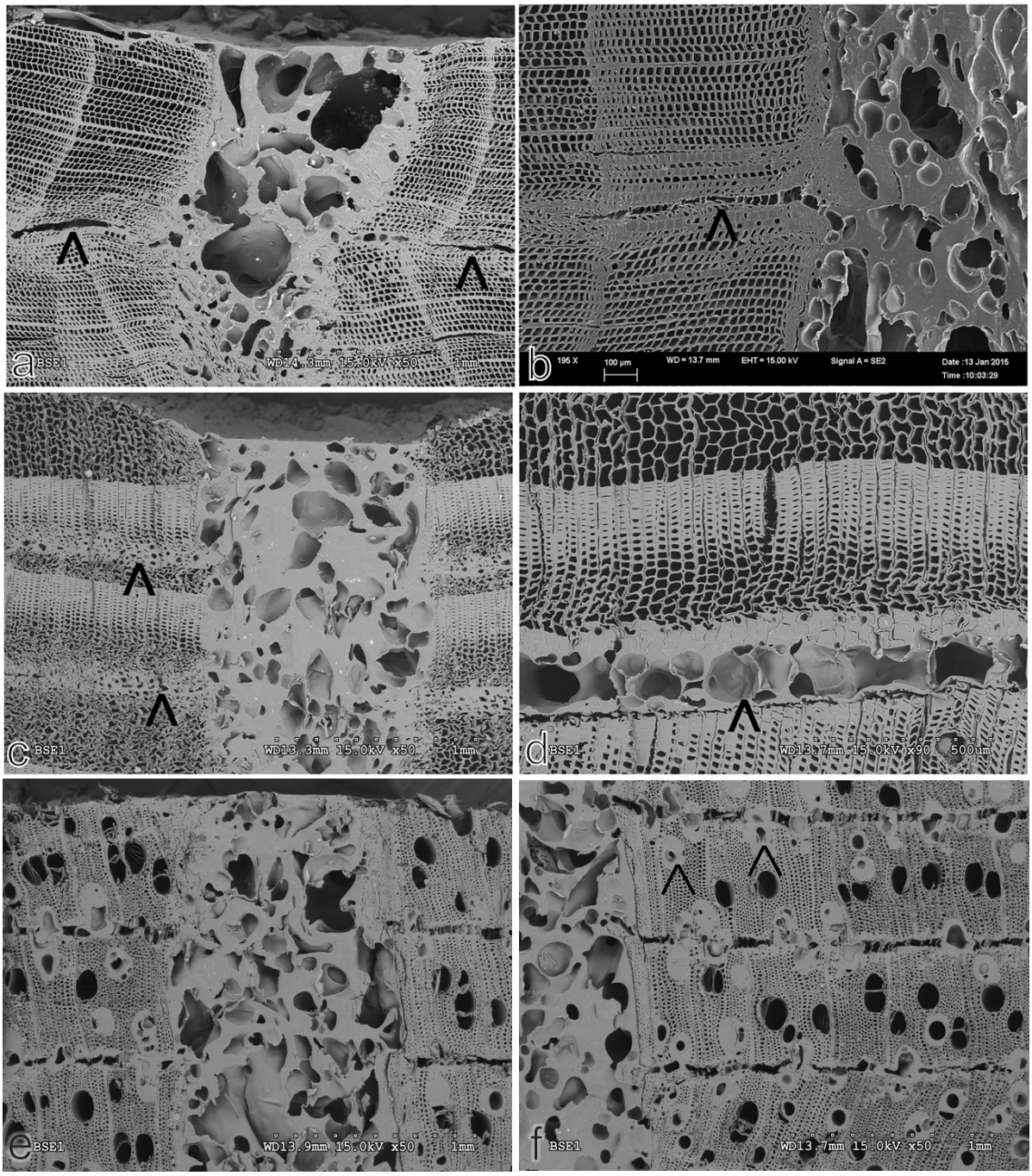

Figure 4.8 Scanning electron photomicrographs of cross-sections of specimens containing adhesive Z-connections after immersion in water and re-drying: (a) Part of a yellow cedar specimen showing an adhesive Z-connection (centre) and a delaminated horizontal glue-line (arrowed); (b) Part of a yellow cedar specimen showing a delaminated horizontal glue-line adjacent to an adhesive Z-connection (arrowed); (c) Part of a white spruce specimen showing an adhesive Z-connection (centre) and two intact horizontal glue-lines (arrowed); (d) A intact horizontal glue-line in a white spruce specimen (arrowed); (e) Part of a yellow birch specimen showing delamination of horizontal glue-lines; (f) Penetration of horizontal glue-lines into vessels in a yellow birch specimen (arrowed)

4.3.2.3 X-ray μCT

X-ray μCT had sufficient resolution to differentiate the adhesive network from wood matrix (Fig 4.9). 3D rendered μCT images of the two types of composites (perforated and control) are shown in Figs 4.9 ~ 4.11. Fig 4.9 shows the entire volume of the wood composites that were imaged. Individual wood veneers can be seen in Fig 4.9. Fig 4.10 shows the spatial distribution of adhesive network in the two wood composites (perforated vs. control). The figure clearly shows the adhesive Z-connections connecting the perforated veneer squares (top part of the figure) as well as the Adhesive X-Y connections in both composite types (arrowed in Fig. 4.10). Connection between individual adhesive Z-connections and adhesive X-Y films can be seen more clearly in Fig. 4.11.

Figure 4.9 3D rendered volume structure of one half of the model spruce wood composites showing the wood veneer

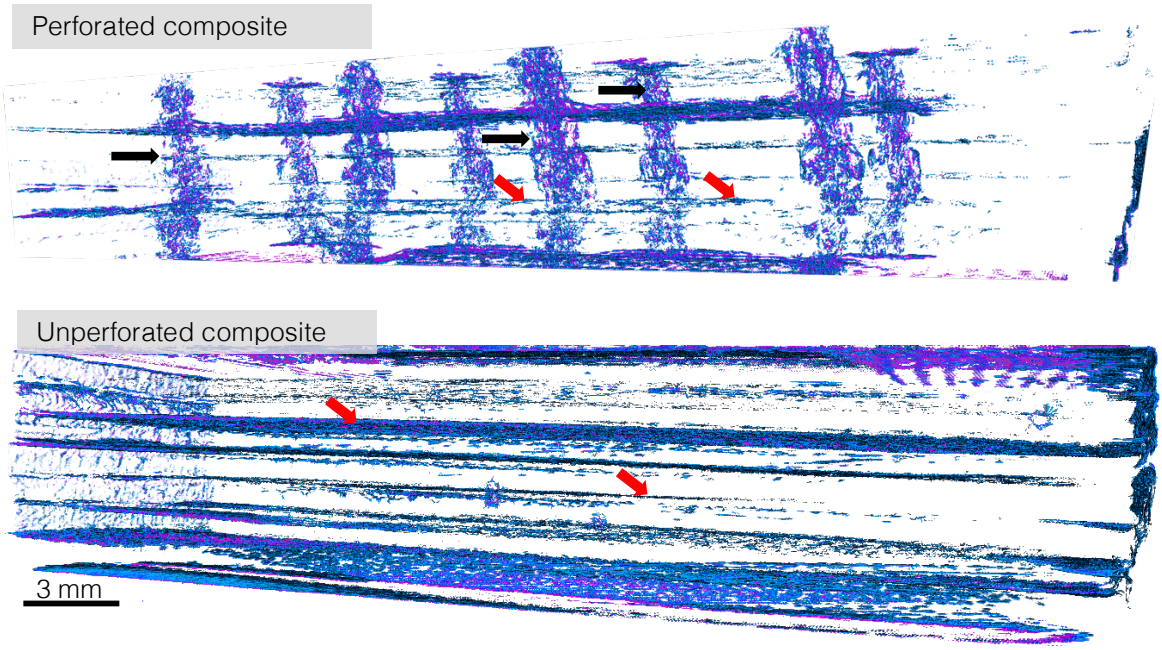

Figure 4.10 3D distribution of adhesive network in the model wood composites. Note the presence of adhesive Z-connections (black arrows) in addition to adhesive (glue-lines) in the X-Y direction (red arrows)

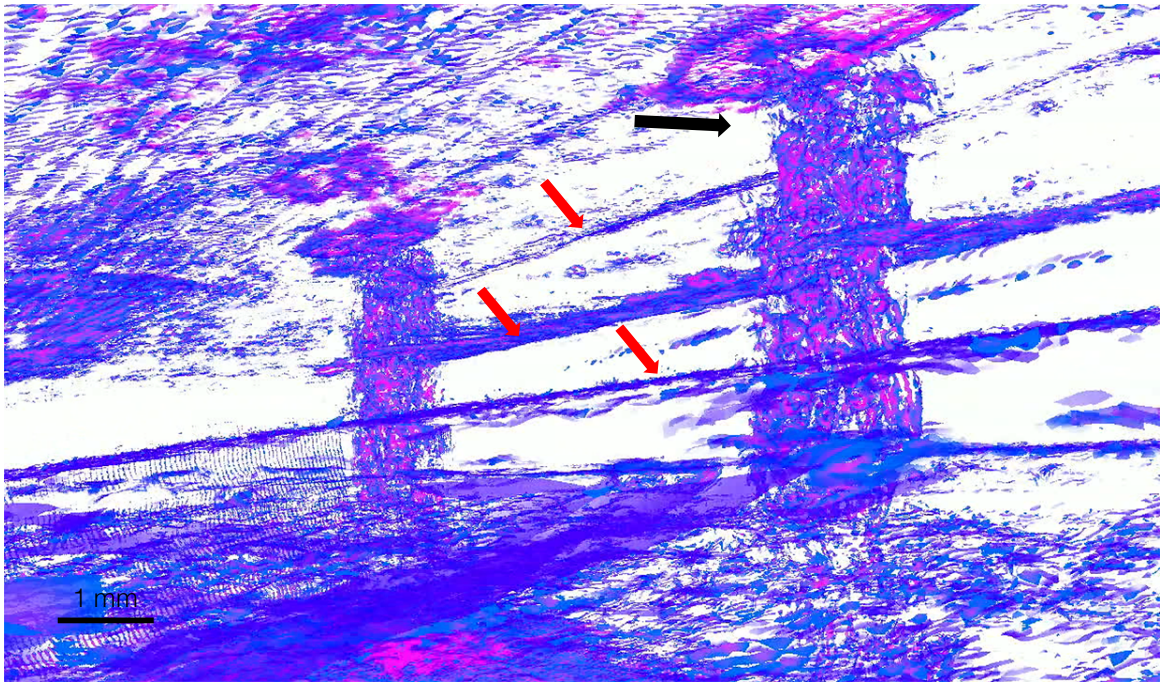

Figure 4.11 Zoom-in view of Fig. 4.11 showing individual adhesive Z-connection (black arrows) connected to horizontal (X-Y) glue-lines (red arrows)

4.4 Discussion

In the introduction, I hypothesized that the creation of adhesive Z-connections would restrain the irreversible thickness swelling of a model composite immersed in water and then re-dried. My results partially support this hypothesis. Adhesive Z-connections were effective at restraining the thickness swelling of model composites made from rotary-peeled spruce and to a lesser extent sliced cedar veneer, but they were ineffective at restraining the swelling of model composites made from rotary-peeled birch veneer. The effectiveness of adhesive Z-connections at restricting swelling appeared to depend, in part, on the presence of strong bonds between veneer in the X-Y directions that were resistant to delamination as well as on the creation of connections in the Z-direction. Such a robust inter-connected adhesive network appeared to be present in spruce specimens, and was able to reduce thickness swelling by 46%, compared to the control that lacked adhesive Z-connections. Such a reduction in thickness swelling compares favourably with other approaches to reducing the thickness swelling of wood composites, including thermal treatments, coatings and water-repellents (Del Menezzi and Tomaselli 2006, Racota 2007, Evans and Cullis 2008).

Adhesive Z-connections were ineffective at restraining thickness swelling of yellow birch composites possibly because penetration of adhesive from X-Y glue-lines into large vessels present in yellow birch reduced bond strength and made the yellow birch composites more prone to delamination than white spruce or yellow cedar composites. In support of this suggestion, Marra (1992), Sernek et al. (1999) and Xing et al. (2005) noted that excessive penetration of adhesive into the wood adjacent to glue-lines may lead to ‘starved’ glue-lines with insufficient adhesive remaining at the bonding interface to strongly bond wood. The effects of wood properties on the ability of adhesive Z-connections to reduce thickness swelling will be examined in more detail in Chapter 5.

Clearly, my approach of precision-drilling veneer to create perforations to allow adhesive to establish adhesive bonds in the Z-direction with those in the *x-y* plane would be difficult to implement in practice. However, an alternative more practical approach could involve passing veneer through a roller containing slitting knives, which would perforate the veneer. Other alternative approaches that can facilitate adhesive Z-connections would also be worth exploring.

4.5 Conclusions

I hypothesized that the creation of coarse adhesive cross-links in the Z-direction would constrain the irreversible moisture-induced thickness swelling of a model wood composites composed of small squares of veneer. My results partially support this hypothesis. I have suggested why the adhesive Z-connections were more effective at restraining swelling of a white spruce composite than yellow cedar or yellow birch composites. If correct my suggestion indicates that the effectiveness of the adhesive Z-connections at restricting swelling depends on the presence of strong bonds between veneer elements as well as the creation of connections in the Z-direction. The establishment of such a strong inter-connected 3-D adhesive network may be a cost-effective way of reducing the swelling of wood composites. Further research is needed to develop practical ways of creating Z direction cross-links in composites that more closely resemble commercial products.

5 Effects of Wood Species and Veneer Type on the Ability of Adhesive Z-connections to Restrain Thickness Swelling of a Model Wood Composite

5.1 Introduction

Chapter 4 showed that adhesive Z-connections (as developed in Chapter 3) can significantly reduce the hygroscopic thickness swelling of a model wood composite. This chapter seeks to further understand how adhesive Z-connections work and which factors influence their effectiveness.

Results in Chapter 4 showed that the effectiveness of adhesive Z-connections at restraining thickness swelling of wood composites varied depending on the wood species used to manufacture the model wood composite. Wood species swell at different rates due to their different water absorption rates as well as density (Hernández 1993, 2007; Glass and Zelinka 2010). Furthermore, the commercial wood veneers that were used to make the composites tested in Chapter 4 were produced using different veneer manufacturing methods. For example, the spruce and birch veneers were rotary cut whereas the cedar veneers were sliced. These different manufacturing methods produced veneers with different grain orientations (tangential vs. radial). Difference in grain orientation can influence the swelling of wood veneer (Glass and Zelinka 2010) and adhesive bond strength with wood (Gavrilović-Grmuša et al. 2016). In general, tangential swelling (or shrinkage) coefficient is 1.5 to 2 times greater than radial swelling (or shrinkage) coefficient (Hernández 1993). Therefore, apart from wood species, grain orientation of veneers could also have influenced the ability of adhesive Z-connections to restrain the thickness swelling of the model wood composites tested in Chapter 4.

Hence, in this chapter I carefully controlled the grain orientation of veneers containing adhesive Z-connections. I also examined the system with three different wood species based on their water absorption and swelling rates. I hypothesize that the effectiveness of adhesive Z-

connections at restraining thickness swelling of wood composites will be influenced by wood species because of differences in water absorption and swelling and strength of glue bonds, and also by veneer type because of differences in tangential/radial swelling ratio.

5.2 Materials and methods

5.2.1 Experimental design

A three-factorial randomized block design was used to test my hypothesis. There were five blocks and hence five replications for each veneer treatment (Z-connections vs. no Z-connections) x species (yellow cedar, eastern red spruce, yellow poplar) x veneer type (radial vs. tangential) (Fig. 5.1). The resulting combinations were randomly assigned to specimens within each block. The effect of each factor and the interaction between the three factors on the thickness swelling of wood composites were tested using analysis of variance (see Section 5.2.4).

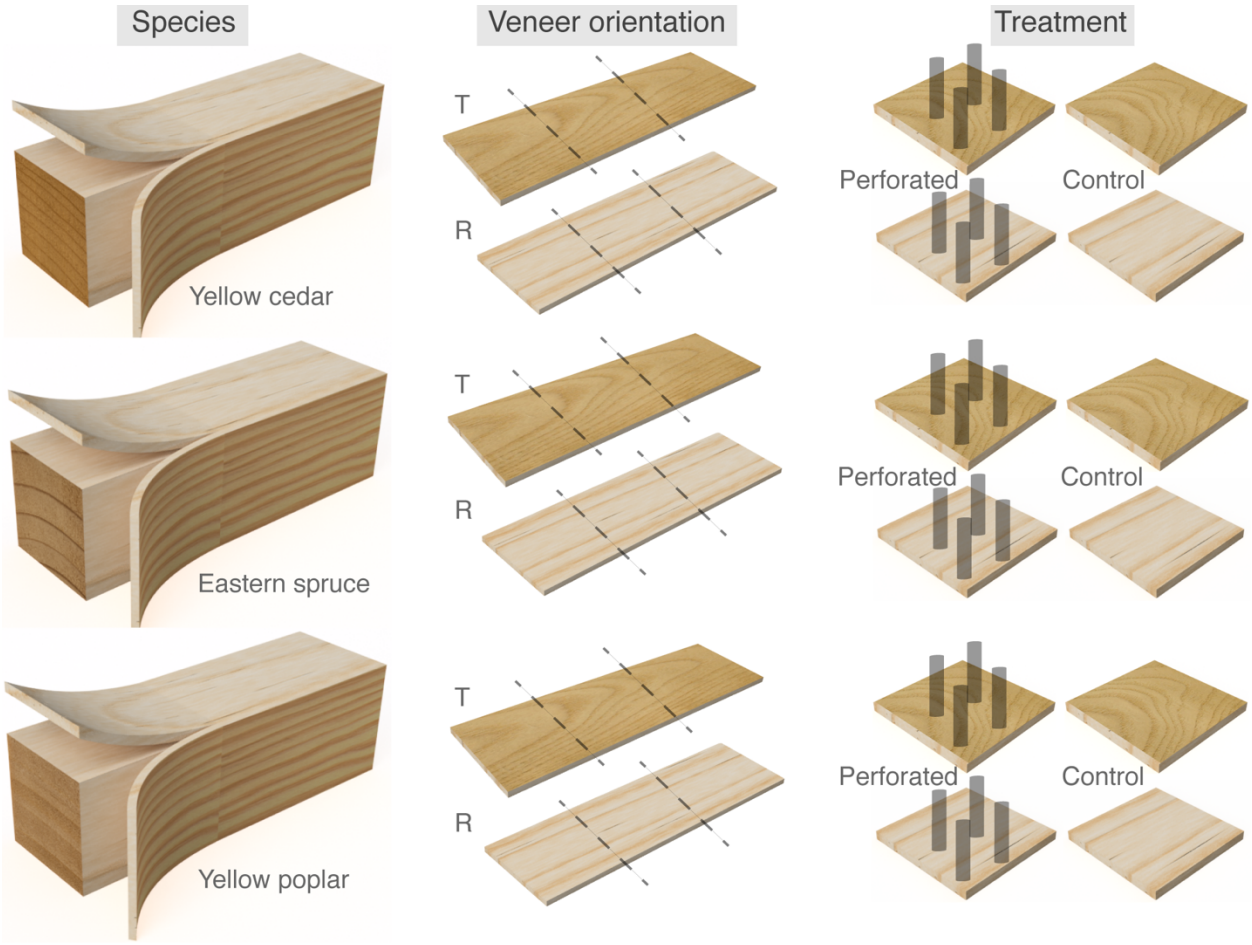

Figure 5.1 Schematic illustration of the experimental design with three experimental factors: (species) x (veneer orientation) x (Z-connections). The three factors were randomly assigned to specimens and repeated in 5 experimental blocks (not shown) to obtain replication at the higher level

5.2.2 Preparation of specimens with and without adhesive Z-connections

Five air-dry wooden boards, of different sizes, with growth rings oriented radially to one of their wide faces were obtained for each of the following wood species: eastern red spruce (*Picea rubens* Sarg.), yellow cedar (*C. nootkatensis*) and yellow poplar (*Liriodendron tulipifera L.*). The fifteen boards (five for each species) were stored in a conditioned environment (20 ± 1ºC temperature and 65 ± 5% relative humidity) for seven days. A sample measuring 35 mm x 35 mm x 300 mm was cut from each board, ensuring that growth rings were oriented radially and tangentially to the side grain of each sample (Figs 5.1 and 5.2). Offcuts measuring 25 mm x 25 mm x 25 mm from original boards were retained and used for the assessment of growth

rates, air-dry densities, and tangential and radial swelling of each parent board. Assessment of growth rate was carried out by measuring annual ring width (Keith 1961; Koga and Zhang 2001). End grain of the offcuts from parent boards was carefully sanded using fine abrasive paper (800 grit) to make it easier to see growth rings (note the end grain of parent boards in Fig. 5.1 represent actual photographs of each wood species). Three annual rings (centre-most, outer-most and the middle one) were chosen from each offcut. The average width of the three annual ring widths was reported for each parent board (Table 5.1). Air-dry densities and tangential and radial swelling were assessed using a modified ASTM standard D143 - Standard test methods for small clear specimens of timber (ASTM 2007). The air-dry weight (g) of each offcut was measured using a digital balance (Fisher® Scientific), and their dimensions (cm^3) were measured using a digital calliper (Mitutoyo®). Air-dry density was calculated as the ratio of weight (g) divided by volume (cm^3) of each offcut (Table 5.1). All offcuts were then submerged in water until they were fully saturated. Their weights and dimensions were re-measured, as above. Tangential and radial swelling were calculated as the increase in dimensions of the offcuts divided by their original dimensions (Table 5.1).

Table 5.1 Basic properties of the wood boards used to manufacture the model composites

Species	Board	Growth rate (annual ring width, mm)	Air-dry density (g/cm^3)	Tangential swelling (%)	Radial swelling (%)
Yellow cedar	1	2.6	0.54	3.2	2.4
	2	2.7	0.51	4.0	0.9
	3	2.0	0.46	3.4	0.8
	4	2.0	0.51	4.3	1.9
	5	2.2	0.51	2.1	1.3
	Mean (standard deviation)	**2.3** (0.1)	**0.51** (0.01)	**3.4** (0.4)	**1.5** (0.3)
Eastern spruce	1	2.6	0.42	4.2	1.5
	2	4.9	0.42	5.5	1.7
	3	3.3	0.46	7.0	2.0
	4	2.3	0.45	5.8	2.4
	5	2.2	0.47	4.7	2.7
	Mean (standard deviation)	**3.1** (0.5)	**0.44** (0.01)	**5.4** (0.5)	**2.1** (0.2)
Yellow poplar	1	3.4	0.58	7.2	2.9
	2	3.5	0.58	7.3	1.6
	3	4.2	0.62	7.1	2.2
	4	3.5	0.53	6.4	1.8
	5	2.9	0.57	6.9	2.1
	Mean (standard deviation)	**3.5** (0.2)	**0.58** (0.02)	**7.0** (0.2)	**2.1** (0.2)

A table saw with a 25 cm (10”) blade (Bosch® 4100) and a purpose-built guide were used to cut radial and tangential veneer strips from samples. Tangential veneers swell radially in the thickness direction, while the opposite is the case for radial veneers. The strips were 1 ± 0.1 mm thick (Fig. 5.3). A veneer guillotine (Boston™ 2658) was used, as described in Chapter 3 to cross-cut veneer strips into veneer squares measuring 25 mm x 25 mm. Veneer squares were perforated with a dental drill as described in Chapter 4. All the perforated and unperforated veneer squares were stored in a conditioned environment at 20 ± 1ºC and 65 ± 5% r.h. for seven days.

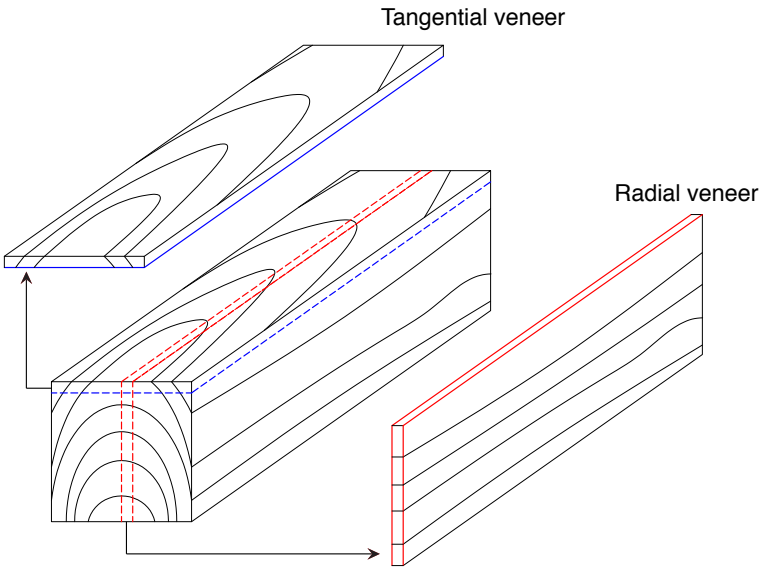

Figure 5.2 Schematic diagram showing growth ring orientations of radial or tangential wood veneer strips sawn from a parent wood sample. Red lines indicate cutting lines for radial veneers; blue lines indicate cutting lines for tangential veneers

Figure 5.3 Table saw with a 25 cm (10”) blade for cutting 1 mm thick veneers. The gap between the blade and the wooden guide which was clamped to the table of the saw was 1 mm

Two groups of matching perforated or unperforated radial veneer squares and another two groups of matching perforated and unperforated tangential veneer squares cut from the same parent wood block for each species were randomly selected, respectively. Composites containing either perforated or unperforated veneer squares were made from veneers, as

described in Chapter 4. The composites were conditioned as above for three days, weighed, and the thickness of each composite was measured at 12 points using a digital calliper (Mitutoyo®) to obtain the initial thickness of each composite specimen.

5.2.3 Thickness swelling measurements and characterization of composites

Specimens made from the first block were submerged in distilled water to a depth of 1 cm for 24 h in a water tank (15 cm x 8 cm x 6 cm). Their thicknesses were re-measured, as above, immediately after 24 h of water soaking. Their weight gains due to water absorption were also measured immediately after 24 h of water soaking. Matching veneer squares from each block and species were also submerged in the water tank for 24 h to obtain water absorption values for individual veneers. Afterwards, specimens were re-conditioned for three days, and their thicknesses re-measured, as above. The increases in thickness of the composites (both absolute value and percentage) were calculated. The changes in surface topography of the composites after immersion in water and re-conditioning were examined using confocal profilometry (Fig. 5.4), as described in Chapter 4. Once all measurements were complete on composites produced from the first wood block for all the species, the experiment was repeated for composites produced from the other 4 blocks. After swelling tests were completed, selected composites were cut in half in the Y-direction using a precision micro-table saw with a 10 cm (4”) blade (Byrnes Model Machines, Orlando, F.L, USA). Then the cross-sections were carefully sliced using a hand-held, single-edged razor blade while being viewed under a stereo-microscope until one row of adhesive Z-columns was completely exposed. Then both macro-photography and scanning electron microscopy, as described in Chapter 4, were used to visualize the cross-sections containing the exposed adhesive Z-columns.

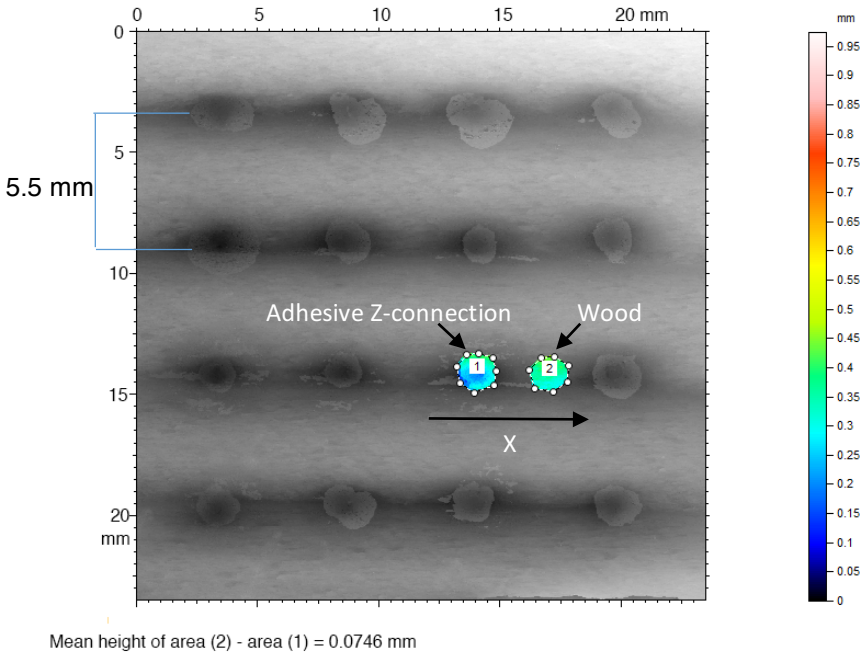

Mean height of area (2) - area (1) = 0.0746 mm

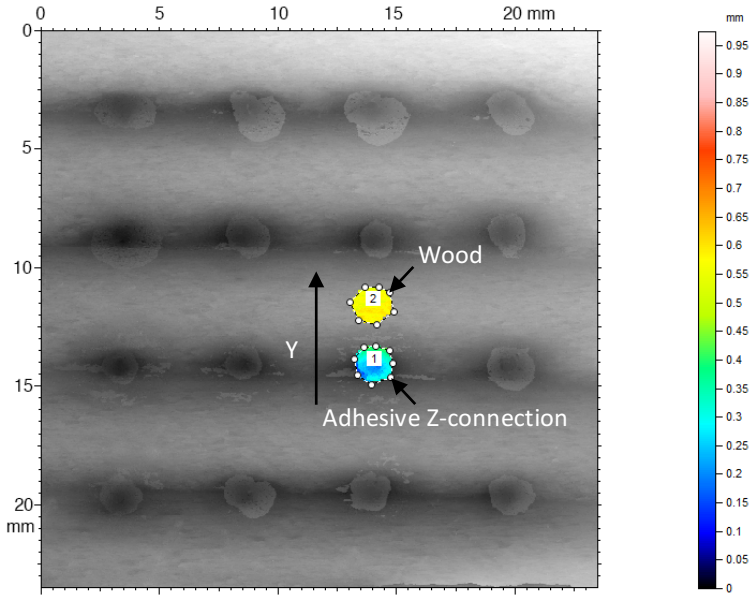

Mean height of area (2) - area (1) = 0.281 mm

Figure 5.4 Measurement of height difference between 'area 2' representing wood material and 'area 1' representing adhesive Z-connections in X and Y directions, respectively. Software calculated the height means of area 2 and area 1 and gave the difference between the two means. The difference is defined as differential thickness swelling (DTS) in X or Y directions. This measurement was repeated 16 times on each composite because each composite contained 16 wood-hole pairs. The average of the 16 measurements was then reported for each composite

Pure adhesive plugs were made, and the swelling of the plugs was measured. The adhesive was inserted using a syringe into six small plastic cylindrical vials (10 mm in diameter,

28 mm in height) with one open end (Fig. 5.5). All of the six vials (containing adhesive) were stored in the conditioned environment (as mentioned above) for three days to allow the adhesive to completely cure. Afterwards, the plastic vials were carefully cut open with a hand-held razor-blade, and adhesive plugs were removed from the vials. The heights of the six adhesive plugs were measured using a calliper (as mentioned above) before and after the plugs were immersed in water for 24 h. The average swelling of the six isolated adhesive plugs was calculated.

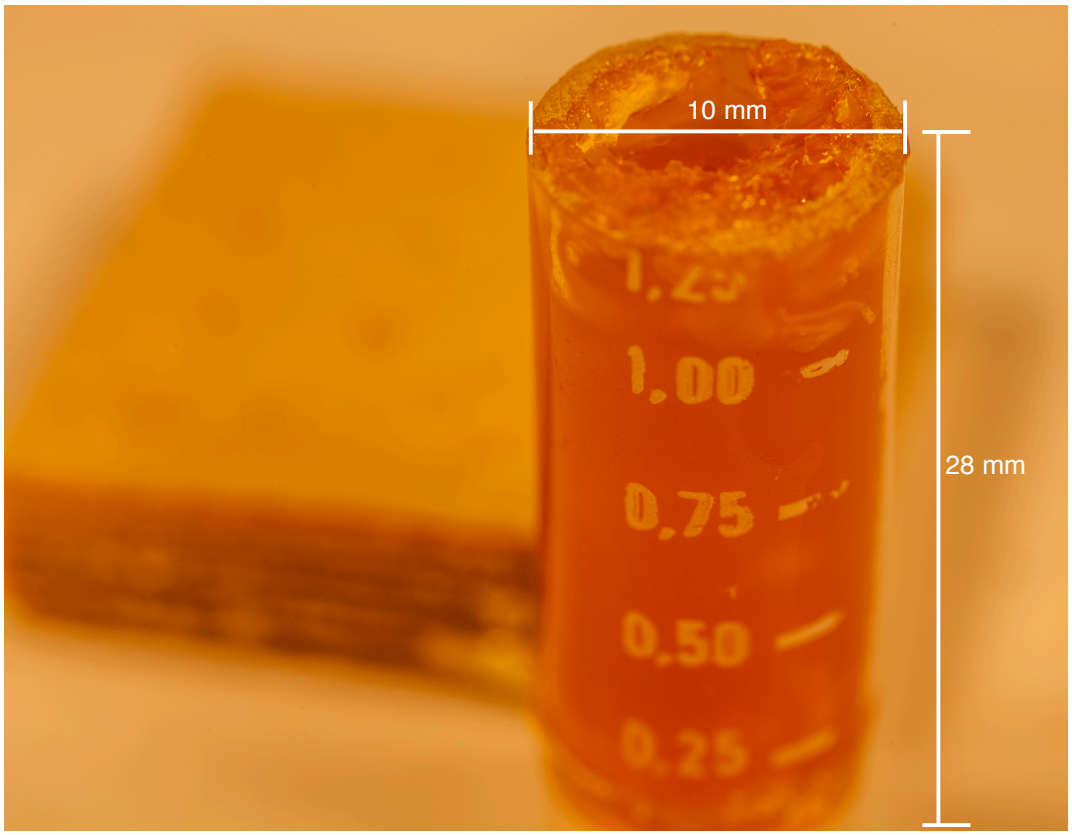

Figure 5.5 Isolated adhesive plug encapsulated in a small plastic vial for 24 h at 20 ± 1°C and 65 ± 5% r.h. and then removed from the plastic vial

5.2.4 Statistical analysis of data

I measured and recorded three variables: (1) thickness swelling of composites after 24 h water soaking; (2) thickness swelling of composites after re-conditioning; and (3) differential thickness swelling (DTS) between wood and adhesive Z-connections in the X and Y directions, respectively.

The effects of the three experimental factors (wood species, veneer type, veneer treatment) as well as the interactions of the three factors on the aforementioned variables were tested for statistical significance using an appropriate multi-factorial analysis of variance (ANOVA) at the 5% significance level ($p < 0.05$). Statistical computation was performed using GenStat® (Release 17.1). Mean values are plotted on graphs, and error bars representing least significant differences are included on graphs. These error bars can be used to assess whether differences between individual means are statistically significant at the 5% level ($p < 0.05$).

5.3 Results

5.3.1 Effects of adhesive Z-connections on thickness swelling of the model wood composite

There was a strong linear relationship ($R^2 = 0.922$) between the thickness swelling of composites after 24 h water soaking and thickness swelling after re-conditioning (Fig. 5.6). The latter represents the irreversible thickness swelling of the composites, i.e. swelling that was not recovered, even though the moisture content of the specimens was returned to its initial starting value by conditioning specimens at 20 ± 1ºC and 65 ± 5% r.h. The slope of Fig. 5.6 indicates that 88% of the water-induced thickness swelling of the composites was irreversible. Hereafter I refer to irreversible thickness swelling as thickness swelling, defined as the thickness increase of the composites after 24 h water soaking and then re-conditioning.

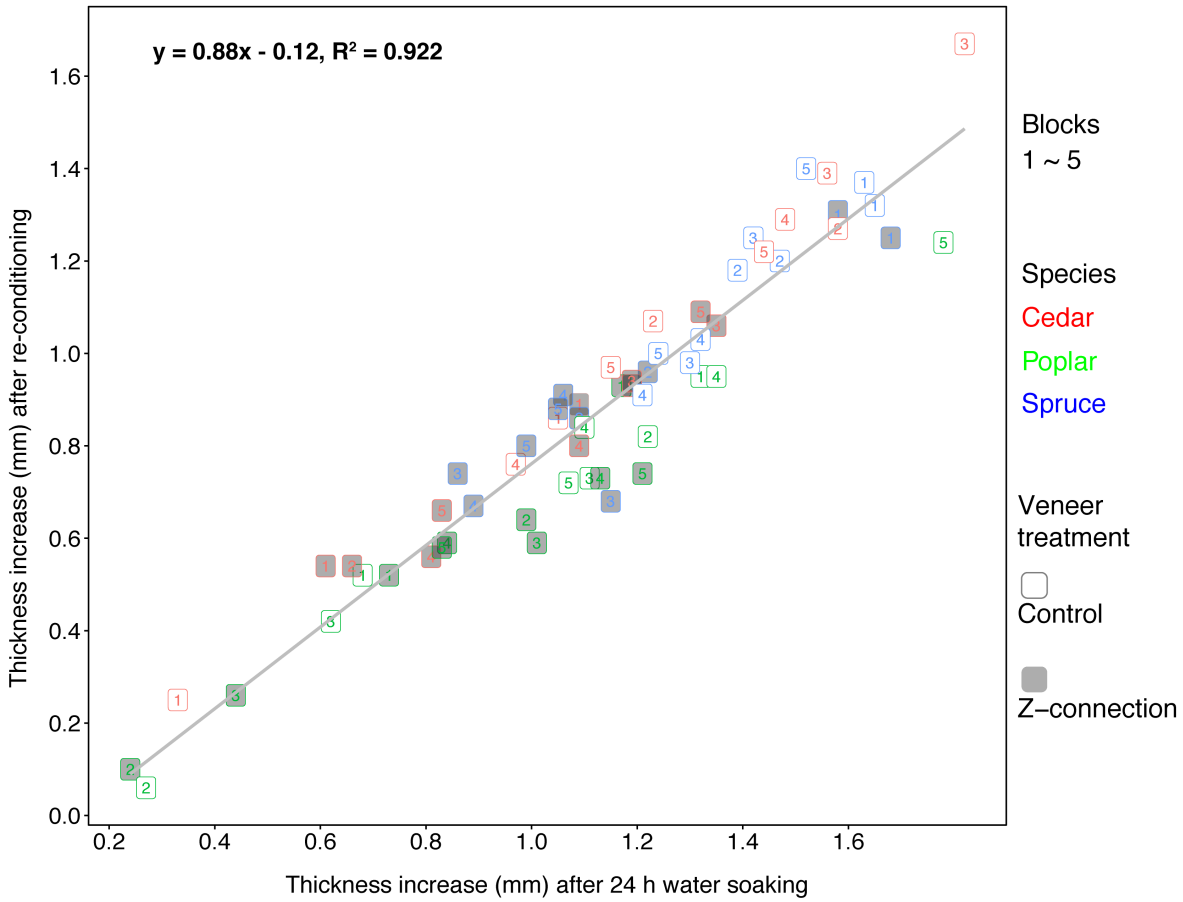

Figure 5.6 Relationship between the thickness increase of all 60 specimens after 24 h water soaking and their thickness increase after re-conditioning

It is apparent from Fig. 5.6 that there is a difference in thickness swelling between blocks within each species. This difference is possibly due to variation in the properties of parent wood boards (Table 5.1). On the other hand, it is also clear from Fig. 5.6 that composites with Z-connections swelled less than the unperforated controls.

Analysis of variance indicated that adhesive Z-connections significantly ($p < 0.001$) reduced the thickness swelling of specimens (Fig. 5.7). This confirms findings from Chapter 4. Analysis of variance also indicated that there were significant effects ($p < 0.05$) of wood species and veneer type on thickness swelling. There was no significant ($p > 0.05$) effect of veneer type on differential thickness swelling in the X or Y directions (Table 5.2). However, there were significant ($p < 0.005$) interactive effects of wood species and veneer type on thickness swelling

of the composites (Table 5.2). This interaction occurred because the thickness swelling of composites made from radial poplar and yellow cedar veneers were significantly ($p < 0.05$) greater than those of composites made from tangential veneers. In contrast, there was no significant ($p > 0.05$) difference in the thickness swelling of composites made from radial vs. tangential spruce veneers (Fig. 5.8).

Table 5.2 Significant effects of, and interactions between, wood species, veneer orientation, and veneer treatment on thickness swelling (TS) and differential thickness swelling (DTS) parameters

Response variables	Experimental factors						
	Wood species (S)	Veneer orientation (O)	Veneer treatment (T)	O x T	S x T	S x O	S x O x T
TS-wet [a]	P=0.001	p<0.001	P=0.002	NS	NS	P=0.004	NS
TS-condit [b]	p<0.001	P=0.002	p<0.001	NS	NS	P=0.004	NS
DTS-X [c]	p<0.001	NS	--	--	--	NS	--
DTS-Y [d]	P=0.003	NS	--	--	--	NS	--

Note: a: thickness swelling after 24 h water soaking; b: thickness swelling after re-conditioning; c: differential thickness swelling in the X-direction; d: differential thickness swelling in the Y-direction.

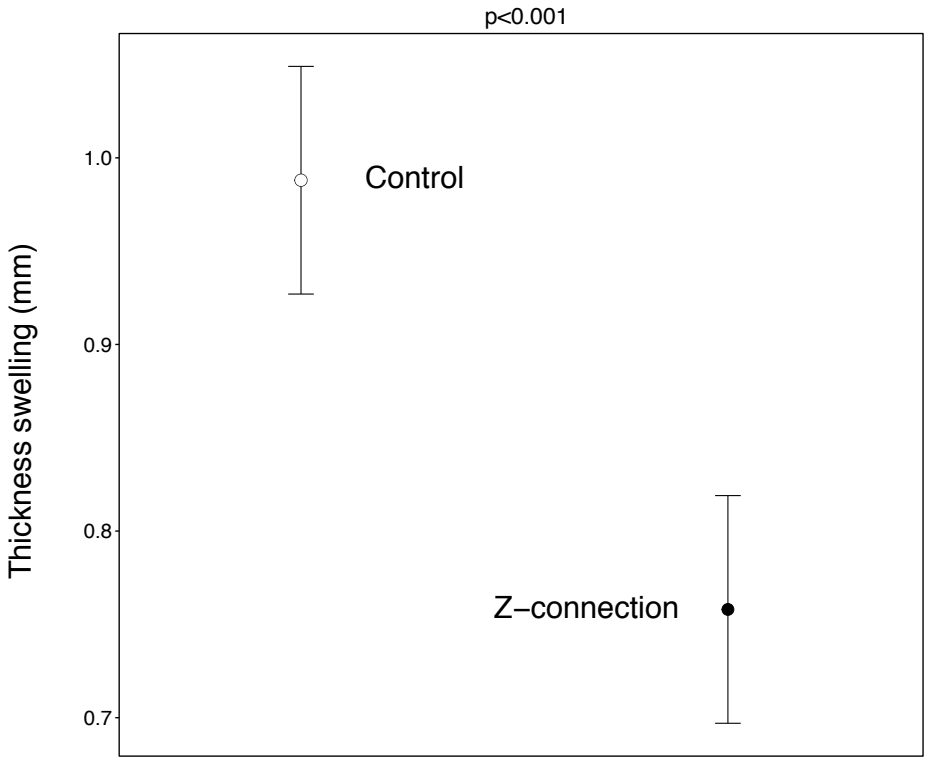

Figure 5.7 Effects of adhesive Z-connections on thickness swelling of model wood composites averaged across all species and veneer types. Error bars represent ± standard error of difference from ANOVA

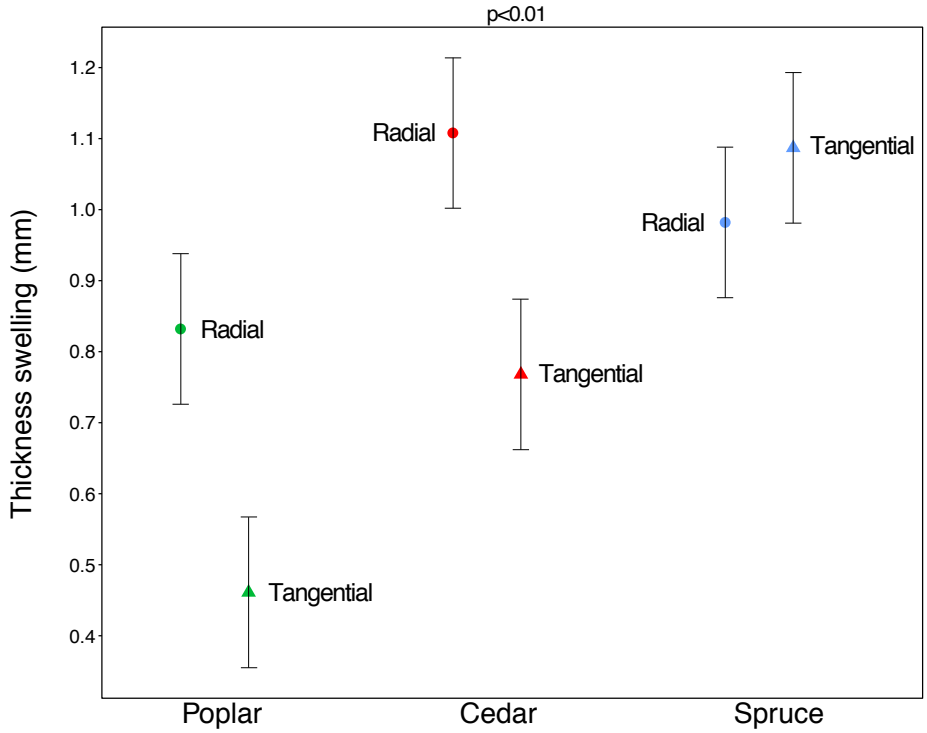

Figure 5.8 Interaction of wood species and veneer type (orientation) on thickness swelling of model wood composites. Error bars represent ± standard error of difference from ANOVA

Table 5.3 lists the thickness swelling in percentages for composites with Z-connections and the controls that lacked Z-connections. These figures make it easier to compare my results with those of other studies that have examined the moisture-induced thickness swelling of wood composites.

Table 5.3 Thickness swelling (TS) percentages (%) of composites with and without adhesive Z-connections after 24 h water soaking and re-conditioning. Note that tangentially-cut veneer swells radially and vice versa

Veneer orientation	Wood species	TS of composites with Z-connections (%)	TS of composites with no Z-connections (control) (%)	Difference (%)
Tangential	Poplar	6.6	8.3	1.7
	Cedar	11.7	16.0	4.3
	Spruce	20.1	27.6	7.5
Radial	Poplar	11.9	15.7	3.8
	Cedar	17.6	24.1	6.5
	Spruce	18.7	22.8	4.1

Fig. 5.9 summarizes and compares the effects of all three experimental factors on the thickness swelling of composites. The number in each bar indicates the % reduction in thickness swelling due to the effects of the adhesive Z-connections. This graph shows that the adhesive Z-connections were able to reduce the thickness swelling of the poplar composites by an average of 21%, even though poplar composites had relatively low absolute thickness swelling. Comparable figures for cedar and spruce composites were 26% and 22%, respectively.

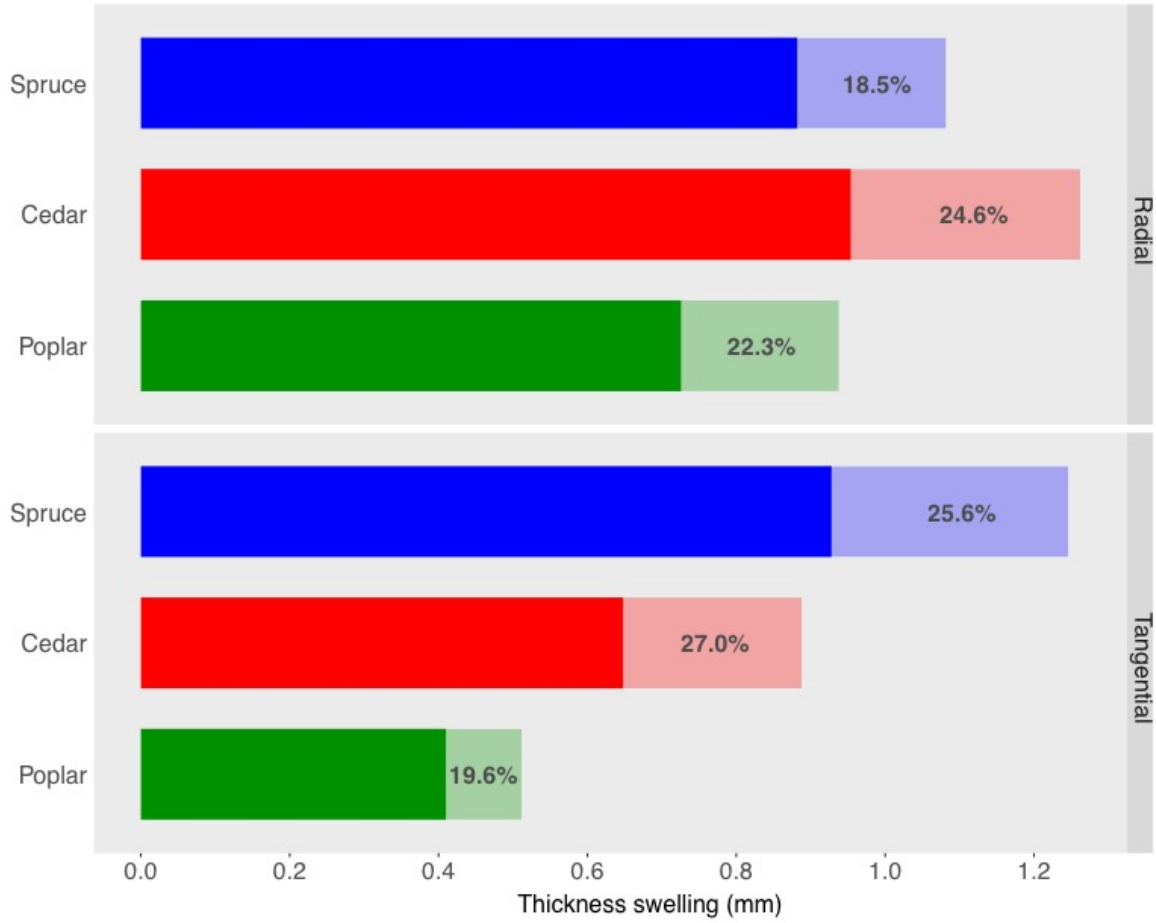

Figure 5.9 Effects of adhesive Z-connections on thickness swelling of model wood composites made from three different wood species (yellow poplar, yellow cedar and red spruce) and two types of veneers (radial vs. tangential veneers). The percentages indicated on the lighter areas of the bars indicate the reduction in thickness swelling resulting from the presence of adhesive Z-connections in the composites

5.3.2 Effects of water absorption and some wood properties on thickness swelling of the composites

The water absorption (%) of both model composites containing no adhesive Z-connections (control) and individual veneers, defined as the ratio of water absorption (g) divided by the original dry mass (g) of either composites or veneers are shown in Tables 5.4 & 5.5, respectively. Individual veneers absorbed more water than composites after 24 h water soaking, as expected. Water absorption of both veneers and composites varied with wood species. Spruce veneer and composites absorbed more water than poplar and particularly cedar veneer and composites.

Table 5.4 Water absorption of individual veneers of different wood species and veneer orientation after 24 h water soaking

Species	Water absorption (g)			Water absorption/veneer original mass (%)		
	Tangential	Radial	Mean	Tangential	Radial	Mean
Spruce	0.19	0.22	0.21	78	80	79
Poplar	0.29	0.25	0.27	81	70	76
Cedar	0.14	0.17	0.16	55	61	58
Mean	**0.21**	**0.21**	**0.21**	**71**	**70**	**71**

Table 5.5 Water absorption of composites containing no adhesive Z-connections (control) made from different wood species and veneer orientation after 24 h water soaking

Species	Water absorption (g)			Water absorption/veneer original mass (%)		
	Tangential	Radial	Mean	Tangential	Radial	Mean
Spruce	0.92	1.08	1.00	44	51	48
Poplar	1.24	1.18	1.21	46	40	43
Cedar	0.73	0.73	0.73	33	32	33
Mean	**0.96**	**1.00**	**0.98**	**41**	**41**	**41**

There was a linear relationship ($R^2 = 0.62$) between the water absorption of composites and the water absorption of individual veneers (Fig. 5.10).

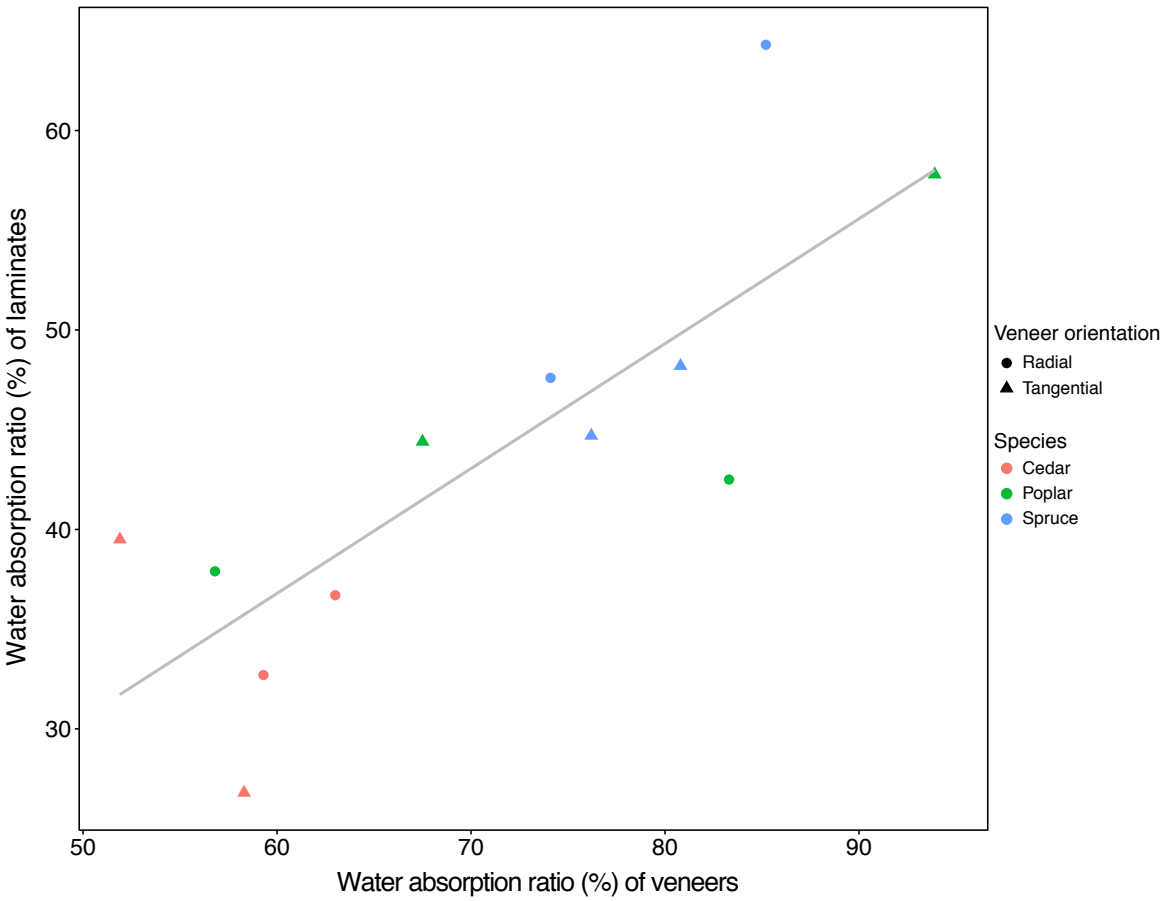

Figure 5.10 Linear regression of water absorption of composites and individual veneers

ANOVA indicated that there was a significant difference ($p < 0.05$) in water absorption of different wood species. However, there was no significant difference ($p > 0.05$) in the water absorption of veneers with different orientations. The water absorption of composites made from the three species is graphed in Fig. 5.11. The figure confirms that spruce composites absorbed more water than cedar and poplar composites, although the difference between spruce and poplar composites was not significant ($p > 0.05$). Fig. 5.11 also shows the thickness swelling (%) of composites containing no adhesive Z-connections made from the three species. Results in Fig. 5.11 indicates that there was a significant difference ($p < 0.05$) in thickness swelling of the wood species. For example, spruce composites swelled significantly more than both cedar and poplar composites.

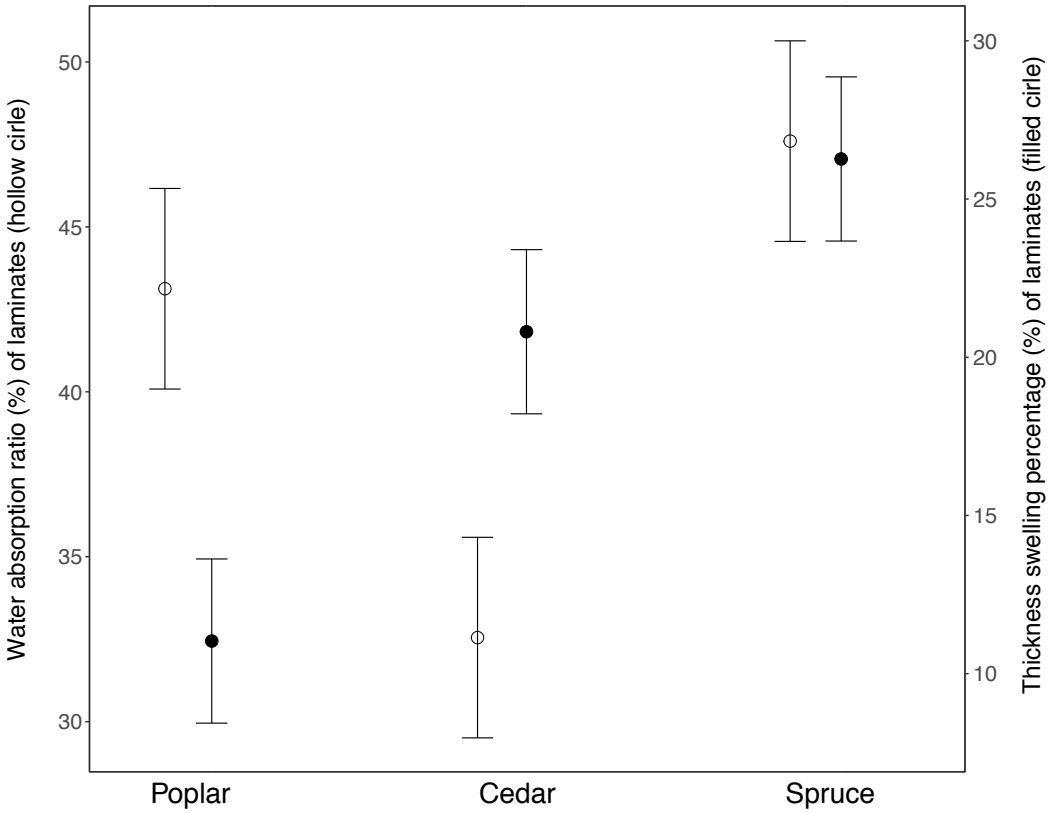

Figure 5.11 Comparison of water absorption (left y-axis) and thickness swelling (right y-axis) of composites containing no adhesive Z-connections made from three different species. Error bars represent ± standard error of difference from ANOVA (different for the two y axis)

Fig. 5.12 shows the differential swelling of wood on its own and isolated adhesive plugs. The swelling of wood varied between species, as mentioned above. Therefore, the difference in swelling between wood and adhesive Z-connections varied between composites made from different species. For example, the difference between wood and adhesive Z-connections was greatest in spruce composites and least in poplar composites.

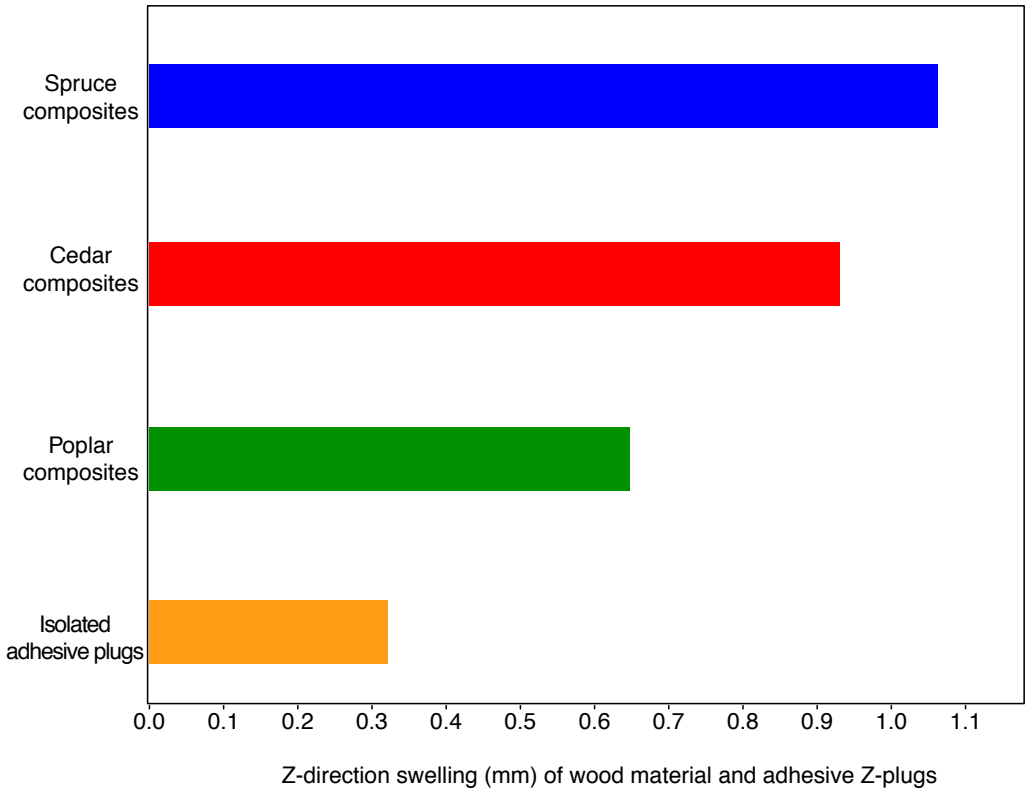

Figure 5.12 Comparison of the swelling of composites made from three wood species and the swelling of isolated adhesive Z-plugs showing the difference in swelling of wood and Z-plugs was highest in spruce composites

5.3.3 Surface topography of composites containing adhesive Z-connections

Confocal profilometry generated colour-coded height maps of the surfaces of the wood composites after water soaking and re-conditioning (Figs. 5.13~5.15). Areas in blue swelled the least (generally around the adhesive Z-connections), whereas orange-coloured areas, swelled the most. In between the blue and orange areas, are green or yellow areas of intermediate heights. The height differences at the surface of composites suggest that the adhesive Z-connections restrict swelling of adjacent wood material. It is also evident from Figs. 5.13~5.15, as I observed in Chapter 4, that the swelling of wood was restricted to different degrees in the X and Y directions. These figures are also in accord with Fig. 5.12, which shows that the height difference between wood and adhesive Z-connections after 24 h water soaking and re-conditioning was highest in spruce composites.

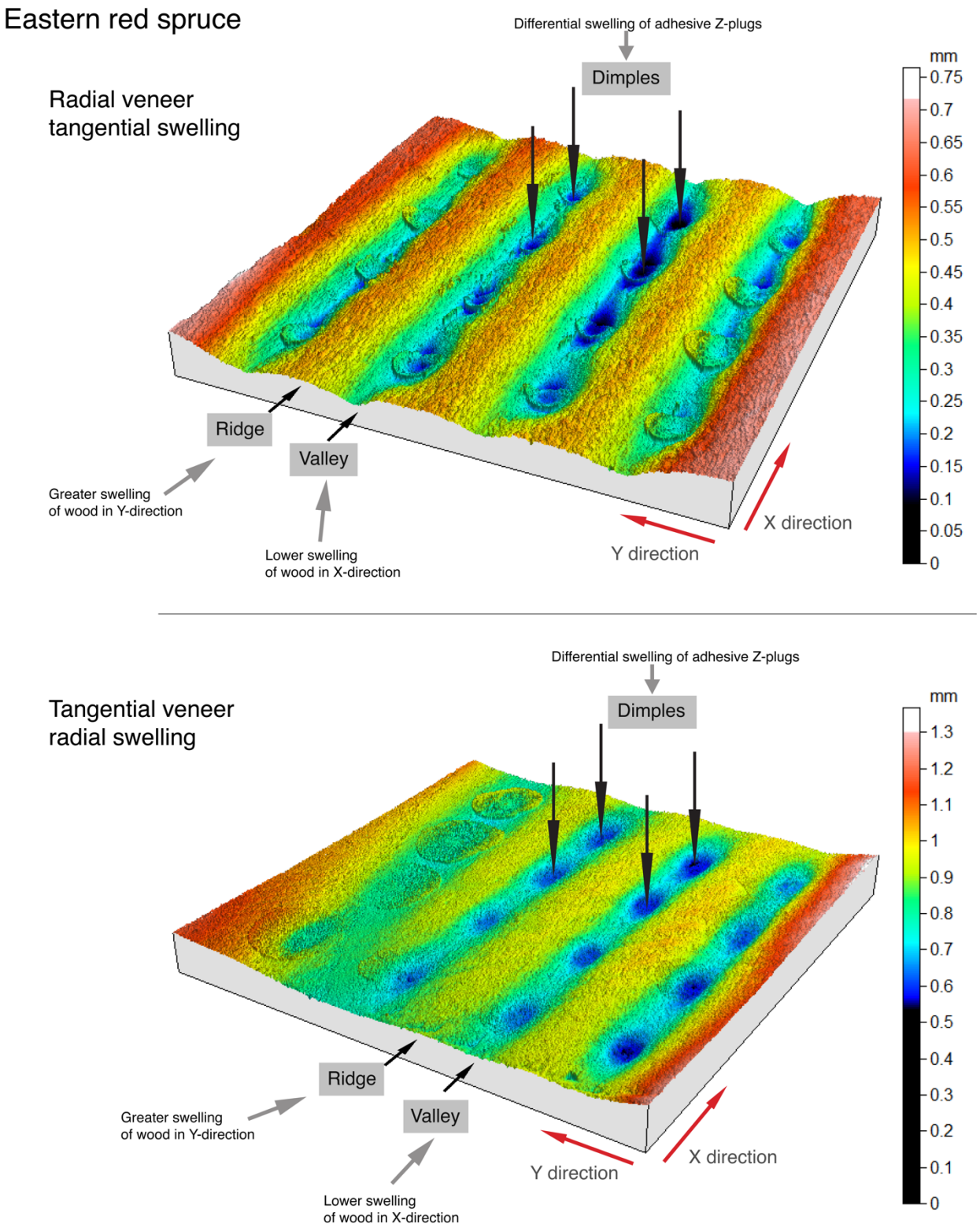

Figure 5.13 Surface topography of eastern red spruce composites after 24 h water soaking and re-conditioning

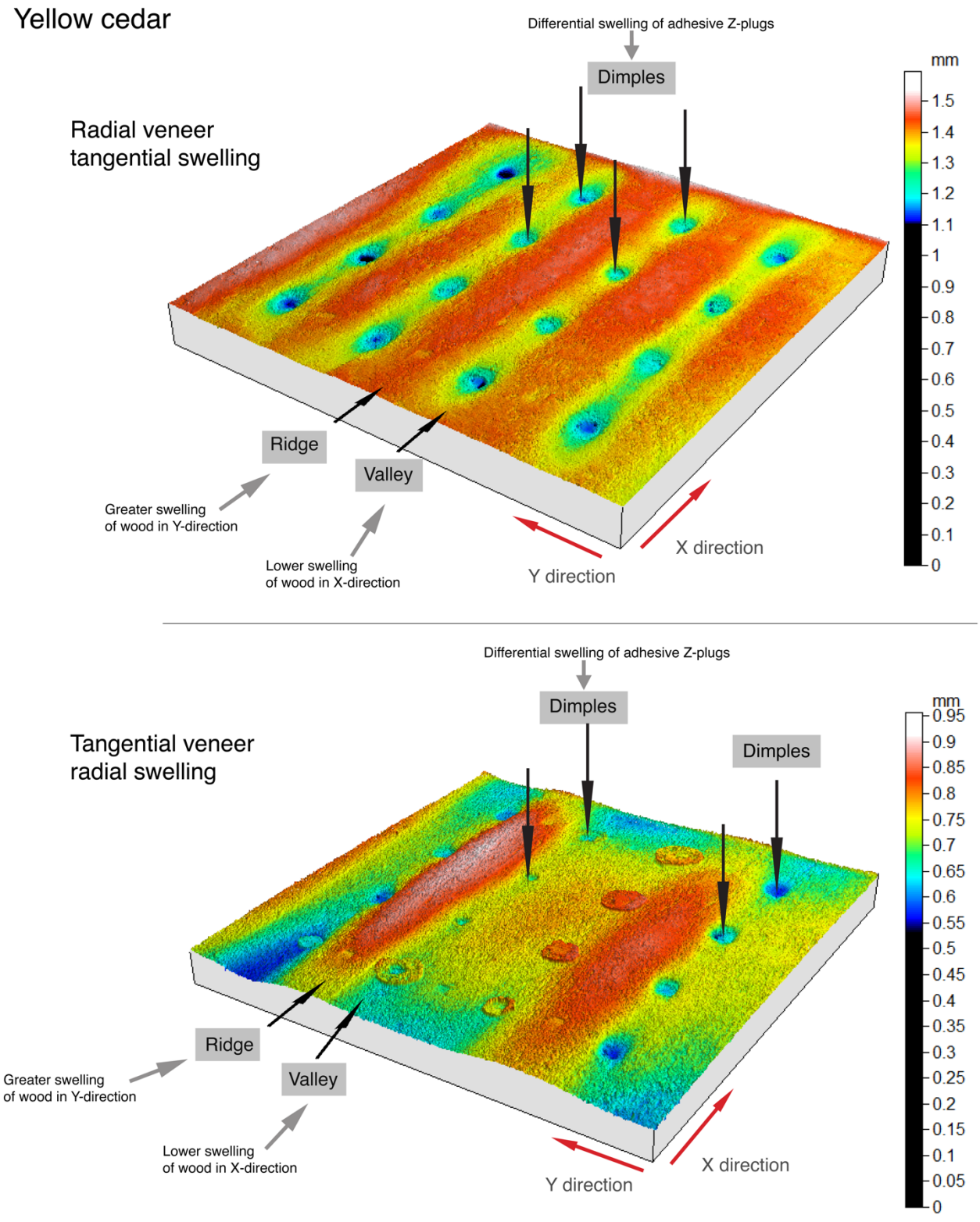

Figure 5.14 Surface topography of yellow cedar composites after 24 h water soaking and re-conditioning

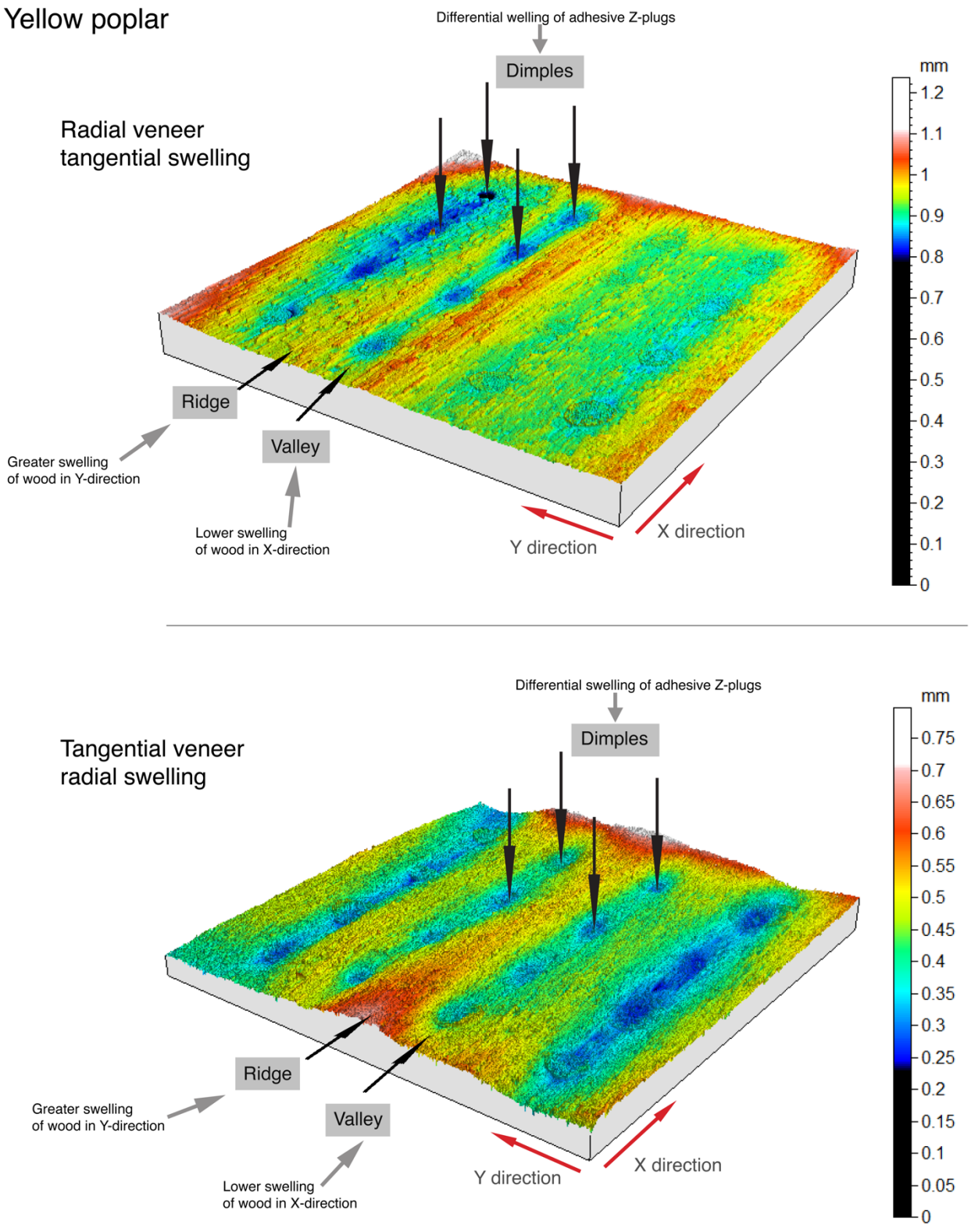

Figure 5.15 Surface topography of yellow poplar composites after 24 h water soaking and re-conditioning

5.3.4 Differential thickness swelling in X and Y directions

The differential thickness swelling of wood and the adhesive Z-connections within the composites was significantly ($p < 0.001$) greater in the X direction than in the Y direction, as observed in Chapter 4. In addition, there was a significant ($p < 0.05$) difference in differential thickness swelling between wood species in both X and Y directions (Fig. 5.16). However, there was no significant effect ($p > 0.05$) of veneer type on differential thickness swelling.

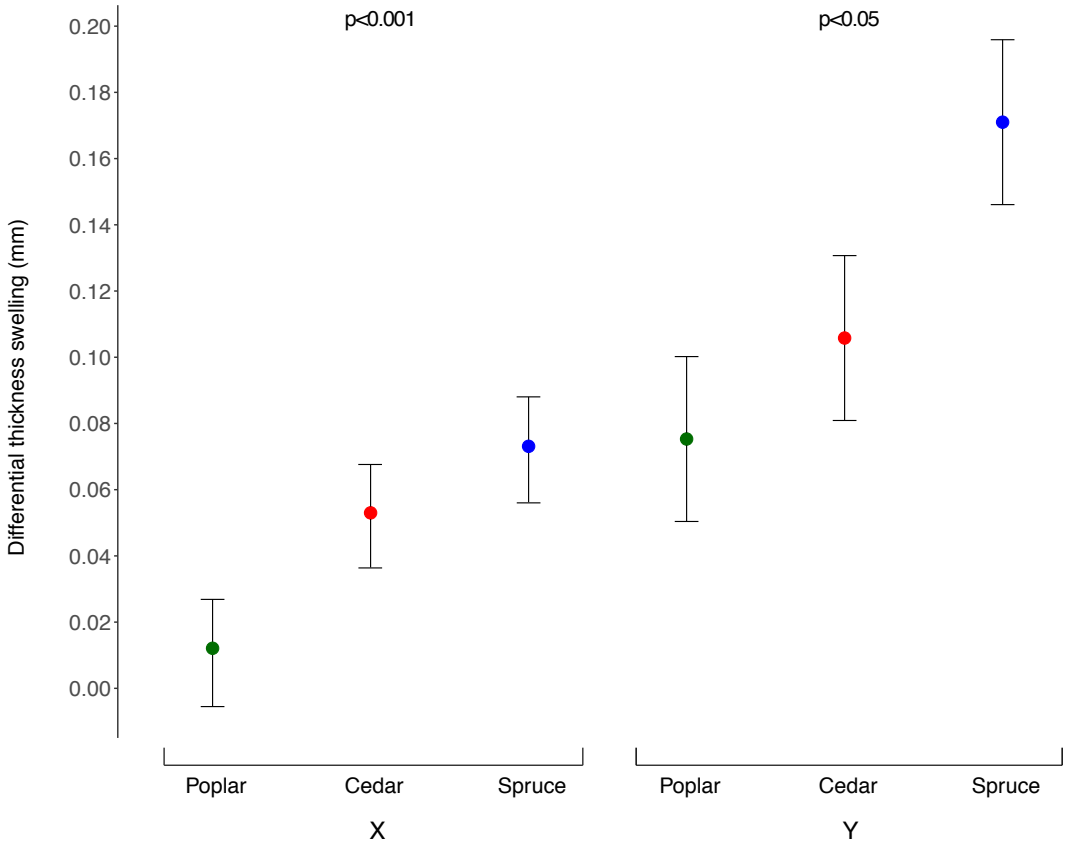

Figure 5.16 Comparison of differential thickness swelling of wood and the adhesive Z-connections in the X-direction (left) and Y-direction (right) of composites made from three wood species after 24 h water soaking and re-conditioning. There are significant differences between wood species. Error bars represent ± standard error of difference from ANOVA

5.3.5 Macro-photographic visualization of adhesive Z-connections

Macro-photographs of cross-sections of composites made from either radially or tangentially cut spruce, cedar and poplar veneers after 24 h water soaking and re-conditioning are shown in Figs 5.17~5.22. The macro-photographs clearly show that the Z-direction adhesive

connections are aligned in the thickness direction of the composites through 7 layers of wood veneer in each composite. Fig. 5.17 confirms that the adhesive Z-connections create profound ‘dimples’ at composite surfaces. Earlywood-latewood boundary in radially cut veneers is oriented approximately parallel to the thickness (Z) direction of the composite, as arrowed in Fig. 5.18 (1). Conversely, earlywood-latewood boundary in tangentially cut veneers is oriented approximately perpendicular to the thickness (Z) direction of the composite, as arrowed in Fig. 5.18 (2).

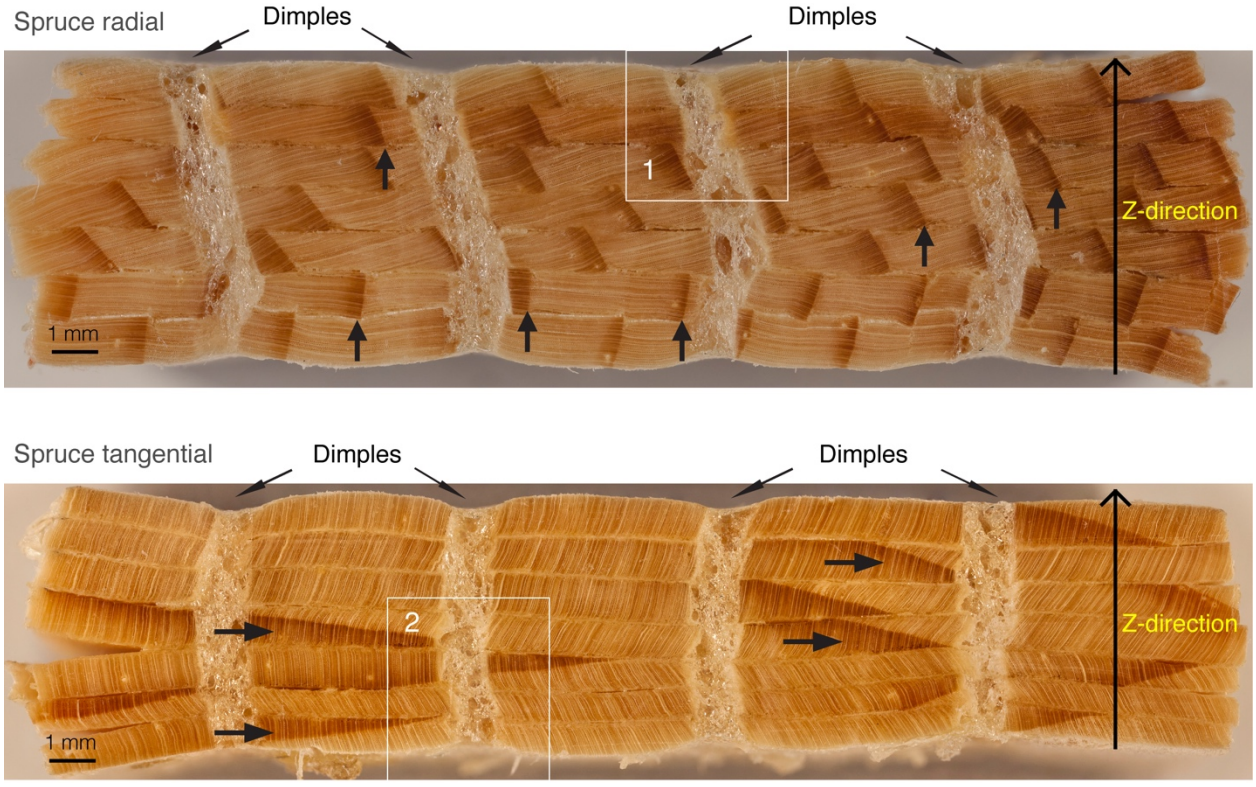

Figure 5.17 Macro-photographs of cross-sections of eastern red spruce composites made from radially and tangentially cut veneers showing one row of adhesive Z-connections through the thickness (Z) direction of composites. Arrows point to orientation of earlywood-latewood boundary

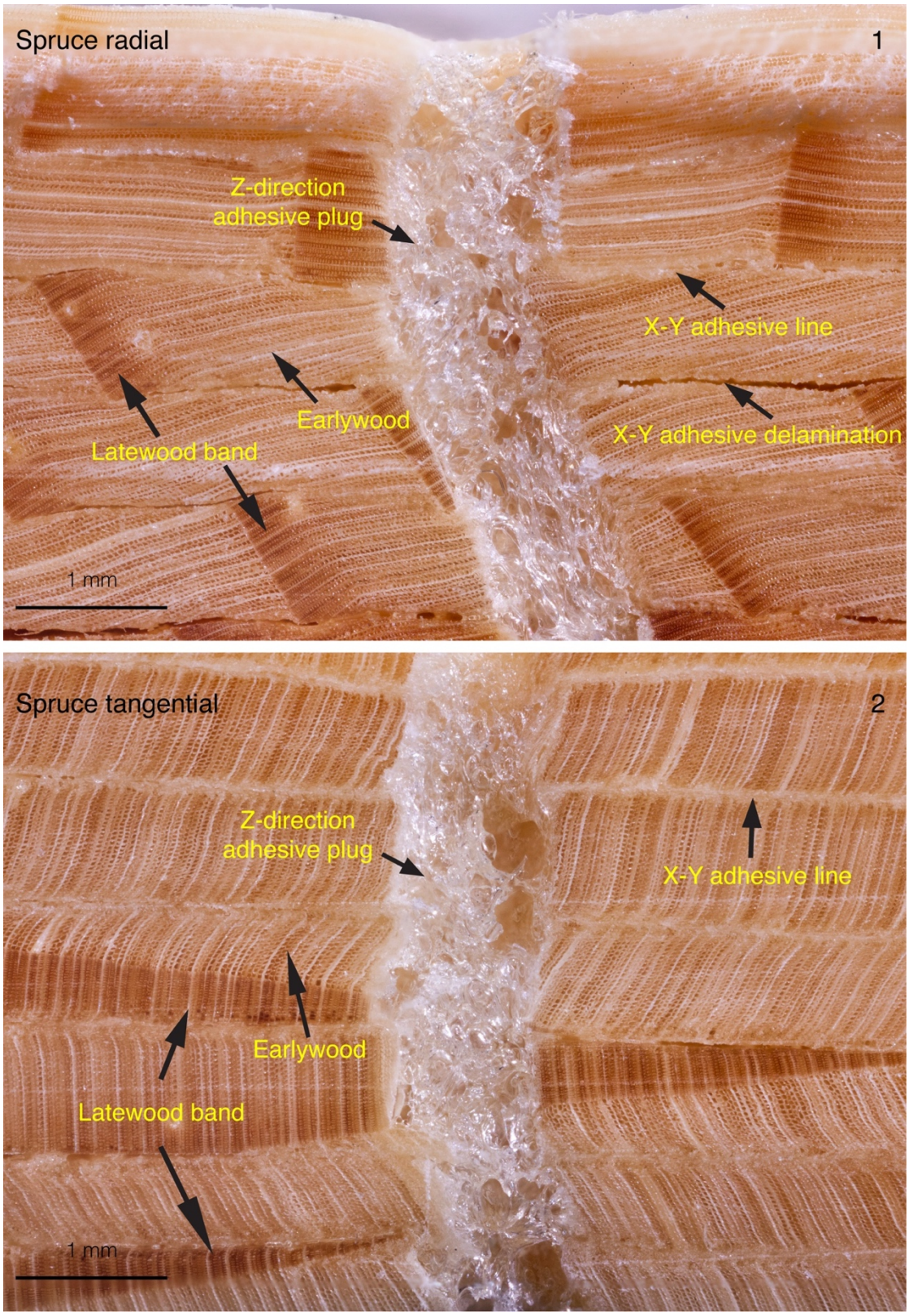

Figure 5.18 Macro-photographs of magnified areas 1 and 2 from Figure 5.17. Note the relative orientation of earlywood-latewood boundary to the adhesive Z-connections. X-Y adhesive bond lines as well as adhesive Z-connections are both visible

Fig. 5.19 shows the ‘dimples’ at cedar composite surfaces, but they are not as pronounced as those found at spruce composite surfaces. Earlywood-latewood boundary in radially cut veneers is oriented approximately parallel to the thickness (Z) direction of the composite, as arrowed in Fig. 5.20 (1). Conversely, earlywood-latewood boundary in tangentially cut veneers is oriented approximately perpendicular to the thickness (Z) direction of the composite, as arrowed in Fig. 5.20 (2). X-Y adhesive bond lines, some of which have delaminated, can be also seen in Figs. 5.19 & 5.20.

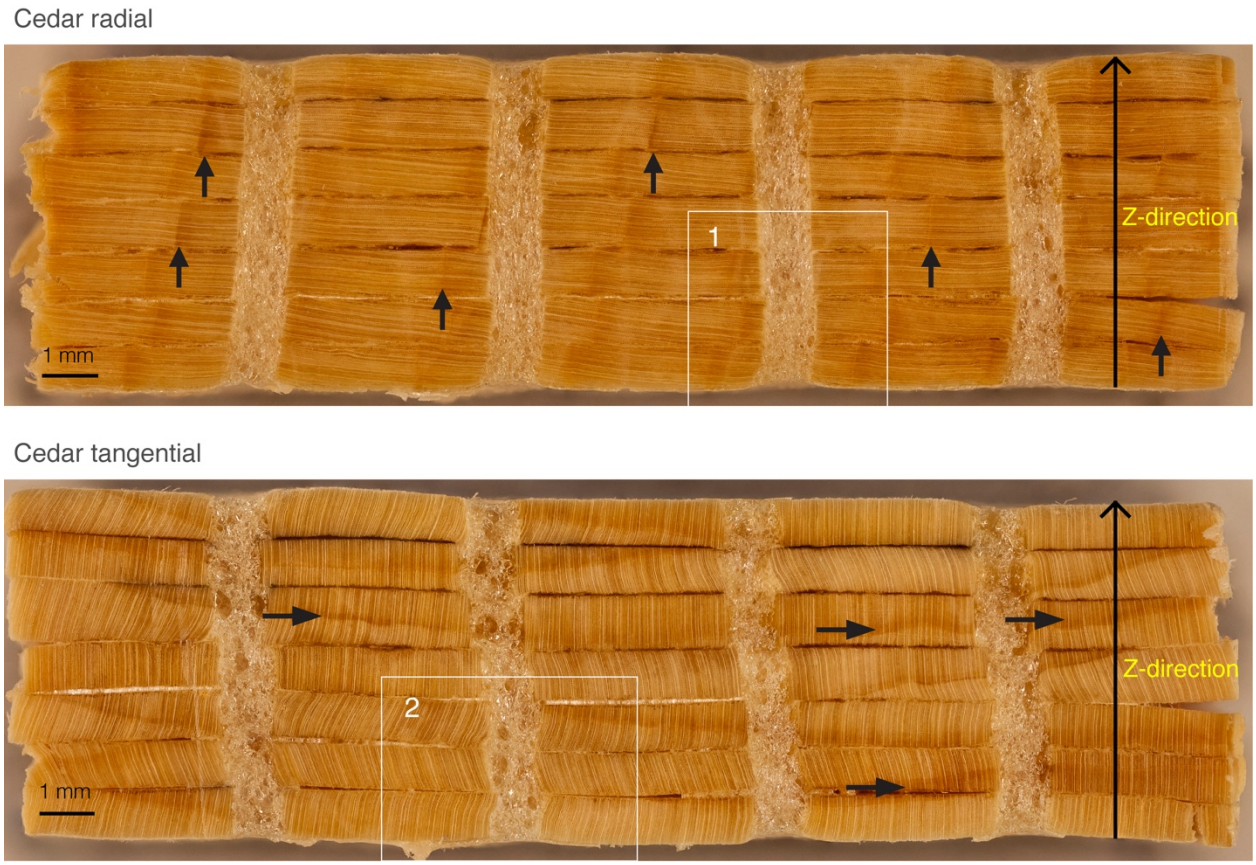

Figure 5.19 Macro-photographs of cross-sections of yellow cedar composites made from radially and tangentially cut veneers showing one row of adhesive Z-connections through the thickness (Z) direction of composites. Arrows point to orientation of ealrywood-latewood boundary

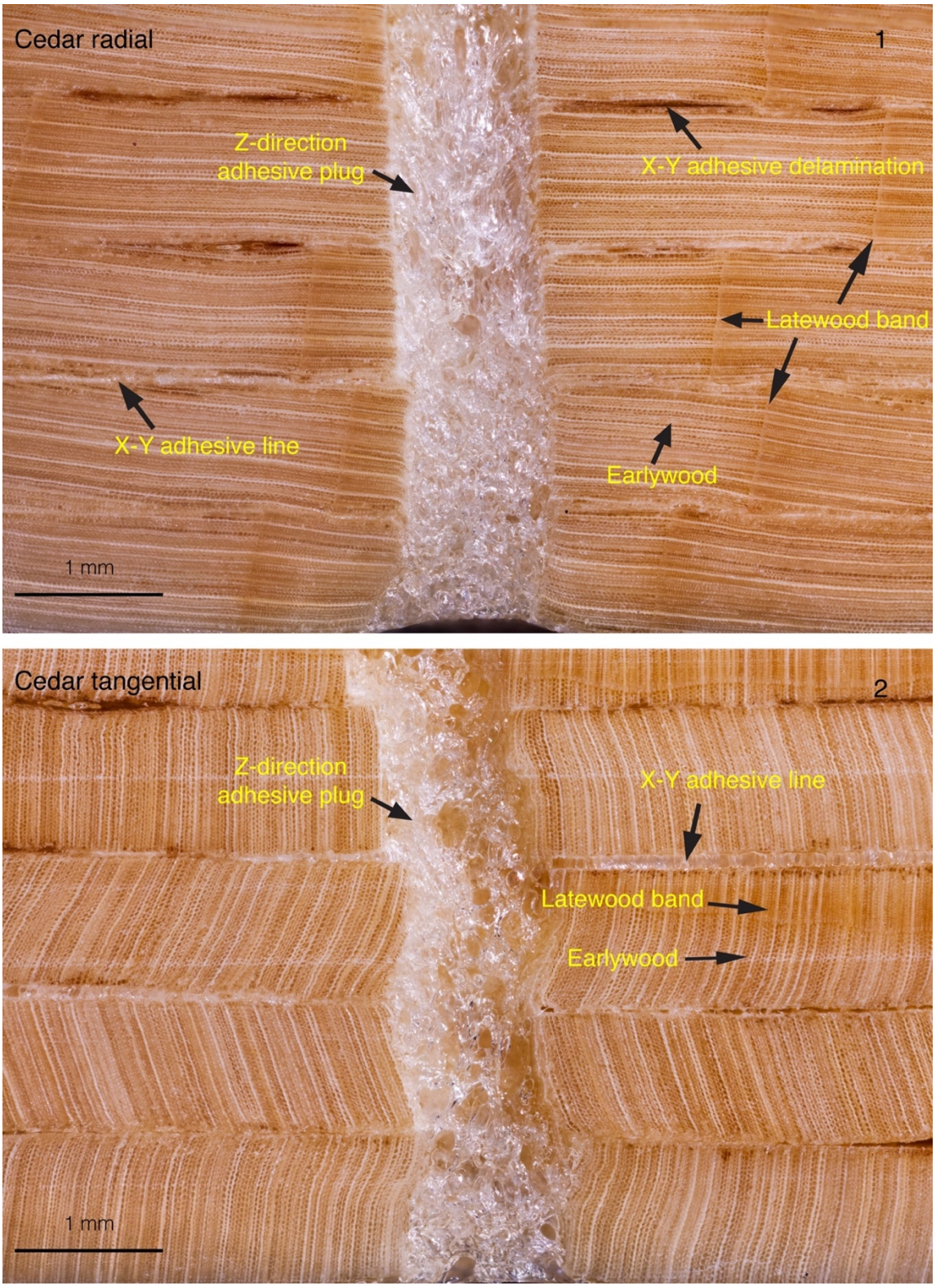

Figure 5.20 Macro-photographs of magnified areas 1 and 2 from Figure 5.19. Note the relative orientation of earlywood-latewood boundary to the adhesive Z-connections. Latewood bands in cedar are narrower than those in spruce but they are still visible. X-Y adhesive bond lines as well as adhesive Z-connections are both visible

‘Dimples’ were least pronounced at the poplar composite surface (Fig. 5.21) which confirms findings from confocal profilometry images. Vessels (pores) can be seen on the cross-sections of poplar composites (Fig. 5.22). Some of the vessels close to X-Y adhesive bond lines are filled with adhesive, as arrowed in Fig. 5.22. Rays can also be seen in poplar composites (Fig. 5.22). Rays in radially cut veneers are oriented approximately perpendicular to the thickness (Z) direction of the composite, as arrowed in Fig. 5.22 (1). Conversely, rays in tangentially cut veneers are oriented approximately parallel to the thickness (Z) direction of the composite, as arrowed in Fig. 5.22 (2).

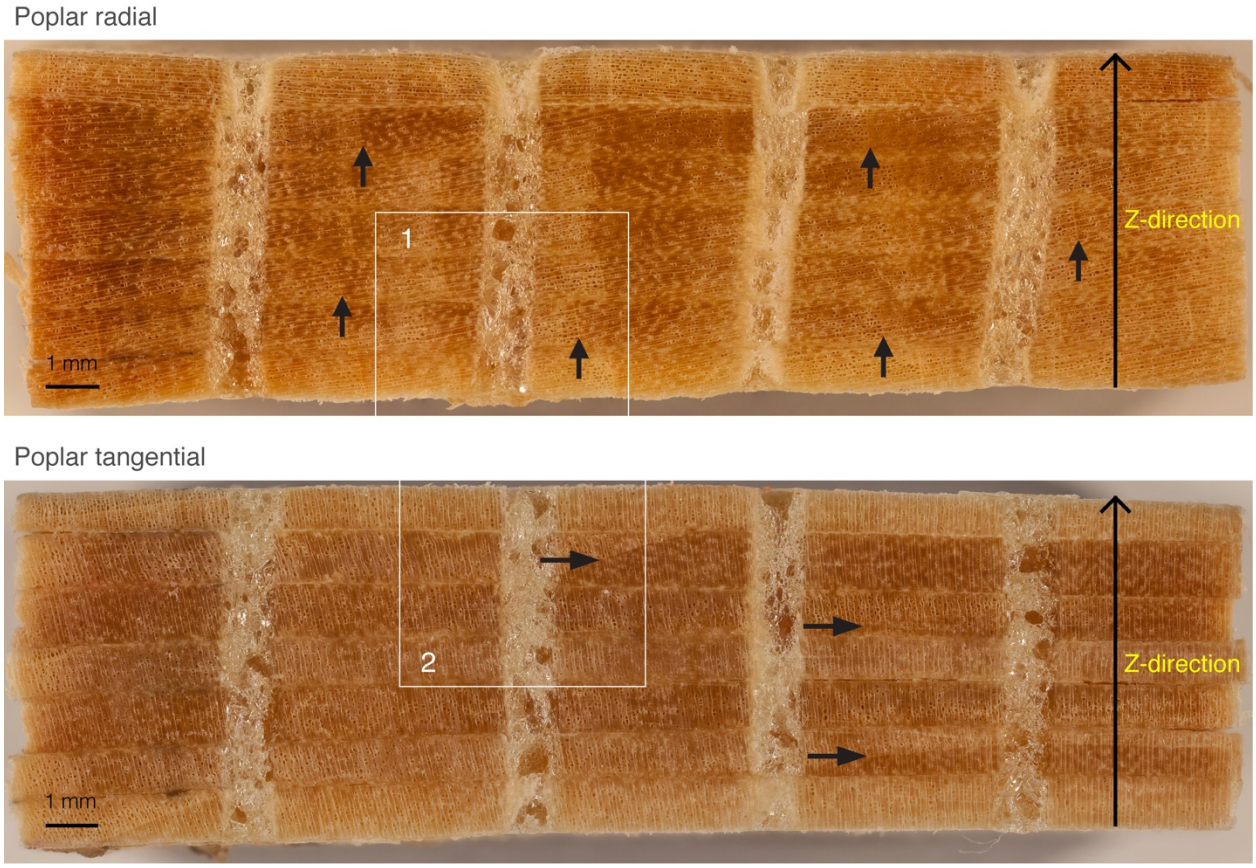

Figure 5.21 Macro-photographs of cross-sections of yellow poplar composites made from radially and tangentially cut veneers showing one row of adhesive Z-connections through the thickness (Z) direction of composites. Arrows point to orientation of ealrywood-latewood boundary

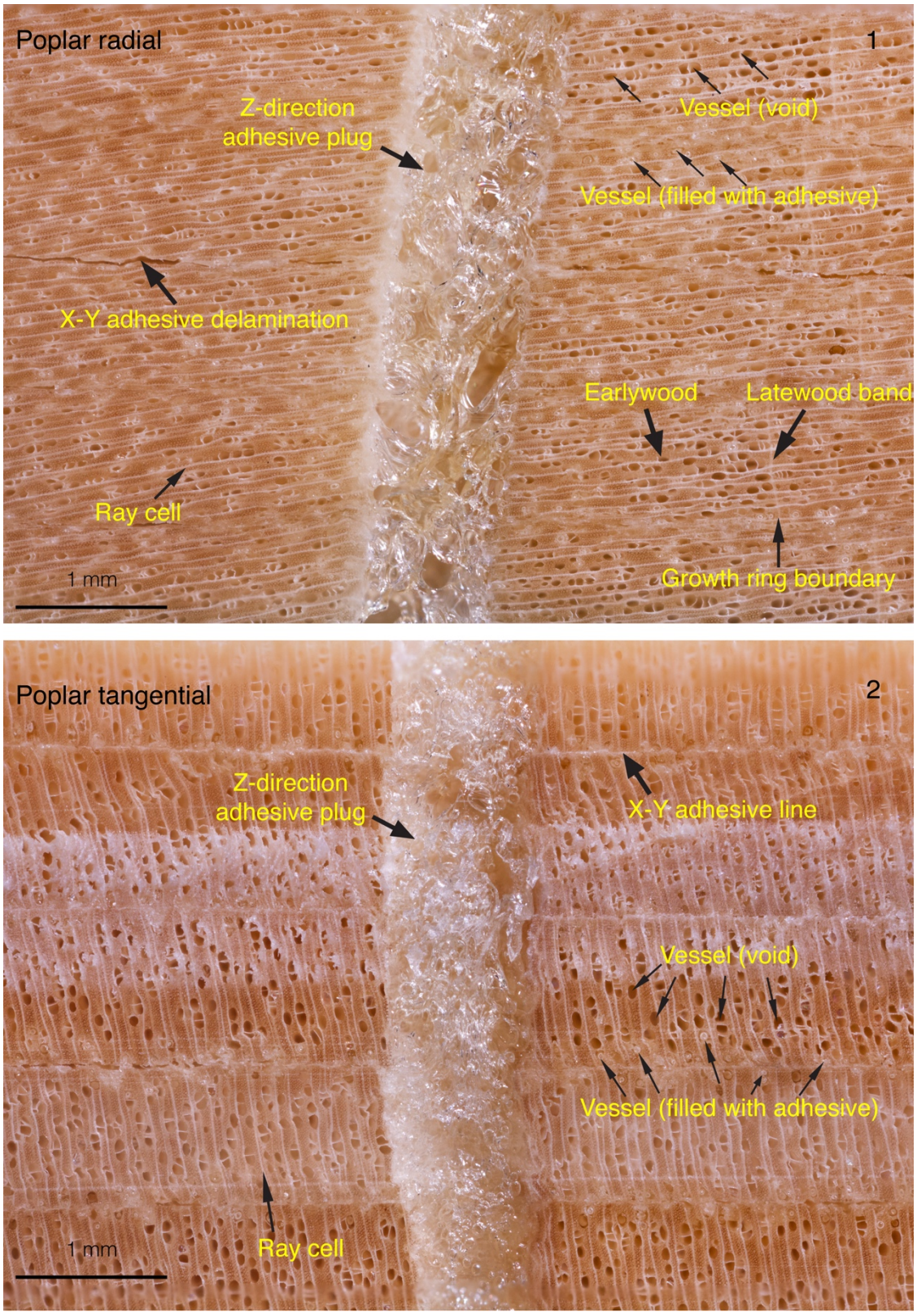

Figure 5.22 Macro-photographs of magnified areas 1 and 2 from Figure 5.21. Note vessel cells close to X-Y adhesive bond lines are filed with adhesive. Also note the different orientations of ray cells in radial and tangential composites

5.3.6 Scanning electron microscopy examination of the X-Y-Z adhesive network in the model wood composite

Scanning electron microscopy (SEM) photomicrographs of cross-sections of composites made from either radially or tangentially cut eastern red spruce, yellow cedar and yellow poplar veneers after 24 h water soaking and re-conditioning are shown in Figs. 5.23~5.25.

In composites made from radially cut spruce veneers, adhesive Z-connections can be clearly seen in Fig. 5.23a. The earlywood-latewood boundary is oriented approximately parallel to the adhesive Z-connection (Fig. 5.23a). X-Y adhesive bond lines are well connected to adhesive Z-connections (Fig. 5.23b). Adhesive in bond lines are present in tracheid cell lumens of adjacent wood. The penetration was as deep as the 3rd row of tracheids adjacent to the adhesive bond line (Fig. 5.23b). Earlywood tracheids near the adhesive Z-connection were deformed (Fig. 5.23b). Such deformation was associated with a decrease in volumes of cell lumens in earlywood tracheids. In contrast, latewood tracheids near the adhesive Z-connection showed little deformation compared to earlywood tracheids (Fig. 5.23c). Resin canals can be seen in spruce composites (Fig. 5.23d). Fig. 5.23d also shows delamination of an X-Y adhesive bond line at the boundary of latewood and earlywood.

In composites made from tangentially cut spruce veneers, adhesive Z-connections can also be seen oriented in the thickness direction of the composite (Fig. 5.23e). Adhesive Z-connections are orientated approximately perpendicular to growth rings (Fig. 5.23e). Connections between X-Y adhesive bond lines and adhesive Z-connections can also be clearly seen (Fig. 5.23f). Deformation of earlywood tracheids occurred near the adhesive Z-connection (Fig. 5.23g). Tracheids were deformed in the Z-direction due to the presence of an adjacent adhesive Z-connection. Such deformation was associated with decreased cell lumen volumes (Fig. 5.23g). Deformation of tracheids also occurred near the ‘dimple’ at the surface of composites (Fig. 5.23h).

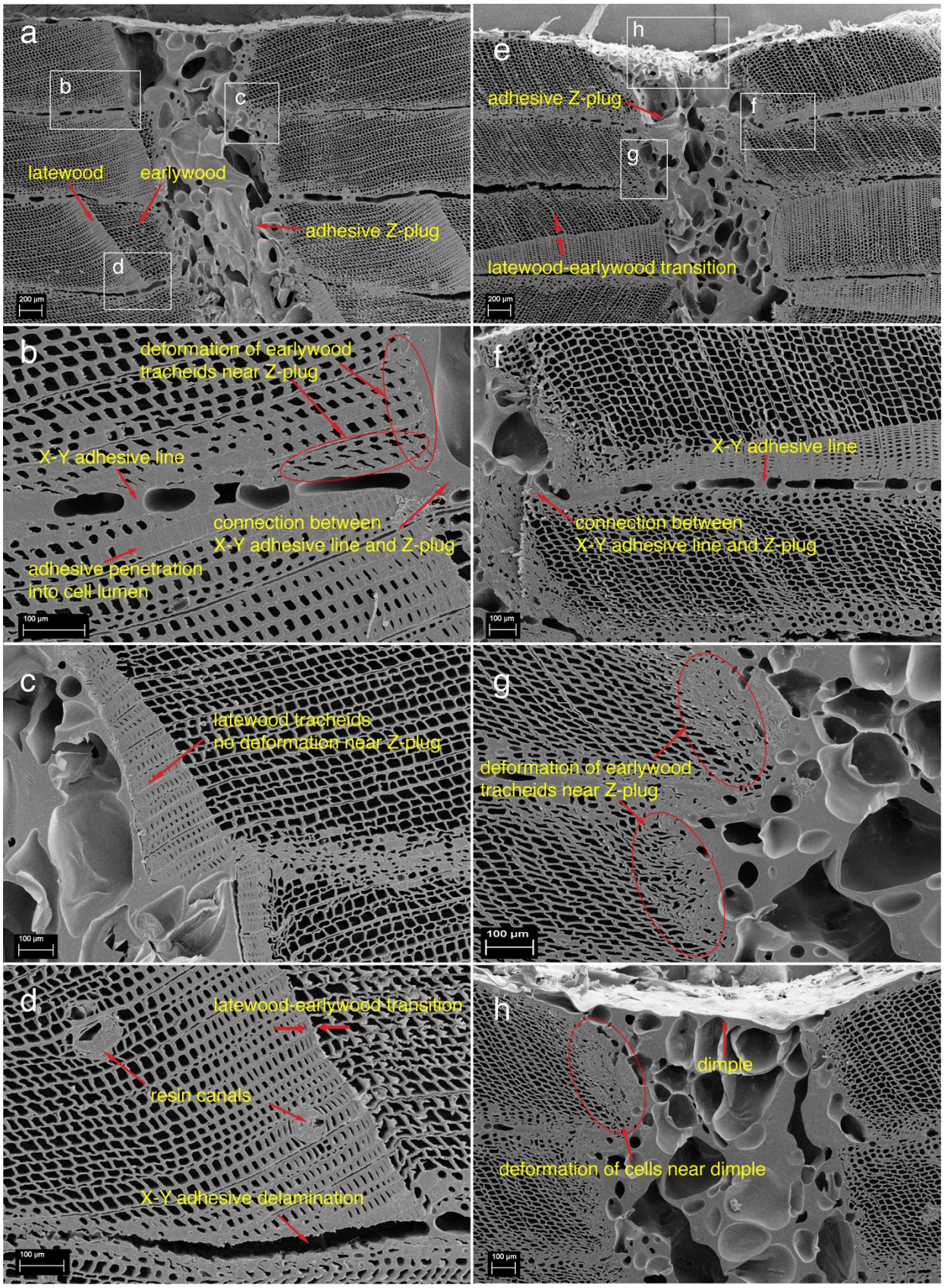

Spruce radial

Spruce tangential

Figure 5.23 Scanning electron photomicrographs of cross-sections of eastern red spruce composites made from radially cut (left-hand side) and tangentially cut (right-hand side) veneers. Figures (b), (c), (d) are higher magnification views of areas in Figure (a). Figures (f), (g), (h) are higher magnification views of areas in Figure (e)

In composites made from radially cut cedar veneers, most of the features noted in spruce composites were present, with some exceptions (Fig. 5.24a~b). Tracheids near the 'dimple' were slightly deformed (Fig. 5.24b), but not to the same extent as those of tracheids in spruce composites. Adhesive in the Z-connection penetrated ray cells perpendicular to the adhesive Z-connection (Fig. 5.24b). Adhesive in the X-Y bond lines penetrated into and filled up cell lumens of adjacent tracheids (Fig. 5.24c), but there was less penetration of adhesive than occurred in spruce composites. Intra-wall as well as inter-wall fractures were associated with delamination of X-Y adhesive bond lines. Intra-wall microfracture was observed in earlywood tracheids (Fig. 5.24c) that were not filled with adhesive, while inter-wall fracture occurred in tracheids that were filled up with adhesive (Fig. 5.24d). Fig. 5.23d also shows that X-Y adhesive bond lines penetrated into both earlywood and latewood tracheids.

In composites made from tangentially cut cedar veneers, adhesive Z-connections are also clearly present in the thickness direction of composite and well connected with X-Y adhesive bond lines (Fig. 5.24e). A series of ray cells are aligned parallel to the adhesive Z-connection and perpendicular to X-Y adhesive bond lines (Fig. 5.24f). Deformation occurred in both earlywood and latewood tracheids near an adhesive Z-connection (Fig. 5.24g). Fig. 5.24g also shows a ray cell oriented in the Z-direction crossing earlywood and latewood zones. Adhesive in the X-Y bond lines penetrated into ray cells that are oriented perpendicular to the adhesive interface (Fig. 5.24h).

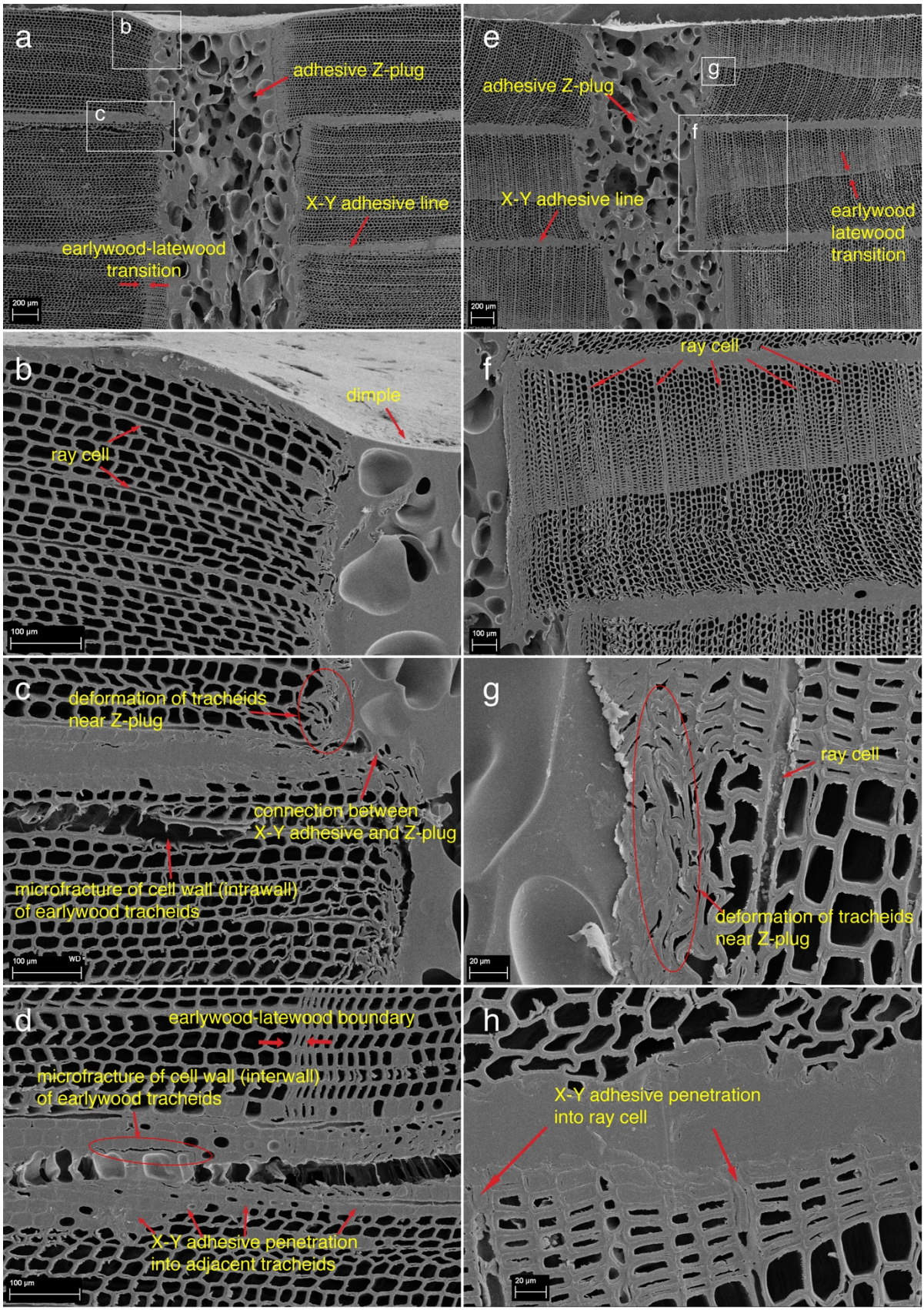

Cedar radial

Cedar tangential

Figure 5.24 Scanning electron photomicrographs of cross-sections of yellow cedar composites made from radially cut (left-hand side) and tangentially cut (right-hand side) veneers. Figures (b), (c) are higher magnification views of areas in Figure (a). Figures (f), (g) are higher magnification views of areas in Figure (e)

In composites made from radially cut poplar veneers, adhesive Z-connections are also clearly visible (Fig. 5.25a). Growth rings are oriented approximately parallel to the adhesive Z-connections (Fig. 5.25a). Large vessels (pores) can be seen in Fig. 5.25b. Ray cells are oriented perpendicular to the adhesive Z-connections in Fig. 5.25b. Adhesive from the X-Y glue-lines penetrated into fibres and large vessels (Fig. 5.25c). Some vessels were completely occluded with adhesive as arrowed in Fig. 5.25c, and in places little adhesive was present at the interface between two wood veneers. In such areas inter-laminar delamination tended to occur (Fig. 5.25c). Where delamination occurred adhesive was stretched in the Z-direction acted as 'bridge' between two adjacent wood veneers (arrowed in Fig. 5.25c). Detachment of adhesive Z-connection and end grain of adjacent wood veneer was observed (Fig. 5.25d), which was not found in either spruce or cedar composites. This suggests poorer bonding between adhesive Z-connections and poplar wood than that in either spruce or cedar composites.

In composites made from tangentially cut poplar veneers, adhesive Z-connections are clearly visible in Fig. 5.25e. Adhesive in the X-Y bond lines penetrated into nearby vessels and filled up their lumens (Fig. 5.25f). Adhesive pulled out where there was inter-laminar delamination (Fig. 5.25f). Adhesive inside a vessel lumens fractured at delamination and acted as a 'bridge' between two adjacent wood veneers (Fig. 5.25g). Detachment between adhesive Z-connection and end grain of adjacent wood veneer also occurred (arrowed in Fig. 5.25g), indicating poor bonding. Deformation of fibres but not vessels near an adhesive Z-connection occurred (Fig. 5.25h).

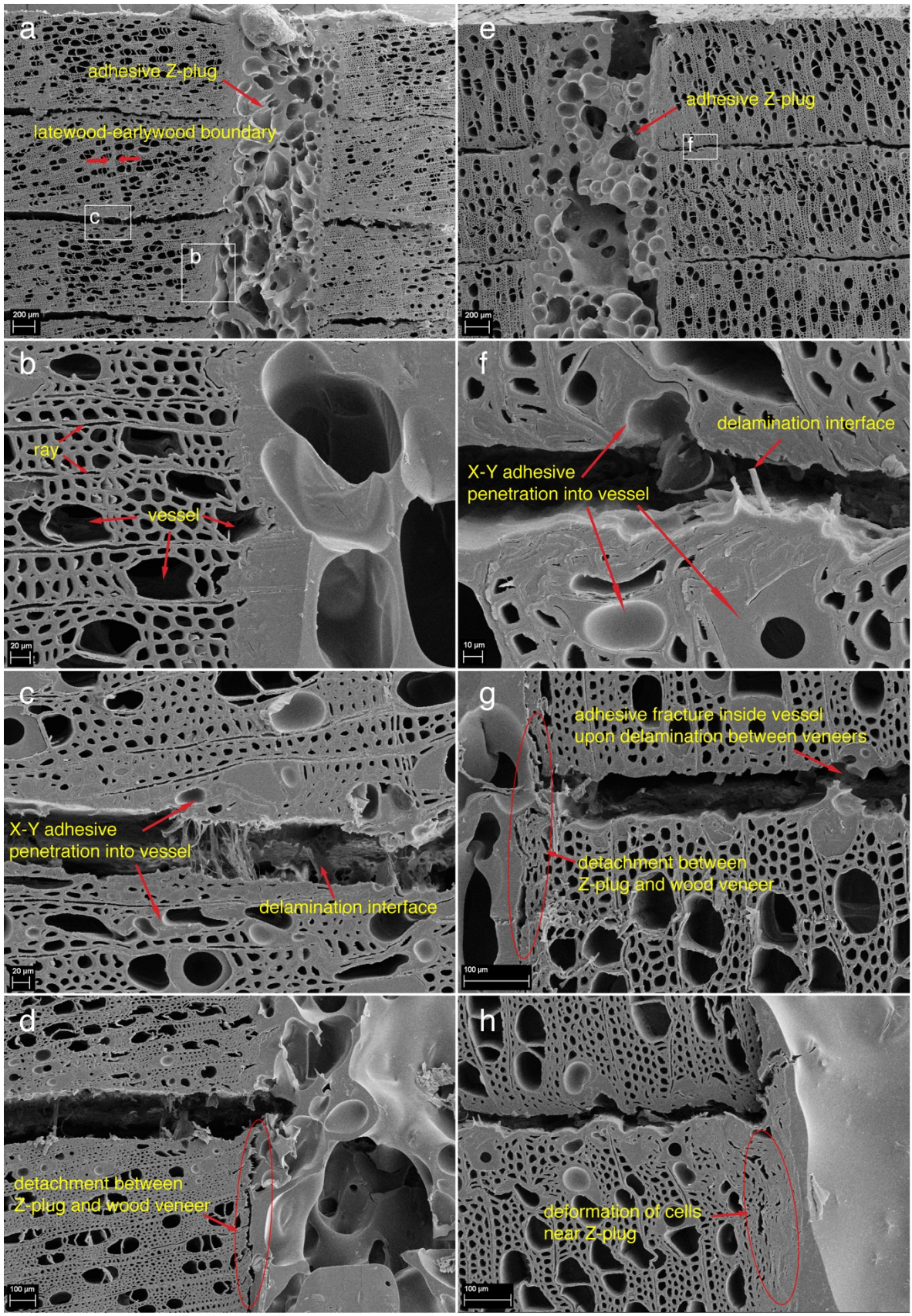

Poplar radial

Poplar tangential

Figure 5.25 Scanning electron photomicrographs of cross-sections of yellow poplar composites made from radially cut (left-hand side) and tangentially cut (right-hand side) veneers. Figures (b), (c) are higher magnification views of areas in Figure (a). Figure (f) is higher magnification views of areas in Figure (e)

5.4 Discussion

My results support the hypothesis that adhesive Z-connections will restrain thickness swelling of my model composite. My results in Chapter 4 showed that adhesive Z-connections were ineffective at restraining the thickness swelling of a composite made from the hardwood birch. In contrast, results here show that adhesive Z-connections are able to restrict the thickness swelling of a composite made from poplar, although, overall, the Z-connections were less effective at restraining thickness swelling of poplar composites than they were at restraining swelling of composites made from either of the two softwoods (spruce and cedar).

The adhesive Z-connections were most effective at reducing the thickness swelling of composites made from either tangential spruce veneer or radial cedar veneer. These composites showed higher swelling and greater resistance to delamination than composites composed of radial (spruce) or tangential (cedar) veneer. These observations suggest an association between degree of thickness swelling & resistance to delamination of the composites and the ability of adhesive Z-connections to reduce swelling of the composites. My results in Chapter 4 showed that adhesive Z-connections were more effective at restraining thickness swelling of spruce composites made from rotary peeled (tangential) veneer than they were at restricting the swelling of cedar composites made from sliced (radial) veneer. In contrast, results here showed that adhesive Z-connections were almost as effective at restraining thickness swelling of cedar composites made from sawn radial veneer as they were at reducing the thickness swelling of spruce composites made from sawn tangential veneer. This discrepancy between results here and those in Chapter 4 may have occurred because the average thickness swelling of composites made from sawn radial cedar veneer here was 24% (Table 5.3) whereas the comparable figure in Chapter 4 was 17% (Fig. 4.4). This suggestion

would accord with my finding of an association between the overall thickness swelling of the composites and the extent to which adhesive Z-connections restrain swelling.

Another factor that may be relevant to the ability of adhesive Z-connections to reduce thickness swelling of the model composites made from different wood species is the extent to which adhesive is able to form solid columns (plugs) in the different species. I noted that adhesive Z-connections in birch composites contained more voids than those in poplar composites (compare Fig. 4.7 (Chapter 4) and Fig. 5.21 (Chapter 5)). Adhesive columns containing voids might be less effective at restraining thickness swelling than those with fewer voids, which would explain why adhesive Z-connections were ineffective at restraining thickness swelling of birch composites whereas they restrained swelling of composites made from poplar.

Surface topography maps obtained using confocal profilometry visualized height differences between wood and adhesive Z-connections after swelling and re-conditioning. They showed that 'dimples' at composite surfaces were most pronounced in spruce composites, which accords with measurements of the swelling of the composites. Differences in surface topography of cedar composites made from tangentially or radially sawn veneer (Fig. 5.14) also accord with measurement values. Measurements of the swelling of wood veneer compared to that of PU adhesive, and also scanning electron microscopy images of composites strongly suggest that the ability of adhesive Z-connections to restrain thickness swelling of model wood composites is related to lower swelling of the adhesive Z-connections than that of the wood connected to the adhesive Z-connections. The restraint of swelling caused by the adhesive Z-connections caused deformation of wood cells adjacent to adhesive Z-connections. Deformation of cells around adhesive Z-connections was found in spruce, cedar and poplar composites (Figs. 5.24~5.26). However, deformation was more pronounced in spruce (Fig. 5.24) than in cedar (Fig. 5.25) or poplar composites (Fig. 5.26), possibly because of the greater swelling of

composites made from spruce, and the lower density of spruce compared to cedar or poplar wood.

Overall, my findings suggest that adhesive Z-connections will work better at restraining swelling of composites made from softwood rather than hardwood veneer. Therefore, selection of wood species has a considerable influence on the ability of adhesive Z-connections to reduce thickness swelling of wood composites. Accordingly, adhesive Z-connections may be effective at reducing thickness swelling of composites made from pine and other softwoods for example western hemlock (Markwardt and Wilson 1935), because they have similar characteristics to the spruce tested here (particularly the ability to form strong glue bonds). Although the effectiveness of adhesive Z-connections at restricting swelling did not vary significantly with veneer type, there was a statistical interaction between veneer type and species on swelling. Therefore, selection of either rotary peeled or sliced veneer may be an important consideration when selecting wood species for the manufacture of composites containing adhesive Z-connections.

5.5 Conclusions

In conclusion, the results in this chapter confirm the findings in Chapter 4 that introducing adhesive Z-connections can reduce thickness swelling of wood composites. Restraint of thickness swelling varies with wood species and is more effective with spruce, than with cedar and particularly poplar. Adhesive Z-connections restrain swelling of both types of veneer that are produced commercially (rotary-peeled or sliced). I have suggested how the Z-connections restrain thickness swelling, and why they might be effective at restraining swelling of other softwoods such as pine or western hemlock. The approach of introducing adhesive Z-connections to reduce swelling does not increase the consumption of adhesive used in the manufacture of wood composites. In contrast, most other methods currently being used to reduce thickness swelling of wood composites require increased amount of adhesive or the use of more costly adhesives. Therefore, my approach to reducing thickness swelling may be cost-

effective. However, further optimization of the adhesive Z-connections as a way of reducing thickness swelling is still possible. Such optimization includes examination of effects of various design parameters including area-density, diameter and spatial distribution on the thickness swelling of composites containing adhesive Z-connections. This topic will be addressed in the following chapter.

6 Finite Element Modelling of the Ability of Adhesive Z-connections to Restrain Thickness Swelling of a Model Wood Composite

6.1 Introduction

Chapters 4 and 5 used experimental approaches to examine the ability of adhesive Z-connections to restrain hygroscopic thickness swelling of a model wood composite. This chapter uses finite element analysis (FEA) to better understand various parameters involved in the design of composites with adhesive Z-connections.

FEA has been extensively used to model hygroscopic swelling of polymeric materials used in integrated circuits as described in Chapter 2 (Lam 2000; Zhou et al. 2005; Hsu et al. 2008; Hsu and Hsu 2009; Shirangi and Michel 2010). Hygroscopic swelling of wood is a physical phenomenon that couples moisture absorption and moisture-induced strain energy. Moisture absorption in wood has been intensively studied and has been widely modeled using Fick's second law of moisture diffusion (Skaar 1988; Shmulsky and Jones 2011a). However, there is little finite element modelling of the hygroscopic swelling of wood or wood composites. Therefore, in this chapter I developed a model for the hygroscopic swelling of wood based on the approaches used to model similar phenomena in polymeric materials, but taking into account the directional properties of wood.

Previous studies of advanced carbon fibre composites have shown that design parameters, such as spacing, diameter and density of Z-direction reinforcement influence their ability to strengthen carbon fibre composites (Partridge et al. 2003a, 2003b; Partridge and Cartié 2005). It is plausible that the same design parameters could influence the ability of adhesive Z-connections to restrain thickness swelling of wood composites. Examination of the effects of Z-connection density and spacing on thickness swelling using an experimental approach would be time consuming and expensive. On the other hand, FEA and computer simulation of effects of Z-connections on the hygroscopic swelling of composites would make it

possible to easily change design parameters, such as density of adhesive Z-connections, and model their effects on thickness swelling.

In this chapter, I hypothesize that area-density, diameter and spatial distribution of adhesive Z-connections will influence the ability of Z-connections to restrain thickness swelling of wood composites. To test this hypothesis I developed a coupled hygroscopic-mechanical finite element model. My model used the ANSYS® Multiphysics FEA program to simulate moisture diffusion and hygroscopic swelling of model wood composites containing adhesive Z-connections with different area densities, diameters and spatial distributions. The thickness swelling of the different wood composites was modelled. The final output of the model is improved design parameters for my model wood composite containing adhesive Z-connections.

6.2 Modelling moisture diffusion and hygroscopic swelling

6.2.1 Physical phenomenon

My model simulated the thickness swelling of a model wood composite submerged in water, as described in Chapters 4 & 5. The wood composite consisted of seven tangentially-cut spruce wood veneers (measuring 25 mm x 25 mm x 1 mm) that were bonded together with a polyurethane adhesive. The wood composite contained adhesive Z-connections with various design configurations as briefly mentioned above.

6.2.2 Modelling of moisture diffusion

Moisture diffusion in wood is governed by Fick's second law, which can be expressed using equation (1) (Hsu and Hsu 2009):

$$\frac{\partial C}{\partial t} = D\left(\frac{\partial^2 C}{\partial x^2} + \frac{\partial^2 C}{\partial y^2} + \frac{\partial^2 C}{\partial z^2}\right) \quad \text{..... (1)}$$

where C stands for the local moisture concentration (kg/m^3), t is time (s), and D is the coefficient of moisture diffusivity (m^2/s). Considering that in terms of moisture diffusion rates, wood is an

orthotropic material in three directions, the 3D moisture diffusion equation for wood can be rewritten as follows (equation 2) (Hsu and Hsu 2009):

$$\frac{\partial C}{\partial t} = D_x \frac{\partial^2 C}{\partial x^2} + D_y \frac{\partial^2 C}{\partial y^2} + D_z \frac{\partial^2 C}{\partial z^2} \quad \text{..... (2)}$$

where D_x, D_y, and D_z represent the coefficient of moisture diffusivity of wood in X (longitudinal), Y (tangential) and Z (radial) directions, respectively.

Most commercial FEA software does not have a moisture diffusion simulation module. However, there is similarity between the governing equations for moisture diffusion and thermal diffusion (Crank 1956). Thermal diffusion (transient heat conduction) can be described using equation (3) (Hsu and Hsu 2009).

$$\frac{\partial T}{\partial t} = \alpha_T \left(\frac{\partial^2 T}{\partial x^2} + \frac{\partial^2 T}{\partial y^2} + \frac{\partial^2 T}{\partial z^2} \right) \quad \text{..... (3)}$$

where T stands for local temperature (K), t is time (s), and α_T is thermal diffusivity (m^2/s), which can be defined as $\alpha_T = K/(\rho C_p)$ where K is thermal conductivity (W/m·C°), ρ is density (kg/m^3), and C_p is specific heat (J/kg·C°). In accord with the 3D moisture diffusion equation, 3D heat conduction for an orthotropic material can be expressed using equation (4) (Hsu and Hsu 2009).

$$\frac{\partial T}{\partial t} = \alpha T_x \frac{\partial^2 T}{\partial x^2} + \alpha T_y \frac{\partial^2 T}{\partial y^2} + \alpha T_z \frac{\partial^2 T}{\partial z^2} \quad \text{..... (4)}$$

where αT_x, αT_y, αT_z represent the coefficients of thermal diffusivity in the X, Y and Z directions, respectively.

The similarity between the two diffusion equations makes it possible to use the thermal diffusion simulation module in the FEA software ANSYS® to solve moisture diffusion problems (Hsu et al. 2008). However, the software is only directly applicable if a homogeneous system is modelled. For heterogeneous composite systems, the moisture concentration is discontinuous

at the multi-material interface (Crank 1956; Wong et al. 1998; Wong et al. 2002a, 2002b). This discontinuity is a barrier to the use of FEA's thermal diffusion module to solve moisture diffusion problems (Zienkiewicz et al. 1967, 2005). But this barrier can be circumvented by introducing a new physical quantity, 'wetness', and modelling moisture diffusion of a composite consisting of two materials, i.e. wood and adhesive. The derivative variable 'wetness', W is defined in equation (5) (Wong et al. 1998):

$$\mathrm{W} = C/C_{sat} \qquad \text{……. (5)}$$

where C_{sat} is saturated moisture concentration (kg/m^3) of a material.

The variable 'wetness', W is continuous across a bi-material interface and therefore obeys Fick's law of diffusion. So, equation (1) can be re-written as equation (6) (Hsu and Hsu 2009):

$$\frac{\partial \mathrm{W}}{\partial \mathrm{t}} = \mathrm{D}\left(\frac{\partial^2 \mathrm{W}}{\partial \mathrm{x}^2} + \frac{\partial^2 \mathrm{W}}{\partial \mathrm{y}^2} + \frac{\partial^2 \mathrm{W}}{\partial \mathrm{z}^2}\right) \qquad \text{……. (6)}$$

where wetness, W has a physical meaning in that W = 0 indicates a completely dry state, and W = 1 indicates a fully saturated state.

Table 6.1 compares thermal diffusion and moisture diffusion including the newly introduced physical quantity, wetness, which was used within the ANSYS® Multiphysics module to simulate moisture diffusion within model wood composites containing various configurations of adhesive Z-connections (area-density, diameter and spatial distribution).

Table 6.1 Parameters used to model thermal and moisture diffusion

Properties	**Thermal diffusion parameters**	**Moisture diffusion parameters**
Field variable	Temperature, T	Wetness, W
Density	ρ	1
Conductivity	K	DC_{sat}
Specific capacity	C_p	C_{sat}
Coefficient of expansion	α	βC_{sat}

6.2.3 Modelling of hygroscopic swelling

Hygroscopic strain, ε_h, induced by hygroscopic stress can be defined using equation (7) (Hsu et al. 2008):

$$\varepsilon_h = \beta C \quad \text{..... (7)}$$

where β is the coefficient of moisture expansion (CME).

Similarly, thermal strain, ε_T induced by thermal stress can be defined using equation (8) (Hsu et al. 2008):

$$\varepsilon_T = \alpha \Delta T \quad \text{..... (8)}$$

where α is the coefficient of thermal expansion (CTE).

The similarity between hygro-mechanical (CME) and the thermal-mechanical (CTE) equations is apparent (Lesse 1972) from the relevant parameters listed in Table 6.1.

In summary, the model developed in this chapter combined a moisture diffusion model with a hygro-mechanical model (as applied to a laminated wood composite). Computer

simulation of moisture-induced swelling of the laminated wood composite was performed using the thermal diffusion and thermal-mechanical modules of the ANSYS® Multiphysics program.

6.2.4 Determination of material properties associated with the model

Saturated moisture concentration, C_{sat} of a material can be calculated using equation (9) (Hsu and Hsu 2009):

$$C_{sat} = \frac{M_{sat}}{abc(100 - \text{vol\% of moisture})} \quad \text{..... (9)}$$

where M_{sat} is saturated mass (kg) and a, b and c are length (m), width (m) and thickness (m) of specimens, respectively.

Wood has a critical moisture content level, the fibre saturation point (FSP), above which its dimensions will not increase with increasing moisture content. Therefore, the saturated moisture concentration of the model composite derived from equation (9) is equal to the FSP of wood.

Moisture diffusion coefficients, D, were taken from the literature (Wadsø 1993; Time 1998). Given that wood veneers in the composite were tangentially sliced, the X, Y and Z directions in the model represent longitudinal, tangential, and radial directions of wood, respectively. Hence, the 3D moisture diffusivity was determined as $D_x = 1000 \times 10^{-12}$ m^2/s, and $D_y = D_z = 52 \times 10^{-12}$ m^2/s. In contrast, the polyurethane adhesive Z-insertions are modelled as an isotropic material. Their isotropic diffusivity is $D = 2 \times 10^{-12}$ m^2/s and they are considered to be uniform regardless of diffusive direction (Hua et al. 2006, 2007, 2008).

The CME was calculated as strain change ($\Delta L/L$) divided by moisture concentration change due to water absorption (kg/m^3). The coefficient of moisture expansion of wood used in the model is based on measurements made in Chapter 5. The moisture diffusion properties of wood and adhesive are listed in Table 6.2.

Table 6.2 Moisture diffusion and hygroscopic swelling properties of spruce (*Picea sp.*) wood and polyurethane adhesive

Material	C_{sat} (kg/m^3)	D_x (m^2/s)	D_y (m^2/s)	D_z (m^2/s)	CMEx	CMEy	CMEz
Spruce veneer	143	$1000x10^{-12}$	$52x10^{-12}$	$52x10^{-12}$	0.001	0.075	0.308
Polyurethane adhesive	20		$2x10^{-12}$			0.001	

Hygro-mechanical properties of the spruce wood and polyurethane adhesive as input values in the ANSYS® module are listed in Table 6.3. The elastic moduli listed in the table were determined from thermo-mechanical analysis (temperature gradient as the driving force of stress development) rather than from traditional strength test (external bending or compression loading as the driving force) (Walter et al. 2013). However, hygro-mechanical behaviour of polymer materials is not fully understood (Walter et al. 2013). Therefore, thermo-mechanical analysis is used in the present work due to the similarity between thermal and hygroscopic stresses (Lesse 1972). On the other hand, thermo-mechanical material data for specific wood species is not readily available in the literature. A frequently used method for the practical problems of stress analysis can be obtained by approximations based on the theory of strength of materials, according to Boley and Weiner (1960) and Lesse (1972). As a result, the thermo-mechanical material input values listed in Table 6.3 are relative values based on strength properties (elastic moduli and shear moduli) of spruce wood and adhesive taken from the papers by Kretschmann (2010) and Hua et al. (2006. 2007, 2008). The purpose of the modelling work in this thesis was to examine the effects of adhesive Z-connection on Z-direction hygroscopic swelling. Therefore, these relative material input values do not influence the comparison between composites with adhesive Z-connections and the controls that lacked adhesive Z-connections.

Table 6.3 Thermo-mechanical properties of spruce wood and polyurethane adhesive used as input values in the model

Material	**Thermal elasticity** (MPa)			**Poisson's ratio**			**Thermal shear modulus** (MPa)		
	E_x	E_y	E_z	μ_{XY}	μ_{YZ}	μ_{XZ}	G_{xy}	G_{yz}	G_{xz}
Spruce veneer	86.9	37.4	67.8	0.467	0.245	0.372	53	26	55.6
Polyurethane adhesive	760			0.35			2.8E5		

6.2.5 Coordinate system, mesh generation and boundary conditions

One eighth of the wood composite was modelled using finite element analysis because of the presence of three symmetrical planes, as arrowed in Fig. 6.1. The use of symmetrical planes can significantly reduce the number of finite elements needed and hence reduce the time to model composites (Meo et al. 2005). The definition of the coordinate system used in the finite element model is shown in Fig. 6.1. The X and Y directions represent grain and cross-grain directions of wood veneer, respectively. Z is the thickness direction of wood veneers. The entire wood composite is submerged in water to simulate the water absorption phenomenon.

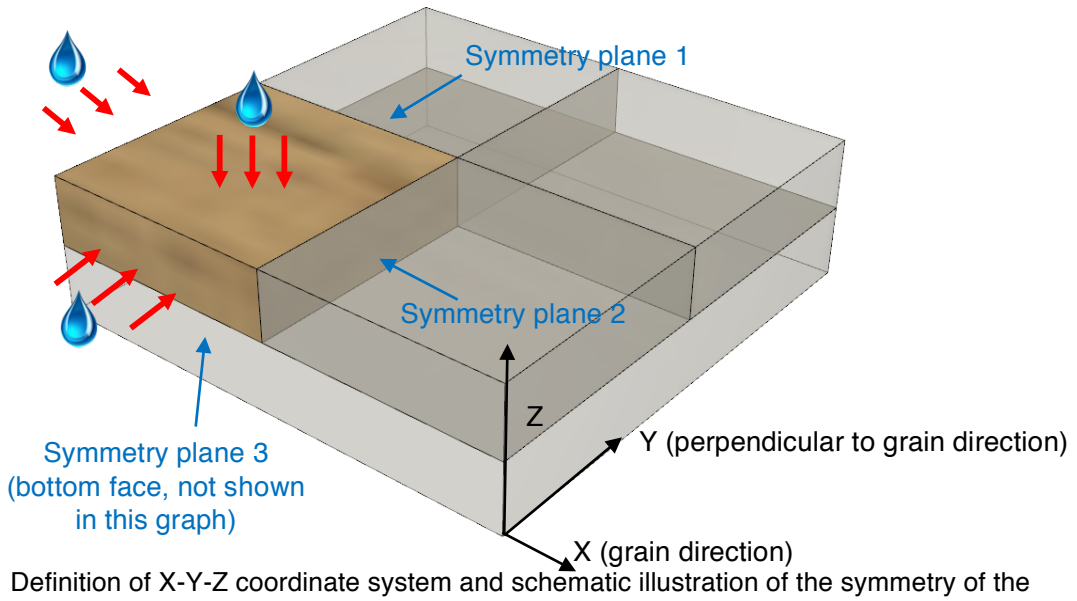

Figure 6.1 Definition of X-Y-Z coordinate system and schematic illustration of the symmetry of the modelled material (arrowed blue) and water absorption planes (arrowed red) in the model

The initial condition of the entire domain was W = 0 to simulate the initial status of a fully unsaturated wood composite (Fig. 6.2). The boundary condition of the three symmetry planes was a zero flux of moisture (Neumann condition), and the boundary condition of the three exposed surfaces was W = 1 (Dirichlet condition) (as arrowed in Fig. 6.2) to simulate the environment surrounding the wood composite. This approach introduced an initial moisture gradient between the surface and the core of the composite and hence allowed moisture diffusion to occur over time. The model was meshed using mainly hexahedron (brick shaped) elements (8-noded) with the following element unit dimensions: 0.33 mm x 0.33 mm x 0.33 mm. Six-faced brick type elements were chosen in this model was because the geometry of the mesh (composite) is hexahedron. In total, there were 11,156 elements generated for one eighth of the wood composite model. The mesh was generated using an adaptive size function in ANSYS that assigned a defined number of elements to the bulk body of wood veneers and adhesive Z-connections. The mesh at the wood-adhesive interface was further refined using a contact area refinement function to ensure smooth transition between the interface and the bulk of the composite (Fig. 6.2). The latter approach was used because an efficient mesh with smooth transition at bi-material interfaces usually improves computation efficiency of finite element models (Madenci and Guven 2006). Mesh size was determined based on computational cost and convergence capacity of a desktop computer (3.40 GHz Intel® Core i7 2600K processor, 24GB of random access memory (RAM), 1 TB of hard disk drive, Nvidia® GeForce GTX 590 graphics card).

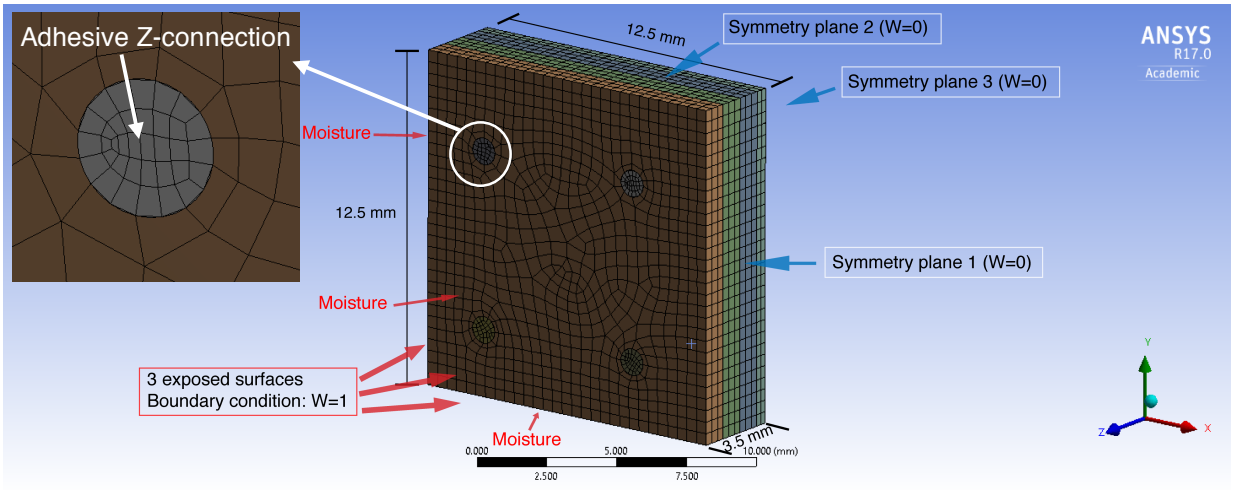

Figure 6.2 Meshed model of 1/8 of the model wood composite (12.5 x 12.5 x 3.5 mm^3) containing 4 adhesive Z-connections (Z-connections) and 3 ½ layers of wood veneers. Boundary conditions at three faces exposed to moisture absorption were arrowed red (W=1). A higher magnification view of refined mesh at the wood-adhesive Z-connection transition area is shown at the top-right corner. Mesh elements were mainly hexahedron shaped; element size was 0.33 x 0.33 x 0.33 mm^3

Moisture diffusion simulation was carried out using the 'transient thermal' module in ANSYS® with an initial time step of 2592 seconds (259.2 s minimum and 25920 s maximum time steps), which produced moisture concentration profiles in the model wood composites. Hygroscopic swelling simulation was carried out using the 'static structural' module with 30 initial substeps (20 minimum and 100 maximum substeps). This module was used to examine moisture-induced swelling and Z-direction deformation of the model wood composites. All modelling using ANSYS® Multiphysics Workbench software was performed on a high-end desktop computer, as mentioned above. Simulated deformation graphs were saved as TIFF files. Average thickness swelling of some key points within the model was calculated to compare effects of different design configurations.

6.3 Results

6.3.1 Simulation of moisture diffusion

Figs. 6.3~6.11 show simulations of moisture concentration over time within the wood composite model. Note in the legend that a blue colour indicates W = 0 (completely dry), a red

colour indicates W = 1 (completely saturated). Hence, it can be observed that the core of the model wood composite (arrowed with a number) was the last to become saturated with water. It is also clear that the moisture diffusion rate in wood was dependent on diffusion direction (Figs. 6.3~6.11). Moisture diffusion was fastest in the X-direction which is aligned with the longitudinal direction of wood. As a result of such orthotropic moisture diffusion, moisture distribution within the model composite at any given time was not uniform. The simulation also suggested that adhesive Z-connections were not as permeable as wood, as indicated by the blue colour of adhesive Z-connections throughout the water soaking process.

Initially, wetness of the core of the model wood composite was 0% (arrowed blue in Fig. 6.3) indicating a completely dry initial state. Surfaces of the model were fully saturated as suggested by the red colour of the moisture profile (Fig. 6.3) indicating the boundary condition, W = 1. This created an initial moisture gradient between the ambient environment and the wood composite enabling moisture absorption to be simulated.

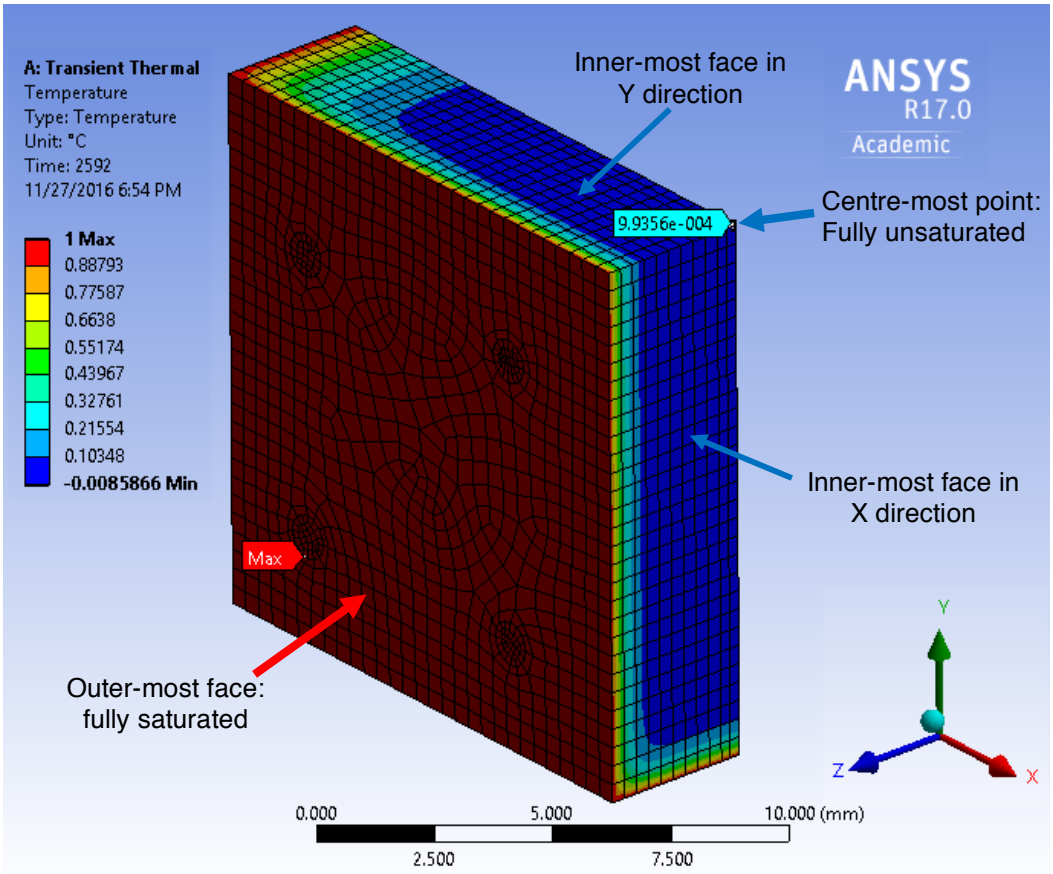

Figure 6.3 Initial 3D moisture distribution in 1/8 of the model wood composite. Moisture contents are colour coded: red = fully saturated; blue = completely dry, etc. (colour scale bars at the left-hand side of figures indicate wetness)

After 2 hours of moisture absorption, wetness of the core of the model wood composite slightly increased to 1.0%, as arrowed in Fig. 6.4. Moisture started to migrate inside the wood composite from three exposed surfaces. However, the rate of moisture diffusion was dependent upon diffusion direction. Moisture diffusion occurred at a faster rate in the X-direction (grain direction) than in the Y-direction (cross-grain direction), as indicated by the colour difference between X and Y directions (arrowed in Fig. 6.4).

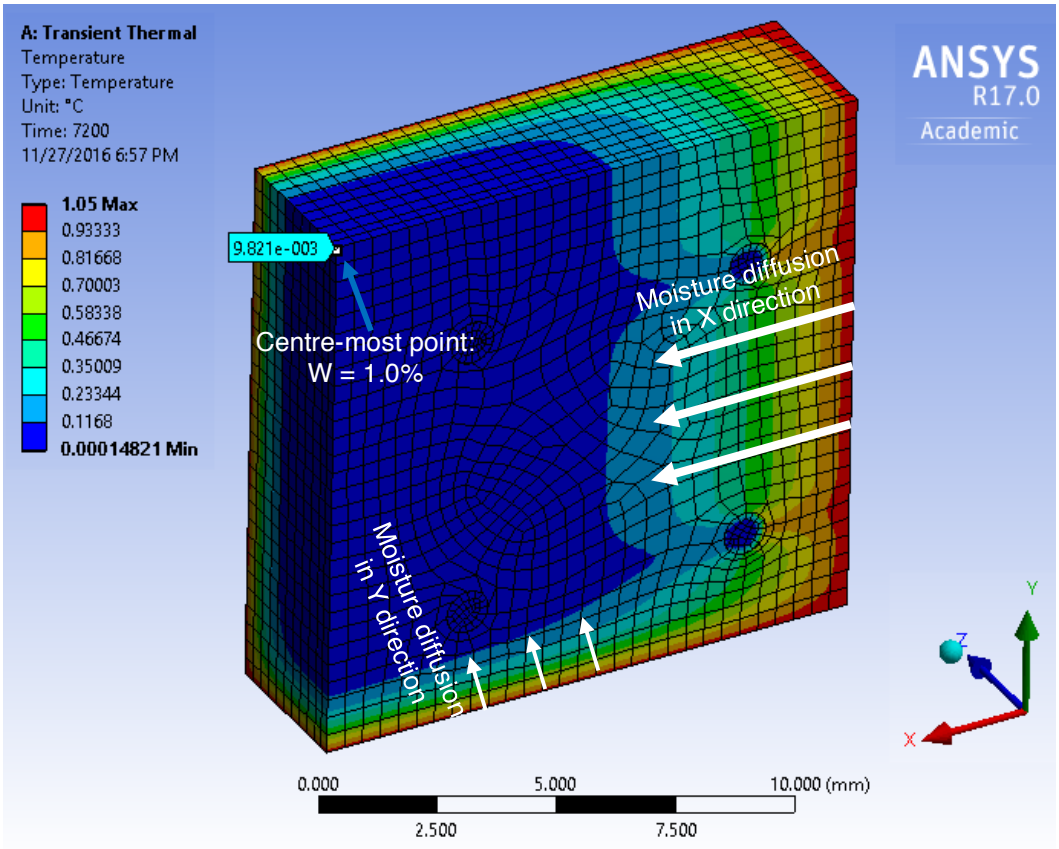

Figure 6.4 3D moisture distribution in 1/8 of the model wood composite after 2 h of simulated water soaking. Colour profile indicates that moisture diffusion was faster in X direction than in Y direction

After 4 hours exposure to water, more moisture migrated into the model wood composite, and the wetness of the core increased to 6.8%, (arrowed in Fig. 6.5a). Fig. 6.5a confirms the orthotropic moisture diffusion characteristics of wood, as indicated by the moisture profile gradient between the X and Y directions. Fig. 6.5a also shows the differential moisture contents of wood veneers and adhesive Z-connections. Adhesive Z-connections contained much less moisture compared to the adjacent wood (Fig. 6.5b). Furthermore, moisture diffusion through adhesive Z-connections was isotropic. However, its moisture content was correlated with the moisture content of the adjacent wood. This is reflected in the moisture profile across the cylindrical adhesive Z-connections (Fig. 6.5c).

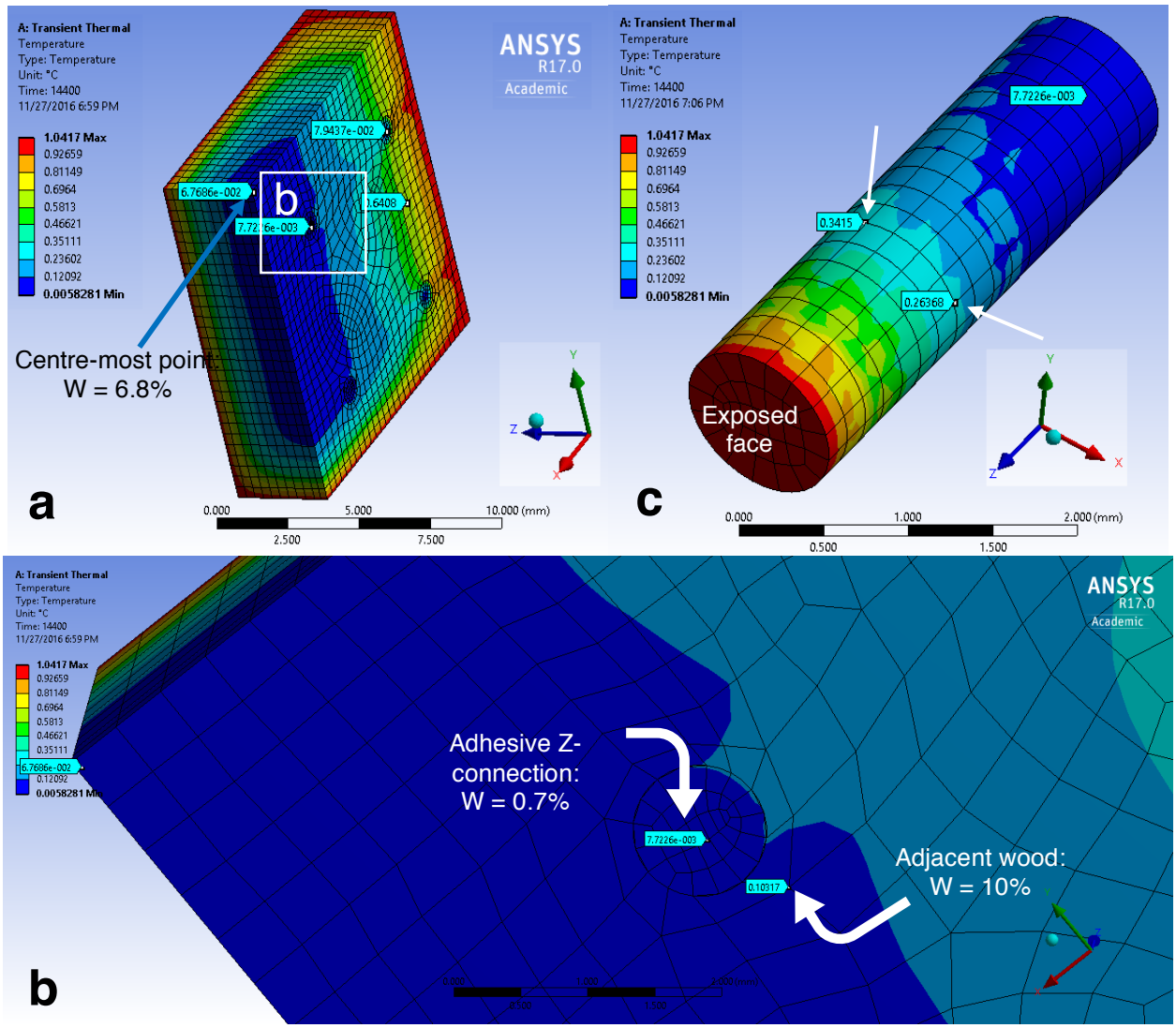

Figure 6.5 (a) 3D moisture distribution in 1/8 of the model wood composite after 4 h of simulated water soaking; (b) Differential moisture content of adhesive Z-connections and adjacent wood; and (c) Moisture profile of an individual adhesive Z-connection

After 6 hours exposure to water, wetness of the core increased to 15.9% (arrowed in Fig. 6.6) and more moisture diffused into the composite in the X, Y and Z directions (Fig 6.6).

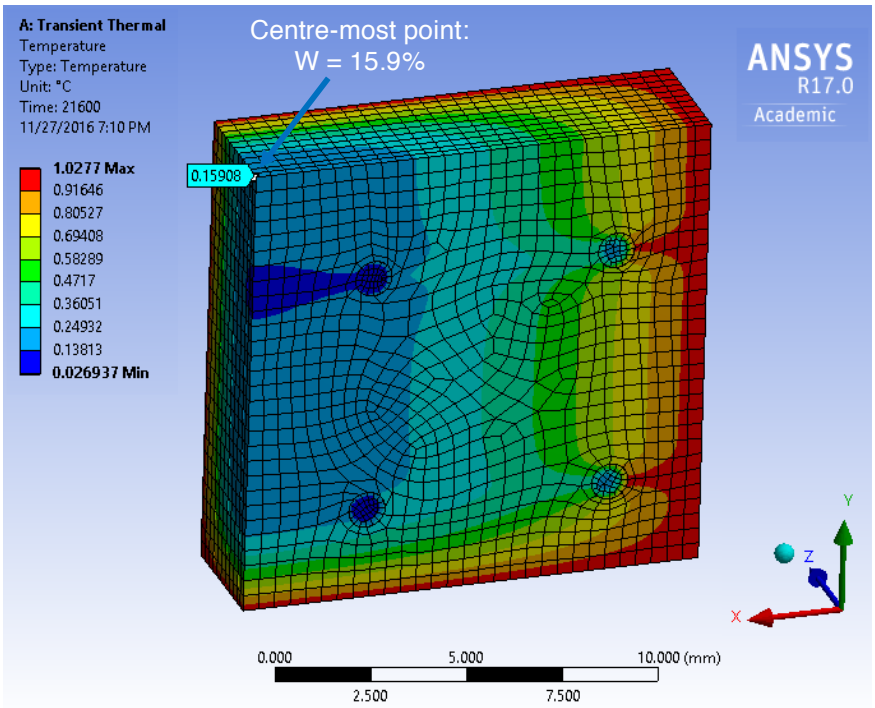

Figure 6.6 3D moisture distribution in 1/8 of the model wood composite after 6 h of simulated water soaking

After 8 hours exposure to water, wetness of the core increased to 25.7% (arrowed in Fig. 6.7). There was still a significant difference in moisture content of wood and adhesive Z-connections. Furthermore, the moisture contents of 4 individual adhesive Z-connections varied considerably depending on their distance from exposed surfaces. For example, 'adhesive Z-connection #1' (arrowed white in Fig. 6.7) had a wetness level of 27.8% whereas the comparable wetness level for 'adhesive Z-connection #2' (arrowed black in Fig. 6.7) was 8.9%, even though they were the same distance from exposed surfaces #1 and #2, respectively (arrowed in Fig. 6.7). This difference is associated with the fact that water diffusion through surface #1 is along the grain (X-direction) whereas water diffusion through surface #2 is across the grain (Y-direction) (Fig. 6.7).

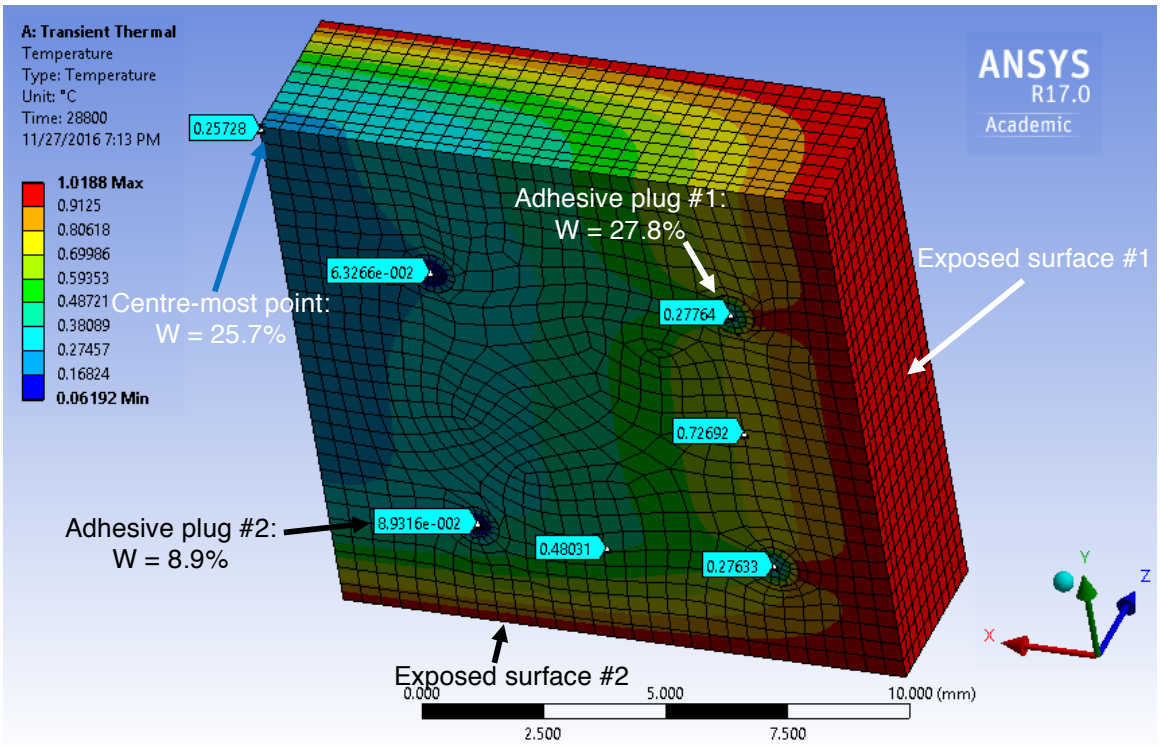

Figure 6.7 3D moisture distribution in 1/8 of the model wood composite after 8 h of simulated water soaking. Note the moisture content difference between adhesive Z-connection #1 (arrowed white) and Z-connection #2 (arrowed black)

After 10 hours exposure to water, wetness of the core increased to 34.7%, as arrowed in Fig. 6.8.

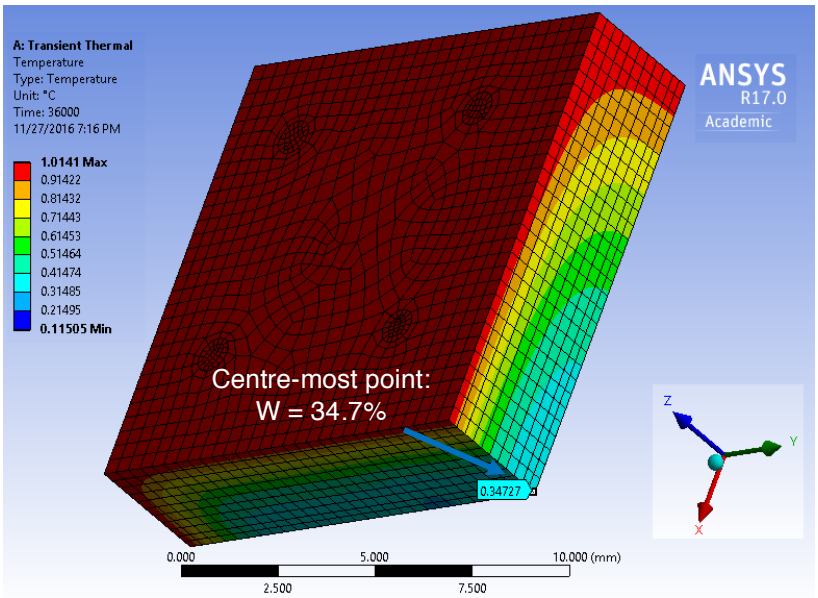

Figure 6.8 3D moisture distribution in 1/8 of the model wood composite after 10 h of simulated water soaking

Wetness of the core of reached 76% after 24 hours of simulated moisture diffusion (Fig. 6.9). The wetness of the centre-most adhesive Z-connection was 53.1% (arrowed in Fig. 6.9). which is lower than those of the other 3 adhesive Z-connections (arrowed in Fig. 6.9).

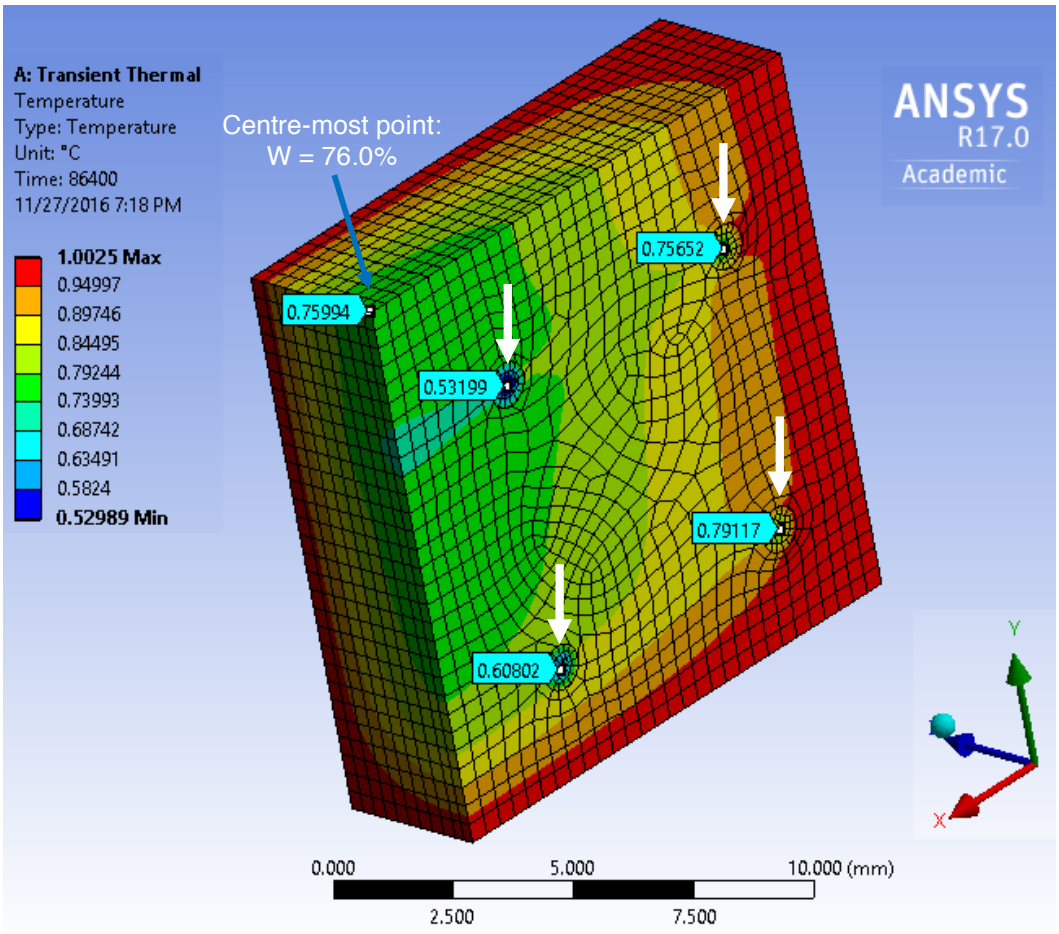

Figure 6.9 3D moisture distribution in 1/8 of the model wood composite after 24 h (1 day) of simulated water soaking. Note the difference in moisture content between the 4 individual adhesive Z-connections (arrowed white)

Wetness of the core of the composite reached 96% (of wood's FSP) after 48 hours of simulated moisture diffusion indicating almost complete saturation of wood. The wetness of the centre-most adhesive Z-connection was 90% indicating that it was not fully saturated (Fig. 6.10).

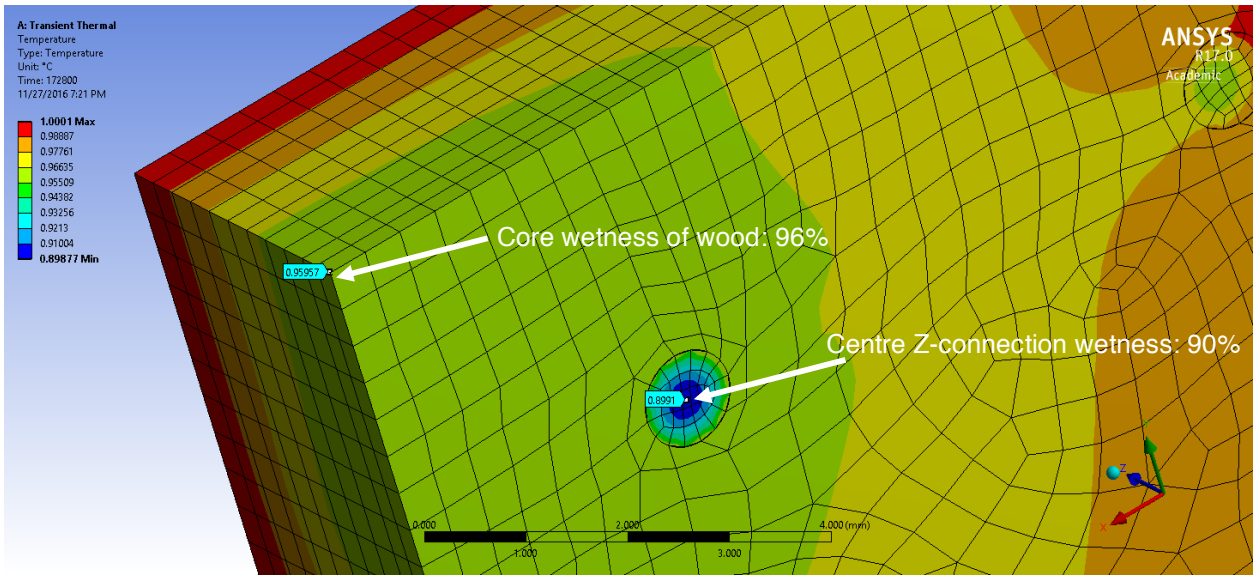

Figure 6.10 3D moisture distribution in 1/8 of the model wood composite after 48 h (2 days) of simulated water soaking. Note the moisture content of the centre-most adhesive Z-connection (not fully saturated)

After 72 hours (3 days) of simulated water diffusion, wetness of the core of the centre-most wood veneer and centre-most adhesive Z-connection were 99.3% and 98.1%, respectively (Fig. 6.11), indicating near-complete saturation. As a result, simulation of water diffusion into the model composite was stopped at 72 hours.

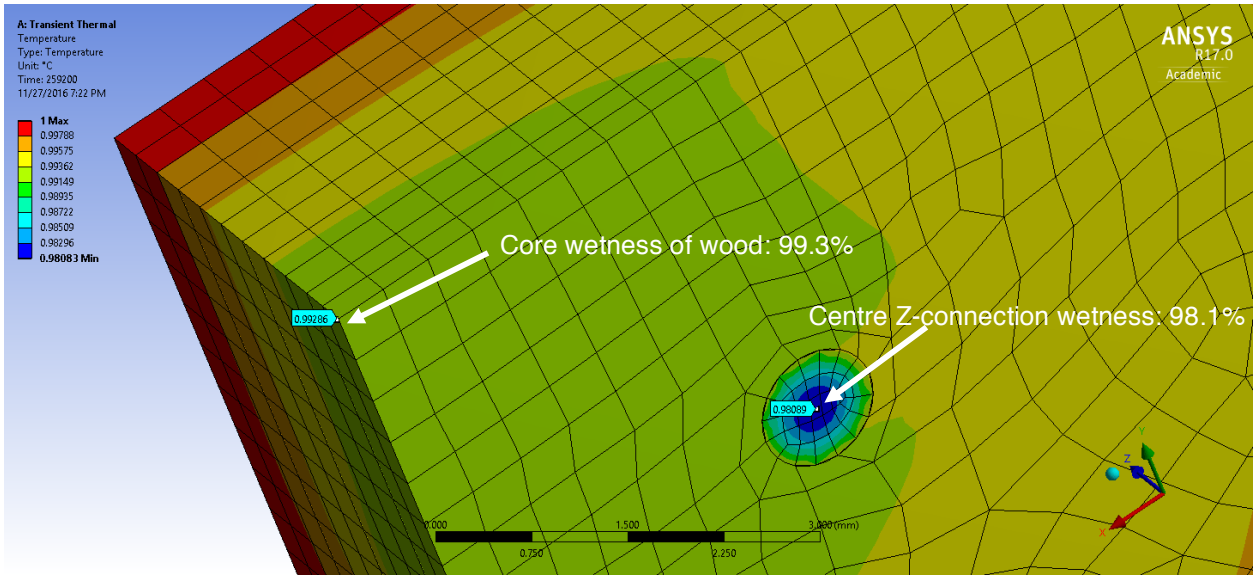

Figure 6.11 3D moisture distribution in 1/8 of the model wood composite after 72 h (3 days) of simulated water soaking. Note that both wood and adhesive Z-connections were fully saturated

Simulated moisture content changes at the core of the model wood composite over time are shown in Fig. 6.12. Moisture change occurred at a faster rate when the simulation began and slowed down after 22 hours. The time-dependent diffusion rate was approximately linear up to 22 hours and became non-linear thereafter.

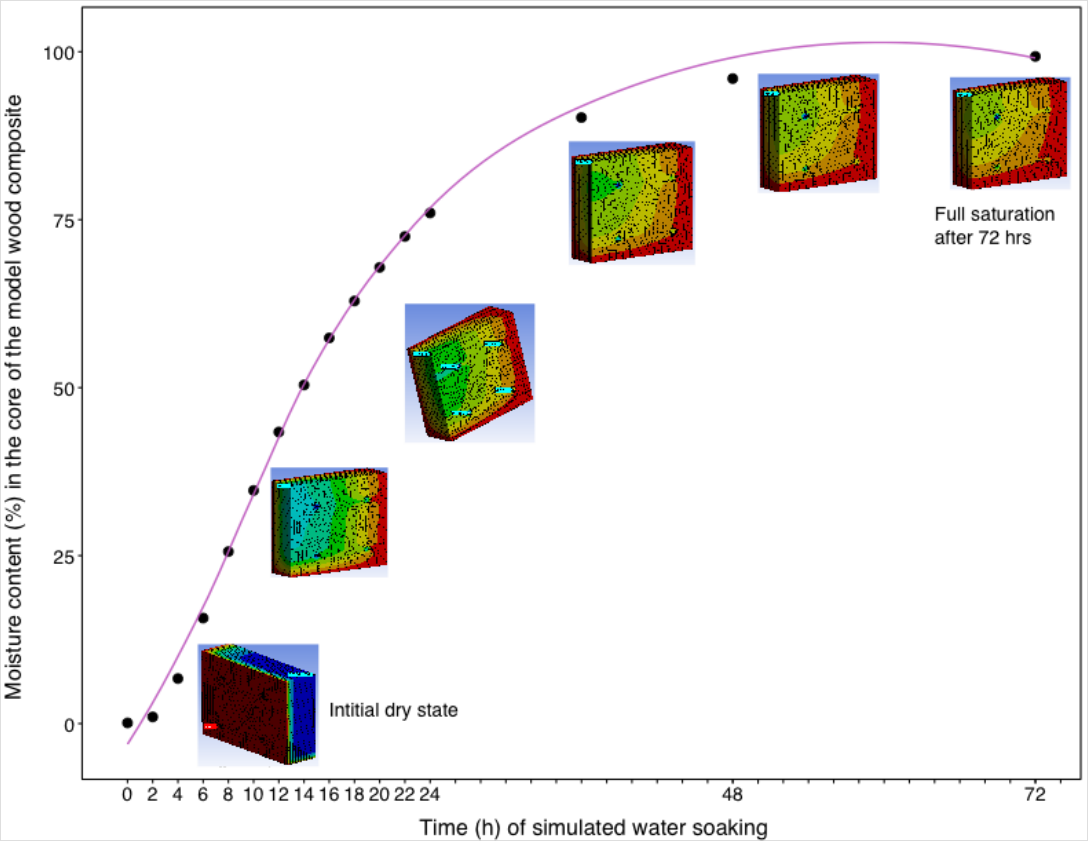

Figure 6.12 Simulated moisture content change over time in the core of the model wood composite

6.3.2 Effects of area-density, diameter, and spatial distribution of adhesive Z-connections on thickness swelling of the model wood composite

As mentioned in Section 6.2.6, Z-direction deformation was modelled using the ANSYS® Multiphysics module for a model wood composite that was saturated. Three main parameters related to the design of adhesive Z-connections were examined using this model, i.e. area-density, diameter and the spatial distribution of adhesive Z-connections.

6.3.2.1 Area-density of adhesive Z-connections

Z-direction (thickness) swelling of model wood composites containing simulated adhesive Z-connections with different area densities are shown in Figs. 6.13 ~ 6.17 (note that in the legend a blue colour indicates no deformation, whereas a red colour indicates maximum deformation). These figures show that the closer adhesive Z-connections were to each other, the better they were at restraining swelling of the composites (Figs. 6.13 ~ 6.17). Restraint of swelling was more continuous in the X-direction than in the Y-direction, as was observed experimentally in Chapters 4 and 5.

When there were 4 simulated adhesive Z-connections distributed uniformly across the model wood composite (Fig. 6.13), the simulated Z-direction (thickness) swelling of wood at positions A and B were 1.24 mm and 1.21 mm, respectively (arrowed in Fig. 6.13), which are lower than the maximum swelling (1.29 mm) of wood at the outer-most surface of the model composite. This indicates that the swelling of wood in between two adhesive Z-connections was decreased.

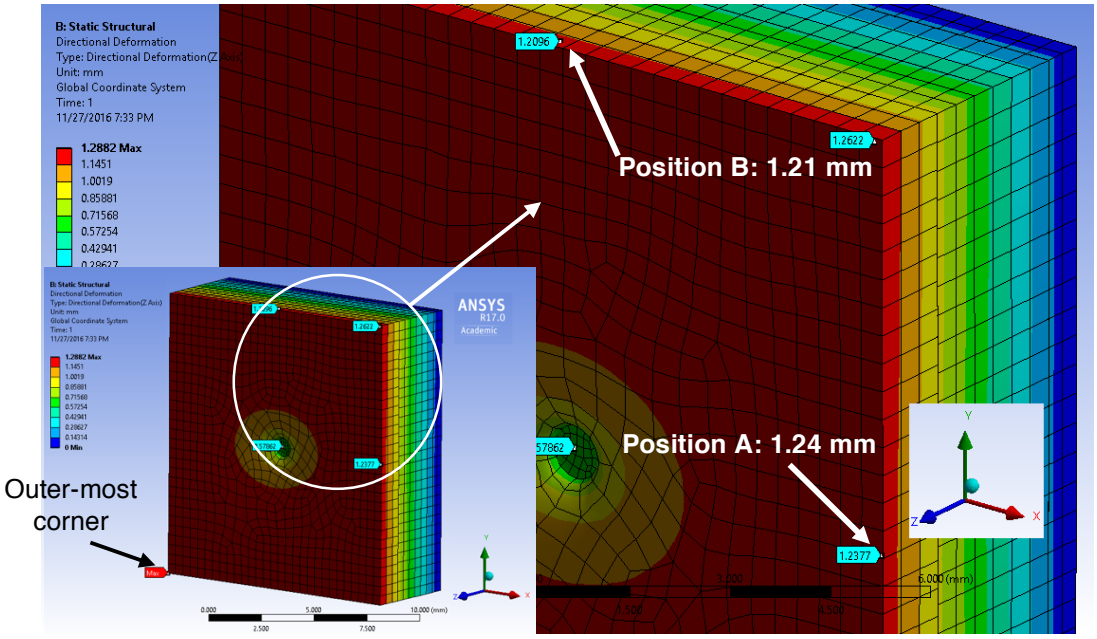

Figure 6.13 Z-direction deformation in 1/8 of the model wood composite containing 4 simulated adhesive Z-connections after 72 h simulated immersion in water. Simulated thickness swelling values of wood at positions A and B are indicated on the figure

When there were 16 simulated adhesive Z-connections in the model wood composite (Fig. 6.14), Z-direction (thickness) swelling of wood at positions A and B were 1.13 mm and 1.20 mm, respectively (arrowed in Fig. 6.14). Comparing these figures with previous ones (Fig. 6.13), it is clear that decreasing the Z-connection interval (increasing Z-connection area-density) further restrained thickness swelling. Furthermore, it appears that decreasing the Z-connection interval in the X-direction was more effective than decreasing the interval in the Y direction, because the reduction in thickness swelling at position A was 0.11 mm whereas at position B it was 0.01 mm (Fig 6.14 vs. 6.13).

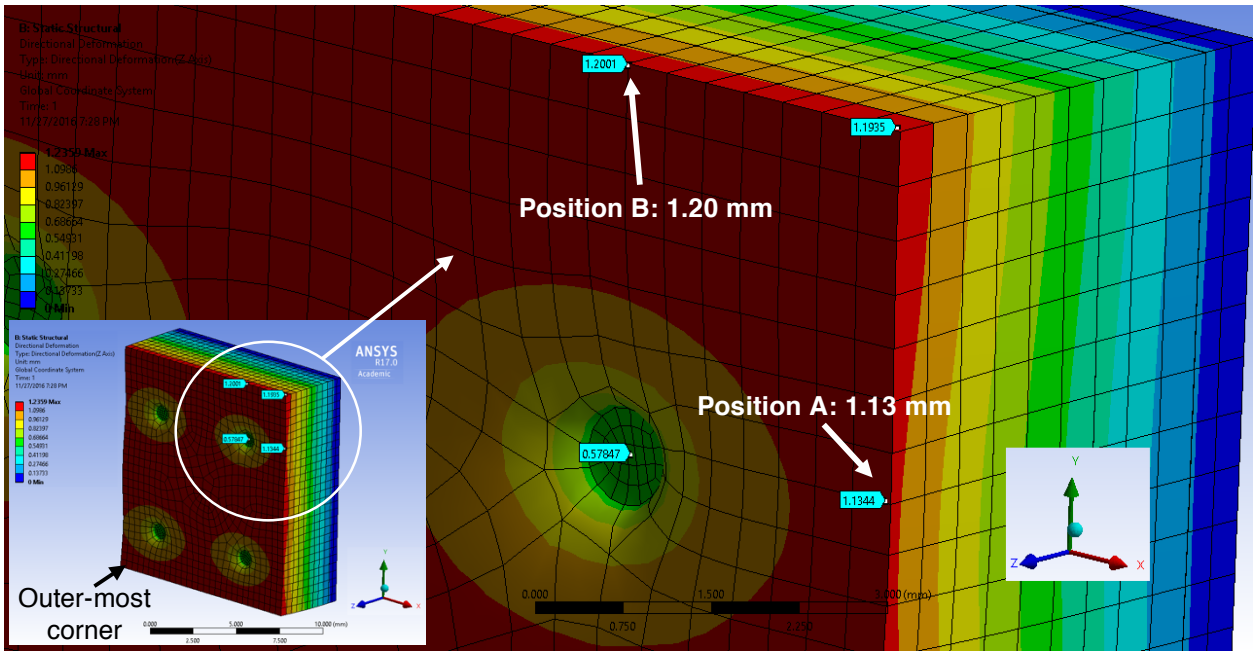

Figure 6.14 Z-direction deformation in 1/8 of the model wood composite containing 16 simulated adhesive Z-connections after 72 h simulated immersion in water. Simulated thickness swelling values of wood at positions A and B are indicated on the figure

Twenty adhesive Z-connections in the model wood composite were created by adding one extra Z-connection in the middle as shown in Fig. 6.15. The resulting simulated Z-direction (thickness) swelling of wood at positions A and B were 1.19 mm and 1.21 mm, respectively (arrowed in Fig. 6.15), which are similar to those of a composite containing 16 Z-connections (Fig. 6.14). However, adding one extra Z-connection in the middle of the array of Z-connections

considerably increased the area of wood whose swelling was restricted by Z-connections (Fig. 6.15).

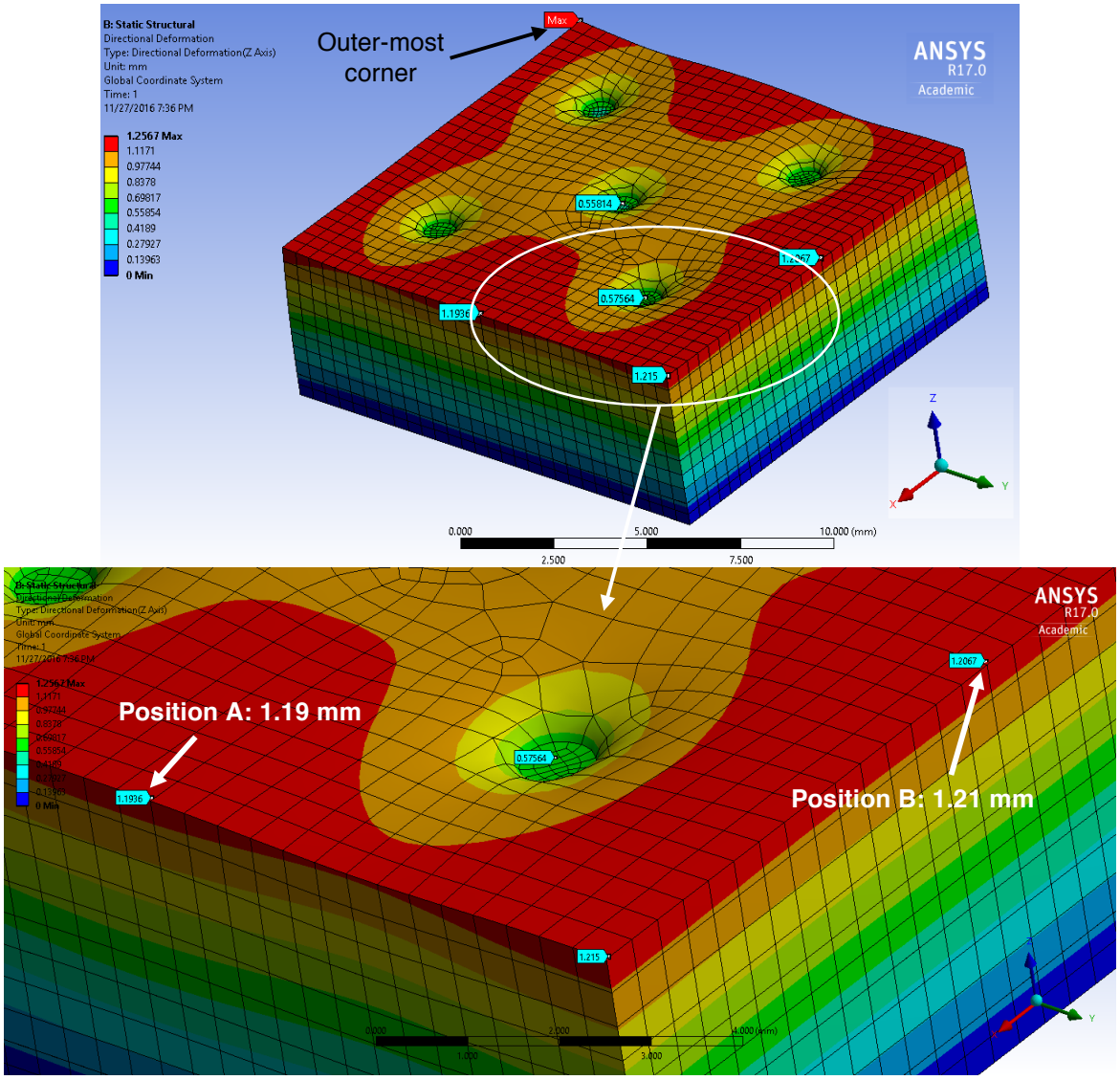

Figure 6.15 Z-direction deformation in 1/8 of the model wood composite containing 20 simulated adhesive Z-connections after 72 h simulated immersion in water. Note that the addition of one Z-connection in the middle of the array of Z-connections increased the overall area of wood whose swelling was restricted by Z-connections. Simulated thickness swelling values of wood at positions A and B are indicated on the figure

When there were 36 adhesive Z-connections in the composite (Fig. 6.16), simulated Z-direction (thickness) swelling of wood at positions A and B were 0.94 mm and 1.02 mm, respectively (arrowed in Fig. 6.16). These figures indicate that thickness swelling of wood was

further restrained as a result of decreased adhesive Z-connection interval. Fig. 6.16 also shows that ‘dimples’ created by Z-connections were better connected in the X-direction than in the Y-direction, manifested by the ‘ridges’ arrowed in Fig. 6.16, which is similar to experimental observations in Chapters 4 and 5.

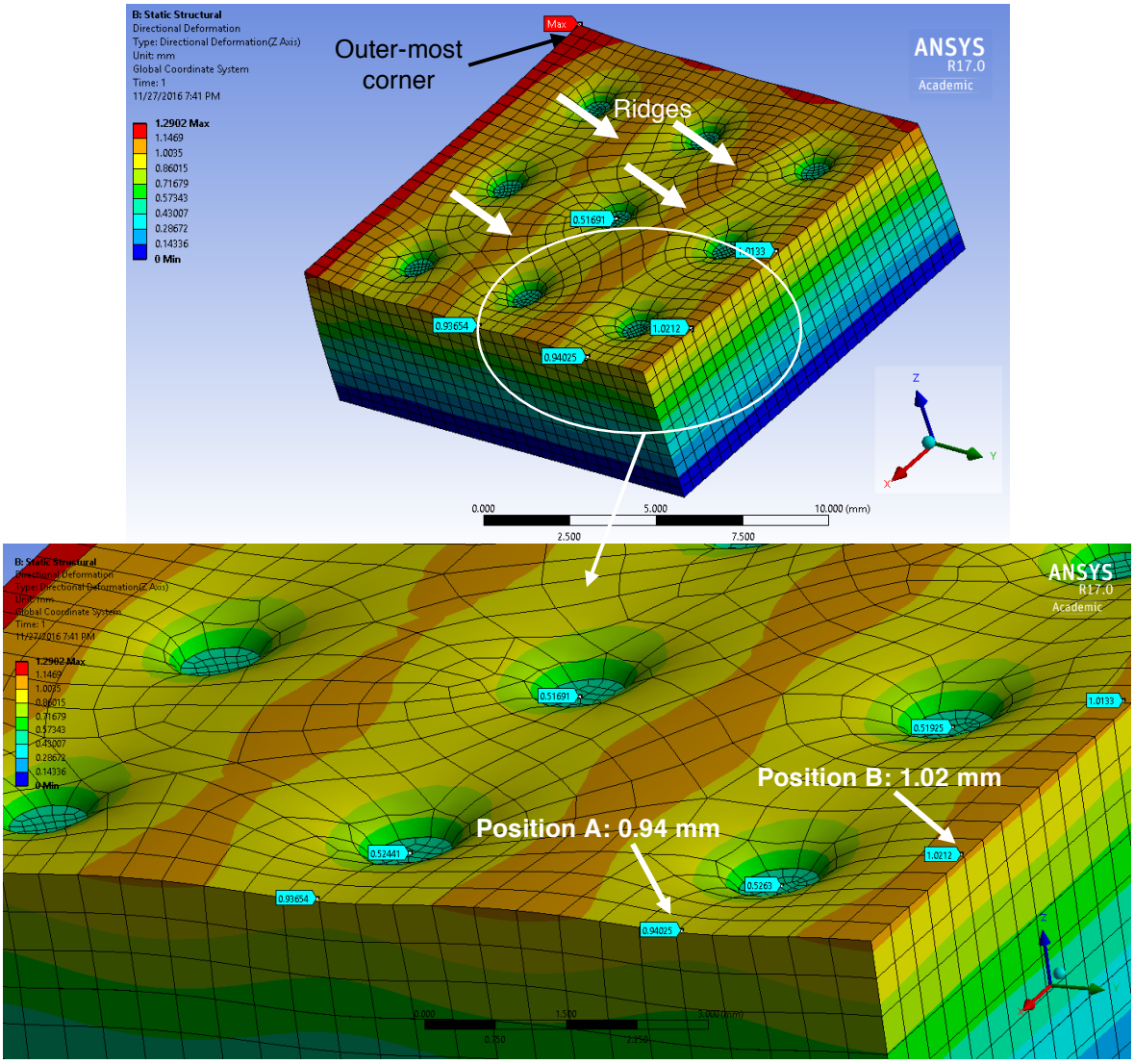

Figure 6.16 Z-direction deformation in 1/8 of the model wood composite containing 36 simulated adhesive Z-connections after 72 h simulated immersion in water. Note the ‘ridges’ running in the X-direction indicating the simulated adhesive Z-connections were better connected in X-direction than in Y-direction. Simulated thickness swelling values of wood at positions A and B are indicated on the figure

48 adhesive Z-connections in the model composite (Fig. 6.17) were created by adding one more row of adhesive Z-connections in the Y-direction of the previous model (Fig. 6.16).

The simulated Z-direction (thickness) swelling of wood at positions A and B decreased to 0.89 mm and 0.87 mm, respectively (arrowed in Fig. 6.17). Hence, the difference in thickness swelling of wood in the X and Y directions was minimal. 'Ridges' between 'dimples' seen in previous models and experimentally disappeared and the 'dimples' were uniformly connected in the X and Y directions across the entire surface of the composite (Fig. 6.17).

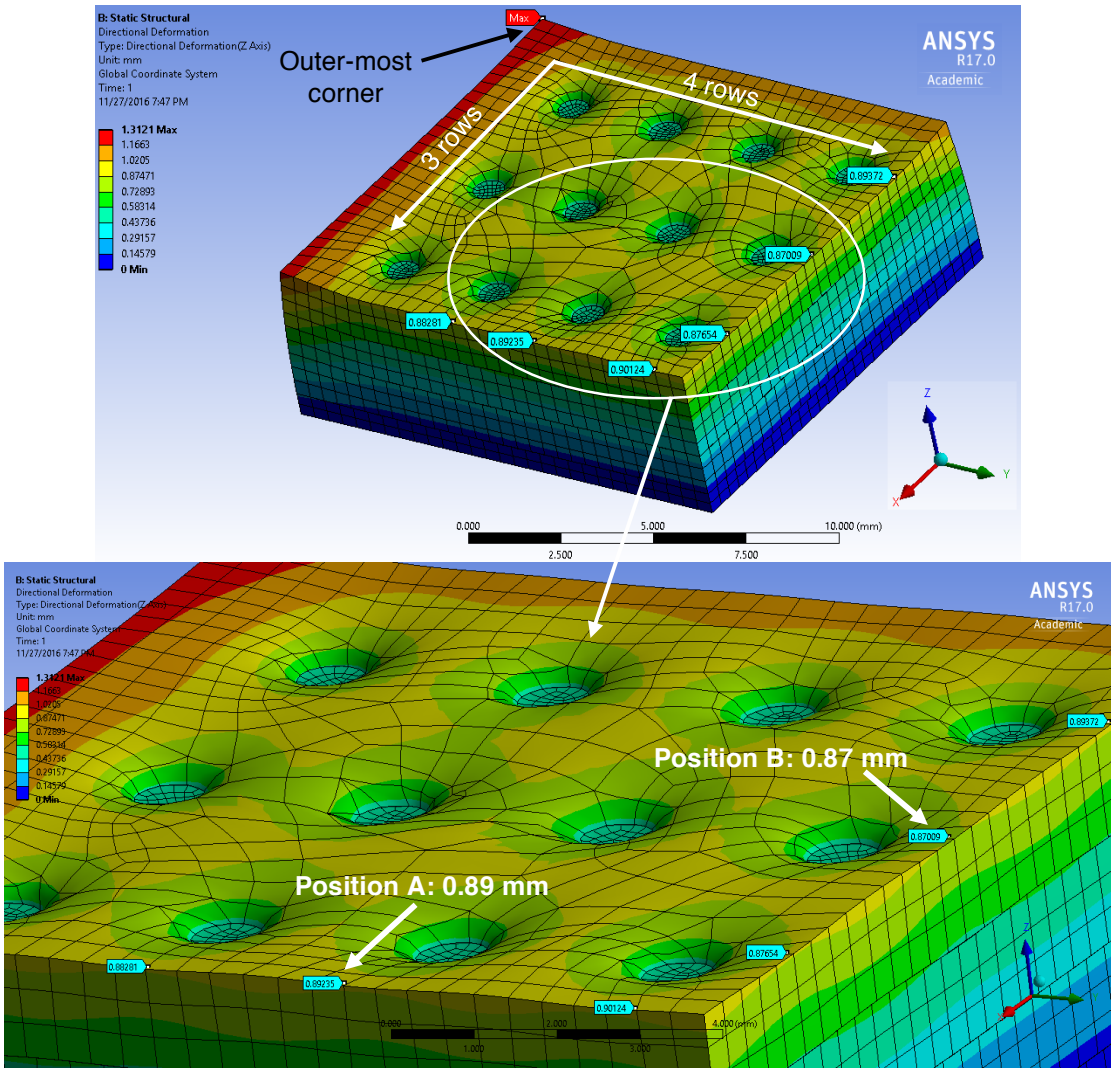

Figure 6.17 Z-direction deformation in 1/8 of the model wood composite containing 48 simulated adhesive Z-connections after 72 h simulated immersion in water. Note 'ridges' disappeared and 'dimples' were evenly distributed and connected across the entire surface of the model wood composite. Simulated thickness swelling values of wood at positions A and B are indicated on the figure

Simulated thickness swelling of wood in the model composites containing adhesive Z-connections with different area-densities are plotted in Fig. 6.18. This figure clearly shows a

positive correlation between the area-density of adhesive Z-connections and their ability to restrain thickness swelling.

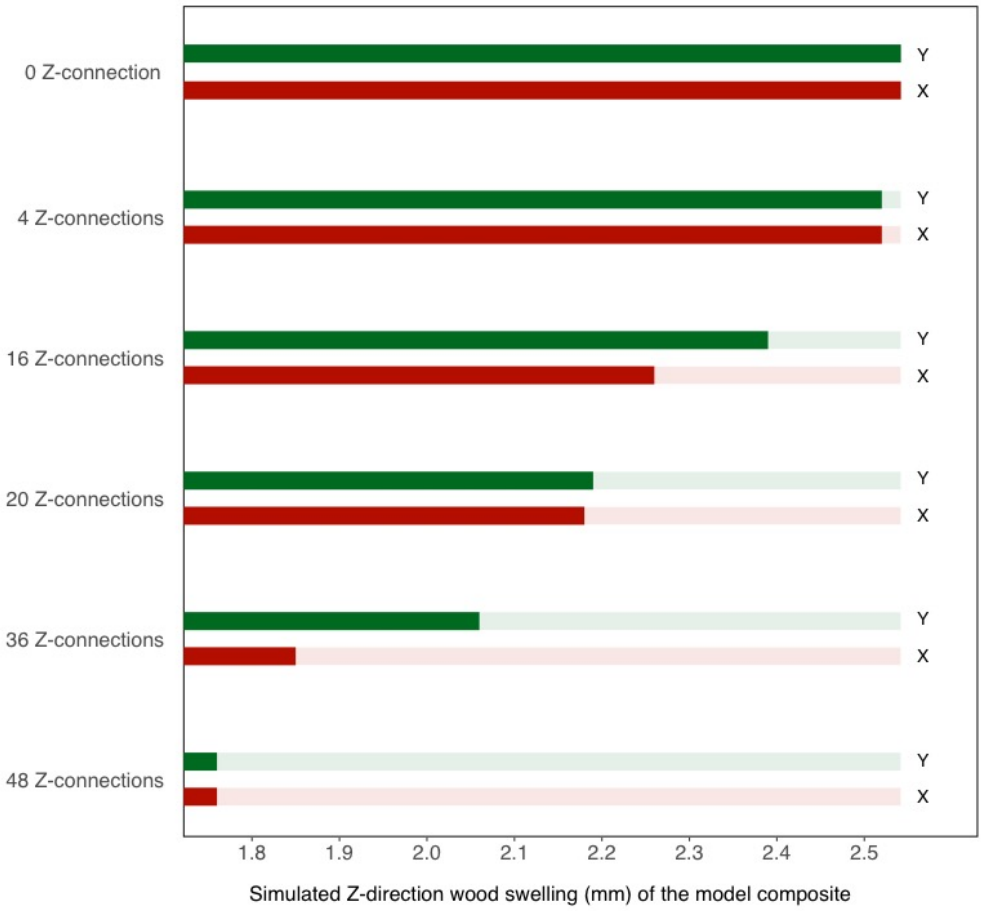

Figure 6.18 Effects of area-density of simulated adhesive Z-connections on thickness swelling of a model wood composite

There was a good (R^2 = 0.99) negative correlation between thickness swelling (mm) of the model wood composites (subtracting area occupied by adhesive Z-connections) and area (mm^2) occupied by adhesive Z-connections at the surfaces of the composites (Fig. 6.19).

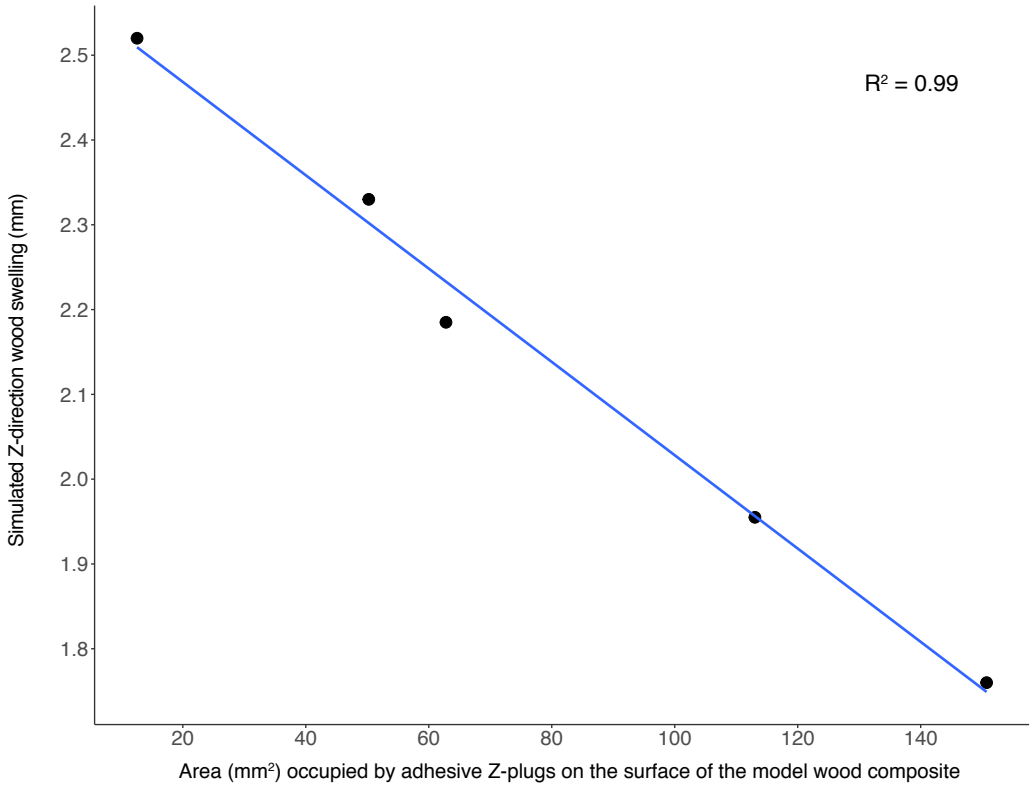

Figure 6.19 Relationship between Z-direction wood swelling (mm) (subtracting areas occupied by adhesive Z-connections) and area (mm^2) occupied by the adhesive Z-connections

6.3.2.2 Diameter of adhesive Z-connections

Effects of diameter of adhesive Z-connections on the thickness swelling of model wood composites are shown in Fig. 6.20. The thickness swelling of wood between two adjacent 1 mm diameter adhesive Z-connections were 1.13 mm and 1.20 mm at positions A and B, respectively (arrowed in Fig. 6.20a). Comparable figures for composites containing 1.5 mm and 2.0 mm diameters adhesive Z-connections were 1.05 mm and 1.15 mm, and 0.96 mm and 1.10 mm, respectively (Figs. 6.20b~c). The size of the 'dimples' around the adhesive Z-connections was positively correlated with the diameter of the Z-connections, as expected.

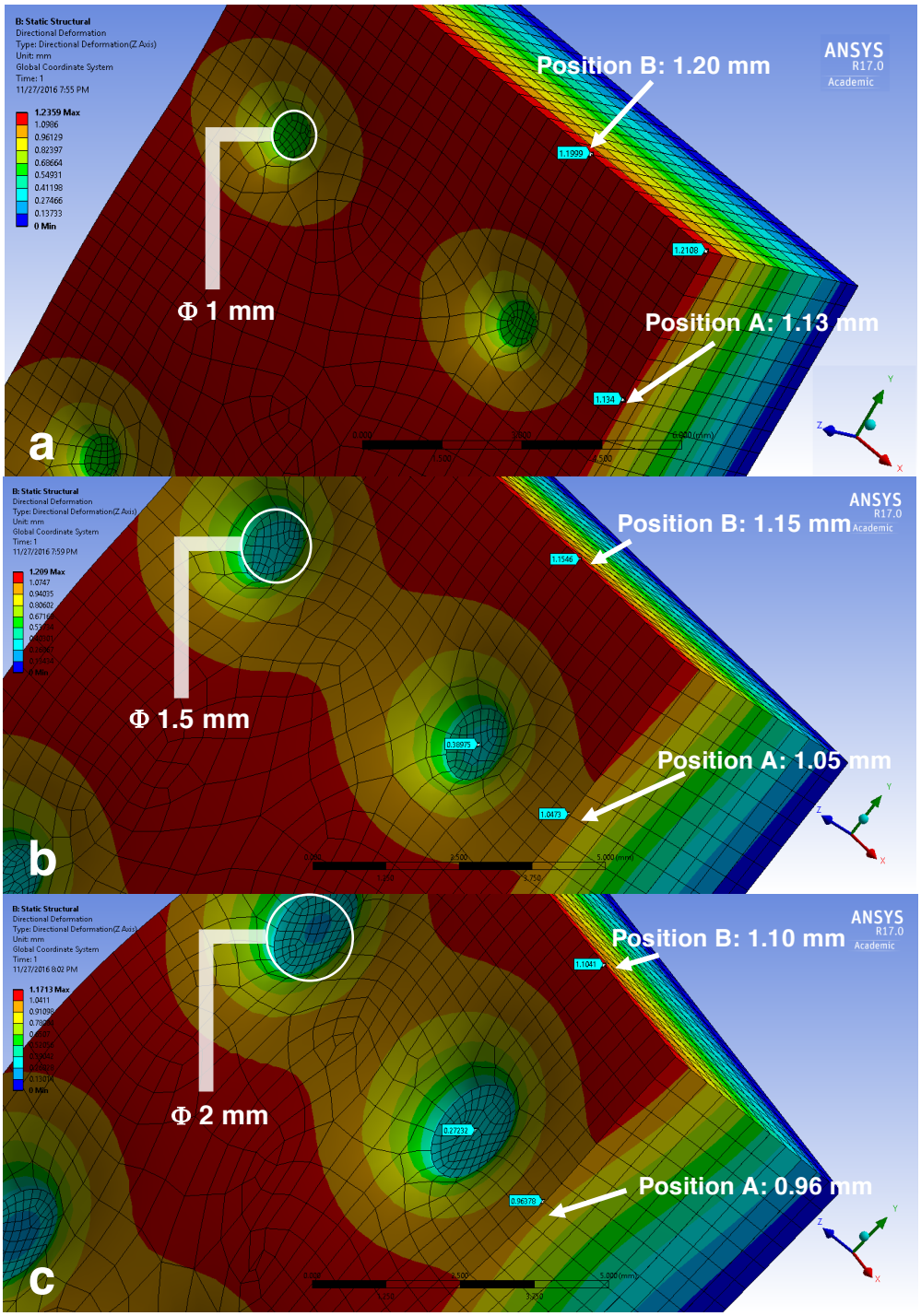

Figure 6.20 Z-direction deformation in 1/8 of model wood composite containing simulated adhesive Z-connections with different diameters (a ~ c) after 72 h simulated immersion in water. Adhesive Z-connections with larger diameter covered a greater area at the surface of the composite and also restrained the thickness swelling of wood to a larger degree. Simulated thickness swelling values of wood at positions A and B are indicated on the figure

Simulated thickness swelling of wood in the X direction (by measuring the Z-direction deformation at position A mentioned above) and in the Y direction (by measuring the Z-direction deformation at position B mentioned above) are plotted in Fig. 6.21. This figure clearly shows the correlation between the diameter of Z-connections and reductions in thickness swelling. It also confirms that the adhesive Z-connections were more effective at restricting swelling in the X-direction than in the Y-direction.

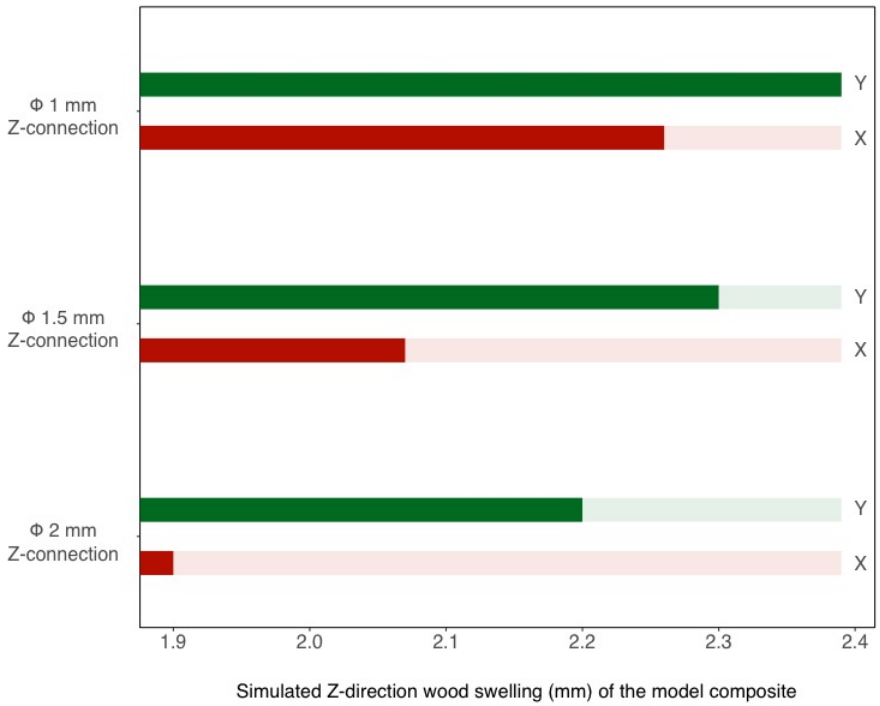

Figure 6.21 Effects of diameter of adhesive Z-connections on thickness swelling of wood in the model wood composite (excluding areas occupied by the adhesive Z-connections)

6.3.2.3 Spatial distribution of adhesive Z-connections

Z-direction (thickness) swelling of the composite containing simulated adhesive Z-connections with different spatial distributions but identical area-densities are shown in Figs. 6.22 & 6.23. Two distributions were modelled: (1) square and; (2) diagonal. These figures suggest that for both 16 Z-connections (Fig. 6.22) and 20 Z-connections (Fig. 6.23), the diagonal spatial distribution restricted thickness swelling over a wider area than the square

distribution, even though both arrangements had the same area-density. This is manifested by the elliptical dimple patterns created by adhesive Z-connections, which covered a greater surface area when the diagonal arrangement was modelled (Fig. 6.22 & 6.23). Fig. 6.22 indicates that the thickness swelling of wood in the centre of the composite was reduced from 1.21 mm to 1.11 mm by adopting a diagonal arrangement in preference to a square one. Fig. 6.23 confirms the superiority of the diagonal arrangement over the square arrangement.

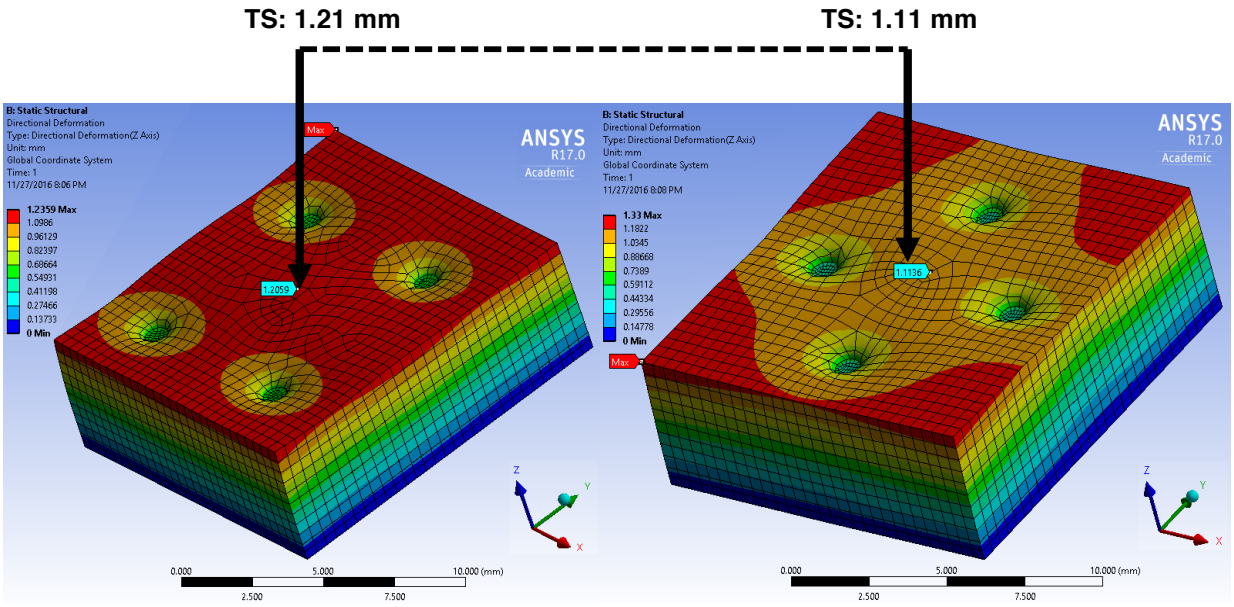

Figure 6.22 Z-direction deformation in 1/8 of a model wood composite containing 16 simulated adhesive Z-connections with different spatial distributions, but same area-density after 72 h simulated immersion in water. Note that the diagonal arrangement has depressed thickness swelling over a greater area at the wood surface than the square arrangement. Simulated thickness swelling values of wood in the centre are indicated on the figure

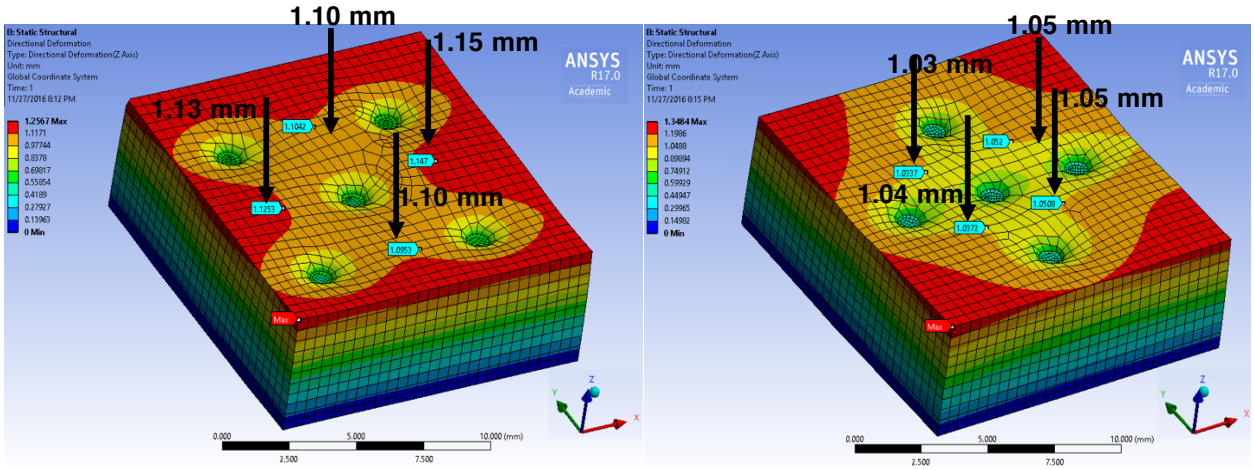

Figure 6.23 Z-direction deformation in 1/8 of a model wood composite containing 20 simulated adhesive Z-connections with different spatial distributions, but same area-density after 72 h simulated immersion in water. Note that the diagonal arrangement depressed thickness swelling over a greater area at the wood surface than the square arrangement. Simulated thickness swelling values of wood at 4 positions are indicated on the figure for comparison (thickness swelling values on the right-hand figure are smaller than the corresponding values on the left-hand figure)

Simulated thickness swelling values of wood (excluding areas occupied by adhesive Z-connections) in the model composite were calculated and averaged to compare the effects of different spatial distributions of Z-connections (square vs. diagonal) on thickness swelling of the model composites (Fig. 6.24). This figure confirms that the diagonal arrangement was more effective at restraining thickness swelling of the model wood composite than the square one (Fig. 6.11).

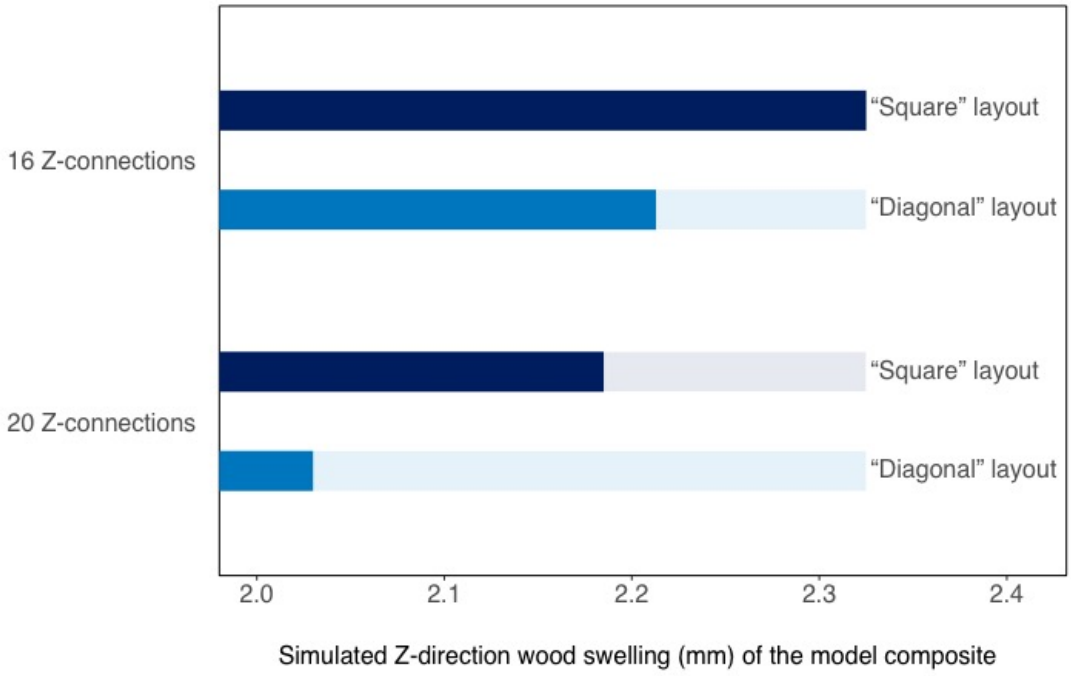

Figure 6.24 Comparison of the effects of the square and diagonal spatial distribution of simulated adhesive Z-connections on thickness swelling of model wood composites

6.4 Discussion

Area-density, diameter and spatial distribution of simulated adhesive Z-connections influenced the ability of the adhesive Z-connections to restrain thickness swelling of the model wood composite, supporting my hypothesis.

As expected, a larger number of adhesive Z-connections over a fixed area was better at restraining thickness swelling of the model wood composite than a lower number of adhesive Z-connections. There was a linear correlation between the thickness swelling of wood (excluding the thickness swelling components of adhesive Z-connections) and the area occupied by adhesive Z-connections (Fig. 6.19). This correlation accords with a study by Partridge and Cartié (2005). They examined the effects of 3 different area-densities (0.5%, 2% and 4%) of Z-pin insertions on the fracture toughness of a carbon fibre/epoxy prepreg composite. They found that the load carrying capability and Mode I fracture toughness of the composite was positively correlated with area-density of Z-pins.

A related approach to increasing the area-density of adhesive Z-connections is to increase the diameter of individual Z-connections. Simulation results suggested that adhesive Z-connections with larger diameters were better than smaller diameter ones at restraining thickness swelling of the model wood composites. This strengthens the correlation between area-density of adhesive Z-connections and reductions in thickness swelling of the model wood composites mentioned above. However, it should be noted that increasing the diameter of adhesive Z-connections also increased the simulated adhesive content of the model. Therefore, my results here are not relevant to those in Chapter 3 which experimentally examined the ability of Z-connections with different diameters to restrain thickness swelling of a model wood composite. In the latter experimental study the adhesive applied on each wood veneer layer remained the same and therefore the larger diameter holes (2 mm in diameter) were not completely filled with adhesive in the Z-direction, in contrast to the simulated adhesive Z-connections modelled in this chapter.

Simulation results clearly suggested that increasing the area-density of adhesive Z-connections better restrained thickness swelling of the model composites. But, from a practical point of view, it would not be realistic to simply increase the area-density of adhesive Z-connections because adhesive is expensive and, accordingly, composites containing large numbers of adhesive Z-connections would not be economic. A more practical approach is to better distribute adhesive Z-connections to reduce thickness swelling. On this topic, one interesting finding from this chapter was that, adding just one extra Z-connection to the middle of a square shaped array formed by four Z-connections improved the ability of the adhesive Z-connections to restrain thickness swelling. This positive effect occurred because the additional Z-connection was able to bridge the four Z-connections at four corners of a square array creating a better connected network of ‘dimples’. This improved array of Z-connections was better at restraining the swelling of the composites. Another related approach is to place

adhesive Z-connections in a way that takes advantage of their ability to restrain swelling to a greater extent in the X-direction than in the Y-direction. For example, adding one extra row of adhesive Z-connections in the Y-direction could reduce the unwanted thickness variation of composites in the X and Y directions (comparing 36 Z-connections with 48 Z-connections). Therefore, a more uniform (even) surface of the composites after thickness swelling might be achieved by unevenly placing adhesive Z-connections across X-Y plane. Another, possibly more practical, approach would be to arrange the adhesive Z-connections diagonally rather than in a square array across the surface of the model wood composites. Because 'dimples' created by adhesive Z-connections were elliptical in shape, it appears that such a diagonal arrangement could take advantage of the directional restraining effects of adhesive Z-connections and hence restrain swelling over a larger surface area than square array. This suggestion accords with research on the optimal packing of ellipses within a constrained area (Galiev and Lisafina 2013; Kallrath and Rebennack 2014; Ilin and Bernacki 2016; Stoyan et al. 2016). For example, a study by Galieve and Lisafina (2013) suggested that a mixed diagonal arrangement of ellipses created by rotating the major axis and varying major/minor axis ratio was able to pack a greater number of ellipses in a given area (Fig. 6.25). However, such an approach would need to take account of the directional nature of the Z-restrain. Nevertheless, the use of adhesive Z-connections of different diameters as a means of creating a more even composite surface after thickness swelling would be worth exploring.

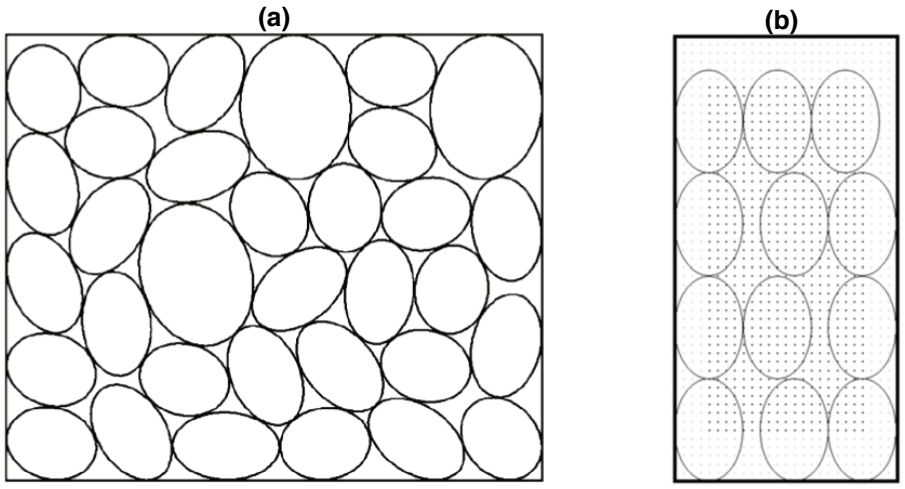

Figure 6.25 Examples of packing of ellipses showing that a diagonal arrangement of ellipses (a) is able to pack a greater number of ellipses in a given area than an arrangement where the ellipses are not rotated (b) (Galieve and Lisafina 2013; Stoyan et al. 2016)

In summary, altering the spatial distribution of adhesive Z-connections appears to be the most practical approach to improving the ability of adhesive Z-connections to more evenly reduce thickness swelling of the model wood composites. Such an approach does not increase the amount of adhesive Z-connections needed in the model wood composites and therefore it is preferable to increasing the number of Z-connections or their diameters.

6.5 Conclusions

In this chapter, I developed a finite element model (FEM) coupling moisture diffusion and hygroscopic swelling of a model laminated wood composite containing adhesive Z-connections. Simulation results using the ANSYS® FEA package supported my 'specific hypothesis' that design parameters, such as area-density, diameter of Z-connections and their spatial arrangement influence the thickness swelling of the model wood composites. In general, as expected, there was a positive relationship between numbers of Z-connections (area-density) and the ability of the Z-connections to restrain thickness swelling. More importantly from a practical point of view, at the same area-density, a diagonal arrangement of Z-connections was better than a square array at restraining thickness swelling.

In conclusion, finite element analysis (FEA) is clearly a useful tool for exploring the effects of various design parameters affecting the ability of adhesive Z-connections to reduce thickness swelling of wood composites. FEA enabled me to explore three design parameters using computer simulation rather than experimental work, which greatly shortened the time frame for product design prototyping. It provided useful information on the effects of area-density, diameter and spatial arrangement of adhesive Z-connections on the thickness swelling of model wood composites, as mentioned above. The modelling approach also opens up opportunities for more complex design of adhesive Z-connections. For example, it would be worthwhile to do further research on using the FEA model to examine effects of wood properties, such as permeability, density and radial/tangential swelling ratio on the thickness swelling of the model wood composites. However, the FEA model developed in this chapter did not take into account the interaction of the Z-connections with the adhesive in the X-Y plane of the wood composites. Future research would be needed to include an X-Y adhesive bond line in an FEA model and explore the relationship between the X-Y adhesive bond lines and the Z-direction adhesive, and their effects on thickness swelling.

7 Adhesive Z-connections Improves the Fracture Toughness of a Laminated Birch Wood Composite

7.1 Introduction

Chapters 4, 5 and 6 examined the effects of adhesive Z-connections on the dimensional stability of a model wood composite. Another important characteristic of wood composites is their mechanical properties, because many wood composites are used in structural applications (Kollmann et al. 1975). For example, fracture toughness is an indicator of the stress required to propagate a pre-existing flaw, and it is a critical property for materials such as laminated composites used in demanding structural applications (Sela and Ishai 1989). Delamination of laminated composites reduces their stiffness and strength and can lead to loss of structural integrity (O'Brien 1982). Hence, there is significant interest in improving the fracture toughness of laminated composites, particularly those used for aircraft construction (Sela and Ishai 1989; Mouritz 2007). Modern high performance aircraft use a range of components made from laminated carbon-fibre/epoxy composites (Franklin and Christopher 2015), but in less demanding aerospace applications plywood is still used (Euro Plywood web source 2016). Plywood, as mentioned in Chapter 2, consists of thin layers of wood veneer that are glued together, with adjacent layers having their wood grain rotated up to 90 degrees to one another (Wood and Linn 1943). The glue-lines of plywood and also other laminated wood composites such as laminated veneer lumber (LVL) and glue-laminated lumber (glulam) often contain flaws, and they can fail by delamination (Bucur 2011). Hence, there has been some interest in improving their fracture toughness (Davalos et al. 2000).

The susceptibility of laminated composites to delamination depends on a variety of intrinsic and extrinsic factors, but the lack of reinforcement of adhesive bond lines is a fundamental reason why cracks propagate between laminae (Franklin and Christopher 2015). Therefore, one obvious route to increasing the fracture toughness of laminated composites is to

provide such reinforcement. For example, numerous studies have shown that the susceptibility of laminated composites to delamination can be reduced by reinforcing adhesive bond lines with fibres that act as bridges to inhibit crack opening (Bloyer et al. 1996; Ritchie 1999; Launey and Ritchie 2009). This approach, and others used to improve fracture toughness of materials, was reviewed by Wegst et al. (2014). Another approach to improving the fracture toughness of composites, which I explore in this chapter, is to alter the geometry of the adhesive network to provide Z-direction adhesive reinforcement across multiple laminae. Such an approach is related, although not identical, to those used to provide through-thickness reinforcement of advanced composites, for example 3D-weaving, stitching, braiding, embroidery, tufting and z-anchoring (Mouritz 2007).

In this Chapter, I test the use of adhesive Z-connections across multiple laminae in combination with glass-fibre reinforcement of adhesive bond lines as means of improving the fracture toughness of a model laminated birch wood composite.

7.2 Materials and methods

7.2.1 Preparation of a laminated birch wood composite with adhesive Z-connections

My main experiment examined the effect of adhesive Z-connections (two levels) and the effect of glass-fibre reinforcement of adhesive bond lines on different measures of fracture toughness of a model laminated birch wood composites (Fig. 7.1). Two different types of samples were prepared: One contained a higher level of Z-connections than the other (39 Z-connections vs. 24 Z-connections). There was only one level of glass-fibre reinforcement of adhesive bond lines (5.5% w/w). Birch was chosen as the test substrate because composites made from this wood species were widely used for the manufacture of aircraft during WWII, and there is also ongoing interest in using birch plywood for the construction of unmanned aerial vehicles, commonly known as drones (Schatzberg 1994; Soutis 2005; Bateman et al. 2007). Eight birch wood veneer sheets were purchased from a retailer (ENE Wood Products, Surrey,

BC, Canada), and stored in a conditioned room (20 ± 1°C and 65 ± 5% relative humidity) for one month to ensure they reached equilibrium moisture content and stable dimensions before the experiment.

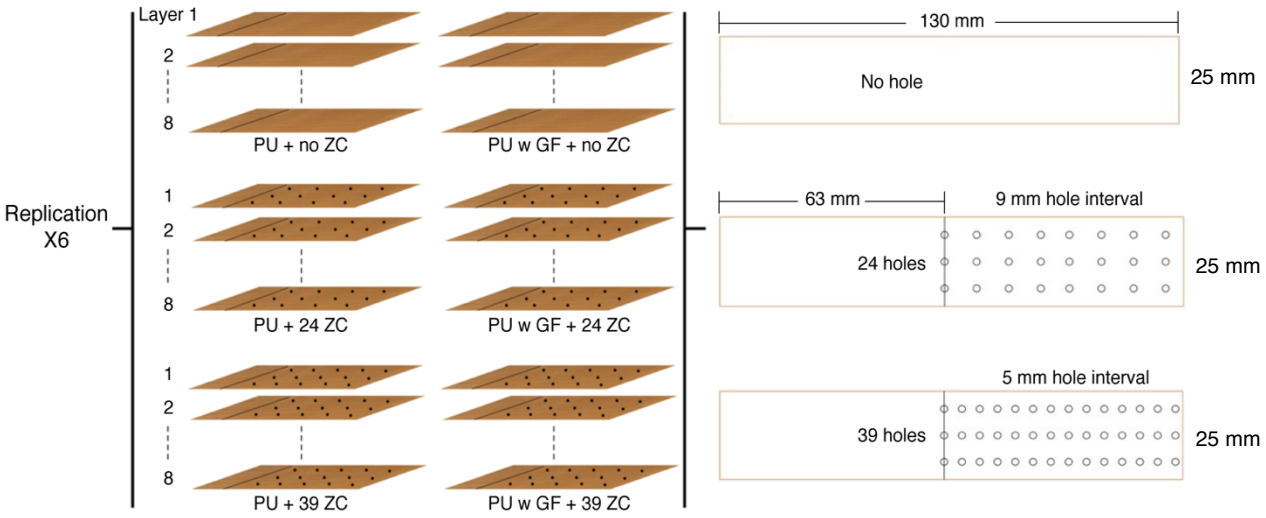

Figure 7.1 Preparation of laminated birch wood composite specimens with two levels of Z-connections (ZC) of laminae and polyurethane (PU) adhesive bond reinforcement with glass-fibre (GF)

Six different types of specimen were made, and there were six replications of each specimen type (Fig. 7.1). Manufacture of specimens was as follows. Each specimen contained eight veneer layers, individually grain matched and selected from eight veneer sheets. Strips measuring 130 mm x 25 mm were cut from veneer sheets using a paper guillotine (Boston™ 2658). These dimensions were chosen because they are the same as those recommended by ASTM standard D5528-13 (ASTM standard 2013). Veneer strips used for specimens with adhesive Z-connections were perforated with a high-speed dental drill as described in Chapter 4. The eight veneer strips used to make each laminated composite were placed in a customized mould to align them vertically, and all eight were perforated together in the mould. Veneer for specimens with a higher number of adhesive Z-connections contained 39 holes (3 rows x 13 columns [density of Z-connections = 2.33/cm^2]) with a spacing of 5 mm (Fig. 7.1). Veneer for specimens with a lower number of adhesive Z-connections contained 24 holes (3 rows x 8

columns [density of Z-connections = 1.43/cm^2]) with a spacing of 9 mm (Fig. 7.1). Control specimens were not perforated.

The same one-component polyurethane adhesive (Gorilla glue Co. USA), used in Chapters 3, 4 and 5 was used to bond veneer strips. The glue was either used in an unmodified form or modified by the addition of 5.5% w/w milled (60 mesh) glass-fibre (Fiber-Tek®, Burnaby, BC, Canada). Unmodified adhesive (0.187 g ± 0.0005 g) was applied to each veneer strip using a syringe (BD® 1 mL syringe) and spread evenly across each veneer using a glass coverslip (Matsunami®). Modified adhesive containing glass fibre was also applied in exactly the same way to veneer strips, and also spread across veneer strips using a coverslip. The same amount of adhesive was applied to perforated and unperforated veneer strips. Veneers were then laid up with their grain direction parallel to each other, to make specimens containing either perforated or unperforated veneer strips. A strip of aluminum measuring 63 mm x 25 mm was inserted into the end of the middle two veneers in each specimen to cover an area of 63 mm x 25 mm. This foil insert served as a crack initiator during fracture testing as recommended by ASTM D5528-13. Specimens were placed in a small laboratory press (Carver® hydraulic press 3912) and pressed at room temperature at 3 MPa for eight minutes. The adhesive penetrated through the Z-direction holes in each veneer, creating adhesive Z-connections across multiple laminae. No such Z-connections occurred in the unperforated veneers. The resulting composites were conditioned at 20 ± 1°C and 65 ± 5% r.h. for seven days.

A second experiment examined the effects of different numbers of adhesive Z-connections (0, 6, 12, 18, 51, and 66 holes) on the fracture toughness of a model laminated birch wood composite bonded with unmodified PU adhesive. This experiment sought to find the lower and upper limits for the ability of adhesive Z-connections to improve the fracture toughness of the birch wood composite. The manufacture and testing of duplicate specimens for

each level of reinforcement in this second experiment was exactly the same as those used in the first experiment.

7.2.2 Fracture toughness testing of laminated wood composites

The geometry of the specimens described above conforms to the requirements of the standard ASTM D5528-13 test for crack opening mode (Mode I) inter-laminar fracture toughness testing of unidirectional polymer composites. The edges of specimens were covered with white correcting tape and marked with length scales (1 mm marks for the first 25 mm followed by 2 mm marks for a further 20 mm, and then 5 mm marks for an additional 20 mm, Fig. 7.2). Opening forces were applied to specimens via hinges attached to the cross-head of a universal tensile testing machine (Instron® M3502) (Fig. 7.2a, b). A cross-head speed of 1 mm/min was used, and crack length propagation was measured using a digital SLR camera (Canon® EOS 5D Mark II) with 24-105 mm zoom lens as shown in Fig. 7.2b. The camera captured an image as soon as the specimen opened. Subsequent images were captured every 20 seconds until failure using the tethering photo-capture software, Breeze® DSLR Remote Pro, on a PC. Each time-lapse image was saved in RAW format so the crack front position could be easily seen at high magnification within the software Adobe Photoshop® Raw processer (Fig. 7.2c, d).

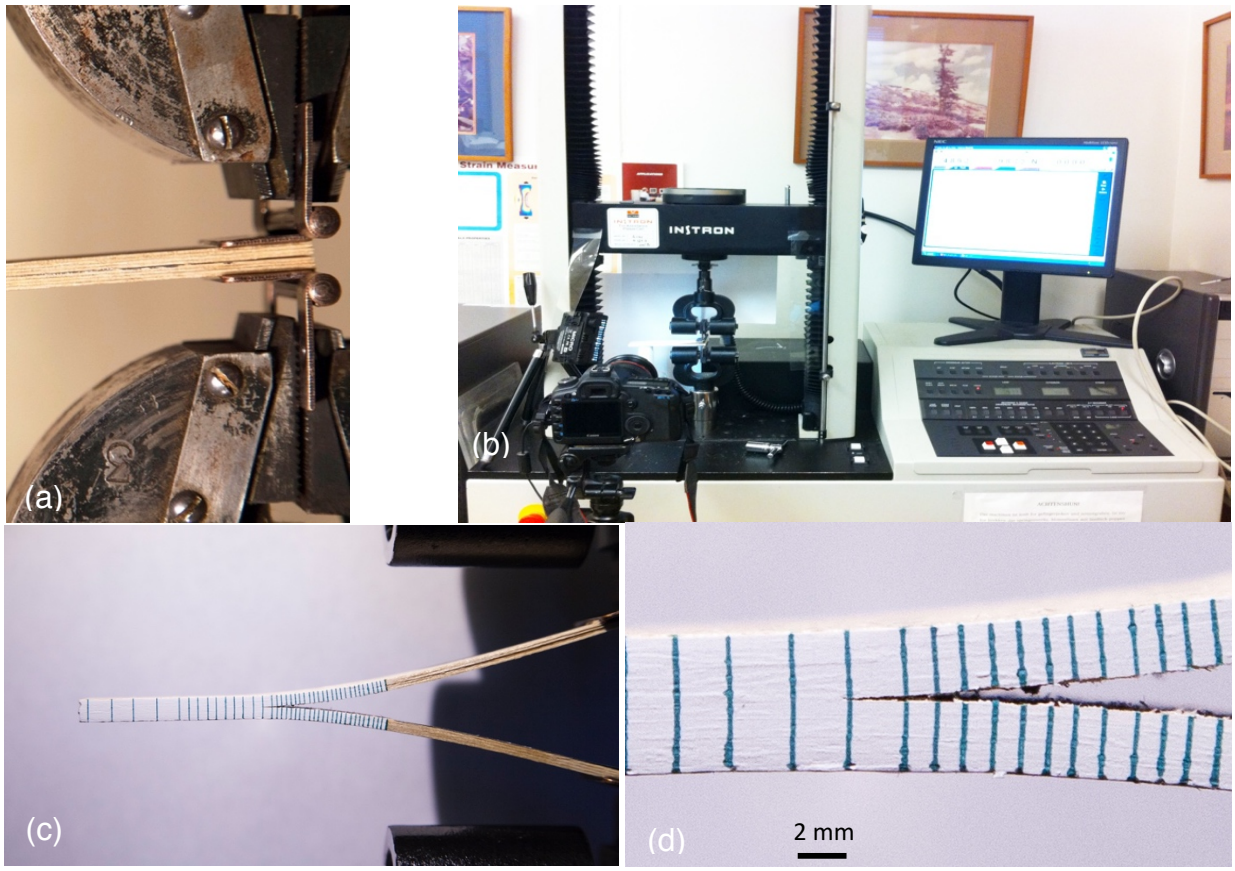

Figure 7.2 Mode I (crack opening mode) fracture toughness testing of a model laminated birch wood composite: (a) Hinges used to attach one end of a specimen to the two crossheads; (b) Universal tensile testing machine with attached computer, and also showing the position of the DSLR camera for measurement of crack propagation and crack length; (c) White coated edge of one side of a specimen with scale markers; (d) Higher magnification image of (c) showing the position of the crack tip front

7.2.3 Fracture toughness calculation and analysis of data

Modified beam theory was used to calculate fracture toughness according to ASTM D5528-13 standard. It should be noted that test results are primarily 'specimen properties' rather than 'material properties', because calculated fracture toughness values are dependent on the geometry of test specimens. The test results should therefore be regarded as 'apparent fracture toughness' as suggested by fracture mechanics principles. Nevertheless, all the specimens (perforated and unperforated controls) consisted of wood veneers with the same grain pattern and similar geometry and they contained identical levels of adhesive. Therefore, the apparent fracture toughness values are comparable between specimens.

Fracture toughness results from the main experiment were subject to analysis of variance to determine the effects of the two experimental factors, adhesive Z-connections (39 Z-connections vs. 24 Z-connections vs. 0 Z-connection) and adhesive modification (PU adhesive vs. glass-fibre reinforced PU adhesive) as well as the interaction of these two factors on fracture toughness. Statistical computation used GenStat® (Release 17.1), and results were tested for statistical significance at the 5% level ($p < 0.05$). Results are presented in graphs plotted using the program R (version 3.2.3) and least significant difference (LSD) bars derived from the ANOVA are included on each graph. These LSD bars can be used to determine if differences between individual means are statistically significant ($p < 0.05$).

7.2.4 Scanning electron microscopy of fracture surfaces

The microstructure of fractured surfaces in tested specimens containing 39 Z-connections was examined using scanning electron microscopy. Small wood specimens measuring 5 mm x 5 mm were carefully cut from the surface of fracture toughness specimens using a precision micro table saw (Byrnes Model Machines Co. USA) equipped with a 10 cm diameter blade. Care was taken to ensure that fracture surfaces were not damaged during the preparation of specimens. Specimens were mounted on aluminium stubs using double-sided adhesive tape. Samples were sputter coated with an 8 nm layer of gold and examined using a Zeiss UltraPlus analytical field emission scanning electron microscope (SEM) operating at 15 kV and a working distance of 13.1 to 14.0 mm. Selected secondary electron images were saved as TIFF files.

7.3 Results

7.3.1 Fracture toughness tests

The adhesive Z-connections in the model birch wood composite significantly improved fracture toughness (Fig. 7.3). The improvement of fracture toughness was significantly ($p < 0.05$) greater in samples containing higher numbers of Z-connections (Fig. 7.3). Fracture

toughness was also significantly improved by reinforcing adhesive bond lines with glass-fibre (Fig. 7.3). Analysis of variance indicated that there was no significant ($p > 0.05$) interaction of Z-connections and addition of glass-fibre to adhesive bond lines on fracture toughness. Nevertheless, the addition of glass-fibre to adhesive bond lines was more effective at improving the fracture toughness of the birch composite containing adhesive Z-connections than it was at improving the fracture toughness of the control. For example, the addition of glass-fibre to adhesive bond-lines improved the fracture toughness of the control by 42%, whereas comparable figures for composites containing adhesive Z-connections were 69% (24 Z-connections) or 67% (39 Z-connections).

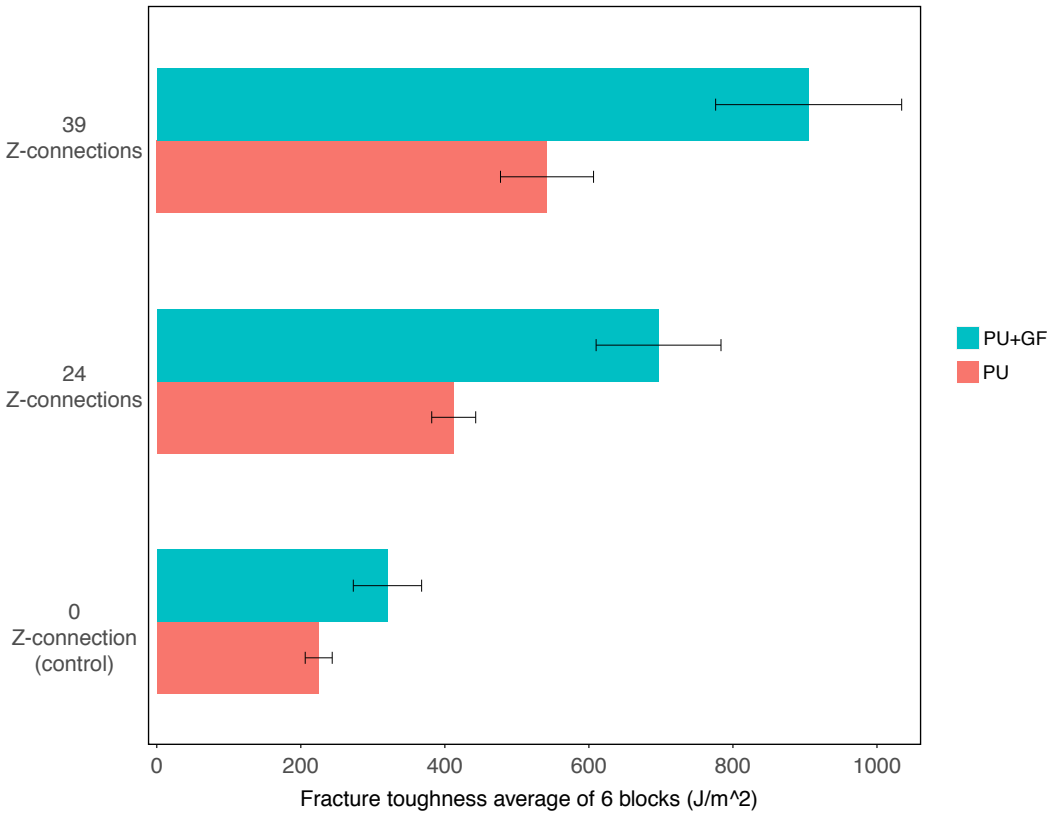

Figure 7.3 Fracture toughness values of specimens containing adhesive Z-connections and glass-fibre in adhesive bond lines vs. fracture toughness of the controls.

The effects of adhesive Z-connections and addition of glass-fibre to adhesive bond lines on 5% maximum fracture toughness values of specimens, a reporting parameter for ASTM

D5528-13, are shown in Figs. 7.4 and 7.5, respectively. These figures also show other critical fracture characteristics of tested specimens, and demonstrate the ability of adhesive Z-connections, and also adhesive bond-line reinforcement to improve the fracture toughness of the birch wood composite.

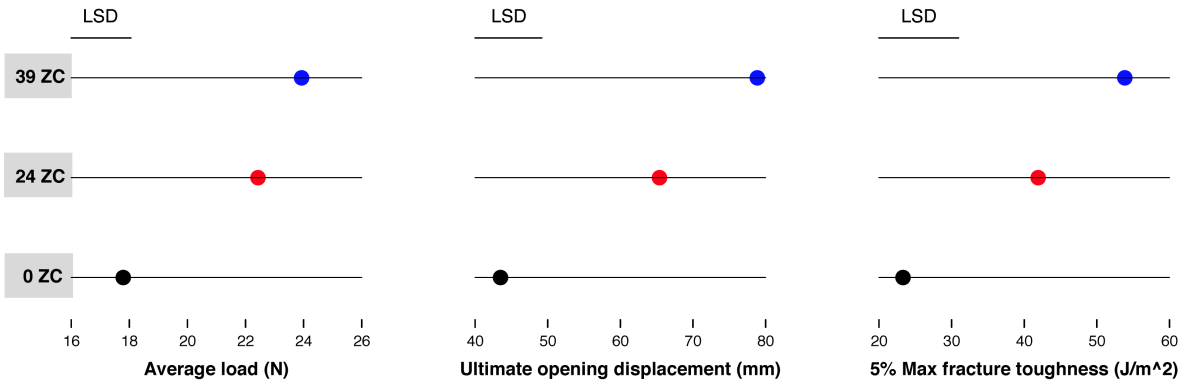

Figure 7.4 Effects of adhesive Z-connections (ZC) (39 Z-connections vs. 24 Z-connections vs. 0 Z-connection) on some critical fracture characteristics of the laminated birch wood specimens

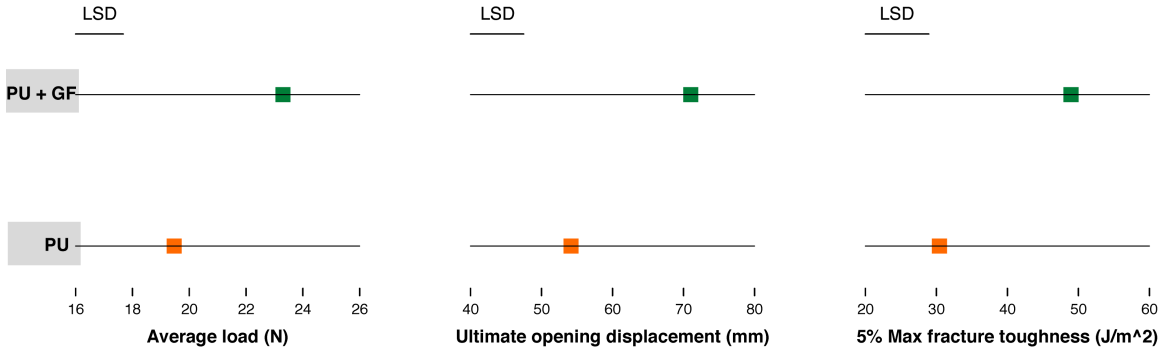

Figure 7.5 Effects of reinforcement of polyurethane adhesive (PU) with glass-fibre (GF) on some critical fracture characteristics of the laminated birch wood specimens

Adhesive Z-connections in the birch composites appeared to arrest propagation of the crack induced during fracture toughness testing. This effect is suggested by load-displacement curves of specimens during testing (Fig. 7.6), which show that load increased abruptly and then increased more slowly. During the latter phase there were increases in load as the crack encountered adhesive Z-connections. Load increases are sinusoidal in specimens containing adhesive Z-connections at the lower level, but the higher level of Z-connections (39 Z-

connections) appears to smooth the sinusoidal variation of load. The load carrying capability (y-axis) of specimens with adhesive Z-connections was generally higher than that of the control. Furthermore, specimens with adhesive Z-connections withstood greater Mode I opening displacement (x-axis) until ultimate failure than the control (Fig. 7.6).

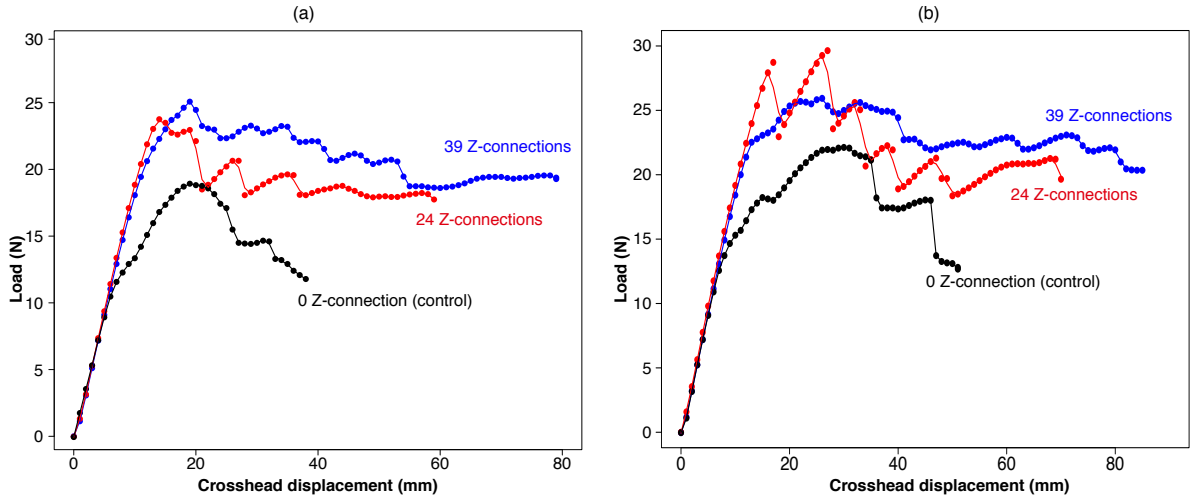

Figure 7.6 Load-displacement curves of specimens with different numbers of adhesive Z-connections and bonded using (a) unmodified polyurethane (PU) adhesive, or (b) a glass-fibre reinforced PU

Results in Fig. 7.6 show the positive effects of the adhesive Z-connections on load sustained by specimens bonded with an unmodified polyurethane adhesive (Fig. 7.6a), and specimens bonded with a polyurethane adhesive reinforced with 5.5% glass-fibre (Fig. 7.6b). The effect of adding glass-fibre to adhesive bond lines on load sustained by specimens can be clearly seen in Fig. 7.7. This figure shows that adding glass-fibre to the PU adhesive increased the load carrying capacity of specimens, and extended the maximum Mode I opening displacement of specimens, irrespective of the presence of adhesive Z-connections (Fig. 7.7).

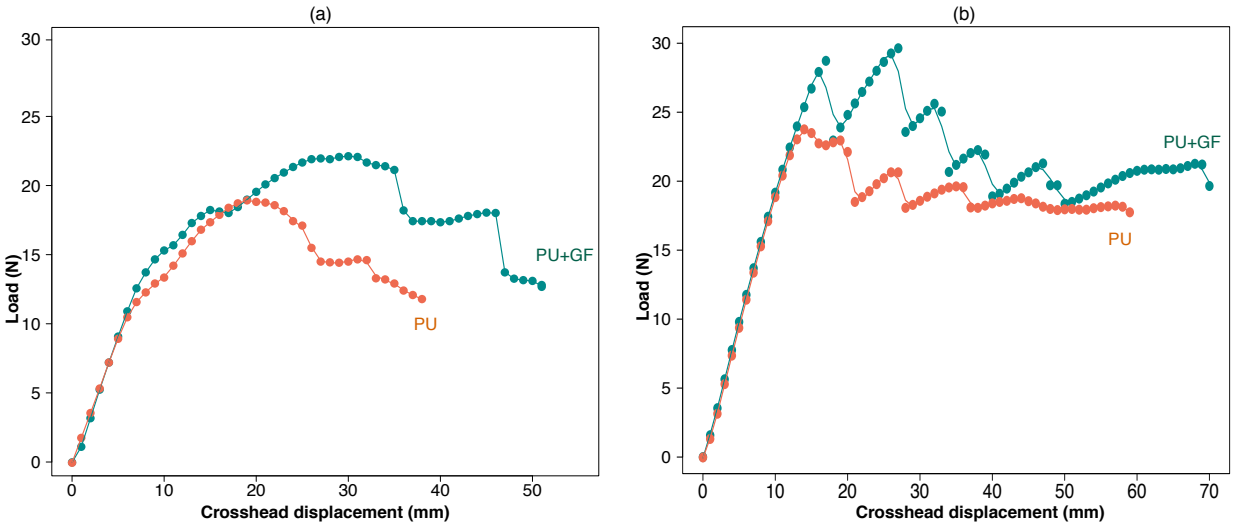

Figure 7.7 Load-displacement curves of specimens with unmodified polyurethane adhesive or adhesive modified by the addition of 5.5% w/w glass-fibre: (a) No adhesive Z-connections; (b) Adhesive Z-connections (24 Z-connections)

Crack resistance curves of specimens, also known as R-curves, accord with load displacement results and indicate the positive effects of adhesive Z-connections and adhesive bond modification (addition of glass-fibre) on fracture toughness (Fig. 7.8). They also support the suggestion that increases in toughness of specimens with adhesive Z-connections resulted from the ability of the Z-connections to arrest crack propagation.

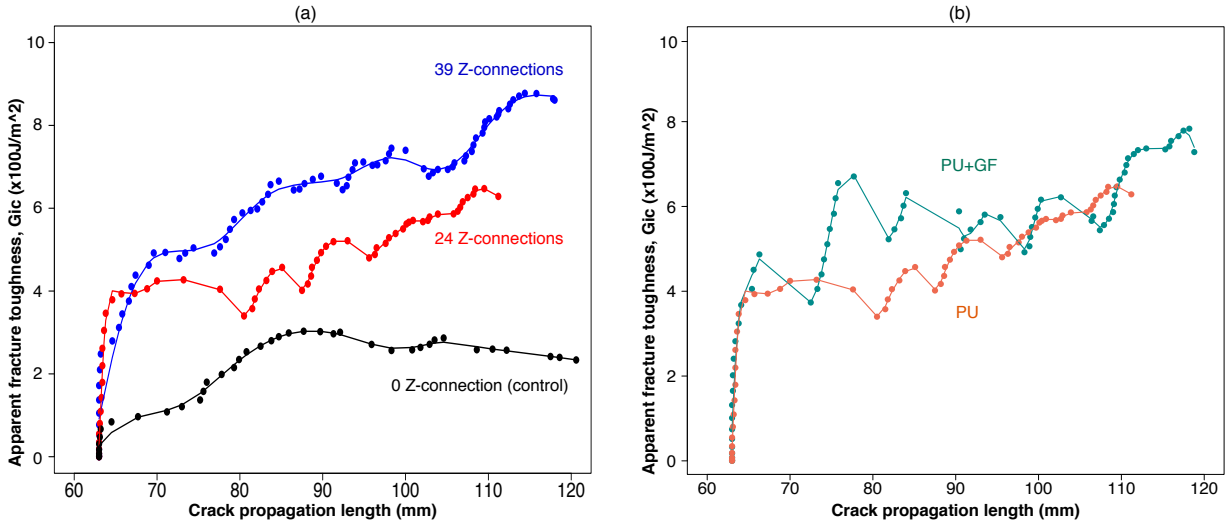

Figure 7.8 Mode I crack growth resistance curves (R-curves) of (a) PU adhesive with different numbers of adhesive Z-connections, and (b) composites bonded with different adhesive types but containing the same number (24) of adhesive Z-connections

Results in Fig. 7.9 show the effects of different numbers of adhesive Z-connections (0, 6, 12, 18, 51, and 66 Z-connections) on the load sustained by specimens bonded with unmodified PU adhesive. Table 7.1 shows the effects of different numbers of adhesive Z-connections on the fracture toughness and Mode I opening displacement of specimens. The results in Fig. 7.9 and Table 7.1 confirm that adhesive Z-connections improve fracture toughness, and indicate that improvements in fracture toughness depend on the number of Z-connections. The optimal number of Z-connections appeared to be 39 per veneer strip (2.33 per cm^2).

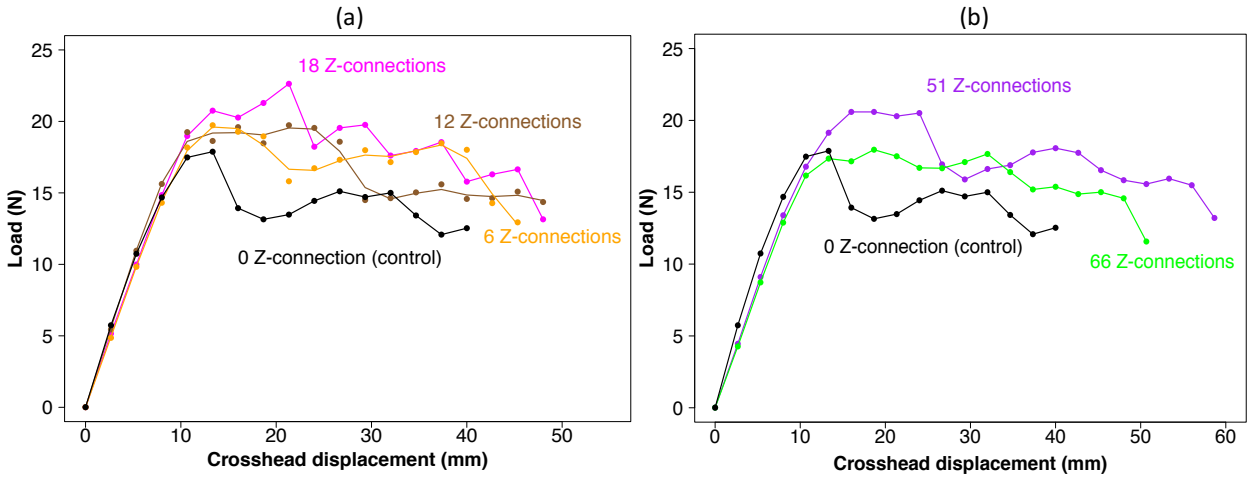

Figure 7.9 Load-displacement curves during double cantilever beam (DCB) Mode I fracture toughness tests of specimens with different numbers of adhesive Z-connections (including the control): (a) Less than 24 Z-connections (<1.43/cm^2); (b) More than 39 Z-connections (>2.33/cm^2)

Table 7.1 Effects of different numbers of adhesive Z-connections on the fracture toughness and Mode I opening displacement of laminated birch wood specimens bonded with an unmodified polyurethane adhesive

No. Z-connections	Density of Z-connections (No./cm^2)	Fracture toughness (J/m^2)	Displacement (mm)
0 (control)	0	225	41
6	0.36	287	40
12	0.72	287	47
18	1.08	327	48
24	1.43	412	56
39	2.33	542	66
51	3.04	340	57
66	3.94	353	52

7.3.2 Scanning electron microscopy of fracture surfaces

Scanning electron photomicrographs of fracture surfaces in laminated birch specimens after mechanical testing suggest how adhesive Z-connections and addition of glass-fibre to adhesive bond lines increased fracture toughness. They also cast some light on the bonding mechanism of polyurethane adhesives used with wood.

Polyurethane adhesive was clearly visible at the fracture surfaces of birch composites bonded with unmodified adhesive (Fig. 7.10a). Residual adhesive at fracture surfaces exhibited tearing and pull-out, which may have contributed to adhesive bond strength (arrowed top left in Fig. 7.10a). In addition, I observed pull-out of adhesive that had penetrated the cells in the rays of birch (arrowed in Figs. 7.10b~c). The pillar-shaped structures that projected from the cells within rays had branches, some of which appeared to have fractured during testing (arrowed in Fig. 7.10d). I also observed fracture, pull-out and lateral displacement of adhesive Z-connections that provided multiple through-reinforcement of the birch composite (arrowed in Figs. 7.10e~f). The same patterns of failure were noted at fracture surfaces of composites

bonded with polyurethane adhesive containing glass-fibre (Figs. 7.11a~c). In addition, I observed pull-out of fibre-bundles at fracture surfaces (arrowed in Fig. 7.11d). Glass-fibre was clearly evident at fracture surfaces, and there was evidence of pull-out of the glass-fibres in horizontal glue-lines (arrowed left in Fig. 7.11a) and also within the adhesive Z-connections (arrowed in Figs. 7.11e~f).

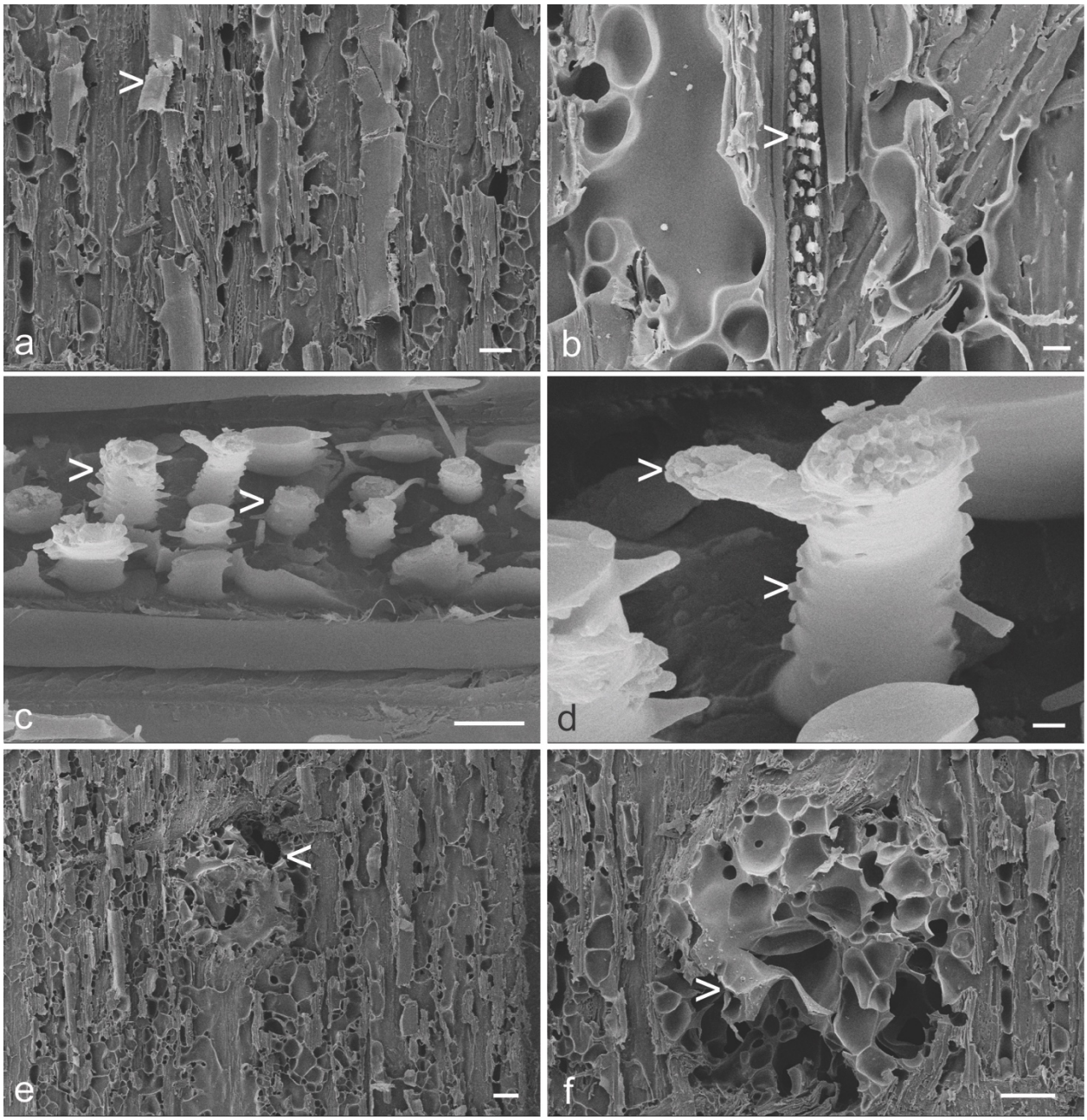

Figure 7.10 Fracture surfaces of a laminated birch composite bonded with unmodified single component polyurethane adhesive: (a) Adhesive on fractured wood surface showing pull-out and micro-fracture of

adhesive that partially covers the wood surface (arrowed left; scale bar = 100 μm); (b) Fractured wood surface showing a multiseriate ray (centre) and pull-out of adhesive from the lumens of individual ray cells (arrowed centre; scale bar = 20 μm); (c, d) Higher magnification photographs showing the pillars of adhesive that pulled out of ray cells shown in (b). Note the fractured ends of the pillars and the intact and fractured side-arms (branches) (arrowed left and centre; scale bars = 10 μm [c] and 1 μm [d]); (e) Fractured column of an adhesive Z-connection that provided through-reinforcement to the composite (arrowed centre) and residual adhesive on the fractured wood surface (scale bar = 200 μm); (f) Higher magnification photograph of the adhesive Z-connection shown in (e). Note the fracture and distortion of the adhesive Z-connection and the distortion of the adjacent wood (as arrowed; scale bar = 200 μm)

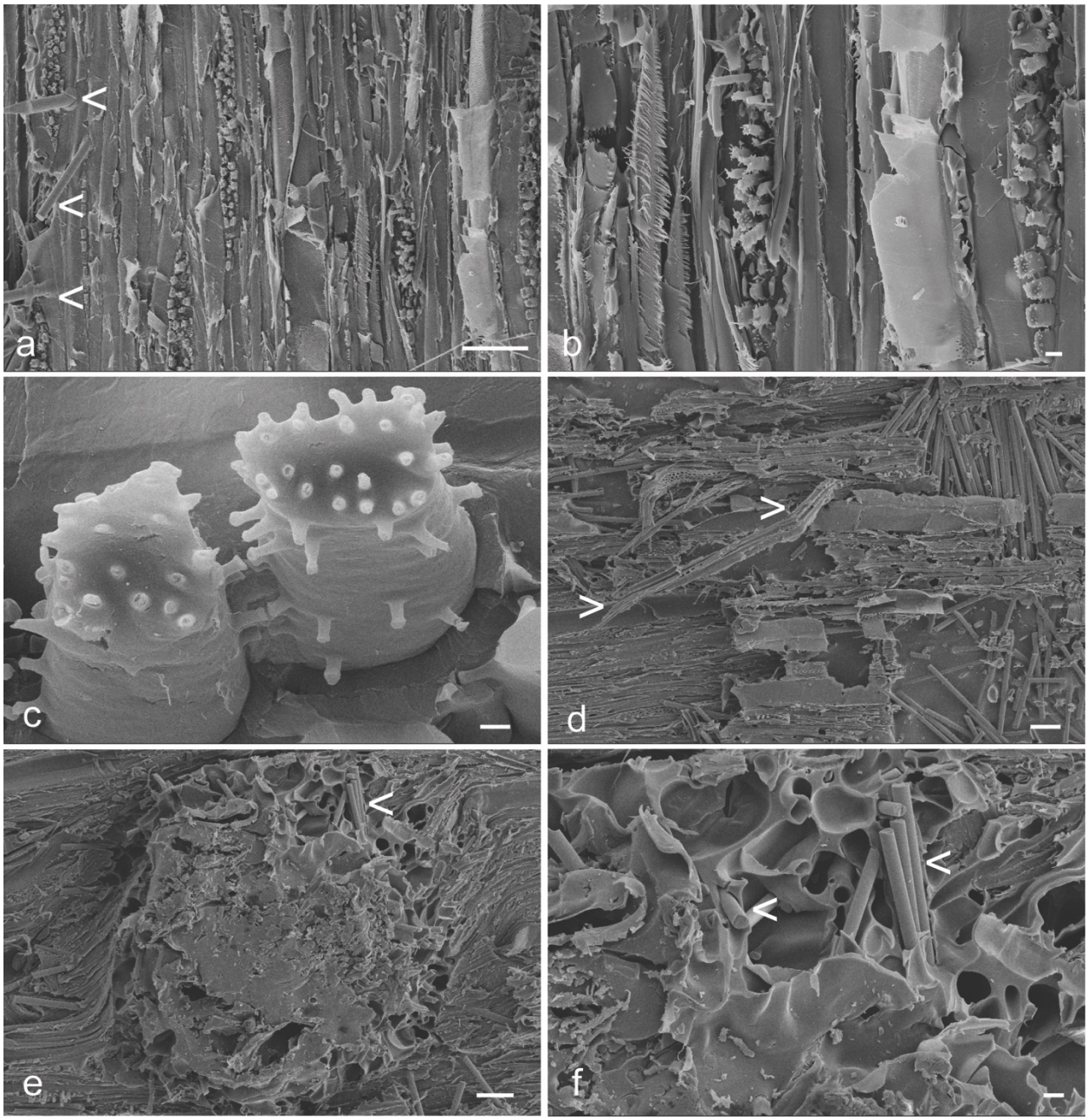

Figure 7.11 Fracture surfaces of a laminated birch composite bonded with a single component polyurethane adhesive containing 5.5% w/w milled (60 mesh) glass-fibre: (a) Fractured wood surface

showing pull-out and fracture of glass-fibre (arrowed left) and wood cells; pull-out of adhesive from ray cells; and adhesive that partially covers the wood surface (scale bar = 100 μm); (b-c) Higher magnification photographs [from (a)] showing fracture of wood cells and pull-out of adhesive from the lumens of individual ray cells (scale bars are 10 μm [b] and 1 μm [c]); (d) Fractured wood surface showing residual adhesive, pull-out of bundles of fibres (arrowed left and centre) and presence of numerous glass-fibre strands (right) (scale bar = 100 μm); (e-f) Fractured column of an adhesive Z-connection containing embedded glass-fibre that provided through-reinforcement to the composite (arrowed top right of centre in e, and centre and right in f). Note the fracture and distortion of the adhesive Z-connection and the distortion of the adjacent wood (scale bars are 100 μm [e] and 20 μm [f])

7.4 Discussion

My results support my hypothesis that adhesive Z-connections increase the fracture toughness of a laminated birch wood composite, and show that improvements in fracture toughness depend on the number of Z-connections. My results also show that glass-fibre reinforcement of adhesive bond lines significantly increases fracture toughness. They also suggest how the two different types of reinforcement increased fracture toughness. The addition of glass-fibre to adhesive bond lines appeared to provide reinforcement during crack propagation, hence consuming fracture energy. This suggestion accords with the results of many studies that have examined the use of glass-fibre to reinforce and improve the toughness of other composite materials, for example vinyl-ester polymer composites (Compston et al. 2001), polypropylene composites (Fu et al. 2002) and dental particulate composites (Dyer et al. 2005). There have been no previous studies, to my knowledge, of the use of adhesive Z-connections to increase the fracture toughness of laminated wood composites. Therefore, I cannot compare my findings with those of previous researchers. However, the multiple through-reinforcement provided by adhesive Z-connections running radially in specimens has some similarities with that provided by rays (radial ribbons of woody tissue), which are aligned in the same direction as the adhesive Z-connections engineered here. My SEM images of fracture surfaces suggested that rays provided reinforcement, and Reiterer et al. (2002) in their study of the fracture toughness of three hardwoods and the softwood, spruce, suggested that ‘the rays (in solid wood) can be considered as reinforcements in the radial directions’. Furthermore, their load displacement graphs obtained during fracture testing of hardwoods have some similarities

to those obtained here (Reiterer et al. 2002). Hence, I suggest that adhesive Z-connections provided reinforcement behind the crack tip, hindering crack propagation and absorbing fracture energy. This suggestion is supported by the wave-shape of the crack propagation resistance curves (R-curves) of specimens containing adhesive Z-connections. The 'wave peaks' indicate abrupt increases in fracture energy when the crack propagated through adhesive Z-connections. This bridging effect occurred at the macro-scale, but it complements that provided by adhesive bond reinforcement with glass-fibre. Such a complementary effect was more pronounced in specimens with adhesive Z-connections than in the controls, possibly because the glass-fibre reinforced the adhesive columns in the birch wood composite, in addition to their ability to reinforce adhesive bond lines aligned in the x-y direction.

Birch plywood is a preferred material use for the construction of wooden aircraft, as mentioned above, and fracture toughness is an important property of composites used for this application. Nevertheless, as pointed out by Reiterer et al. (2002) there are few studies of the fracture toughness properties of hardwoods such as birch. The fracture toughness properties of composites depend on good adhesion between adhesive and the matrix (Ashcroft et al. 2001). Adhesive bonding of wood involves a mix of physico-chemical interactions including mechanical interlocking provided by the penetration of adhesive into the porous microstructure of wood (Vick 1999). Penetration of adhesives into hardwoods occurs easily via the open pores (vessels) as was observed in Chapters 4 and 5. Hence, reviews of wood adhesion have focused on such an effect (Vick 1999; Kamke and Lee 2007). The penetration of adhesives into rays was mentioned by Vick (1999) as possibly having a detrimental effect on adhesion because 'radially oriented rays can allow excessive flow and overpenetration' (of adhesive). My SEM photomicrographs showed pullout of adhesive from cells in rays suggesting that penetration of adhesive into the rays located at the tangential surface of rotary peeled birch veneer improved adhesion. The pillars of adhesive that pulled out from ray cells had side arms possibly produced

by penetration of adhesive from ray cell lumens through pits (openings) into the lumens of an adjacent cell. Some of these side arms were fractured, possibly indicating that they contributed to the fracture toughness of the composite. This observation suggests that penetration of adhesive into rays can have a positive effect on adhesion, and underscores the need for further studies of the effects of wood microstructure on the adhesive properties and fracture toughness of composites made from hardwoods.

The fracture toughness of the model composite I tested was clearly improved by the introduction of adhesive Z-connections, and also by the addition of glass-fibre to adhesive bond lines. Glass-fibre has been added to composites to improve their mechanical properties (Fu et al. 2002), and a study by Dorey and Cheng (1996) showed that the mechanical properties of laminated spruce-pine-fir (SPF) beams was significantly improved by reinforcing the phenol-resorcinol glue-lines of the composite with pultruded glass-fibre straps. They concluded that 'the application of glass-fibre reinforcing has a potential to play a significant role in glulam structures' (Dorey and Cheng 1996). Hence, the addition of glass-fibre to adhesives could be a practical means of improving the fracture toughness of veneer-based wood composites used in demanding applications. Clearly, my means of creating through-reinforcement using adhesive Z-connections, which also significantly improved the fracture toughness of our model composite, would be more difficult to implement in practice than adding glass-fibre to adhesive bond lines. However, the approach is attractive because significant increases in fracture toughness were achieved without increasing the level of adhesive in the composite. Therefore, it would be worthwhile to explore approaches that are more practical than precision drilling as a means of perforating veneer. One possible approach, as mentioned in Chapter 4, as a way of creating adhesive Z-connections, would be to pass veneer through a roller containing slitting knives. Such an approach, as mentioned in Chapter 4, has been used in the past to 'reduce the tendency of rotary peeled veneer to distort when it is used to manufacture plywood' (Perry

1948). An alternative related approach to improving fracture toughness would be to nail the composite in the Z-direction using thermo-plastic polymer nails. Laminated wood composites that are bonded together with nails are available commercially (Boyle and Gafner 2013), and such an approach might work with other types of wood composites. In support of this suggestion, the automated insertion of thin metal wires through laminates (Z-pinning) is highly effective at improving the fracture toughness of laminated synthetic composites, and is used commercially to improve the properties of aerospace and automotive composites (Mouritz 2007). The Z-pins used in these applications are made from materials such as titanium alloy that are strong and stiff. This desirable property of Z-pins suggests that adhesives that are stronger than the polyurethane adhesive tested here might be better at increasing fracture toughness of laminated wood composites via adhesive Z-connection reinforcement. Further research would be needed to test this hypothesis. Further research is also needed to examine the effect of adhesive Z-connections on other mechanical properties of laminated wood composites. Significant improvements to such composites and also others derived from renewable materials, for example bamboo, could allow them to compete more effectively in some applications with synthetic composites, with resulting benefits in terms of sustainability and the environment (Koronis et al. 2013).

7.5 Conclusions

I hypothesized that introduction of adhesive Z-connections, and glass-fibre reinforcement of adhesive bond lines would significantly increase the fracture toughness of a laminated birch wood composite. My results support this hypothesis, and I have shown that improvements in fracture toughness are related to the number of adhesive Z-connections. I have suggested how through-reinforcement with adhesive Z-connections and glass-fibre reinforcement of adhesive bond lines increase the fracture toughness of the composite. I have also suggested how the ability of adhesive Z-connections to increase fracture toughness could

be improved further. Through-reinforcement using adhesive Z-connections is potentially an attractive, cost-effective approach to improving fracture toughness, because increases in this property were achieved without the use of additives or increasing the level of adhesive in the composite. However, further research is needed to develop practical ways of creating the perforations that facilitate through-reinforcement using adhesive Z-connections in laminated wood composites.

8 General Discussion, Suggestions for Further Research and Conclusions

8.1 General discussion

In this thesis, I hypothesized that creating a 3-dimensionally inter-connected adhesive network by introducing adhesive Z-connections in a model wood composite would improve some properties of the composite. I performed experiments and computer modelling (finite element analysis) to test this hypothesis and examined factors affecting the ability of adhesive Z-connections to improve the dimensional stability and fracture toughness of the composite.

I have shown that adhesive Z-connections (Chapters 3~5) can restrain thickness swelling of the model wood composite. Chapter 3 showed that the optimal diameter for the adhesive Z-connections to restrain thickness swelling of the model composite was 1 mm rather than 2 mm or 3 mm. Chapters 4 and 5 showed that adhesive Z-connections reduced the thickness swelling of the model wood composites by 20 ~ 25%, depending on wood species and veneer type. In comparison, other approaches appear to be more effective at reducing thickness swelling of wood composites. For example, thermal treatments have been reported to reduce the thickness swelling of OSB panels by 67% (Hsu et al. 1989) and 44% (Menezzi and Tomaselli 2006). Surface coatings reduced the thickness swelling of OSB by 69% (Evans and Cullis 2008). Increasing the level of adhesive in OSB was able to reduce thickness swelling of OSB by 52% (Taylor et al. 2008). However, it is important to note that these figures are relevant to a composite composed of veneer flakes, rather than a laminated wood composite made from wood veneer. One attractive aspect of my approach to reducing thickness swelling of composites is that it does not increase the overall level of adhesive in the composites.

I observed that the ability of the adhesive Z-connections to restrain swelling varied with level of adhesive (Chapter 3), wood species (Chapter 4) and veneer type (Chapter 5). Chapter 3 demonstrated that a polyurethane adhesive could form Z-connections in wood composites.

However, it is still not clear whether all adhesives will be able to form Z-connections. My preliminary (unpublished) results suggest that PF and epoxy adhesives can form Z-connections in a model composite and restrain swelling of the composite. However, a protein-based adhesive (rabbit skin glue) and a hot-melt glue both failed to form Z-connections in my model composite. However, these findings are not definitive and further studies would be needed to confirm my preliminary findings. Nevertheless, it appears that some common adhesives (PU, PF and epoxy) can form adhesive Z-connections and reduce thickness swelling of wood composites.

The ability of adhesive Z-connections to reduce thickness swelling was also dependent upon the diameter of the Z-connections (Chapter 3). Larger diameter Z-connections contained voids, and they were less effective at restraining thickness swelling (when they contained the same quantity of adhesive as smaller diameter holes). However, modelling in Chapter 6 demonstrated that larger Z-connections were more effective than smaller ones when they were completely filled with adhesive. However, the latter approach may not be cost effective. A more cost effective and practical method of increasing the ability of adhesive Z-connections to restrain thickness swelling, as results in Chapter 6 suggested, would be to alter their spatial distribution. My method of drilling holes in wood veneer employed precision dental drilling equipment. One of the main challenges to the use of adhesive Z-connections as a way of reducing thickness swelling of wood composites is to develop a method of perforating veneer on a large scale that could be adopted by industry (see the next section on further research).

The effectiveness of adhesive Z-connections at reducing swelling was also affected by wood species (Chapters 4 & 5). The main effect of ‘species’ on thickness swelling was the reduced ability of adhesive Z-connections to reduce the thickness swelling of composites made from hardwoods compared to those made from softwoods. This ‘species’ effect appeared to be related to the lower overall swelling of hardwood composites and possibly their ability to form

good bonds with adhesives (Chapter 5). Adhesive Z-connections were most effective at restraining swelling of spruce composites (Chapters 4 & 5). Spruce is widely used for the manufacture of composites including plywood which is used in demanding applications, for example, the manufacture of aircraft. Nevertheless, the effect of 'species' on the performance of adhesive Z-connections would appear to restrict their use to softwoods and limit their use with hardwoods such as birch, which is widely used to manufacture plywood in North America (Chapter 2).

Chapter 7 supports my hypothesis that adhesive Z-connections (through-reinforcement) improves fracture toughness of my model composite. The effectiveness of adhesive Z-connections on fracture toughness was influenced by the number of adhesive Z-connections as well as the addition of glass-fibre to the adhesive bond lines (Chapter 7). It is clear that any number of adhesive Z-connections (from 6 up to 66) over a fixed area improved fracture toughness of the model composite. However, from a practical point of view it would be desirable to use a smaller number of Z-connection reinforcement (holes). In addition, drilling larger numbers of holes might weaken wood veneer and impair static mechanical properties, such as flexural strength and internal bond strength of composites. Therefore, a way of maximizing the positive effect of adhesive Z-connections on toughness while reducing their effects on other mechanical properties would need to be found. One possible solution would be to design adhesive Z-connections with different shapes and forms rather than the cylindrical form employed in this thesis. For example, polygonal FRP rebars were better at reinforcing concrete than round rebars (Nanni et al. 1995). Perhaps, adhesive Z-connections with different cross-sectional shapes would be better at restricting thickness swelling of wood composites than the cylindrical Z-connections used here. Another possible approach worthy of consideration would be to insert the adhesive Z-connections at an angle of 45°, rather than the 90° used here. In support of this suggestion, Rugg et al. (1998) demonstrated superior delamination resistance of

carbon-epoxy polymer composites reinforced with Z-fibres inserted at 45° than composites reinforced with Z-fibres inserted at 90° to the delamination plane.

In summary, my findings suggest that adhesive Z-connections show promise as a way of improving the dimensional stability and fracture toughness of a model laminated wood composite. The results demonstrate proof of concept, but the approach is a long way from commercial applications. It is most likely that adhesive Z-reinforced wood composites would have a place in composites used in very demanding applications (aerospace, wind towers, etc.). Such applications require high strength-to-weight ratios and superior resistance to delamination. Z-reinforcement could be used to significantly improve through-the-thickness properties particularly the fracture toughness of these wood composites. Most importantly, the concept of adhesive Z-connections opens up a new approach to composite product design that looks at modification of the 3D distribution of adhesive in composites as a way of enhancing properties. Such an approach may be able to improve the properties of wood composites to enable them to compete more efficiently with advanced polymer composites in demanding applications.

8.2 Further research

The precision drilling methodology developed and deployed in this thesis provided a way of creating Z-direction pathways to facilitate adhesive through-reinforcement of a model wood composite. More practical methods of perforating veneer, however, would be needed for composites that resemble those used commercially. The approaches that might be suitable include incising (Evans 2016), laser drilling/cutting (Bromberg 1991), high pressure water jet cutting (Leach and Walker 1966) and air knife drilling (Industrial Laser Solutions Magazine, USA). Further research would be needed to determine whether these alternative ways of perforating veneer would be as effective as the cylindrical drill holes used in this thesis. Another way of introducing Z-connections into wood composites would be to nail the composites in the Z-direction using thermo-plastic polymer nails. Polymer nail guns are already commercially

available and they are cheap to operate (Raptor® nailers, Utility Composites, Inc., USA). Computer numerically controlled nail guns (Lander 2008) could reinforce large composite panels in areas requiring increased fracture toughness and resistance to delamination. This approach would be worthy of further exploration.

My findings imply that adhesive Z-connections will work best with lower density wood species that can be well bonded with adhesive. Further research would be needed to test this hypothesis and also to develop ways of improving the ability of Z-connections to reduce the thickness swelling of hardwoods such as birch and poplar. FEA could be used to explore the effects of parameters such as wood permeability, density, and radial/tangential swelling ratio on the thickness swelling of wood composites. Further improvements to the FEA model used in Chapter 7 would also be desirable. For example, it would be worthwhile to model a thin layer of X-Y adhesive bond line in the FEA model, and explore the relationship between the X-Y adhesive bond lines and the Z-direction adhesive, and their effects on thickness swelling.

I examined the effects of adhesive Z-connections on the fracture toughness of a birch wood composite. Further research is needed to examine effects of such Z-reinforcement on additional mechanical properties of composites made from birch and also other wood species.

8.3 Conclusions

Adhesive Z-connections were explored as a means of creating a novel 3-dimensionally inter-connected adhesive network in wood composites. Wood composites were made from different wood species, veneer type, and with different levels of reinforcement. Significant improvements in dimensional stability and fracture toughness of some of the model wood composites were observed. I have established some key design parameters for the adhesive Z-connections, and have shown how they influence the thickness swelling and fracture toughness of a model wood composite. Much more work needs to be done but the approach of introducing adhesive Z-connections into wood composites has merit because it does not increase the level

of costly adhesive used in the composite. Significant improvements to such composites and also others derived from renewable materials, for example bamboo, could allow them to compete more effectively in some applications with synthetic composites, with resulting benefits in terms of sustainability and the environment (Koronis et al. 2013). The effects of adding glass-fibre, carbon fibre and other fibre additives to adhesive bond lines in combination with adhesive Z-connections on the properties of wood composites would be worth exploring in the future.

Bibliography

Abdalla, A.M.F. and Sekino, N. 2004. Veneer strand flanged I-beam with MDF or particleboard as web material II: effect of resin type, application rate, strand dimension, and pressing time on the basic properties. Journal of Wood Science, 50(5): 400-406.

Acda, M.N., Devera, E.E., Cabangon, R.J., Ramos, H.J. 2012. Effects of plasma modification on adhesion properties of wood. International Journal of Adhesion and Adhesives, 32(1): 70-75.

Altimet Altisurf operator's manual. 2007. Website: http://www.altimet.fr/?page_id=234&lang=en.

American Society for Testing and Materials (ASTM) standard D143. 2007. Standard test methods for small clear specimens of timber. ASTM International, USA.

American Society for Testing and Materials (ASTM) standard D5528-13. 2013. Standard test method for mode I interlaminar fracture toughness of unidirectional fiber-reinforced polymer matrix composites. ASTM International, USA.

American Society for Testing and Materials (ASTM) standard D7519-11. 2011. Standard test method for internal bond strength and thickness swell of cellulosic-based fiber and particle panels after repeated wetting. ASTM International, USA.

American Society for Testing and Materials (ASTM) standard D905-08. 2013. Standard Test Method for Strength Properties of Adhesive Bonds in Shear by Compression Loading. ASTM International, USA.

Anwar Hossain, K.M. 2008. Bond characteristics of plain and deformed bars in lightweight pumice concrete. Construction and Building Materials, 22(7): 1491-1499.

Archer, E., Buchanan, S., McIlhagger, A.T. and Quinn, J.P. 2010. The effect of 3D weaving and consolidation on carbon fiber tows, fabrics, and composites. Journal of Reinforced Plastics and Composites, 29(20): 3162-3170.

Ashcroft, I.A., Hughes, D.J. and Shaw, S.J. 2001. Mode I fracture of epoxy bonded composite joints: 1. Quasi-static loading. International Journal of Adhesion and Adhesives, 21(2): 87-99.

Avramidis, G., Scholz, G., Nothnick, E., Militz, H., Viöl, W. and Wolkenhauer, A. 2011. Improved bondability of wax-treated wood following plasma treatment. Wood Science and Technology, 45(2): 359-368.

Avramidis, S. and Smith, L.A. 1989. The effect of resin content and face-to-core ratio on some properties of oriented strand board. Holzforschung, 43(2): 131-133.

Aydin, I. 2004. Activation of wood surfaces for glue bonds by mechanical pre-treatment and its effects on some properties of veneer surfaces and plywood panels. Applied Surface Science, 233(1): 268-274.

Baileys, J.K., Marks, B.M., Ross, A.S., Crawford, D.M., Krzysik, A.M., Muehl, J.H. and Youngquist, J.A. 2003. Providing moisture and fungal protection to wood-based composites. Forest Products Journal, 53(1): 76-81.

Baldwin, R.F. 1981. Plywood Manufacturing Practices. Miller Freeman Publications Inc., San Francisco, C.A, USA.

Bartell, F.E. and Osterhof, H.J. 1927. Determination of the wettability of a solid by a liquid: Relation of adhesion tension to stability of colour varnish and lacquer systems. Industrial and Engineering Chemistry, 19(11): 1277-1280.

Bateman, T.A., Nelson, J.D. and Argrow, B.M. 2007. A low cost, rapid construction unmanned aircraft design. In: Proceedings of American Institute of Aeronautics and Astronautics Conference and Exhibition. pp 2007-2703.

Beele, P. 1983. The microdistribution of urea formaldehyde resin in particleboard, and its significance. Ph.D dissertation, University of Wales, Bangor, UK.

Belfas, J., Groves, K.W. and Evans, P.D. 1993. Bonding surface-modified karri and jarrah with resorcinol formaldehyde I. The effect of sanding on wettability and shear strength. Holz als Roh- und Werkstoff, 51(4): 253-259.

Benmokrane, B., Zhang, B., Laoubi, K., Tighiouart, B. and Lord, I. 2002. Mechanical and bond properties of new generation of carbon fibre reinforced polymer reinforcing bars for concrete structures. Canadian Journal of Civil Engineering, 29(2): 338-343.

Bianchi, F., Koh, T.M., Zhang, X., Partridge, I.K. and Mouritz, A.P. 2012. Finite element modelling of z-pinned composite T-joints. Composites Science and Technology, 73(1): 48-56.

Biblis, E.J. 1990. Performance of southern OSB overlaid with resin-impregnated paper. Forest Products Journal, 40(4): 55-62.

Bikerman, J.J. 1961. The Science of Adhesive Joints. The Academic Press, New York, N.Y, USA.

Bloyer, D.R., Venkateswara Rao, K.T. and Ritchie, R.O. 1996. Resistance-curve toughening in ductile/brittle layered structures: behavior in Nb/Nb_3Al laminates. Materials Science and Engineering A, 216(1-2): 80-90.

Boley, B.A. and Weiner, J.H. 1960. Theory of Thermal Stress. Wiley, New York, N.Y, USA.

Boyle, I. and Gafner, B. 2013. Mass timber: Knowing your options, Available at http://www.fastepp.com/images/attachments/Final_AIBC_AIA%20Conference%20for%20Uploaded%20ibbg_Oct24_2013%2010%2025.pdf [accessed 29 June, 2016]

Brady, D.E. and Kamke, F.A. 1988. Effects of hot-pressing parameters on resin penetration. Forest Products Journal, 38(11/12): 63-68.

British Standard (BS) 1204. 1993. Specification for Type MR Phenolic and Aminoplastic Synthetic Resin Adhesives for Wood. British Standards Institution (BSI), UK.

Brochmann, J., Edwardson, C. and Shmulsky, R. 2004. Influence of resin type and flake thickness on properties of OSB. Forest Products Journal, 54(3): 51-55.

Brodersen, C.R. 2013. Visualizing wood anatomy in three dimensions with high-resolution X-ray micro-tomography (μCT): a review. International Association of Wood Anatomists (IAWA) Journal, 34(4): 408-424.

Bromberg, J.L. 1991. The Laser in America, 1950-1970. The Massachusetts Institute of Technology Press, Cambridge, M.A, USA.

Browne, F.L. and Brouse, D. 1929. Nature of adhesion between glue and wood: A criticism of the hypothesis that the strength of glued wood joints is due chiefly to mechanical adhesion. Industrial and Engineering Chemistry, 21(1): 80-84.

Browne, M.A., Akinyemi, O. and Boyde, A. 1992. Confocal surface profiling utilizing chromatic aberration. Scanning, 14(3): 145-153.

Bucur, V. 2011. Delamination in Wood, Wood Products and Wood-based Composites. Springer Science + Business Media B.V, Dordrecht Heidelberg London New York.

Burgoyne, C.J. 2001. Rational use of advanced composites in concrete. In: Proceedings of the 3rd international symposium on non-metallic (FRP) reinforcement for concrete structures, the Institution of Civil Engineers: Structures and Buildings, 146(3): 253-262.

Burrows, C.H. 1961. Some factors affecting resin efficiency in flake board. Forest Products Journal, XI(1): 27-33.

Byrd, L.W. and Birman, V. 2006. Effect of temperature on stresses and delamination failure of z-pinned joints. International Journal of Mechanical Sciences, 48(9): 938-949.

Chapman, K.M. 2006. Wood-based panels: particleboard, fibreboards and oriented strand board. In: (Walker, J.C.F. et al. ed.): Primary Wood Processing: Principles and Practice (2nd edition). Springer Science + Business Media B.V, London, UK.

Chen, C.M. and Wangaard, F.F. 1968. Wettability and hysteresis effect in sorption of water vapor by wood. Wood Science and Technology, 2(3): 177-187.

Chou, S., Chen, H. and Wu, C. 1992. BMI resin composites reinforced with 3D carbon-fibre fabrics. Composites Science and Technology, 43(2): 117-128.

Chow, S. 1975. Minimizing wood surface inactivation at high temperatures by boron compounds. Forest Products Journal, 25(5): 41-48.

Cloutier, A., Gendron, G., Blanchet, P., Ganev, S. and Beauregard, R. 2001. Finite element modeling of dimensional stability in layered wood composites. In: Proceedings of the 35th International Particleboard/Composite Materials Symposium. Washington State University, Pullman, W.A, USA. pp 63-72.

Collett, B.M. 1972. A review of surface and interfacial adhesion in wood science and related fields. Wood Science and Technology, 6(1): 1-42.

Compston, P., Jar, P.-Y.B., Burchill, P.J. and Takahashi, K. 2001. The effect of matrix toughness and loading rate on the mode-II interlaminar fracture toughness of glass-fibre/vinyl-ester composites. Composites Science and Technology, 61(2): 321-333.

Comyn, J. 2006. Theories of adhesion. In: (Cognard, P. ed.): Handbook of Adhesives and Sealants, Volume 2 - General Knowledge, Application of Adhesives, New Curing Techniques. Elsevier Publisher.

Constant, T., Badia, M.A. and Mothe, F. 2003. Dimensional stability of Douglas fir and mixed beech-poplar plywood: experimental measurements and simulations. Wood Science and Technology, 37(1): 11-28.

Cool, J. and Hernández, R.E. 2011. Evaluation of four surfacing methods on black spruce wood in relation to poly (vinyl acetate) gluing performance. Wood and Fiber Science, 43(2): 194-205.

Cosenza, E., Manfredi, G. and Realfonzo, R. 1997. Behavior and modeling of bond of FRP rebars to concrete. Journal of Composites for Construction, 1(2): 40-51.

Côté, W.A. and Vasishth, R.C. 1970. Light and electron microscopic studies of wood/wood coating systems. In: Proceedings of the 10th Fatipec Congress. pp 57-65.

Crank, J. 1956. The Mathematics of Diffusion. The Oxford University Press, London, UK.

Cyr, P.L., Riedl, B. and Wang, X.M. 2008. Investigation of urea-melamine-formaldehyde (UMF) resin penetration in medium-density fiberboard (MDF) by high resolution confocal laser scanning microscopy. Holz als Roh- und Werkstoff, 66(2): 129-134.

Dai, C., He, G. and Jin, J. 2011. Press-induced lateral resin flow and its effects on resin area coverage on composite wood strands. Wood Science and Technology, 45(2): 269-280.

Dai, C. and Steiner, P.R. 1993. Compression behavior of randomly formed wood flake mats. Wood and Fiber Science, 25(4): 349-358.

Dai, C., Yu, C. and Zhou, C. 2007. Theoretical modeling of bonding characteristics and performance of wood composites: Part I. Inter-element contact. Wood and Fiber Science, 39(1): 48-55.

Dai, C., Yu, C., Groves, K. and Lohrasebi, H. 2007. Theoretical modeling of bonding characteristics and performance of wood composites: Part II. Resin distribution. Wood and Fiber Science, 39(1): 56-70.

Davalos, J.F., Qiao, P. and Trimble, B.S. 2000. Fiber-reinforced composite and wood bonded interfaces: Part 2. Fracture. Journal of Composites Technology and Research, 22(4): 232-240.

Davis, J. and Wells, P. 1992. Computed tomography measurements on wood. Industrial Metrology, 2(3-4): 195-218.

Delmonte, J. 1947. The Technology of Adhesives. Reinhold Publication Co., New York, N.Y, USA.

Deppe, H.J. 1977. Technical progress in using isocyanate as an adhesive in particleboard manufacture. In: Proceedings of the 11th International Particleboard/Composite Materials Symposium. Washington State University, Pullman, W.A, USA. pp 13-31.

Deteix, J., Blanchet, P., Fortin, A. and Cloutier, A. 2008. Finite element modeling of laminate wood composites hygromechanical behavior considering diffusion effects in the adhesive layers. Wood and Fiber Science, 40(1): 132-143.

Deutsches Institut für Normung (DIN) EN 205: 2016-12. 2016. Adhesives - Wood Adhesives for Non-structural Applications - Determination of Tensile Shear Strength of Lap Joints. Deutsches Institut für Normung (German Institute for Standardization), Germany.

DeVallance, D.B., Funck, J.W. and Reeb, J.E. 2007. Douglas-fir plywood gluebond quality as influenced by veneer roughness, lathe checks, and annual ring characteristics. Forest Products Journal, 57(1/2): 21-28.

Dierick, M., Van Loo, D., Masschaele, B., Van den Bulcke, J., Van Acker, J., Cnudde, V., and Van Hoorebeke, L. 2014. Recent micro-CT scanner developments at UGCT. In: Proceedings of 1st International Conference on Tomography of Materials and Structures, Nuclear Instruments and Methods in Physics Research Section B: Beam Interactions with Materials and Atoms, 324(1): 35-40.

Ding, Y.Q., Yan, Y., McIlhagger, R. and Brown, D. 1995. Comparison of the fatigue behaviour of 2-D and 3-D woven fabric reinforced composites. Journal of Materials Processing Technology, 55(3-4): 171-177.

Dollhausen, M. 1983. Polyurethane. In: (Vieweg, R. and Becker, E. ed.): Kunststoff-Handbuch (Plastics Handbook). Hanser, Munich Vienna.

Dorey, A.B. and Cheng, J.J.R. 1996. Glass Fiber Reinforced Glued Laminated Wood Beams. A joint publication of the Canadian Forest Service and Land and Forest Services, Minister of Supply and Services Canada.

Drolet, F. and Dai, C. 2010. Three-dimensional modeling of the structure formation and consolidation of wood composites. Holzforschung, 64(5): 619-626.

Dunky, M. 2002. Formaldehyde resins. In: (Dunky, M., Pizzi, T. and Van Leemput, M. ed.): COST Action E13 Wood Adhesion and Glued Products, Working Group 1: Wood Adhesives State-of-the-Art Report, Volume 1 (1st edition). Office for Official Publications of the European Communities, Luxembourg.

Dunky, M., Grunwald, D. and Haelvoet, W. 2002. Emission. In: (Johansson, C.J., Pizzi, T. and Van Leemput, M. ed.): COST Action E13 Wood Adhesion and Glued Products, Working Group 2: Glued Wood Products State-of-the-Art Report, Volume 2 (2nd edition). Office for Official Publications of the European Communities, Luxembourg.

Durand-Raute Industries Ltd. 1988. Laminated veneer lumber from aspen veneer. Company report.

Dyer, S.R., Lassila, L.V.J., Jokinen, M. and Vallittu, P.K. 2005. Effect of cross-sectional design on the modulus of elasticity and toughness of fiber-reinforced composite materials. The Journal of Prosthetic Dentistry, 94(3): 219-226.

Ellis, S. 1993. Effect of resin particle size on waferboard adhesive efficiency. Wood and Fiber Science, 25(3): 214-219.

Ellis, S.C. and Steiner, P.R. 1991. Characterization of chemical properties and flow parameters of powdered phenol-formaldehyde resins. Wood and Fiber Science, 23(1): 85-97.

Euro Plywood web source: http://europlywood.com/catalogue/aircraft-plywood/.

Evans, P.D. and Cullis, I. 2008. Effect of sanding and coating with UV-cured finishes on the surface roughness, dimensional stability and fire resistance of oriented strandboard. Holz als Roh- und Werkstoff, 66(3): 191-199.

Evans, P.D., Lube, V., Averdunk, H., Limaye, A., Turner, M., Kingston, A. and Senden, T.J. 2015. Visualizing the micro-distribution of zinc borate in oriented strand board using X-ray micro-computed tomography and SEM-EDX. Journal of Composites, DOI: http://dx.doi.org/10.1155/2015/630905.

Evans, P.D., Miesner, M. and Rogerson, D. 2013. Machined tapers reduce the differential edge swelling of oriented strand board exposed to water. Composites Part B: Engineering, 50(1): 15-21.

Evans, P.D., Morrison, O., Senden, T.J., Vollmer, S., Roberts, R.J., Limaye, A., Arns, C.H., Averdunk, H., Lowe, A. and Knackstedt, M.A. 2010. Visualization & numerical analysis of adhesive distribution in particleboard using X-ray micro-computed tomography. International Journal of Adhesion and Adhesives, 30(8): 754-762.

Evans, P.D., Morrison, O., Averdunk, H., Turner, M., Limaye, A., Arns, C.H., Lube, V., Vollmer, S., Roberts, R., Kingston, A., Knackstedt, M. and Senden, T.J. 2015. Probing the structure of particulate wood composites using X-ray micro-computed tomography. In: Proceedings of the International Panel Products Symposium, Wales, UK. p 3-16.

Evans, P.D. 2016. The effects of incising on the checking of wood: A review. International Wood Products Journal, 7(1): 12-25.

Farley, G.L. and Dickinson, L.C. 1992. Mechanical response of composite materials with through-the-thickness reinforcement. In: Proceedings of the 5th Conference on Advanced Engineering Fibers and Textile Structures for Composites, NASA Langley Research Center, FIBER-TEX 1991. pp 123-143.

Farley, G.L., Smith, B.T. and Maiden, J. 1992. Compression response of thick layer composite laminates with through-the-thickness reinforcement. Journal of Reinforced Plastics and Composites, 11(7): 787-810.

Franklin, V.A. and Christopher, T. 2015 Interlaminar fracture toughness estimation of aerospace composites by weighted residual approach. Strength of Materials, 47(6): 789-796.

Fratzl, P. and Weinkamer, R. 2007. Nature's hierarchical materials. Progress in Materials Science, 52(8): 1263-1334.

Freitas, G., Fusco, T., Campbell, T., Harris, J. and Rosenberg, S. 1996. Z-Fiber technology and products for enhancing composite design. In: Proceedings of the 83rd Meeting of the Advisory Group for Aerospace Research & Development (AGARD) Structures and Materials Panel, AGARG-CP-590. pp: 17-1 ~ 8.

Freitas, G., Magee, C., Dardzinski, P. and Fusco, T. 1994. Fiber insertion process for improved damage tolerance in aircraft laminates. Journal of Advanced Materials, 25(4): 36-43.

Freyburger C., Longuetaud, F., Mothe, F., Constant, T. and Leban, J.M. 2009. Measuring wood density by means of X-ray computer tomography. Annals of Forest Science, 66(8): 804-804.

Frihart, C.R. 2006. Wood structure and adhesive bond strength. In: (Stokke, D.D. and Groom, L.H. ed.): Characterization of the Cellulosic Cell Wall. Blackwell Publishing Ltd., I.A, USA.

Frihart, C.R. and Hunt, C.G. 2010. Adhesives with wood materials bond formation and performance. In: (Ross, R.J. ed.): Wood Handbook - Wood as an Engineering Material. USDA General Technical Report FPL-GTR-190, Madison, WI: Forest Service, Forest Products Laboratory, USA.

Fu, S.Y., Mai, Y.W., Lauke, B. and Yue, C.Y. 2002. Synergistic effect on the fracture toughness of hybrid short glass fiber and short carbon fiber reinforced polypropylene composites. Materials Science & Engineering A, 323(1): 326-335.

Galbraith, C.J. 1986. Recent developments in the full-time manufacture of all-isocyanate bonded structural composite boards. In: Proceedings of 20th International Particleboard/Composite Materials Symposium. Washington State University, Pullman, W.A, USA. pp 55-81.

Ganev, S., Cloutier, A., Gendron, G. and Beauregard, R. 2005. Finite element modeling of the hygroscopic warping of medium density fiberboard. Wood and Fiber Science, 37(2): 337-354.

Garay, R.M.M, Poblete, H.W. and Karsulovic, J.T.C. 2009. Evaluation of oriented strandboard and plywood subjected to severe relative humidity and temperature conditions. Forest Products Journal, 59(3): 84-90.

Gardner, D.J. 2006. Adhesion mechanisms of durable wood adhesive bonds. In: (Stokke, D.D. and Groom, L.H. ed.): Characterization of the Cellulosic Cell Wall. Blackwell Publishing Ltd., I.A, USA.

Gardner, D.J. and Elder, T.J. 1988. Surface activation treatment of wood and its effect on the gel time of phenol-formaldehyde resin. Wood and Fiber Science, 20(3): 378-385.

Gardner, D.J., Generalla, N.C., Gunnells, D.W. and Wolcott, M.P. 1991. Dynamic wettability of wood. Langmuir, 7(11): 2498-2502.

Gavrilović-Grmuša, I., Dunky, M., Djiporović-Momčilović, M., Popović, M. and Popović, J. 2016. Influence of pressure on the radial and tangential penetration of adhesive resin into poplar wood and on the shear strength of adhesive joints. Bioresources, 11(1): 2238-2255.

Generalla, N.C., Biblis, E.J. and Carino, H.F. 1989. Effect of two resin levels on the properties of commercial southern OSB. Forest Products Journal, 39(6): 64-68.

Ginzel, W. and Stegmann, G. 1970. Nachträgliche anfärbung von harnstoff-formaldehydharz-bindemitteln auf beleimten holzspänen zur visuellen beurteilung der leimverteilung (Subsequent colouring of urea-formaldehyde resins on glued wood particles for visual estimation of glue distribution). Holz als Roh- und Werkstoff, 28(8): 289-292.

Glass, S.V. and Zelinka, S.L. 2010. Moisture relations and physical properties of wood. In: (Ross, R.J. ed.) Wood Handbook - Wood as an Engineering Material (centennial edition). USDA General Technical Report FPL-GTR-190, Madison, WI: Forest Service, Forest Products Laboratory, USA.

Grassi, M., Zhang, X. and Meo, M. 2002. Prediction of stiffness and stresses in z-fibre reinforced composite laminates. Composites Part A, 33(12): 1653-1664.

Gray, V.R. 1962. The wettability of wood. Forest Products Journal, 12(9): 452-461.

Grigsby, W.J. and Thumm, A. 2002. Interaction of wax and UF resin in MDF: quantification of wax and resin distribution by confocal microscopy. In: Proceedings of the 6th Pacific Rim Bio-Based Composites Symposium & Workshop on the Chemical Modification of Cellulosics, Portland, O.R, USA. pp 94-103.

Grigsby, W.J. and Thumm, A. 2012. The interactions between wax and UF resin in medium density fibreboard. European Journal of Wood and Wood Products, 70(4): 507-517.

Grigsby, W.J., McDonald, A.G., Thumm, A. and Loxton, A. 2004. X-ray photoelectron spectroscopy determination of urea formaldehyde resin coverage on MDF fibre. Holz als Roh- und Werkstoff, 62(5): 358-364.

Groom, L., Mott, L., Shaler, S.M. 1999. Relationship between fiber furnish properties and the structural performance of MDF. In: Proceedings of the 33rd international particleboard/composite materials symposium, Washington State University, Pullman, W.A, USA. pp 89-100.

Grunwald, D. 2002. Analysis of resins and adhesives. In: (Dunky, M., Pizzi, T. and Van Leemput, M. ed.): COST Action E13 Wood Adhesion and Glued Products, Working Group 1: Wood Adhesives State-of-the-Art Report, Volume 1 (1st edition). Office for Official Publications of the European Communities, Luxembourg.

Grunwald, D. 2002. Polyurethane adhesives. In: (Dunky, M., Pizzi, T. and Van Leemput, M. ed.): COST Action E13 Wood Adhesion and Glued Products, Working Group 1: Wood Adhesives State-of-the-Art Report, Volume 1 (1st edition). Office for Official Publications of the European Communities, Luxembourg.

Gustafsson, P.J. 2002. Tests and test results on mechanical properties of adhesive bond lines. In: (Johansson, C.J., Pizzi, T. and Van Leemput, M. ed.): COST Action E13 Wood Adhesion and Glued Products, Working Group 2: Glued Wood Products State-of-the-Art Report, Volume 2 (2nd edition). Office for Official Publications of the European Communities, Luxembourg.

Halligan, A.F. 1970. A review of thickness swelling in particleboard. Wood Science and Technology, 4(4): 301-312.

Harajli, M., Hamad, B. and Karam, K. 2002. Bond-slip response of reinforcing bars embedded in plain and fiber concrete. Journal of Materials in Civil Engineering, 14(6): 503-511.

Hare, D.A. and Kutscha, N.P. 1974. Microscopy of eastern spruce plywood gluelines. Wood Science, 6(3): 294-304.

Hassoun, M.N. and Al-Manaseer, A. 2012. Structural Concrete: Theory and Design (5th edition). John Wiley & Sons, Inc., Hoboken, N.J, USA.

He, G., Yu, C. and Dai, C. 2007. Theoretical modeling of bonding characteristics and performance of wood composites. Part III. Bonding strength between two wood elements. Wood and Fiber Science, 39(4): 566-577.

He, W. and Evans, P.D. 2016. Reducing the thickness swelling of a model wood composite by creating a three-dimensional adhesive network. International Wood Products Journal, 7(4): 202-207.

Hernández, R.E. 1993. Influence of moisture sorption history on the swelling of sugar maple wood and some tropical hardwoods. Wood Science and Technology, 27(5): 337-345.

Hernández, R.E. 2007. Swelling properties of hardwoods as affected by their extraneous substances, wood density, and interlocked grain. Wood and Fiber Science, 39(1): 146-158.

Hesterman, N.D. and Gorman, T.M. 1992. Mechanical properties of laminated veneer lumber made from interior Douglas-fir and lodgepole pine. Forest Products Journal, 42(11-12): 69-73.

Hoover, W.L., Eckelman, C.A., Ringe, J.M. and Youngquist, J.A. 1987. Markets for hardwood laminated-veneer-lumber. Forest Products Journal, 37(10): 57-62.

Hoover, W.L., Ringe, J.M., Eckelman, C.A. and Youngquist, J.A. 1987. Material design factors for hardwood laminated-veneer-lumber. Forest Products Journal, 37(9): 15-23.

Hsu, H.C. and Hsu, Y.T. 2009. Characterization of hygroscopic swelling and thermo-hygro-mechanical design on electronic package. Journal of Mechanics, 25(2): 225-232.

Hsu, H.C., Hsu, Y.T., Hsich, W.L., Weng, M.C., ZhangJian, S.T., Hsu, F.J., Chen, Y.F. and Fu, S.L. 2008. Hygroscopic swelling effect on polymeric materials and thermo-hygro-mechanical design on finger printer package. In: Proceedings of the 3rd International Microsystems, Packaging, Assembly & Circuits Technology Conference, Institute of Electrical and Electronics Engineers (IEEE), New York, N.Y, USA. pp 291-294.

Hsu, W.E. 1988. Laminated veneer lumber from aspen. In: Proceedings of 22nd International Particleboard/Composite Symposium, Washington State University, Pullman, W.A, USA. pp 257-269.

Hsu, W.E., Schwald, W., Schwald, J. and Shields, J. A. 1988. Chemical and physical changes required for producing dimensionally stable wood-based composites, Part 1: steam pretreatment. Wood Science and Technology, 22(3): 281-289.

Hsu, W.E., Schwald, W. and Shields, J.A. 1989. Chemical and physical changes required for producing dimensionally stable wood-based composites, Part 2: heat post-treatment. Wood Science and Technology, 23(3): 281-288.

Hua, Y., Crocombe, A.D., Wahab, M.A. and Ashcroft, I.A. 2006. Modelling environmental degradation in EA9321-bonded joints using a progressive damage failure model. The Journal of Adhesion, 82(2): 135-160.

Hua, Y., Crocombe, A.D., Wahab, M.A. and Ashcroft, I.A. 2007. Continuum damage modelling of environmental degradation in joints bonded with E32 epoxy adhesive. Journal of Adhesion Science and Technology, 21(2): 179-195.

Hua, Y., Crocombe, A.D., Wahab, M.A. and Ashcroft, I.A. 2008. Continuum damage modelling of environmental degradation in joints bonded with EA9321 epoxy adhesive. International Journal of Adhesion and Adhesives, 28(6): 302-313.

Huang, C.L. 2011. Industry prospective of delamination in wood and wood products. In: (Bucur, V. ed.): Delamination in Wood, Wood Products and Wood-Based Composites. Springer Science + Business Media B.V, Dordrecht Heidelberg London New York.

Huang, H. and Waas, A.M. 2009. Compressive response of Z-pinned woven glass fiber textile composite laminates: Experiments. Composites Science and Technology, 69(14): 2331-2337.

Humphrey, P.E. 1982. Physical aspects of wood particleboard manufacture. Ph.D dissertation. University of Wales, Bangor, UK.

Ilin, D.N. and Bernacki, M. 2016. Advancing layer algorithm of dense ellipse packing for generating statistically equivalent polygonal structures. Granular Matter, DOI: 10.1007/s10035-016-0646-9.

Irle, M. and Barbu, M.C. 2010. Wood-based panel technology. In: (Thoemen, H., Irle, M. and Sernek, M. ed.): Wood-Based Panels - An Introduction for Specialists. Brunel University Press, London, UK.

Jacquier, N. and Girhammar, U.A. 2014. Tests on glulam-CLT shear connections with double-sided punched metal plate fasteners and inclined screws. Construction and Building Materials, 72(1): 444-457.

Jakal, L. 1984. Effect of the penetration of adhesive on the strength of adhesion. Faipar, 34(2): 59-60.

Jakes, J.E., Hunt, C.G., Yelle, D.J., Lorenz, L., Hirth, K., Gleber, S.C., Vogt, S., Grigsby, W. and Frihart, C.R. 2015. Synchrotron-based X-ray fluorescence microscopy in conjunction with nanoindentation to study molecular-scale interactions of phenol-formaldehyde in wood cell walls. Applied Material Interfaces, 7(12): 6584-6589.

Jamali, A. and Evans, P.D. 2010. Etching of wood surfaces by glow discharge plasma. Wood Science and Technology, 45(1): 169-182.

Jeronimidis, G. 2000. Structure-property relationships in biological materials. In: (Elices, M. ed.): Structural Biological Materials, Design and Structure-Property Relationships. Pergamon Materials Series, New York, N.Y, USA.

Johansson, J. 1988. Determination of UF-glue distribution by staining and image analysis. In: FESYP Technical Conference, Munich, Germany.

Johns, W.E. 1989. The chemical bonding of wood. In: (Pizzi, A. ed.): Wood Adhesives: Chemistry and Technology, Volume 2. Marcel Dekker Inc., New York, N.Y, USA.

Johnson, J.W. 1964. Effect of exposure cycles on stability of commercial particleboard. Forest Products Journal, 14(7): 277-282.

Johnson, R.E. 1984. Sealing edges and faces of structural particleboard. In: Proceedings of 18th International Particleboard/Composite Materials Symposium. Washington State University, Pullman, W.A, USA. pp 271-283.

Johnson, S.E. and Kamke, F.A. 1992. Quantitative analysis of gross adhesive penetration in wood using fluorescence microscopy. Journal of Adhesion, 40(1): 47-61.

Jordan, D.L. and Wellons, J.D. 1977. Wettability of dipterocarp veneers. Journal of Wood Science, 10(1): 22-27.

Kajita, H. and Imamura, Y. 1991. Improvement of physical and biological properties of particleboards by impregnation with phenolic resin. Wood Science and Technology, 26(1): 63-70.

Kallrath, J. and Rebennack, S. 2014. Cutting ellipses from area-minimizing rectangles. Journal of Global Optimization, 59(2): 405-437.

Kamke, F.A. 2004. Adhesive penetration. In: Wood Adhesion Problem Solving - The Isocyanate Dimension. Wood-Based Composites Center, Virginia Polytechnic Institute and State University, Blacksburg, V.A, USA.

Kamke, F.A. and Lee, J.N. 2007. Adhesive penetration in wood - A review. Wood and Fiber Science, 39(2): 205-220.

Kamke, F.A., Lenth, C.A. and Saunders, H.G. 1996. Measurement of resin and wax distribution on wood flakes. Forest Products Journal, 46(6): 63-68.

Kasper, B.J. and Chow, S. 1980. Determination of resin distribution in flakeboard using X-ray spectrometry. Forest Products Journal, 30(7): 37-40.

Keating, W.G. 1973. Nail laminating. Commonwealth Scientific and Industrial Research Organisation (CSIRO) Forest Products Newsletter, 393(1): 3-4.

Kedziersk, A. 1986. Effect of adhesive penetration into wood on the strength of glued joints. Przemys Drzewny, 37(3): 18-20.

Feldkamp, L.A., Davis, L.C. and Kress, J.W. 1984. Practical cone-beam algorithm. Journal of the Optical Society of America A: Optics, Image Science, and Vision, 1(6): 612-619.

Keith, C.T. 1961. Characteristics of annual rings in relation to wood quality for white spruce. Forest Products Journal, 11(3): 122-126.

Kelly, M.W. 1977. Critical literature review of relationships between processing parameters and physical properties of particleboard. USDA General Technical Report FPL-10, Madison, WI: Forest Service, Forest Products Laboratory, USA.

Kim, J.W. and Humphrey, P.E. 2001. The effect of testing temperature on the strength of partially cured phenol-formaldehyde adhesive bonds. In: Proceedings of Wood Adhesives 2000, Forest Products Society, South Lake Tahoe, N.V, USA. pp 386-388.

Koch, P. 1967. Super-strength beams laminated from rotary-cut southern pine veneer. Forest Products Journal, 17(6): 42-48.

Koch, G.S., Klareich, F. and Exstrum, B. 1987. Adhesives for the Composite Wood Panel Industry. Noyes Data Corporation, Park Ridge, N.J, USA.

Koga, S. and Zhang, S.Y. 2001. Relationships between wood density and annual growth rate components in Balsam fir (*abies balsamea*). Wood and Fiber Science, 34(1): 146-157.

Kollmann, F.F.P., Kuenzi, E.W. and Stamm, A.J. 1975. Principles of Wood Science and Technology II: Wood Based Materials. Springer - Verlag, Berlin Heidelberg New York.

Koran, Z. and Vasishth, R.C. 1972. Scanning electron microscopy of plywood glue-lines. Wood and Fiber, 3(4): 202-209.

Koronis, G., Silva, A. and Fontul, M. 2013. Green composites: a review of adequate materials for automotive applications. Composites Part B: Engineering, 44(1): 120-127.

Kretschmann, D.E. 2010. Mechanical properties of wood. In: (Ross, R.J. ed.): Wood Handbook - Wood as an Engineering Material (centennial edition). USDA General Technical Report FPL-GTR-190, Madison, WI: Forest Service, Forest Products Laboratory, USA.

Krzysik, A. and Young, R.A. 1986. A lignin adhesive system for flakeboard production. Forest Products Journal, 36(11/12): 39-44.

Kumar, S., Kumar, A., Shukla, A., Devi, G.R. and Gupta, A.K. 2009. Investigation of thermal expansion of 3D-stitched C-SiC composites. Journal of the European Ceramic Society, 29(13): 2849-2855.

Kurt, R., Krause, A., Militz, H. and Mai, C. 2008. Hydroxymethylated resorcinol (HMR) priming agent for improved bondability of wax-treated wood. Holz als Roh- und Werkstoff, 66(5): 333-338.

Lam, T.F. 2000. FEA simulation on moisture absorption in PBGA packages under various moisture pre-conditioning. In: Proceedings of the 50th Electronic Components and Technology Conference, Institute of Electrical and Electronics Engineers (IEEE), New York, N.Y, USA. pp 1078-1082.

Lander, J.K. 2008. Designing with z-pins: locally reinforced composite structures. Ph.D dissertation. Cranfield University, Cranfield, UK.

Launey, M.E. and Ritchie, R.O. 2009. On the fracture toughness of advanced materials. Advanced Materials, 21(20): 2103-2110.

Lawniczak, M. and Nowak, K. 1962. Der Einfluß hydrophobierender Imprägniermittel auf feuchtigkeitsbedingte (Effect of water repellents on the deformations in particleboards and flaxboards caused by moisture changes). Holz als Roh- und Werkstoff, 20(2): 68-72.

Lay, D.G. and Cranley, P. 1994. In: (Pizzi, A. and Mittal, K.L. ed.): Handbook of Adhesive Technology. Marcel Dekker Inc., New York, N.Y, USA. pp 405-430.

Leach, S.J. and Walker, G.L. 1966. The application of high speed liquid jets to cutting. Philosophical Transactions of the Royal Society of London Series A, Mathematical and Physical Sciences, 260(1110): 295-310.

Lehmann, W.F. 1965. Improved particleboard through better resin efficiency. Forest Products Journal, XV(4): 155-161.

Lehmann, W.F. 1968. Resin distribution in flakeboard shown by ultraviolet light photography. Forest Products Journal, 18(10): 32-34.

Lehmann, W.F. 1970. Resin efficiency in particleboard as influenced by density, atomization, and resin content. Forest Products Journal, 20(11): 48-54.

Lesse, P.F. 1972. Osmotic stress in wood – Part I: the analogy between thermal and swelling stress. Wood Science and Technology, 6(3): 204-214.

Li, W., Van den Bulcke, J., Mannes, D., Lehmann, E., De Windt, I., Dierick, M. and Van Acker, J. 2014. Impact of internal structure on water-resistance of plywood studied using neutron radiography and X-ray tomography. Construction and Building Materials, 73(1): 171-179.

Linville, J.D. and Wolcott, M.P. 2001. Controlling thickness swell in oriented strand composites. In: Proceedings of 35th International Particleboard/Composite Materials Symposium. Washington State University. Pullman, W.A, USA. pp 91-101.

Industrial Laser Solutions. 2017. Clean air cutting. Available at: http://www.industrial-lasers.com/articles/print/volume-18/issue-9/features/clean-air-cutting.html [accessed 20 Jan, 2017].

Lukkaroinen, J. and Dunky, M. 2005. European market for adhesives for panel board products: current state and challenges for the future. In: Proceedings of Wood Adhesives 2005, Forest Products Society, San Diego, C.A, USA.

Lux, J., Deliseée, C., Thibault, X. 2006. 3D characterization of wood based fibrous materials: an application. Image Analysis Stereology, 25(1): 25-35.

Madenci, E. and Guven, I. 2006. The Finite Element Method and Applications in Engineering using ANSYS®. Springer Science + Business Media, LLC, New York, N.Y, USA.

Mantanis, G.I. and Papadopoulos, A.N. 2010. Reducing the thickness swelling of wood based panels by applying a nanotechnology compound. European Journal of Wood and Wood Products, 68(2): 237-239.

Marcinko, J., Devathala, S., Rinaldi, P.L. and Bao, S. 1998. Investigating the molecular and bulk dynamics of PMDI/wood and UF/wood composites. Forest Products Journal, 48(6): 81-84.

Marcinko, J., Phanopolus, C. and Teachy, P. 2001. Why does chewing gum stick to hair and what does this have to do with lignocellulosic structural composite adhesion? In: Proceedings of Wood Adhesives 2000, Forest Products Society, South Lake Tahoe, N.V, USA. pp 111-121.

Markwardt, L.J. and Wilson, T.R.C. 1935. Strength and related properties of woods grown in the United States. USDA Technical Bulletin No. 479, Madison, WI: Forest Service, Forest Products Laboratory, USA.

Marra, A.A. 1992. Technology of Wood Bonding: Principles in Practice. Van Nostrand Reinhold, New York, N.Y, USA.

Mattheck, C. and Kubler, H. 1997. Wood - The Internal Optimization of Trees. Springer-Verlag, Berlin.

McBain, J.W. and Hopkins, D.G. 1926. Films of adhesives. Journal of Physical Chemistry, 30(1): 114-125.

Del Menezzi, C.H.S. and Tomaselli, I. 2006. Contact thermal post-treatment of oriented strandboard to improve dimensional stability: a preliminary study. Holz als Roh- und Werkstoff, 64(3): 212-217.

Meo, M., Achard, F. and Grassi, M. 2005. Finite element modelling of bridging micro-mechanics in through-thickness reinforced composite laminates. Composite Structures, 71(3-4): 383-387.

Mouritz, A.P. 2007. Review of z-pinned composite laminates. Composites Part A, 38(12): 2383-2397.

Mouritz, A.P., Bannister, M.K., Falzon, P.J. and Leong, K.H. 1999. Review of applications for advanced three-dimensional fibre textile composites. Composites Part A, 30(12): 1445-1461.

Murmanis, L., Myers, G.C. and Youngquist, J.A. 1986. Fluorescence microscopy of hardboards. Wood and Fiber Science, 18(2): 212-219.

Murmanis, L., River, B.H. and Stewart, H. 1983. Microscopy of abrasive-planed and knife-planed surfaces in wood-adhesive bonds. Wood and Fiber Science, 15(2):102-115.

Murmanis, L., Youngquist, J.A. and Myers, G.C. 1986. Electron microscopy study of hardboards. Wood and Fiber Science, 18(3): 369-375.

Nanni, A. and Dolan, C.W. 1993. Nonmetallic reinforcement and prestressing. American Concrete Institute Special Publication SP-138, Proceedings of International Symposium on Fiber Reinforced Plastic Reinforcement for Concrete Structures, Vancouver, Canada.

Nanni, A., Bakis, C.E. and Boothby, T.E. 1995. Test methods for FRP-concrete systems subjected to mechanical loads: state of the art review. Journal of Reinforced Plastics and Composites, 14(6): 524-558.

Nearn, W.T. 1974. Application of the ultrasound concept in industrial wood products research. Wood Science, 6(3): 285-293.

Neusser, H., Krames, U. and Haidinger, K. 1965. Das verhalten von spanplatten gegeniiber feuchtigkeit unter besonderer beriicksichtigung der quellung. Holzforschung und Holzverwertung, 17(3): 43-69.

O'Brien, T.K. 1982. Characterization of delamination onset and growth in a composite laminate. In: Proceedings of American Society for Testing and Materials (ASTM) Symposium on Damage in Composite Material: Basic Mechanic, Accumulation, Tolerance, and Characterization, Bal Harbour, F.L, USA.

O'Halloran, M. 1995. Hardwood LVL in North America. The American Engineered Wood Association report.

Ormarsson, S. and Dahlblom, O. 2013. Finite element modelling of moisture related and visco-elastic deformations in inhomogeneous timber beams. Engineering Structures, 49(1): 182-189.

Ormarsson, S., Dahlblom, O. and Petersson, H. 1998. A numerical study of the shape stability of sawn timber subjected to moisture variation Part 1: Theory. Wood Science and Technology, 32(5): 325-334.

Ormarsson, S., Dahlblom, O. and Petersson, H. 1999. A numerical study of the shape stability of sawn timber subjected to moisture variation Part 2: Simulation of drying board. Wood Science and Technology, 33(5): 407-423.

Otterstätter, G. 1995. Färbung von Lebensmitteln, Arzneimittel, Kosmetika. Behr's Verlag, Hamburg, Germany.

Ozarska, B. 1999. A review of the utilisation of hardwoods for LVL. Wood Science and Technology, 33(4): 341-351.

Pakdel, H., Cyr, P.L., Riedl, B. and Deng, J. 2008. Quantification of urea formaldehyde resin in wood fibers using X-ray photoelectron spectroscopy and confocal laser scanning microscopy. Wood Science and Technology, 42(2): 133-148.

Park, R. and Gamble, W.L. 1980. Reinforced Concrete Slabs. John Wiley & Sons, Inc., New York, N.Y, USA.

Partridge, I.K. and Cartié, D.D.R. 2005. Delamination resistant laminates by Z-Fiber® pinning: Part I manufacture and fracture performance. Composites Part A, 36(1): 55-64.

Partridge, I.K., Cartié, D.D.R, Troulis, M., Grassi, M. and Zhang, X. 2003. Evaluating the mechanical effectiveness of Z-pinning. In: Proceedings of SAMPE Technical Conference Materials and Processing - Enabling Flight, Our Legacy and Our Future, Dayton, O.H, USA.

Partridge, I.K., Cartié, D.D.R. and Bonnington, T. 2003. Manufacture and performance of Z-pinned composites. In: (Shonaike, G.O. and Advani, S.G. ed.): Advanced Polymeric Materials: Structure Property Relationships. CRC Press, Boca Raton, F.L, USA.

Perry, T.D. 1948. Modern Plywood. Pitman Publishing Corporation, New York, N.Y, USA.

Petri, D.F.S., Pereira, E.M.A. and Carmona-Rtbeiro, A.M. 2002. Wettability and adhesion of bilayer-forming lipids onto polymeric films. In: (Mittal, K.L. ed.): Contact Angle, Wettability and Adhesion, Volume 2. VSP Publisher, The Netherlands.

Pizzi, A. 1994. Advanced Wood Adhesives Technology. Marcel Dekker Inc., New York, N.Y, USA.

Pocius, A.V. 2012. Adhesion and Adhesives Technology: an Introduction (3rd edition). Hanser, Munich, Germany.

Podgorski, L., Chevet, B., Onic, L. and Merlin, A. 2000. Modification of wood wettability by plasma and corona treatments. International Journal of Adhesion and Adhesives, 20(2): 103-111.

Quirk, J.T., Kozlowski, T.T. and Blomquist, R.F. 1968. Contributions of end-wall and lumen bonding to strength of butt joints. USDA Research Note FPL-0179, Madison, WI: Forest Service, Forest Products Laboratory, USA.

Racota, M. 2007. Process for imparting water resistance to wood-based products. United States Patent 20070059509. Washington, DC: U.S. Patent and Trademark Office.

Rehn, P., Wolkenhauer, A., Bente, M., Forster, S. and Viöl, W. 2003. Wood surface modification in dielectric barrier discharges at atmospheric pressure. Surface and Coatings Technology, 174-175(1): 515-518.

Reiterer, A., Sinn, G. and Stanzl-Tschegg, S.E. 2002. Fracture characteristics of different wood species under mode I loading perpendicular to the grain. Materials Science & Engineering A, 332(1-2): 29-36.

Rice, J.T. 1965. The effect of urea-formaldehyde resin viscosity on plywood bond durability. Forest Products Journal, 15(3): 107-112.

Riegler, M., Gindl-Altmutter, W., Hauptmann, M. and Müller, U. 2012. Detection of UF resin on wood particles and in particleboards: potential of selected methods for practice-oriented offline detection. European Journal of Wood and Wood Products, 70(6): 829-837.

Ritchie, R.O. 1999. Mechanisms of fatigue-crack propagation in ductile and brittle solids. International Journal of Fracture, 100(1): 55-83.

River, B. 1984. Method for evaluating nonrigid adhesives for use in structural joints. Journal of Applied Polymer Science, Proceedings of Applied Polymer Symposium 40, pp 235-250.

Rowell, R.M. and Banks, W.B. 1985. Water Repellency and Dimensional Stability of Wood. USDA General Technical Report FPL-50, Madison, WI: Forest Service, Forest Products Laboratory, USA.

Rowell, R.M. and Ellis, W.D. 1981. Bonding of isocyanates to wood. In: (Edwards, K.N. ed.): Urethane Chemistry and Applications, based on the 2nd symposium of chemical congress of the North American Continent (180th ACS National Meeting), Las Vegas, N.V, USA. pp 263-284.

Rowell, R.M., Simonson, R. and Tillman, A.M. 1986. A simplified procedure for the acetylation of chips for dimensionally stabilized particleboard products. Paperi ja Puu (Paper and Timber), 68(10): 740-744.

Rowell, R.M., Simonson, R. and Tillman, A.M. 1990. Acetyl balance for the acetylation of wood particles by a simplified procedure. Holzforschung, 44(4): 263-269.

Rowell, R.M., Tillman, A.M. and Simonson, R. 1986. A simplified procedure for the acetylation of hardwood and softwood flaxes for flakeboard production. Journal of Wood Chemistry and Technology, 6(3): 427-448.

Rugg, K.L., Cox, B.N. and Massabò, R. 2002. Mixed mode delamination of polymer composite laminates reinforced through the thickness by z-fibers. Composites Part A, 33(2): 177-190.

Rugg, K.L., Cox, B.N., Ward, K.E. and Sherrick, G.O. 1998. Damage mechanisms for angled through-thickness rod reinforcement in carbon-epoxy laminates. Composites Part A, 29(12): 1603-1613.

Sakellariou, A., Sawkins, T.J., Senden, T.J. and Limaye, A. 2004. X-ray tomography for mesoscale physics applications. Physica A: Statistical Mechanics and its Applications, 339(1-2): 152-158.

Saleem, M.A., Mirmiran, A., Xia, J. and Mackie, K. 2013. Development length of high-strength steel rebar in ultrahigh performance concrete. Journal of Materials in Civil Engineering, 25(8): 991-998.

Sarkar, S. and Adhikari, B. 2000. Lignin-modified phenolic resin: synthesis optimization, adhesive strength, and thermal stability. Journal of Adhesion Science and Technology, 14(9): 1179-1193.

Sayed Ahmad, F., Foret, G., and Le Roy, R. 2011. Bond between carbon fibre-reinforced polymer (CFRP) bars and ultra high performance fibre reinforced concrete (UHPFRC): experimental study. Construction and Building Materials, 25(2): 479-485.

Schaffer, E.L., Jokerst, R.W., Moody, R.C., Peters, C.C., Tschernitz, J.L. and Zahn, J.J. 1972. Feasibility of producing a high-yield laminated structural product: general summary. USDA Research Paper FPL-RP-175, Madison, WI: Forest Service, Forest Products Laboratory, USA.

Schatzberg, E. 1994. Ideology and technical choice: the decline of the wooden airplane in the United States, 1920-1945. Technology and Culture, 35(1): 34-69.

Scholz, G., Nothnick, E., Avramidis, G., Krause, A., Militz, H., Viöl, W. and Wolkenhauer, A. 2010. Adhesion of wax impregnated solid beech wood with different glues and by plasma treatment. European Journal of Wood and Wood Products, 68(3): 315-321.

Schultz, J. and Nardin, M. 2003. Theories and mechanisms of adhesion. In: (Pizzi, A. and Mittal, K.L. ed.): Handbook of Adhesive Technology (2nd edition), Revised and Expanded. CRC Press, Taylor & Francis Publisher, London, UK.

Sela, N. and Ishai, O. 1989. Interlaminar fracture toughness and toughening of laminated composite materials: a review. Composites, 20(5): 423-435.

Sellers, Jr., T. 1994. Adhesives in the Wood Industry. In: (Pizzi, A. and Mittal, K.L. ed.): Handbook of Adhesive Technology. Marcel Dekker, Inc., New York, N.Y, USA. pp. 599-614.

Sernek, M., Resnik, J. and Kamke, F.A. 1999. Penetration of liquid urea-formaldehyde adhesive into beech wood. Wood and Fiber Science, 31(1): 41-48.

Shaler, S.M., Wang, H., Landis, E., Keane, D.T., Mott, L. and Holzman, L. 1998. Microtomography of cellulosic structures. In: Proceedings of Process and Product Quality Conference and Trade Fair, Technical Association of the Pulp and Paper Industry (TAPPI), Atlanta, G.A, USA. pp 89-96.

Shen, K.C. 1974. Improving the surface quality of particleboard by high-temperature pressing. Forest Products Journal, 24(10): 36-39.

Shi, S.Q. and Gardner, D.J. 2001. Dynamic adhesive wettability of wood. Wood Fiber Science, 33(1): 58-68.

Shirangi, M.H. and Michel, B. 2010. Mechanism of moisture diffusion, hygroscopic swelling, and adhesion degradation in epoxy molding compounds. In: (Fan, X.J. and Suhir, E. ed.): Moisture Sensitivity of Plastic Packages of IC Devices, Micro- and Opto- Electronic Materials, Structures, and Systems. Springer Science + Business Media.

Shmulsky, R. and Jones, P.D. 2011. Chapter 7, Wood and water. In: Forest Products and Wood Science: An Introduction (6th edition). John Wiley & Sons, Inc. Publication, West Sussex, UK.

Shmulsky, R. and Jones, P.D. 2011. Chapter 13, Structural composites. In: Forest Products and Wood Science: an Introduction (6th edition). John Wiley & Sons, Inc. Publication, West Sussex, UK.

Skaar, C. 1988. Wood-Water Relations. Springer, Berlin, Germany.

Smith, L.A. 1971. Resin penetration of wood cell walls – implications for adhesion of polymers to wood. Ph.D dissertation, State University College of Forestry at Syracuse University, Syracuse, N.Y, USA.

Soutis, C. 2005. Fibre reinforced composites in aircraft construction. Progress in Aerospace Sciences, 41(2): 143-151.

Spelter, H., McKeever, D.B., and Alderman, M. 2006. Status and trends: Profile of structural panels in the United States and Canada. USDA Research Paper FPL-RP-636, Madison, WI: Forest Service, Forest Products Laboratory, USA.

Sperling, L.H. 1981. Interpenetrating Polymer Networks and Related Materials. Plenum Press, New York, N.Y, USA.

Šrajer, J., Král, P., Čermák, M. and Mazal, P. 2013. Structure evaluation of compressing of spruce and beech plywoods Part 1: microscopic structure. Wood Research, 58(1): 101-112.

Stamm, A.J. 1964. Wood and Cellulose Science. Ronald Press Co., New York, N.Y, USA.

Stamm, A.J. and Baechler, R.H. 1960. Decay resistance and dimensional stability of five modified woods. Forest Products Journal, 10(1): 22-26.

Stark, N.M., Cai, Z., Carll, C. 2010. Wood-based composite materials: panel products, glued-laminated timber, structural composite lumber, and wood-nonwood composite materials. In: (Ross, R.J. ed.): Wood Handbook - Wood as an Engineering Material (centennial edition).

USDA General Technical Report FPL-GTR-190, Madison, WI: Forest Service, Forest Products Laboratory, USA.

Steeves, C.A. and Fleck, N.A. 2006. In-plane properties of composite laminates with through-thickness pin reinforcement. International Journal of Solids and Structures, 43(10): 3197-3212.

Stehr, M. 1999. Adhesion to Machined and Laser Ablated Wood Surfaces. Ph.D dissertation, KTH Royal Institute of Technology, Stockholm, Sweden.

Stephens, R.S. and Kutscha, N.P. 1987. Effect of resin molecular weight on bonding flakeboard. Wood and Fiber Science, 19(4): 353-361.

Stoyan, Y., Pankratov, A. and Romanova, T. 2016. Quasi-phi-functions and optimal packing of ellipses. Journal of Global Optimization, 65(2): 283-370.

Suchsland, O. 1959. An analysis of the particle board process. Quarterly Bulletin: Michigan State University Agricultural Experiment Station, 42(2): 350-372.

Suchsland, O. 1962. The density distributions in strand boards. Quarterly Bulletin: Michigan State University Agricultural Experiment Station, 45(1): 104-121.

Suchsland, O. and McNatt, J.D. 1986. Computer simulation of laminated wood panel warping. Forest Products Journal, 36(11-12): 16-23.

Suchsland, O. and Xu, H. 1991. Model analysis of flakeboard variables. Forest Products Journal, 41(11-12): 55-60.

Sugimori, M. and Lam, F. 1999. Macro-void distribution analysis in strand-based wood composites using an X-ray computer tomography technique. Journal of Wood Science, 45(3): 254-257.

Sweeting, R.D. and Thomson, R.S. 2004. The effect of thermal mismatch on Z-pinned laminated composite structures. Composite Structures, 66(1): 189-195.

Tackie, A.D., Wang, S. and Bennett, R.M. 2008. Investigation of OSB thickness-swell based on a 3-D density distribution, Part II: variations in thickness-swell and internal stresses. Wood and Fiber Science, 40(3): 352-361.

Taylor, A., Wang, S., Freitag, C. and Morrell, J.J. 2008. Properties of “enhanced” OSB subfloor panels. Forest Products Journal, 58(5): 77-79.

Thompson, D.W. 1917. On Growth and Form. The University Press, Cambridge, UK.

Tighiouart, B., Benmokrane, B. and Gao, D. 1998. Investigation of bond in concrete member with fibre reinforced polymer (FRP) bars. Construction and Building Materials, 12(8): 453-462.

Time, B. 1998. Hygroscopic moisture transport in wood. Ph.D dissertation, Building and Construction Engineering, Norwegian University of Science and Technology, Trondheim, Norway.

Tong, L., Mouritz, A.P. and Bannister, M. 2002. 3D Fibre Reinforced Polymer Composites. Elsevier Science Ltd., Oxford, UK.

Tong, Y. and Suchsland, O. 1993. Application of finite element analysis to panel warping. Holz als Roh- und Werkstoff, 51(1): 55-57.

Troughton, G.E. 1967. Kinetic evidence for covalent bonding between wood and formaldehyde glues. Information Report VP-X-26, Forest Products Laboratory, Vancouver, B.C., Canada.

Vick, C.B. 1999. Adhesive bonding of wood materials. In: Wood Handbook - Wood as an Engineering Material. USDA General Technical Report FPL-GTR-113, Madison, WI: Forest Service, Forest Products Laboratory, USA

Vincent, J.F.V. and Mann, D.L. 2002. Systematic technology transfer from biology to engineering. Philosophical Transactions: Mathematical, Physical and Engineering Sciences, 360(1791): 159-173.

Vlassenbroeck, J., Dierick, M., Masschaele, B., Cnudde, V., Van Hoorebeke, L. and Jacobs, P. 2007. Software tools for quantification of X-ray microtomography at the UGCT. In: Proceedings of the 10th International Symposium on Radiation Physics, Nuclear Instruments and Methods in Physics Research Section A: Accelerators, Spectrometers, Detectors and Associated Equipment, 580(1): 442-445.

Vlosky, R.P., Smith, P.M., Blankenhorn, P.R. and Haas, M.P. 1994. Laminated veneer lumber: a United States market overview. Wood and Fiber Science, 26(4): 456-466.

Voronko, Y., Chernev, B.S. and Eder, G.C. 2014. Spectroscopic investigations on thin adhesive layers in multi-material laminates. Applied Spectroscopy, 68(5): 584-592.

Wadsø, L. 1993. Studies of water vapor transport and sorption in wood. Ph.D dissertation, Report TVBM-1013, Building Materials, Lund University, Lund, Sweden.

Walker, J.C.F. 1993. Wood panels: plywoods. In: (Walker, J.C.F. et al. ed.): Primary Wood Processing: Principles and Practice (1st edition). Springer Science + Business Media B.V, London, UK.

Hedberg, Y.S., Hedberg, J.F., Herting, G., Goidanich, S. and Wallinder, I.O. 2014. Critical review: Copper runoff from outdoor copper surfaces at atmospheric conditions. Environmental Science and Technology, 48(3): 1372-1381.

Wallinder, I.O. and Herting, G. 2016. Metal surface and bioelution - the KTH approach. In: Proceedings of the 8th International Meeting of the Task Force on Exposure Assessment (OECS), Dortmund, Germany.

Walther, T. and Thoemen, H. 2009. Synchrotron X-ray microtomography and 3D image analysis of medium density fiberboard (MDF). Holzforschung, 63(5): 581-587.

Wang, H. and Shaler, S.M. 1998. Computer-simulated three-dimensional microstructure of wood fibre composite materials. Journal of Pulp and Paper Science, 24(10): 314-319.

Wang, S. and Winistorfer, P.M. 2000. The effect of species and species distribution on the layer characteristics of OSB. Forest Products Journal, 50(4): 37-44.

Wegst, U.G.K., Bai, H., Saiz, E., Tomsia, A.P. and Ritchie, R.O. 2014. Bioinspired structural materials. Nature Materials, 14(1): 23-36.

Weiner, S. and Wagner, HD. 1998. The material bone: structure - mechanical function relations. Annual Review of Materials Science, 28(1): 271-298.

Wernersson, H. 1990. Wood adhesive bonds - fracture softening properties in shear and in tension. Report TVSM-3012, Division of Structural Mechanics, Lund University, Lund, Sweden.

White, M.S., Ifju, G. and Johnson, J.A. 1977. Method for measuring resin penetration into wood. Forest Products Journal, 27(7): 52-54.

Williams, R.S., Swan, L., Sotos, P., Knaebe, M. and Feist, W.C. 2005. Performance of finishes on western juniper lumber and particleboard during outdoor exposure. Forest Products Journal, 55(11): 65-72.

Wilson, J.B. 1980. Is there an isocyanate in your future? Property and cost comparisons. In: Proceedings of the 14th International Particleboard/Composite Materials Symposium. Washington State University, Pullman, W.A, USA. pp 185-193.

Winterowd, J.G., Lewis, C.E., Izan, J.D., and Shantz, R.M. 2003. Edge sealant formulation for wood-based panels. United States Patent: 6608,131 B1. Washington, DC: U.S. Patent and Trademark Office.

Wong, E.H., Koh, S.W., Lee, K.H. and Rajoo, R. 2002. Advanced moisture diffusion modeling & characterisation for electronic packaging. In: Proceedings of the 52nd Institute of Electrical and Electronics Engineers (IEEE) Electronic Components and Technology Conference. pp 1297-1303.

Wong, E.H., Koh, S.W., Lee, K.H. and Rajoo, R. 2002. Comprehensive treatment of moisture induced failure - recent advances. Transactions on Electronics Packaging Manufacturing, 25(3): 223-230.

Wong, E.H., Teo, Y.C. and Lim, T.B. 1998. Moisture diffusion and vapor pressure modeling of IC packaging. In: Proceedings of the 48th Institute of Electrical and Electronics Engineers (IEEE) Electronic Components and Technology Conference. pp 1372-1378.

Wood, A.D. and Linn, T.G. 1943. Plywoods, their Development, Manufacture and Application. Chemical Publishing Co., Brooklyn, N.Y, USA.

Wu, Q.L. and Suchsland, O. 1996. Linear expansion and its relationship to moisture content change for commercial oriented strandboard. Forest Products Journal, 46(11/12): 79-83.

Wu, Q.L. and Suchsland, O. 1997. Effect of moisture on the flexural properties of commercial oriented strandboards. Wood and Fiber Science, 29(1): 47-57.

Wu, Q.L., Lee, S.Y. and Lee J.N. 2002. Mechanical, physical, and biological properties of borate-modified oriented strandboard. In: (Anson, M., Ko, J.M. and Lam, E.S.S. ed.): Advances in Building Technology: Proceedings of the International Conference on Advances in Building Technology (ABT 2002). Elsevier Science. pp 137-144.

Xing, C., Riedl, B. and Cloutier, A. 2004. Measurement of urea-formaldehyde resin distribution as a function of MDF fiber size by laser scanning microscopy. Wood Science and Technology, 37(6): 495-507.

Xing, C., Riedl, B., Cloutier, A. and Shaler, S.M. 2005. Characterization of urea-formaldehyde resin penetration into medium density fiberboard fibers. Wood Science and Technology, 39(5): 374-384.

Yeih, W., Huang, R., Chang, J.J. and Yang, C.C. 1997. A pullout test for determining interface properties between rebar and concrete. Advanced Cement Based Materials, 5(2): 57-65.

Young, T. 1805. An essay on the cohesion of fluids. Philosophical Transactions of the Royal Society of London, 95(1): 65-87.

Young, R.A. 1976. Wettability of wood pulp fibers - Applicability of methodology. Wood and Fiber, 8(2): 120-128.

Youngquist, J.A., Myers, G.C. and Murmanis, L. 1987. Resin distribution in hardboard: evaluated by internal bond strength and fluorescence microscopy. Wood and Fiber Science, 19(2): 215-224.

Zackay, V.F., Mitchell. D.W., Mitoff, S.P. and Pask, J.A. 1953. Fundamentals of glass-to-metal bonding: I, Wettability of some group I and group VIII metals by sodium silicate glass. Journal of the American Ceramic Society, 36(3): 84-89.

Zhou, J., Lahoti, S. and Kallolimath, K. 2005. Investigation of non-uniform moisture distribution on determination of hygroscopic swelling coefficient and finite element modeling for a flip chip package. In: Proceedings of the 6th Institute of Electrical and Electronics Engineers (IEEE) International Conference on Thermal, Mechanical and Multiphysics Simulation and Experiments in Micro-Electronics and Micro-Systems (EuroSime), Berlin, Germany. pp 112-119.

Zienkiewicz, O.C., Taylor, R.L. and Zhu, J.Z. 2005. Finite Element Method - Its Basis and Fundamentals (6th edition) (first published in 1967 by McGraw-Hill). Elsevier Butterworth-Heinemann.

Zisman, W.A. 1963. Influence of constitution on adhesion. Industrial and Engineering Chemistry, 55(10): 19-38.

Appendices

Appendix A: Confocal profilometry images of model composites showing the adhesive Z-connections from 2D and 3D views (different viewing angles) (Chapter 4)

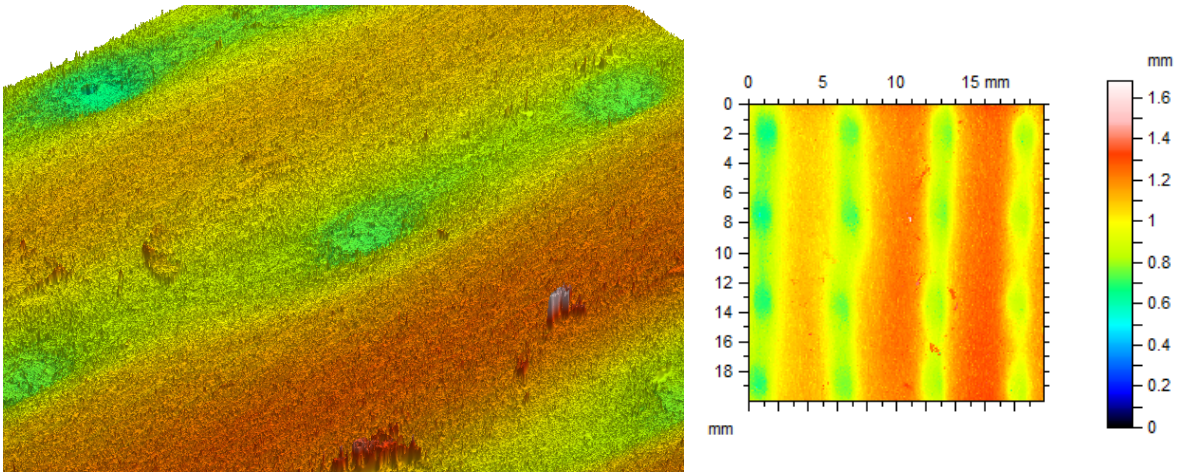

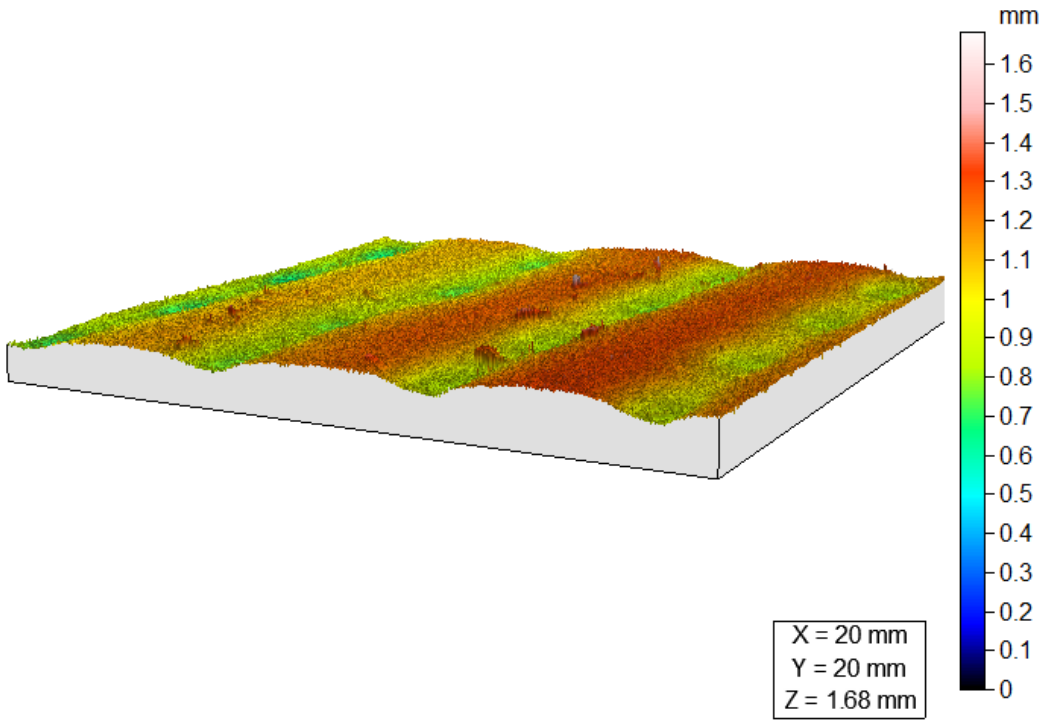

Appendix B: Macro-photographs of cross-sections of model composites showing some adhesive Z-connections containing voids (Chapter 4)

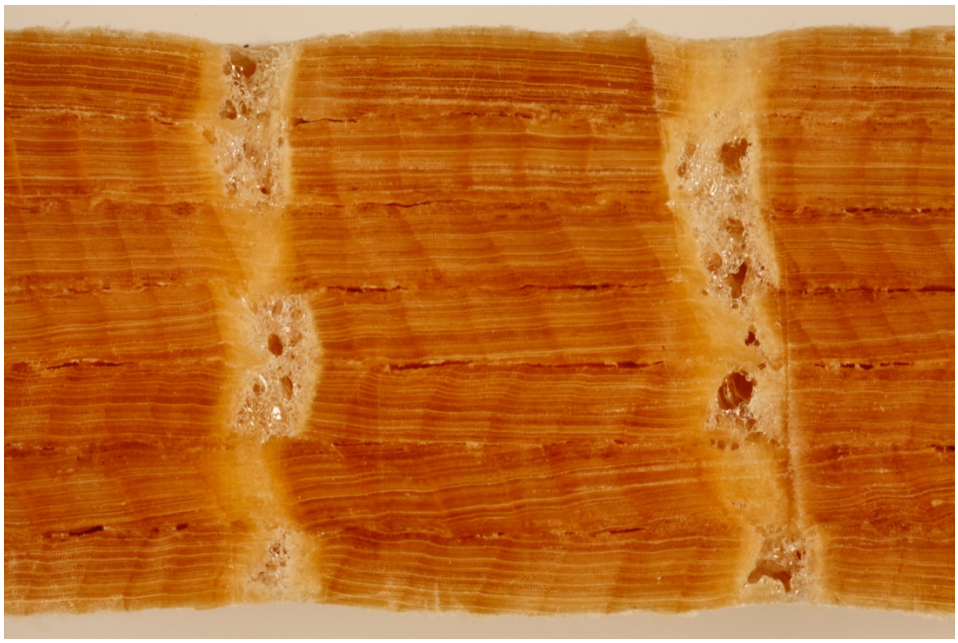

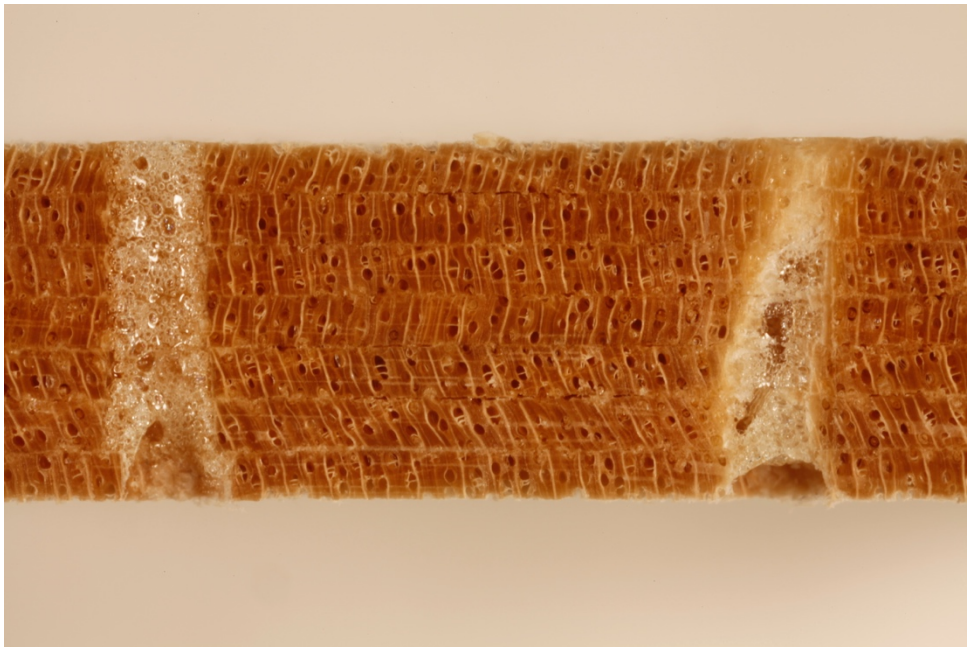

Appendix C: SEM images of cross-sections of model composites showing connections of adhesive Z-connections with X-Y adhesive bond lines (Chapter 4)

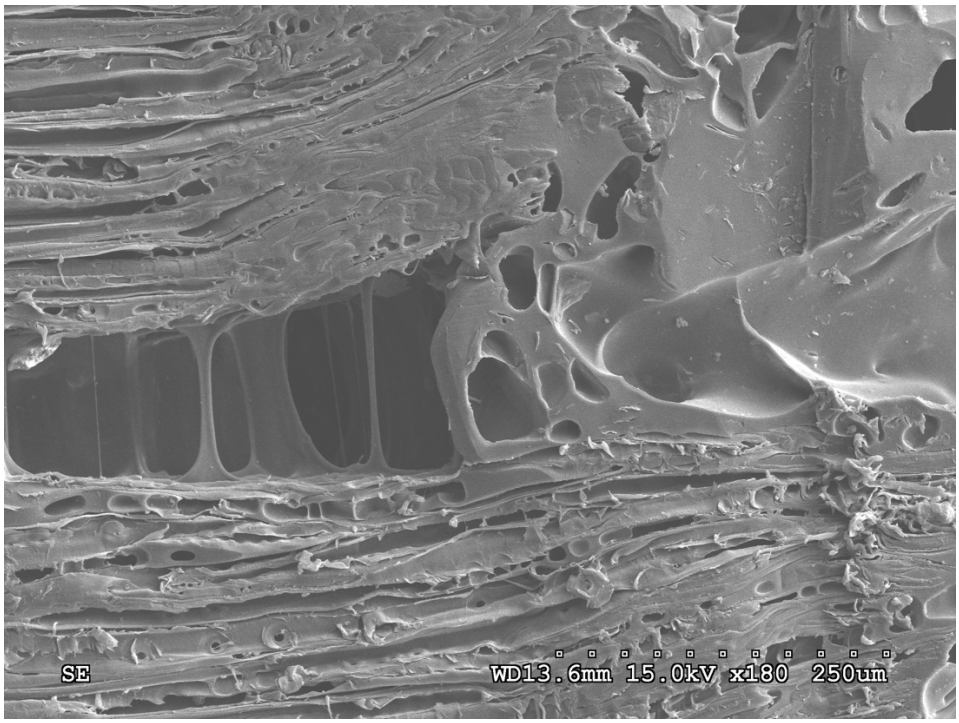

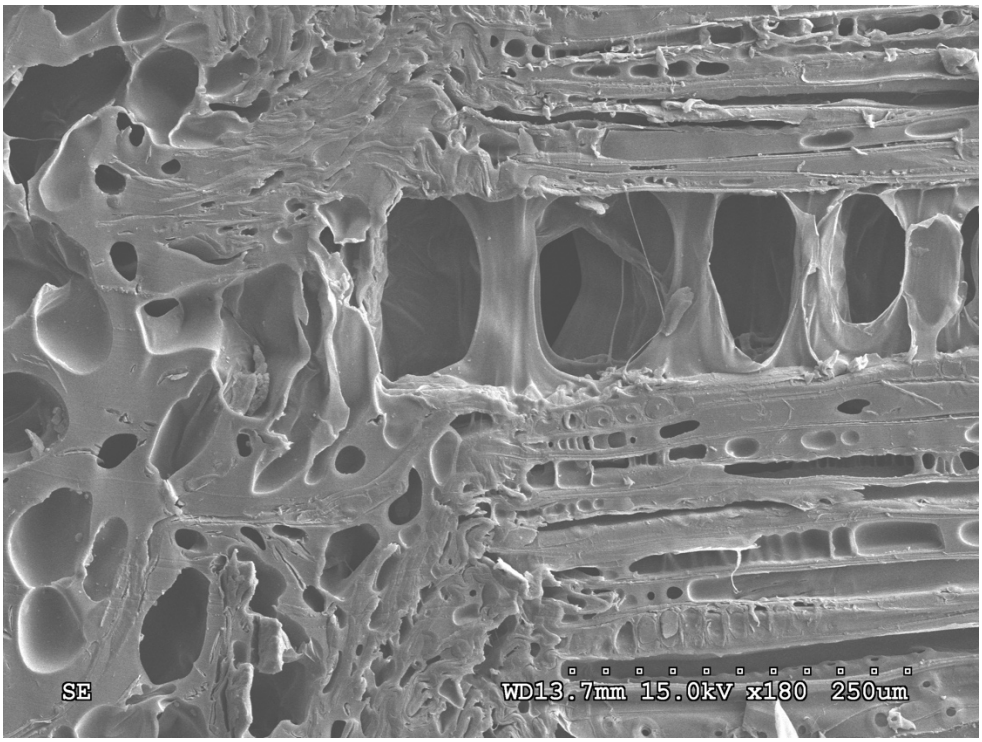

Appendix D: Confocal profilometry images of model composites showing measurement of wood swelling (2D view) and differential swelling between wood and adhesive Z-connections (mesh 3D view) (Chapter 5)

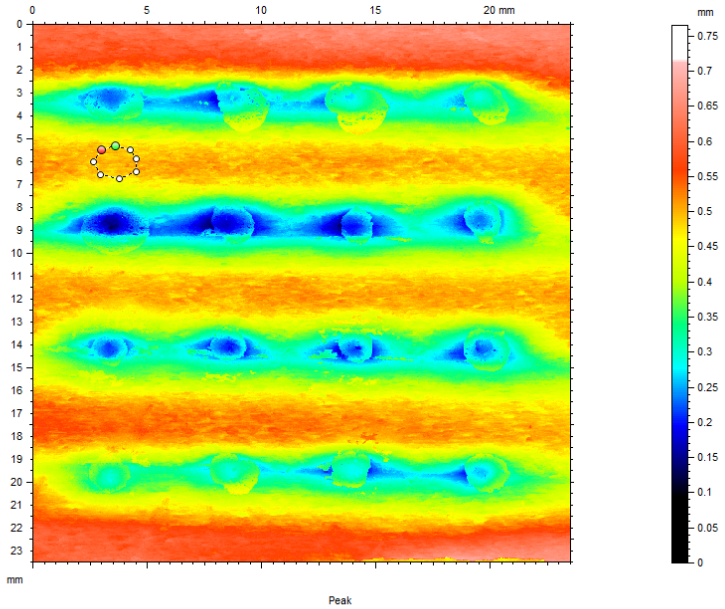

Surface (mm²)	2.01
Mean depth/height (mm)	0.0873

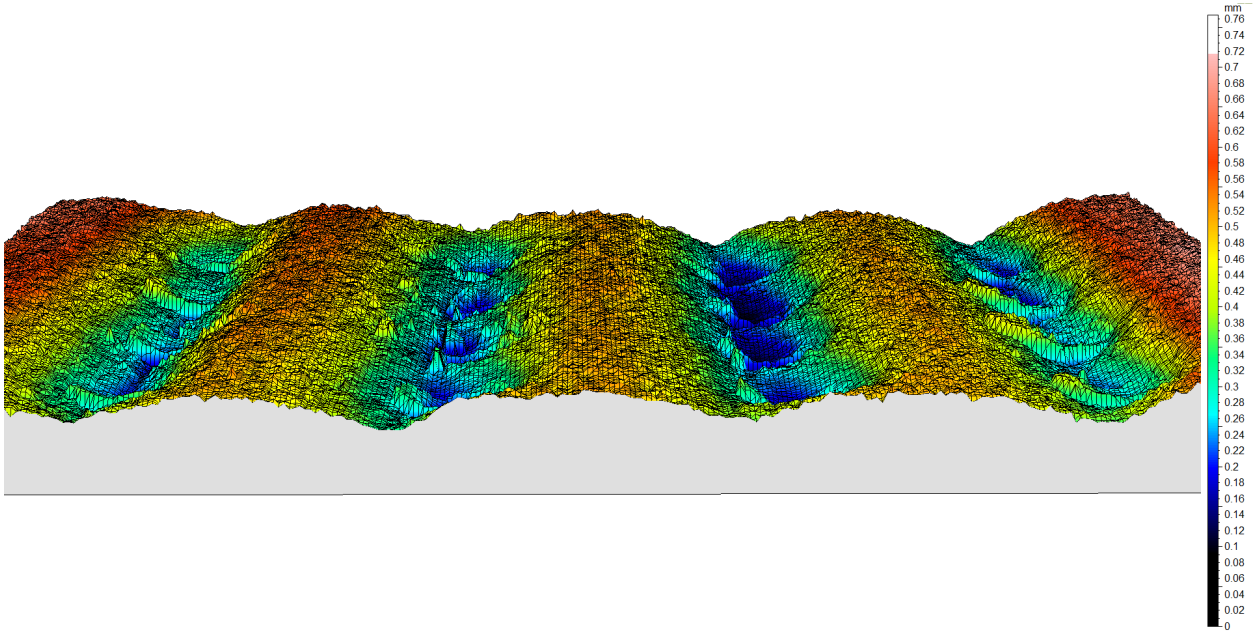

Appendix E: SEM image of cross-section of a model composite showing the penetration of X-Y adhesive bond lines into adjacent tracheids (Chapter 5)

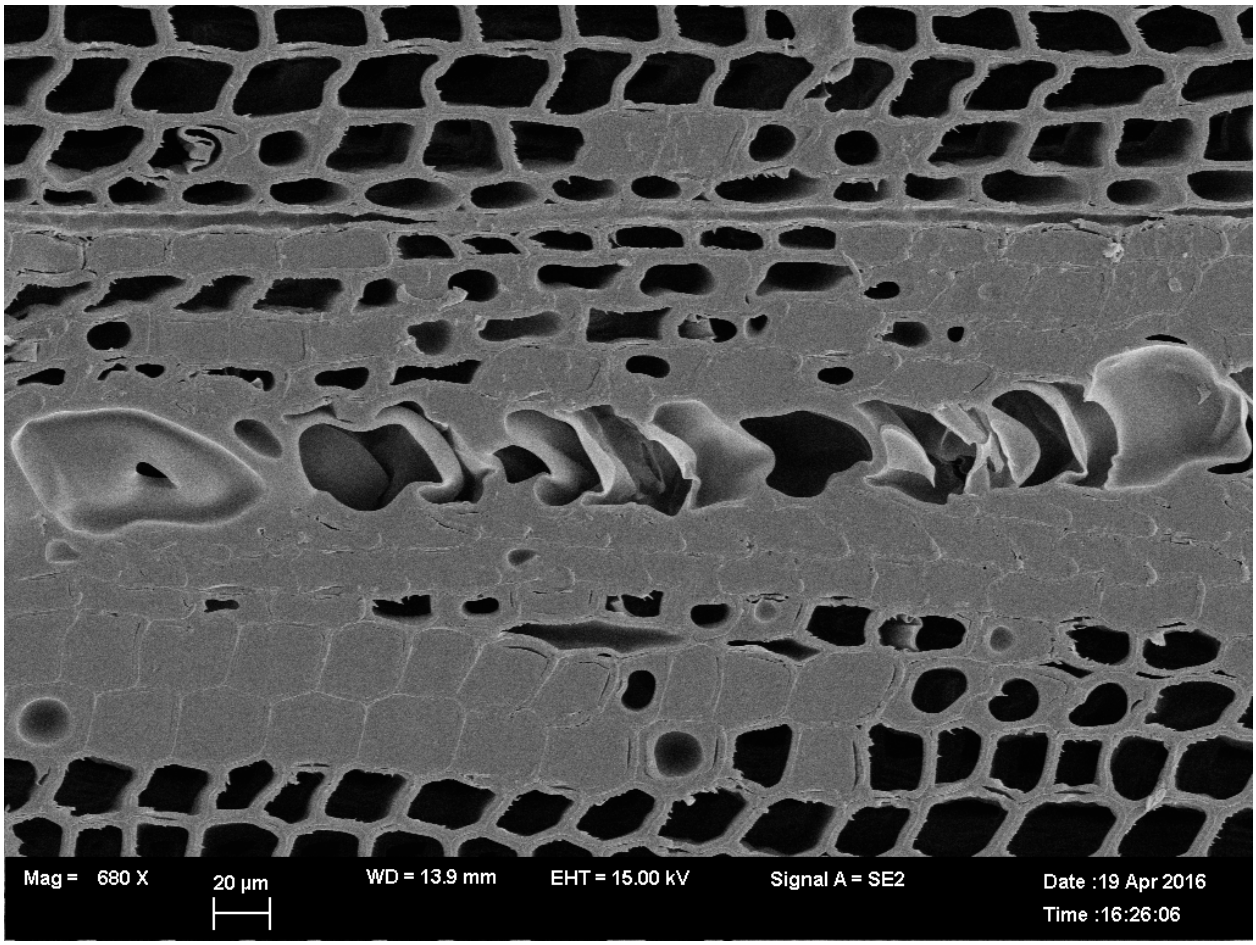

Appendix F: SEM images of fracture surfaces of model birch composites bonded with GF reinforced PU adhesive showing GF embedded in and around the adhesive Z-connections (Chapter 7)